MATERIALS CHARACTERISATION OF CRYSTALLINE BECLOMETHASONE DIPROPIONATE: IMPACT OF MANUFACTURING CONDITIONS ON PHYSICOCHEMICAL PROPERTIES

Cordula Weiss

Waterford Institute *of* Technology
INSTITIÚID TEICNEOLAÍOCHTA PHORT LÁIRGE

A dissertation submitted to Waterford Institute of Technology for the Degree of Doctor of Philosophy

May 2018

Prepared under the supervision of Dr Peter McLoughlin and Dr Helen Cathcart

Ireland's EU Structural Funds Programmes 2007 - 2013
Co-funded by the Irish Government and the European Union
EUROPEAN REGIONAL DEVELOPMENT FUND
HEA
Higher Education Authority
An tÚdarás um Ard-Oideachas
ENTERPRISE IRELAND
SFI
Science Foundation Ireland

DECLARATION

I hereby certify that this material, which I now submit for assessment is entirely my own work and has not been taken from the work of others, save to the extent that such work has been cited and acknowledged within the text of my work.

Signed: Date: 10 May 2018

ACKNOWLEDGEMENTS

Thank you to my amazing supervisors Dr Helen Cathcart and Dr Peter McLoughlin for their continuous support of my research. Thank you for providing excellent guidance and advice at all times – you have no idea how much every single meeting added to my motivation and kept me going those last few months. I would also like to thank you for giving me so many opportunities outside the actual PhD work, this really made moving to Ireland and finding and getting into a career I love so much easier.

I would like to thank my family and friends in Germany, Ireland and abroad for supporting me around the clock throughout the years. A special thank you to all for helping me stay awake late at night, sending my favourite coffee straight from the stores in Munich and getting my favourite chocolate for me during the last stages of writing up.

I also thank the WIT Scholarship Programme for financial support.

ABSTRACT

Active pharmaceutical ingredients in dry powder inhaler (DPI) formulations need to have well-defined material properties. These can be influenced by the choice of processing parameters. The impact of methanol, ethanol, 1-propanol, 2-propanol, 1-butanol, 1-pentanol and acetone on the crystallisation of beclomethasone dipropionate (BDP), an anti-inflammatory agent, was studied using infrared spectroscopy, X-ray powder diffraction, thermal analysis, gas chromatography with mass spectrometry, scanning electron microscopy and atomic force microscopy. Crystallisation from methanol, 1-butanol and 1-pentanol resulted in particulate BDP with a predominantly anhydrous character. In contrast, BDP solvates were formed using ethanol, 1-propanol, 2-propanol and acetone. The physical properties of the solvates were found to depending on the solvent used.

Single crystal X-ray diffraction and solid state NMR confirmed the inclusion of ethanol, 1-propanol, 2-propanol and acetone within the crystalline BDP host. Based on NMR titration, DOSY, thermal analysis and XRD, the intermolecular interactions leading to the preferred formation of either solvated or anhydrous BDP from solution were analysed. The same combination of techniques can be potentially used to predict the formation of solvated compounds in general by assessing the forces acting between the host and guest molecules and analysing their impact on solvate formation and stability.

The size, shape and surface characteristics of the crystalline particles were found to be influenced by the choice of solvent in a reproducible way. These properties were also found to translate to the anhydrous products prepared from the solvates through controlled desolvation. Thus, anhydrous BDP with defined surface properties were prepared. AFM was used to evaluate the adhesive and cohesive forces between lactose, a commonly used carrier material in DPI formulations, and anhydrous BDP prepared from the BDP ethanol, 1-propanol and 2-propanol solvates.

The interparticulate forces in a DPI formulation depend to a large part on the surface roughness of the drug particles and the carrier material. It was demonstrated that the surface roughness of anhydrous BDP can be controlled through the manufacturing process. This is an important step towards the targeted preparation of well-defined formulations which have the potential to be tailored to specific patient needs.

CONTENTS

ABBREVIATIONS

AFM	Atomic force microscopy or atomic force microscope
ah	anhydrous
API	Active pharmaceutical ingredient
BDP	Beclomethasone dipropionate
BET	Brunauer Emmet Teller
CCDC	Cambridge Crystallographic Data Centre
$CDCl_3$	Deuterated chloroform
COPD	Chronic obstructive pulmonary disease
COSY	Correlation spectroscopy
CP	Cross polarisation
DEPT	Distortion enhancement by polarisation transfer
DLS	Dynamic light scattering
DOSY	Diffusion ordered spectroscopy
DPI	Dry powder inhaler
DSC	Differential scanning calorimetry
DVS	Dynamic vapour sorption
FPF	Fine particle fraction
FTIR	Fourier transform infrared spectroscopy
GC-MS	Gas chromatography with mass spectrometry
HMBC	Heteronuclear multiple bond correlation
HSQC	Heteronuclear single quantum coherence
HSQC-TOCSY	Heteronuclear single quantum coherence - total correlation spectroscopy
LD	Laser diffraction
MAS	Magic angle spinning
NGI	Next generation impactor
NMR	Nuclear magnetic resonance spectroscopy
NOESY	Nuclear Overhauser effect spectroscopy
PFQNM	Peak force quantitative nanomechanical mapping
Ph. Eur.	European Pharmacopoeia
PSD	Particle size distribution
RH	Relative humidity
SEM	Scanning electron microscopy or scanning electron microscope
SSNMR	Solid state nuclear magnetic resonance spectroscopy
TGA	Thermogravimetric analysis
XRD	X-ray diffraction
XRPD	X-ray powder diffraction

LIST OF FIGURES

LIST OF TABLES

CHAPTER 1

DRY POWDER INHALER FORMULATIONS FOR PULMONARY DRUG DELIVERY

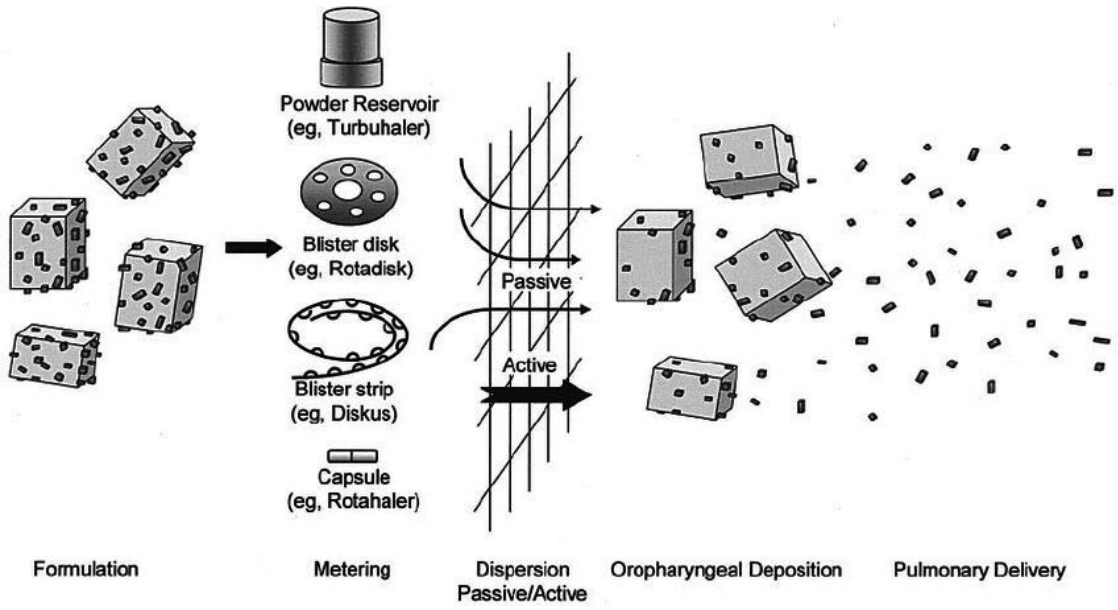

Figure 1. Pulmonary drug delivery using dry powder inhaler formulations (Telko and Hickey, 2005).

1 Dry Powder Inhaler Formulations for Pulmonary Drug Delivery

Respiratory disorders such as asthma and chronic obstructive pulmonary disorder (COPD) are usually treated by direct pulmonary delivery of drug formulations via inhalation (GINA, 2014). Owing to the rapid onset of action, the circumvention of first pass metabolism and a generally lower risk of side effects, inhalation formulations are generally considered superior to conventional oral dose alternatives (Sung et al., 2007, Patton and Byron, 2007, Wang et al., 2014, Hoppentocht et al., 2014). Delivery relies on nebulisers, metered dose inhalers (MDI) or dry powder inhalers (DPI), with the latter providing a convenient way of delivering the drug with unique advantages such as easy handling and relatively high patient compliance (Labiris and Dolovich, 2003a, Labiris and Dolovich, 2003b, Sung et al., 2007, Patton and Byron, 2007, Wang et al., 2014, Hoppentocht et al., 2014). In terms of shelf life and drug stability, DPI formulations benefit from being stored in the solid state which makes the active pharmaceutical ingredient (API) less susceptible to degradation and therefore superior to MDI suspensions (Zeng et al., 2000).

Particles for DPI formulations, however, need to fulfil certain requirements. Size regulations are among the most important limitations when preparing particulate APIs: Only particles with a diameter between 1 and 5 µm are therapeutically active as smaller and larger ones do not proceed to the site of action deep within the respiratory tract. Further limiting factors are the reproducibility of the method, the mechanical and physicochemical characteristics of the particles within the formulation and the interparticulate forces acting between them.

The efficient delivery of drugs into the respiratory system is controlled and limited by several factors. The process of drug delivery itself is subject to continuous development and the composition of the administered medication also holds potential for substantial improvement. One of the main issues is the delivery of sufficient doses of therapeutic substances. Another issue is the use of a propellants in devices such as the MDI. Propellants are prone to remain in the lungs instead of being exhaled again in the course of the respiratory cycle which is due to their greater density compared to the inhaled air. Patients already suffering from respiratory diseases may thus experience additional breathing problems (Kruber, 1981). They may even be exposed to higher medical risks on account of inhaling potentially carcinogenic materials. Propellants such as hydrofluoroalkenes (HFA) are also known to affect the environment by contributing to current climate issues (Zeng et al., 2000).

A number of developments in the second half of the 20th century (Zeng et al., 2000, Kruber, 1981, Bell et al., 1971, Sung et al., 2007), however, led to the establishment and improvement of propellant-free devices such as the nebuliser or the DPI. While nebulisers generate a mist of particles from solution and benefit from administration doses of up to 1 g at a time, DPIs are

controlled by the inhalation effort of the patient. Nebulisers tend to be of poor storage stability (McAffer et al., 2011) and their application is limited by the instability of drugs in aqueous solution (Zeng et al., 2000). DPIs, in contrast, contain only dry substances, either in form of a single drug or a combination formulation. This enhances the shelf live and stability of the therapeutic agent (Zeng et al., 2000, Chougule et al., 2007), thus reducing risks caused by premature degradation. Further advantages include easy handling, the capacity of the device to carry large doses and the reduced time exposure for administration (Sudhamani et al., 2010, Geller et al., 2011, Zeng et al., 2000, Chougule et al., 2007), which is conducive to patience compliance. DPI based respiratory drug delivery further benefits from a rapid onset of action and a generally lower risk of side effects (Sung et al., 2007, Patton and Byron, 2007, Wang et al., 2014, Hoppentocht et al., 2014).

1.1 Dry Powder Inhalers

The high patient compliance (Zeng et al., 2000, Chougule et al., 2007) to DPI treatment has been subject to a number of comparative studies. Comparing the success of MDI and DPI supported delivery of the same API reveals a small but undeniable preference of DPI based delivery (Hoppentocht et al., 2014). A large variety of DPIs are currently in use or in development (Saritha et al., 2013, Demoly et al., 2014, Wang et al., 2014, Healy et al., 2014). The devices can be differentiated into single- and multi-dose, active and passive devices with the latter being the most common ones (Chougule et al., 2007). It is the patient's own respiratory effort that triggers the actuation of the API. Studies concentrating on the efficiency of drug administration compared the performance of DPIs and other devices (Kanniess et al., 2014, Chrystyn and Price, 2009, Crowther Labiris et al., 1999, Cui et al., 2014) and found that respiratory drugs are best delivered when allowing for air flow-dependent dosage. A high internal resistance is beneficial to regulate the air flow and results in conveniently sized doses. To ensure correct use as well as patient compliance - which is crucial for therapeutic success - the inhalation device needs to be easily operated (Demoly et al., 2014, Chrystyn and Price, 2009). Current approaches to maximise the success of inhalation therapy focus on understanding the factors affecting the performance of DPIs and DPI formulations (Hoppentocht et al., 2014) and work towards matching formulation and device (Zhou et al., 2014).

Even though progress is being made in terms of device and drug development, patient compliance and adherence to therapy is still an issue. Therefore, studies are carried out to improve the process of drug administration by inhalation with regard to patients' preferences as well as cost and therapy effectiveness (Jentzsch et al., 2009, Lasmar et al., 2009).

Dispersion and flow related properties are also crucial for the success of inhalation therapy. For example, flowability affects the mixing and capsule filling performance (Neumann, 1967, Tan

and Newton, 1990), and the detachment of the API from the carrier during inhalation (Zeng et al., 2000).

1.2 Drug Delivery and Clearance Mechanism

Upon inhalation, the drug particles proceed into the bronchi and bronchioli of the lungs and, depending on their size, are able to access the alveoli directly (Patton et al., 2010, Crampton et al., 2004), from where they can easily penetrate the circulatory system. Thus, therapeutic efficacy and rapid onset are facilitated which is of specific importance in the treatment of respiratory diseases. Pulmonary drug delivery additionally benefits from being non-invasive and targeting a large surface area (Zeng et al., 2000, Rogueda and Traini, 2007).

Being the site of oxygen and carbon dioxide exchange, the lungs are highly vascularised (Weibel, 1965) and have a large surface area of about 75 to 140 m² (Groneberg et al., 2003). This is due to many kilometres of airways, the bronchi branching into bronchioles and about 500 million alveoli. The surface area of the blood-gas barrier at the alveoli in the alveolar ducts and sacs makes up about 70 m² which is created by a network of more than 280 billion capillaries. It is at the interface between the alveoli and the capillaries that the gas exchange occurs by diffusion through an easily permeable layer of epithelium, endothelium and interstitial cells. This makes the lungs an ideal target for not only targeting pulmonary but also systematic diseases. Owing to the likewise present lymph vessels they are also well suited for the administration of drugs to the lymphatic system (Wang et al., 2014, Patton et al., 2010, Weibel, 1965, Todoroff and Vanbever, 2011).

Drug delivery via DPI means exposing the airways to fine particles. The lungs are constructed in a way that prevents the uptake of particular matter larger than 10 µm. Cilia and mucus help remove contaminants from the inhaled air and the increasingly narrow airways additionally prevent the passage of too large particles. This protects the lungs from injuries and reduces the risk of pollutants reaching the deep lung and potentially entering the circulatory system. However, the same mechanisms also significantly restrict respiratory drug delivery to the administration of particles with a diameter of 10 µm or less, ideally within the size range between 1 and 5 µm.

Depending on the patient's inhalation effort and technique, their breathing pattern, the geometry of the patient's airway and environmental factors such as humidity but also powder specific properties like morphology, geometry and mainly size or aerodynamic diameter, the drug is transported to different parts of the respiratory system and deposited either via impaction, sedimentation or diffusion (Todoroff and Vanbever, 2011, Heyder, 2004, Hoppentocht et al., 2014). The mechanical forces controlling the fate of the drug particles are gravity, inertia and

impulse transfer (Heyder, 2004) with gravity being the driving force that allows appropriately sized particles to reach the small branches in the lower part of the respiratory tract.

Deposition by impaction means deposition in the upper airways, the oropharynx part of the respiratory tract. Particles larger than 5 μm impinge on the wall of these parts due to their high momentum and the impact of centrifugal forces. Speed and deposited amount also depend strongly on the flow rate, thus on the patient's inhalation effort.

Sedimentation, in contrast, leads to particles below 5 μm depositing in the smaller airways, including bronchi and bronchioles, by gravitational forces. Again, the patient's breathing pattern is crucial as the particles are not deposited immediately but need sufficient time to settle. As the settling velocity correlates directly to the square of the particle diameter, sedimentation depends considerably on particle size leading to particles below 1 μm being unsuitable for sedimentation (Frijlink and De Boer, 2004).

Very small particles, in particular those below 0.5 μm, are either exhaled by the patient or get drawn into the alveoli where they deposit due to diffusion. Brownian motion on the inner surface of the lungs induces random particle movement which facilitates the diffusion of drug into the smallest branching of the lung where the particles can permeate the thin cellular layer to get into the circulatory system.

Particles can also be subject to the lung's natural cleaning mechanism (Rogueda and Traini, 2007, Todoroff and Vanbever, 2011, Fernández Tena and Casan Clarà, 2012). A protective layer of thick mucus catches particles in the upper airways from where they are cleared through mucociliary clearance, the movement of thousands of cilia. Particles thus kept from proceeding into the lungs are coughed out or simply swallowed. Tight junctions additionally hinder small particles from further entering the deepest regions of the lung. Eventually, alveolar macrophages help removing foreign bodies from the lung through phagocytisis (Todoroff and Vanbever, 2011, Geiser, 2010).

These mechanisms are only effective if the lung itself is healthy. Organs affected by asthma, COPD or other pulmonary issues most likely react differently. The pathophysiology of a diseased lung and the impact of this on drug deposition, dissolution and absorption need to be considered when developing formulations for respiratory delivery (Wang et al., 2014).

1.3 Inhaler Formulation

DPI formulations typically consist of coarse carrier material and fine particulate API. Due to their small surface area, the tiny drug particles in a DPI formulation experience substantial cohesive forces which leads to poor dispersion and flow properties (Telko and Hickey, 2005). Excipients, often α-lactose monodydrate, are added to the formulation to improve this. The small

drug particles adhere to the coarse carrier material which prevents the former from agglomerating. Furthermore, the mass added to the formulation has a positive effect on handling and facilitates the administration of small doses (Healy et al., 2014). Carrier materials, their bulk and particle properties and their impact on the finished product are an important factor in the development of formulations for respiratory drug delivery and DPIs (Guenette et al., 2009, Kaialy and Nokhodchi, 2012, Louey et al., 2001, Donovan and Smyth, 2010, Louey et al., 2004, De Boer et al., 2003, Bosquillon et al., 2001).

Coarse excipient particles, usually in the range of 50 to 100 μm, facilitate the delivery of respirable drug particles as they improve fluidisation, dispersion and disaggregation properties (Telko and Hickey, 2005, Cui et al., 2014, Hickey, 2003). Together with the micronised API, the excipient forms an interactive homogeneous mixture with the drug-to-carrier ratio depending on type of API, the DPI device, the objective of the treatment, the amount of drug needed to cause relief and other factors. The adhesive mixture is prepared by blending drug powder with carrier material, resulting in the fine particles sticking to the surface of the excipient. The total API surface available for inter-particle interaction thus decreases (Cui et al., 2014). Carrier and drug particles are dispersed by the flow shear and turbulent stress caused by inhalation and by inertial forces due to acceleration and deceleration during the inhalation process (Telko and Hickey, 2005, De Boer et al., 2006). To achieve optimal results, DPIs are designed to transfer kinetic energy into drag, inertial and frictional forces (De Boer et al., 2006). Due to size differences, only API particles can reach the target region within the lung (Heyder et al., 1986, Usmani et al., 2005) but the DPI formulation must be designed in a way to facilitate formulation, preparation and storage while also ensuring particle detachment upon inhalation. This means that the adhesive properties need to be strong enough to enable handling and low enough to not hinder dispersion (Cui et al., 2014). The required inter-particle forces can be governed by surface modification and size control (Donovan and Smyth, 2010, De Boer et al., 2005).

The most common excipient is lactose which is safe to use, chemically stable, widely available and compatible with a large number of APIs (Adi et al., 2007, Rowe et al., 2006). A small number of drugs tend to react in an undesired way with the carrier (Begat et al., 2009) and patients suffering from lactose intolerance may encounter problems which encouraged the search for alternatives such as mannitol (Karner et al., 2014, Kaialy and Nokhodchi, 2013), cyclodextrins (Cabral-Marques and Almeida, 2009) or erythritol (Jones et al., 2008). Yet lactose is still the most common excipient and the characteristics of lactose, lactose based formulations and the beneficial influence of fines (fine lactose particles) on the performance of DPI formulations have been studied widely (Tee et al., 2000, Shur et al., 2008, Young et al., 2007, Louey and Stewart, 2002, Pilcer et al., 2012).

Successful API delivery through DPI formulations is influenced by particle shape, size and size distribution, and also by surface morphology (De Boer et al., 2005, Neumann, 1967). Where excipients are included in the formulation, carrier particle size and texture also have to be considered. The forces acting both between drug particles and between drug and excipient particles are of high importance: they have to be strong enough to allow for easy formulation preparation and to prevent segregation during transport and storage (Cui et al., 2014). At the same time, they need to be low enough to ensure dispersion and disaggregation during inhalation (Cui et al., 2014), as only small particles and agglomerates (< 5 μm) can penetrate the deep lung and be therapeutically active (Cui et al., 2014, Zeng et al., 2000). The drug load itself also affects formulation performance along with the choice of inhaler device (De Boer et al., 2005) and the patient's individual breathing pattern (Heyder, 2004, Chrystyn and Price, 2009). The relationship between particulate characteristics and their respective effects on formulation performance have been studied and reviewed widely over the years (Adi et al., 2013, Chow et al., 2007, Zeng et al., 2000, Chan, 2008, Donovan and Smyth, 2010, Guenette et al., 2009, Healy et al., 2014, Zellnitz et al., 2014, Zhang et al., 2011).

The manufacturing process of API particles for respiratory delivery has a large impact on their properties and the performance of the finished product. Adhesive and cohesive characteristics and aerodynamic diameter, all key to the successful delivery of the drug into the deeper respiratory tract, can be manipulated in various ways during API production and processing.

1.4 Drugs for Pulmonary Delivery

Drugs for the treatment of asthma, COPD and other respiratory diseases counteract infection and inflammation, dilate the airways to ease constriction and lower the frequency of exacerbations (Powell and Gibson, 2003, Kirsten and Watz, 2014). They are divided into form groups: inhaled corticosteroids (ICS), long-acting muscarinic antagonists (LAMA) and long and short acting ß$_2$-agonists (LABA/SABA) (Kirsten and Watz, 2014, GINA, 2014). ICS have anti-inflammatory properties (Powell and Gibson, 2003, GINA, 2014). LAMA, LABA and SABA are bronchodilators, they facilitating breathing by dilating the airways (GINA, 2014). Depending on the nature of the disease, certain kinds or combinations of drugs may be better suited than others (Wang et al., 2014, Kirsten and Watz, 2014, Cazzola and Matera, 2006). New APIs for inhalation via DPI, (fixed) dual or even triple drug combinations (Cazzola and Matera, 2006, Tashkin and Ferguson, 2013, Wang et al., 2014, Van Noord et al., 2010, Huchon et al., 2009, Hanania et al., 2012) and carrier materials (Cabral-Marques and Almeida, 2009, Karner et al., 2014, Kaialy and Nokhodchi, 2013, Zellnitz et al., 2013) are continuously under investigation. As discussed by Tashkin et al.(Tashkin and Ferguson, 2013), muscarinic antagonist-ß$_2$-agonists (MABA) seem to be a promising approach. The author also refers to the development of dilating agents that relieve bronchoconstriction in a different way from hitherto known bronchodilators.

Only recently, the bronchodilators vilanterol (Kirsten and Watz, 2014) and olodaterol (Kirsten and Watz, 2014) as well as the combinations indacaterol/glycopyronium (Kirsten and Watz, 2014) and vilanterol/umeclidinium (Scott and Hair, 2014) have been approved for therapeutic use. It has to be noted, that so far no cure for COPD has been found (Tashkin et al., 2008). Not even the rate of mortality is lowered by the drugs currently on the market (Calverley et al., 2007). Currently, the main treatment objectives are to limit the risk of exacerbation, facilitate breathing and reduce the symptoms (Kirsten and Watz, 2014) as stated by the Global Initiative for Chronic Obstructive Lung Disease (GOLD) (Vestbo et al., 2013).

1.5 Beclomethasone Dipropionate: Structure of Anhydrate and Solvates

This study focuses on beclomethasone dipropionate (BDP, Figure 1-1), a glucocorticosteroid that acts as an anti-inflammatory drug, reducing irritation and swelling of the respiratory tract and suitable for long-term treatment. BDP and BDP based treatments have been improved over the years (Petersen et al., 2004, Huchon et al., 2009, Jentzsch et al., 2009, Kanniess et al., 2014). For respiratory drug delivery, BDP is used in either its anhydrous form (e.g. Beclazone, IVAX Pharmaceuticals/TEVA; Beclate, Cipla Pharmaceuticals) or as monohydrate (e.g. Beconase Hayfever, Chefaro Ireland Ltd.) (Bouhroum et al., 2010, Wang et al., 2007, Duax et al., 1981, Millard and Myrdal, 2002).

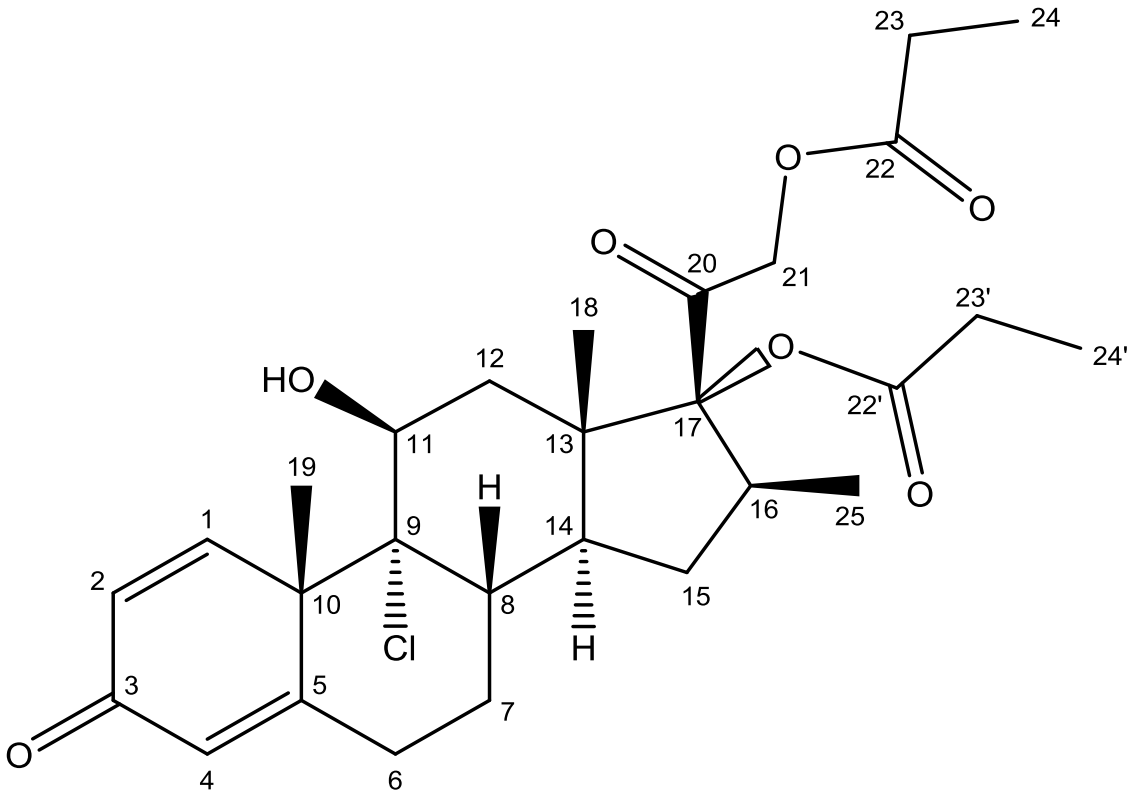

Figure 1-1. Molecular structure of beclomethasone dipropionate.

BDP has a relatively short biological half-life (Wood and Barnes, 1995). The rapid degradation and de-esterification of BDP into the active metabolite beclomethasone-17-monopropionate (17-BMP) due to hydrolysis (Othman et al., 2008) is mediated by esterase enzymes within the metabolism (Mutch et al, 2007, Roberts et al, 2013). Side products are propionic acid and beclomethasone-21-monopropionate (21-BMP) (Figure 1-2).

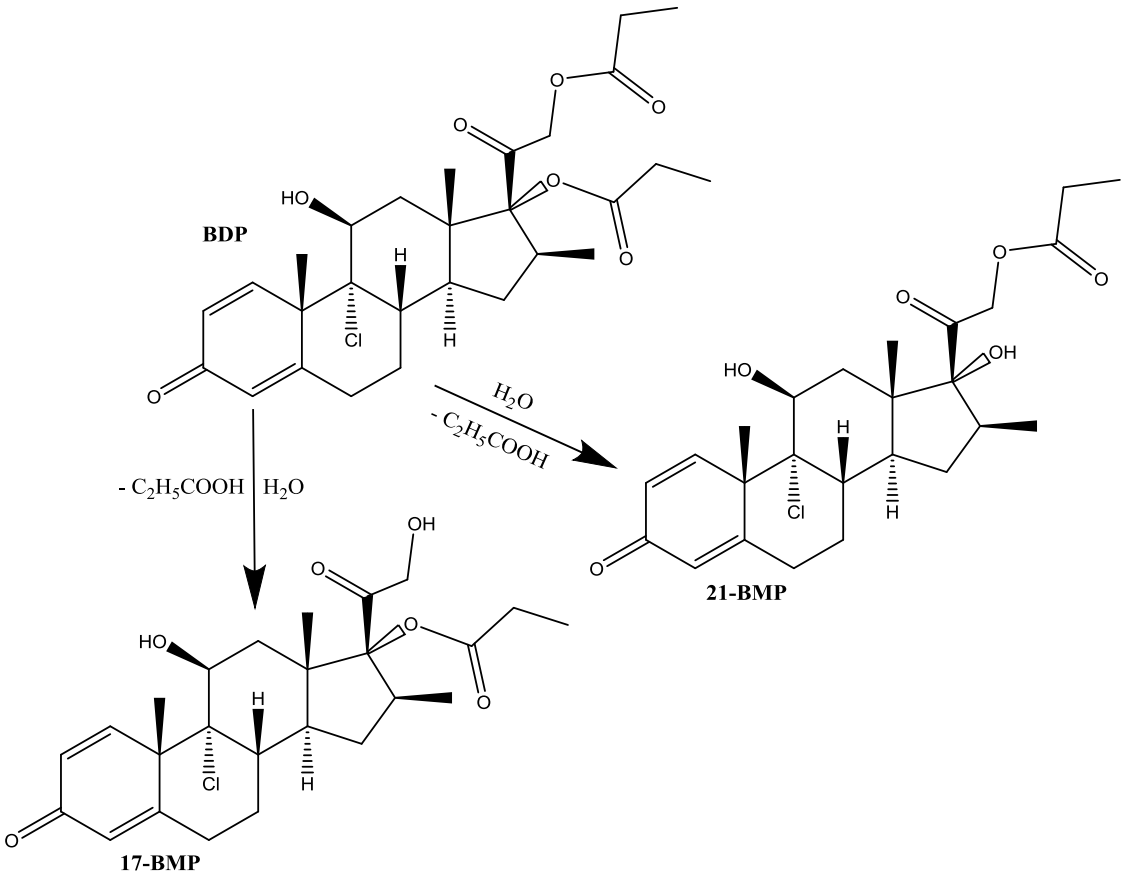

Figure 1-2. Hydrolysis of BDP into propionic acid and 17-BMP and 21-BMP, respectively (Othman et al, 2008).

BDP also undergoes oxygenation, mediated by cytochrome P450 (Mutch et al, 2007, Roberts et al, 2013). The active metabolite, however, is then further hydrolysed and metabolised by esterase into beclomethasone (BOH) and finally releases HCl in favour of an epoxy ring (Figure 1-3). Due to transesterification processes, the two intermediate products 17-BMP and 21-BMP can transform into each other. The release of HCl and hydrolysis of both, however, results in the same degradation compound 19β, 11β-epoxy-16β-methyl-1,4-pregnadiene-17, 21-diol-3,20-dione (Othman et al, 2008).

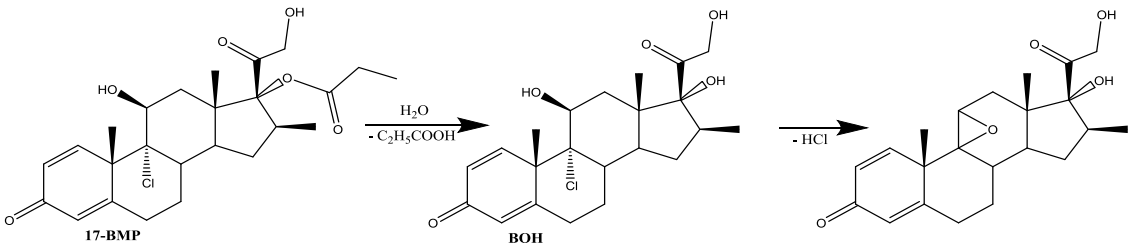

Figure 1-3. Hydrolysis of 17-BMP into BOH and HCl release in favour of epoxy ring formation (Othman et al, 2008).

In its anhydrous form, BDP forms stable crystals. The individual molecules are connected through hydrogen bridges between the hydroxyl group of one molecule and the carbonyl group of a second molecule. The crystalline material melts at 210 ºC (Sahib et al., 2012, Nachiengtung, 1997) and is commonly characterised by XRPD and FTIR (Nachiengtung, 1997, Wang et al., 2007).

The BDP monohydrate is known to be stable at standard conditions but dehydrates at about 120 ºC (Nachiengtung, 1997). XRPD and FTIR spectra allow the distinction between the BDP monohydrate and the anhydrate (Nachiengtung, 1997, Hunt and Padfield, 1989). The water molecules act as structural agents. Each water molecule forms hydrogen bonds to three functional groups on two BDP molecules, thus keeping the channel structure in place.

Apart from the BDP monohydrate, several solvated forms are known, with the BDP ethanol solvate being the most extensively studied one. The solvate was crystallised from direct precipitation (Jinks, 1989) and grown from a supersaturated solution at low temperature (Kuehl et al., 2003). A similar solvate was prepared from a suspension of BDP in ethanol and 1,1,1,2-tetrafluoroethane (HFA-134a) (Harris et al., 2003), resulting in a BDP-HFA-134-ethanol solvate from which the highly volatile HFA-134a evaporates immediately after preparation (Harris et al., 2003). The solvate is thought to have a channel structure. Intermolecular hydrogen bonds and chlorine-chlorine interactions maintain the channel structure in which solvent molecules such as ethanol (Kuehl et al., 2003) are retained. Hydrogen bonding between the BDP and the enclosed solvent molecules additionally helps to hold the structure in place (Bouhroum et al., 2010). Contradictory results were reported on the stability of BDP ethanol solvates (Bouhroum et al., 2010, Jinks, 1989). The carbonyl oxygen in the C_{22}' position of one BDP molecule forms a hydrogen bond to the alcohol group in the C_{11} position of a second BDP molecule. The carbonyl oxygen of the longer chain in the C_{22} position and the ester oxygen in the C_{20} position reach into the channels and are potentially available to interact with the solvent molecules (Harris et al., 2003). The BDP ethyl acetate solvate has a similar structure with the ethyl acetate being incorporated as highly mobile guest molecules inside the BDP clathrate (Othman et al., 2008).

Further alcohol based BDP solvates have been identified and the stability of their particle size was determined over six months at different conditions (Jinks, 1989). However, their particulate characteristics and their exact structure have not been investigated. Solvate formation was also observed from di-isopropylether (Page and Heggie, 1990) and short-chained alkanes (5 to 8 carbons) (Finckenor, 1980)

To date, the solvent dependent characteristics of BDP solvates, the details of solvate formation and the possible use of BDP solvates as precursors for anhydrous BDP for inhalation have not been investigated. While the influence of manufacturing and processing conditions on the physicochemical properties of the BDP monohydrate are known (Wang et al., 2007), similar studies have not yet been carried out with regard to BDP alcohol solvates.

1.6 Aims and Objectives

This study aimed at investigating the formation of BDP solvates from solution, their characteristics and their potential use as precursors for anhydrous BDP with well-defined physical properties.

Studying the contribution of the mobile alcohol molecules to the maintenance of the channel structure and the possible formation of weak intermolecular bonds between host and guest would add to the understanding of why certain solvates form and how they can be used in pharmaceutical applications such as respiratory drug delivery. Controlled crystal growth followed by controlled desolvation to anhydrous BDP may yield particles with well-known physicochemical characteristics. In contrast to random micronisation using, for example, ball milling or another high energy process, solvate desolvation would not result in high-energy surfaces and/or spontaneous recrystallisation of induced amorphous content which would negatively impact the performance of a DPI formulation.

In-depth knowledge of how solvent properties influence the characteristics of an API is of large benefit to the pharmaceutical industry and the patient. If it were possible to prepare crystalline API with preferred characteristics by using a particular solvent, it would also be possible to adjust these material characteristics in a way that improves the performance of a drug formulation. Knowledge of the impact of processing parameters including the use of solvents thus potentially offers a pathway to manufacture drug formulations that meet specific requirements. The development of analytical techniques to assess the relevant properties would also be of value for the pharmaceutical industry and chemical research in general. The formation of solvates is very common and having the tools to predict their formation, the interaction between solvent and host, the stability of the structure and the possible implications of desolvation would add to the understanding of solvated structures.

1.7 References

Adi, H., Larson, I. & Stewart, P. J. 2007. Adhesion and redistribution of salmeterol xinafoate particles in sugar-based mixtures for inhalation. *International journal of pharmaceutics,* 337**,** 229-238.

Adi, S., Adi, H., Chan, H.-K., Tong, Z., Yang, R. & Yu, A. 2013. Effects of mechanical impaction on aerosol performance of particles with different surface roughness. *Powder Technology,* 236**,** 164-170.

Begat, P., Morton, D. A., Shur, J., Kippax, P., Staniforth, J. N. & Price, R. 2009. The role of force control agents in high-dose dry powder inhaler formulations. *Journal of pharmaceutical sciences,* 98**,** 2770-2783.

Bell, J., Hartley, P. & Cox, J. 1971. Dry powder aerosols I: a new powder inhalation device. *Journal of pharmaceutical sciences,* 60**,** 1559-1564.

Bosquillon, C., Lombry, C., Preat, V. & Vanbever, R. 2001. Influence of formulation excipients and physical characteristics of inhalation dry powders on their aerosolization performance. *Journal of controlled release,* 70**,** 329-339.

Bouhroum, A., Burley, J. C., Champness, N. R., Toon, R. C., Jinks, P. A., Williams, P. M. & Roberts, C. J. 2010. An assessment of beclomethasone dipropionate clathrate formation in a model suspension metered dose inhaler. *International journal of pharmaceutics,* 391**,** 98-106.

Cabral-Marques, H. & Almeida, R. 2009. Optimisation of spray-drying process variables for dry powder inhalation (DPI) formulations of corticosteroid/cyclodextrin inclusion complexes. *European Journal of Pharmaceutics and Biopharmaceutics,* 73**,** 121-129.

Calverley, P. M., Anderson, J. A., Celli, B., Ferguson, G. T., Jenkins, C., Jones, P. W., Yates, J. C. & Vestbo, J. 2007. Salmeterol and fluticasone propionate and survival in chronic obstructive pulmonary disease. *New England Journal of Medicine,* 356**,** 775-789.

Cazzola, M. & Matera, M. G. 2006. The effective treatment of COPD: anticholinergics and what else? *Drug Discovery Today: Therapeutic Strategies,* 3**,** 277-286.

Chan, H.-K. 2008. What is the role of particle morphology in pharmaceutical powder aerosols? *Expert Opinion on Drug Delivery,* 5**,** 909-914.

Chougule, M. B., Padhi, B. K., Jinturkar, K. A. & Misra, A. 2007. Development of dry powder inhalers. *Recent Patents on drug delivery & formulation,* 1**,** 11-21.

Chow, A. H., Tong, H. H., Chattopadhyay, P. & Shekunov, B. Y. 2007. Particle engineering for pulmonary drug delivery. *Pharmaceutical research,* 24**,** 411-437.

Chrystyn, H. & Price, D. 2009. Not all asthma inhalers are the same: factors to consider when prescribing an inhaler. *Prim Care Respir J,* 18**,** 243-9.

Crampton, M., Kinnersley, R. & Ayres, J. 2004. Sub-micrometer particle production by pressurized metered dose inhalers. *Journal of aerosol medicine,* 17**,** 33-42.

Crowther Labiris, N., Holbrook, A. M., Chrystyn, H., Macleod, S. M. & Newhouse, M. T. 1999. Dry powder versus intravenous and nebulized gentamicin in cystic fibrosis and bronchiectasis: a pilot study. *American journal of respiratory and critical care medicine,* 160**,** 1711-1716.

Cui, Y., Schmalfuß, S., Zellnitz, S., Sommerfeld, M. & Urbanetz, N. 2014. Towards the optimisation and adaptation of dry powder inhalers. *International journal of pharmaceutics,* 470**,** 120-132.

De Boer, A., Dickhoff, B., Hagedoorn, P., Gjaltema, D., Goede, J., Lambregts, D. & Frijlink, H. 2005. A critical evaluation of the relevant parameters for drug redispersion from adhesive mixtures during inhalation. *International journal of pharmaceutics,* 294**,** 173-184.

De Boer, A., Hagedoorn, P., Gjaltema, D., Goede, J. & Frijlink, H. 2006. Air classifier technology (ACT) in dry powder inhalation: part 4. Performance of air classifier technology in the Novolizer® multi-dose dry powder inhaler. *International journal of pharmaceutics,* 310**,** 81-89.

De Boer, A., Hagedoorn, P., Gjaltema, D., Goede, J., Kussendrager, K. & Frijlink, H. 2003. Air classifier technology (ACT) in dry powder inhalation Part 2. The effect of lactose

carrier surface properties on the drug-to-carrier interaction in adhesive mixtures for inhalation. *International journal of pharmaceutics,* 260**,** 201-216.
Demoly, P., Hagedoorn, P., de Boer, A. H. & Frijlink, H. W. 2014. The clinical relevance of dry powder inhaler performance for drug delivery. *Respiratory Medicine,* 108**,** 1195-1203.
Donovan, M. J. & Smyth, H. D. 2010. Influence of size and surface roughness of large lactose carrier particles in dry powder inhaler formulations. *International journal of pharmaceutics,* 402**,** 1-9.
Duax, W. L., Cody, V. & Strong, P. D. 1981. Structure of the asthma drug beclomethasone dipropionate. *Acta Crystallographica Section B: Structural Crystallography and Crystal Chemistry,* 37**,** 383-387.
Fernández Tena, A. & Casan Clarà, P. 2012. Deposition of Inhaled Particles in the Lungs. *Archivos de Bronconeumología (English Edition),* 48**,** 240-246.
Finckenor, L. E. 1980. *Beclomethasone dipropionate-hexane solvate and aerosols prepared therefrom*. US Patent 4,225,597
Frijlink, H. & De Boer, A. 2004. Dry powder inhalers for pulmonary drug delivery. *Expert opinion on drug delivery,* 1**,** 67-86.
Geiser, M. 2010. Update on macrophage clearance of inhaled micro-and nanoparticles. *Journal of aerosol medicine and pulmonary drug delivery,* 23**,** 207-217.
Geller, D. E., Weers, J. & Heuerding, S. 2011. Development of an inhaled dry-powder formulation of tobramycin using PulmoSphere™ technology. *Journal of aerosol medicine and pulmonary drug delivery,* 24**,** 175-182.
GINA. 2014. *Pocket Guide for Asthma Management and Prevention* [Online]. GINA. Available: http://www.ginasthma.org/documents/1 [Accessed].
Groneberg, D. A., Peiser, C., Dinh, Q., Matthias, J., Eynott, P. R., Heppt, W., Carlstedt, I., Witt, C., Fischer, A. & Chung, K. F. 2003. Distribution of respiratory mucin proteins in human nasal mucosa. *The Laryngoscope,* 113**,** 520-524.
Guenette, E., Barrett, A., Kraus, D., Brody, R., Harding, L. & Magee, G. 2009. Understanding the effect of lactose particle size on the properties of DPI formulations using experimental design. *International journal of pharmaceutics,* 380**,** 80-88.
Hanania, N. A., Crater, G. D., Morris, A. N., Emmett, A. H., O'Dell, D. M. & Niewoehner, D. E. 2012. Benefits of adding fluticasone propionate/salmeterol to tiotropium in moderate to severe COPD. *Respiratory medicine,* 106**,** 91-101.
Harris, J. A., Carducci, M. D. & Myrdal, P. B. 2003. Beclomethasone dipropionate crystallized from HFA-134a and ethanol. *Acta Crystallographica Section E: Structure Reports Online,* 59**,** o1631-o1633.
Healy, A. M., Amaro, M. I., Paluch, K. J. & Tajber, L. 2014. Dry powders for oral inhalation free of lactose carrier particles. *Advanced drug delivery reviews*.
Heyder, J. 2004. Deposition of inhaled particles in the human respiratory tract and consequences for regional targeting in respiratory drug delivery. *Proceedings of the American Thoracic Society,* 1**,** 315-320.
Heyder, J., Gebhart, J., Rudolf, G., Schiller, C. F. & Stahlhofen, W. 1986. Deposition of particles in the human respiratory tract in the size range 0.005–15 μm. *Journal of Aerosol Science,* 17**,** 811-825.
Hickey, A. J. 2003. *Pharmaceutical inhalation aerosol technology,* CRC Press.
Hoppentocht, M., Hagedoorn, P., Frijlink, H. W. & de Boer, A. H. 2014. Technological and practical challenges of dry powder inhalers and formulations. *Adv Drug Deliv Rev,* 75**,** 18-31.
Huchon, G., Magnussen, H., Chuchalin, A., Dymek, L., Gonod, F. B. & Bousquet, J. 2009. Lung function and asthma control with beclomethasone and formoterol in a single inhaler. *Respiratory medicine,* 103**,** 41-49.
Hunt, J. H. & Padfield, J. M. 1989. *Micronised beclomethasone dipropionate monohydrate compositions and methods of use*. US Patent 4,866,051.

Jentzsch, N., Camargos, P., Colosimo, E. & Bousquet, J. 2009. Monitoring adherence to beclomethasone in asthmatic children and adolescents through four different methods. *Allergy,* 64**,** 1458-1462.

Jinks, P. A. 1989. *Physically modified beclomethasone dipropionate suitable for use in aerosols*. US Patent 4,810,488.

Jones, M. D., Harris, H., Hooton, J. C., Shur, J., King, G. S., Mathoulin, C. A., Nichol, K., Smith, T. L., Dawson, M. L. & Ferrie, A. R. 2008. An investigation into the relationship between carrier-based dry powder inhalation performance and formulation cohesive–adhesive force balances. *European Journal of Pharmaceutics and Biopharmaceutics,* 69**,** 496-507.

Kaialy, W. & Nokhodchi, A. 2012. Antisolvent crystallisation is a potential technique to prepare engineered lactose with promising aerosolisation properties: effect of saturation degree. *International journal of pharmaceutics,* 437**,** 57-69.

Kaialy, W. & Nokhodchi, A. 2013. Freeze-dried mannitol for superior pulmonary drug delivery via dry powder inhaler. *Pharmaceutical research,* 30**,** 458-477.

Kanniess, F., Scuri, M., Vezzoli, S., Francisco, C. & Petruzzelli, S. 2014. Extrafine beclomethasone/formoterol combination via a dry powder inhaler (NEXThaler< sup>®</sup>) or pMDI and beclomethasone monotherapy for maintenance of asthma control in adult patients: A randomised, double-blind trial. *Pulmonary pharmacology & therapeutics*.

Karner, S., Maier, M., Littringer, E. & Urbanetz, N. A. 2014. Surface roughness effects on the tribo-charging and mixing homogeneity of adhesive mixtures used in dry powder inhalers. *Powder Technology*.

Kirsten, A. & Watz, H. 2014. LABA, LAMA und Kombinationen. *Der Pneumologe,* 11**,** 127-134.

Kruber, H. 1981. *Hand-held atomizer especially for dispensing inhalation-administered medicaments*.

Kuehl, P. J., Carducci, M. D. & Myrdal, P. B. 2003. An ethanol solvate of Beclomethasone dipropionate. *Acta Crystallographica Section E: Structure Reports Online,* 59**,** 1888-1890.

Labiris, N. & Dolovich, M. 2003a. Pulmonary drug delivery. Part I: physiological factors affecting therapeutic effectiveness of aerosolized medications. *British journal of clinical pharmacology,* 56**,** 588-599.

Labiris, N. R. & Dolovich, M. B. 2003b. Pulmonary drug delivery. Part II: the role of inhalant delivery devices and drug formulations in therapeutic effectiveness of aerosolized medications. *British journal of clinical pharmacology,* 56**,** 600-612.

Lasmar, L., Camargos, P., Champs, N., Fonseca, M., Fontes, M., Ibiapina, C., Alvim, C. & Moura, J. 2009. Adherence rate to inhaled corticosteroids and their impact on asthma control. *Allergy,* 64**,** 784-789.

Louey, M. D., Mulvaney, P. & Stewart, P. J. 2001. Characterisation of adhesional properties of lactose carriers using atomic force microscopy. *Journal of Pharmaceutical and Biomedical analysis,* 25**,** 559-567.

Louey, M. D. & Stewart, P. J. 2002. Particle interactions involved in aerosol dispersion of ternary interactive mixtures. *Pharmaceutical research,* 19**,** 1524-1531.

Louey, M. D., Van Oort, M. & Hickey, A. J. 2004. Aerosol dispersion of respirable particles in narrow size distributions using drug-alone and lactose-blend formulations. *Pharmaceutical Research,* 21**,** 1207-1213.

McAffer, I. G. C., Tasko, P. E., Swift, G. J. & Giafrancesco, S. 2011. *Steroid Nebuliser Formulation*.

Millard, J. W. & Myrdal, P. B. 2002. Anhydrous beclomethasone dipropionate. *Acta Crystallographica Section E: Structure Reports Online,* 58**,** o712-o714.

Mutch, E., Nave, R., McCracken, N., Zech, K. & Williams, F. M. (2007). The Role of Esterases in the Metabolism of Ciclesonide to Desisobutyryl-Ciclesonide in Human Tissue. *Biochemical pharmacology*, 73, 1657-1664.

Nachiengtung, N. 1997. Solid-state characterization of beclomethasone dipropionate solvates and polymorphs. PhD Thesis, Purdue University, IN, USA.
Neumann, B. S. 1967. The flow properties of powders. *Advances in pharmaceutical sciences,* 2**,** 191-221.
Othman, A., Harris, R. K., Hodgkinson, P., Christopher, E. A. & Lancaster, R. W. 2008. Structural characterisation of two pharmaceutically important steroids by solid-state NMR. *New Journal of Chemistry,* 32**,** 1796-1806.
Page, P. R. & Heggie, W. 1990. *Preparation and use of new solvates of beclomethasone 17, 21-dipropionate*. US Patent 4,913,892.
Patton, J. S., Brain, J. D., Davies, L. A., Fiegel, J., Gumbleton, M., Kim, K.-J., Sakagami, M., Vanbever, R. & Ehrhardt, C. 2010. The particle has landed—characterizing the fate of inhaled pharmaceuticals. *Journal of aerosol medicine and pulmonary drug delivery,* 23**,** S-71-S-87.
Patton, J. S. & Byron, P. R. 2007. Inhaling medicines: delivering drugs to the body through the lungs. *Nature Reviews Drug Discovery,* 6**,** 67-74.
Petersen, R., Agertoft, L. & Pedersen, S. 2004. Treatment of exercise-induced asthma with beclomethasone dipropionate in children with asthma. *European Respiratory Journal,* 24**,** 932-937.
Pilcer, G., Wauthoz, N. & Amighi, K. 2012. Lactose characteristics and the generation of the aerosol. *Advanced drug delivery reviews,* 64**,** 233-256.
Powell, H. & Gibson, P. G. 2003. Inhaled corticosteroid doses in asthma: an evidence-based approach. *Medical journal of Australia,* 178**,** 223-225.
Roberts, J. K., Moore, C. D., Ward, R. M., Yost, G. S. & Reilly, C. A. 2013. Metabolism of Beclomethasone Dipropionate by Cytochrome P450 3a Enzymes. *Journal of Pharmacology and Experimental Therapeutics,* 345, 308-316.
Rogueda, P. G. & Traini, D. 2007. The nanoscale in pulmonary delivery. Part 1: deposition, fate, toxicology and effects.
Rowe, R. C., Sheskey, P. J., Owen, S. C. & Association, A. P. 2006. *Handbook of pharmaceutical excipients*, Pharmaceutical press London.
Sahib, M. N., Abdulameer, S. A., Darwis, Y., Peh, K. K. & Tan, Y. T. F. 2012. Solubilization of beclomethasone dipropionate in sterically stabilized phospholipid nanomicelles (SSMs): physicochemical and in vitro evaluations. *Drug design, development and therapy,* 6**,** 29.
Saritha, M., Rao, S. & Movva, B. 2013. Inhalers: Back to the Future. *International Journal of Current Trends in Pharmaceutical Research,* 1**,** 256-266.
Scott, L. J. & Hair, P. 2014. Umeclidinium/Vilanterol: First Global Approval. *Drugs,* 74**,** 389-395.
Shur, J., Harris, H., Jones, M. D., Kaerger, J. S. & Price, R. 2008. The role of fines in the modification of the fluidization and dispersion mechanism within dry powder inhaler formulations. *Pharmaceutical research,* 25**,** 1631-1640.
Sudhamani, T., Reddy, K. N., Kumar, V. R., Revathi, R. & Ganesan, V. 2010. Preparation and evaluation of ethyl cellulose microspheres of ibuprofen for sustained drug delivery. *Int J Pharm Res Dev,* 2**,** 119-125.
Sung, J. C., Pulliam, B. L. & Edwards, D. A. 2007. Nanoparticles for drug delivery to the lungs. *Trends in biotechnology,* 25**,** 563-570.
Tan, S. & Newton, J. 1990. Powder flowability as an indication of capsule filling performance. *International Journal of Pharmaceutics,* 61**,** 145-155.
Tashkin, D. P., Celli, B., Senn, S., Burkhart, D., Kesten, S., Menjoge, S. & Decramer, M. 2008. A 4-year trial of tiotropium in chronic obstructive pulmonary disease. *New England Journal of Medicine,* 359**,** 1543-1554.
Tashkin, D. P. & Ferguson, G. T. 2013. Combination bronchodilator therapy in the management of chronic obstructive pulmonary. *Respir Res,* 14**,** 49.
Tee, S., Marriott, C., Zeng, X. & Martin, G. 2000. The use of different sugars as fine and coarse carriers for aerosolised salbutamol sulphate. *International journal of pharmaceutics,* 208**,** 111-123.

Telko, M. J. & Hickey, A. J. 2005. Dry powder inhaler formulation. *Respiratory care,* 50**,** 1209-1227.

Todoroff, J. & Vanbever, R. 2011. Fate of nanomedicines in the lungs. *Current Opinion in Colloid & Interface Science,* 16**,** 246-254.

Usmani, O. S., Biddiscombe, M. F. & Barnes, P. J. 2005. Regional lung deposition and bronchodilator response as a function of β2-agonist particle size. *American journal of respiratory and critical care medicine,* 172**,** 1497-1504.

Van Noord, J., Aumann, J.-L., Janssens, E., Smeets, J., Zaagsma, J., Mueller, A. & Cornelissen, P. 2010. Combining tiotropium and salmeterol in COPD: effects on airflow obstruction and symptoms. *Respiratory medicine,* 104**,** 995-1004.

Vestbo, J., Hurd, S. S., Agusti, A. G., Jones, P. W., Vogelmeier, C., Anzueto, A., Barnes, P. J., Fabbri, L. M., Martinez, F. J. & Nishimura, M. 2013. Global strategy for the diagnosis, management, and prevention of chronic obstructive pulmonary disease: GOLD executive summary. *American journal of respiratory and critical care medicine,* 187**,** 347-365.

Wang, Y.-B., Watts, A. B., Peters, J. I. & Williams III, R. O. 2014. The impact of pulmonary diseases on the fate of inhaled medicines—A review. *International journal of pharmaceutics,* 461**,** 112-128.

Wang, Z., Chen, J.-F., Le, Y., Shen, Z.-G. & Yun, J. 2007. Preparation of ultrafine beclomethasone dipropionate drug powder by antisolvent precipitation. *Industrial & engineering chemistry research,* 46**,** 4839-4845.

Weibel, E. R. 1965. *Morphometry of the human lung,* Heidelberg, Germany, Springer.

Wood, A. J. & Barnes, P. J. 1995 Inhaled Glucocorticoids for Asthma. *New England Journal of Medicine,* 332, 868-875

Young, P. M., Chan, H. k., Chiou, H., Edge, S., Tee, T. H. & Traini, D. 2007. The influence of mechanical processing of dry powder inhaler carriers on drug aerosolization performance. *Journal of pharmaceutical sciences,* 96**,** 1331-1341.

Zellnitz, S., Redlinger-Pohn, J. D., Kappl, M., Schroettner, H. & Urbanetz, N. A. 2013. Preparation and characterization of physically modified glass beads used as model carriers in dry powder inhalers. *International journal of pharmaceutics,* 447**,** 132-138.

Zellnitz, S., Schroettner, H. & Urbanetz, N. A. 2014. Surface modified glass beads as model carriers in dry powder inhalers—Influence of drug load on the fine particle fraction. *Powder Technology,* 268**,** 377-386.

Zeng, X. M., Martin, G. P. & Marriott, C. 2000. *Particulate Interactions in Dry Powder Formulation for Inhalation,* Taylor & Francis.

Zhang, J., Wu, L., Chan, H.-K. & Watanabe, W. 2011. Formation, characterization, and fate of inhaled drug nanoparticles. *Advanced drug delivery reviews,* 63**,** 441-455.

Zhou, Q. T., Tang, P., Leung, S. S. Y., Chan, J. G. Y. & Chan, H.-K. 2014. Emerging inhalation aerosol devices and strategies: Where are we headed? *Advanced drug delivery reviews*.

CHAPTER 2

CHARACTERISATION OF ANHYDROUS BECLOMETHASONE DIPROPIONATE

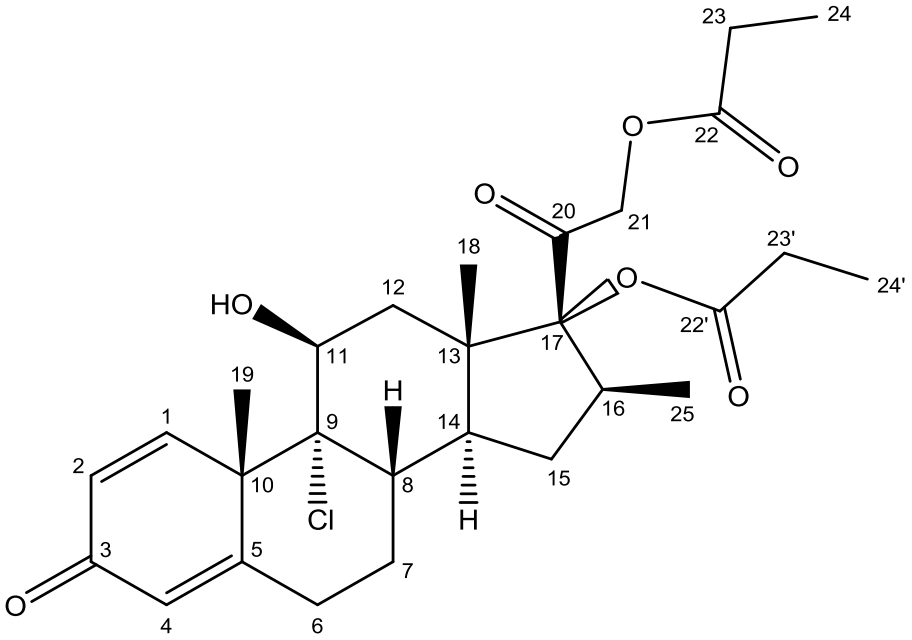

Figure 2. Molecular structure of BDP.

2 Characterisation of Anhydrous Beclomethasone Dipropionate

The anti-inflammatory agent beclomethasone dipropionate (BDP; IUPAC name: 2-[(8S,9R,10S,11S,13S,14S,16S,17R)-9-chloro-11-hydroxy-10,13,16-trimethyl-3-oxo-17-propanoyloxy-6,7,8,11,12,14,15,16-octahydrocyclopenta[a]phenanthren-17-yl]-2-oxoethyl] propanoate), has the chemical composition $C_{28}H_{37}ClO_7$ and is based on a steroid structure (Figure 2-1).

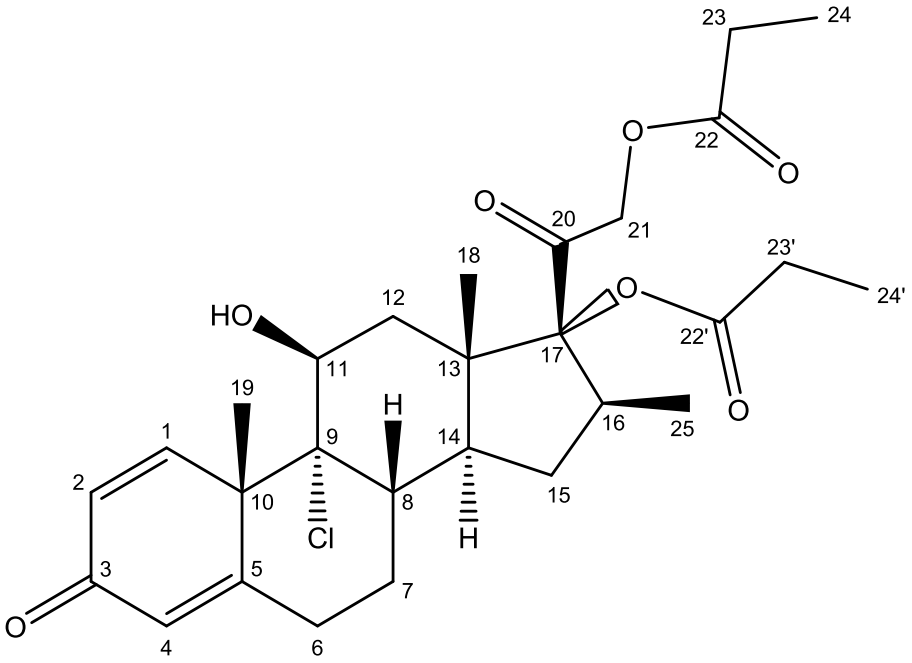

Figure 2-1. Molecular structure of BDP.

The structure of anhydrous BDP has been analysed using Fourier transform infrared (FTIR) spectroscopy (Sahib et al., 2012), X-ray powder diffraction (XRPD) (Nachiengtung, 1997, Wang et al., 2007, Ooi et al., 2014), single X-ray diffractometry (XRD) (Millard and Myrdal, 2002), solid state nuclear magnetic resonance (NMR) spectroscopy (Christopher, 1993) and partially analysed using solution state NMR in deuterated chloroform ($CDCl_3$) (Christopher, 1993, Othman et al., 2008, Foe et al., 1998). Thermogravimetric analysis (TGA) and differential scanning calorimetry (DSC) have been used to determine the thermal stability of the crystalline compound (Nachiengtung, 1997, Ooi et al., 2014). The specific surface area of anhydrous BDP has been analysed based on nitrogen sorption and a method has been developed to measure the particle size distribution (PSD) of particulate BDP (Ooi et al., 2014). Optical and scanning electron microscope (SEM) images of anhydrous BDP prepared in different ways have been published (Ooi et al., 2014, Wang et al., 2007) and were used for comparison.

Prior to any further experimental studies, the properties of anhydrous BDP as-received were confirmed and additional studies were carried out to obtain a thorough understanding of the

structural and physicochemical properties of anhydrous BDP. The results were used as references in further studies.

2.1 Materials and Methods

Anhydrous BDP was supplied by Intatrade Chemicals GmbH, Germany, and used as received.

2.1.1 Fourier Transform Infrared Spectroscopy

Fourier transform infrared (FTIR) spectroscopy uses infrared (IR) radiation to induce vibration within molecules. The IR spectrum covers wavelengths from 0.8-1000 µm which can be divided into near-IR (0.8-2.5 µm), mid-IR (2.5-50 µm) and far-IR (50-1000 µm). IR measurements are usually performed within the mid-IR range between 2.5-25 µm, or 400-4000 cm^{-1} on the wavenumber scale. Together with other structural analysis techniques such as NMR spectroscopy or XRD/XRPD, FTIR spectroscopy is commonly used to identify the structural composition of a molecule (Hesse and Meier, 2014, Schwedt, 1997).

The technique relies on IR light passing through a sample. The energy provided by electromagnetic radiation excites the atomic bonds within the molecules and facilitates transitions between energy levels. Yet in order to be FTIR active, the molecule's dipole moment also needs to change. Symmetric molecules such as the diatomic N_2 or O_2 are therefore not IR-active. IR-active molecules have a unique IR spectrum which shows the absorption of energy within the IR range as light absorption at certain wavenumbers, $\tilde{\upsilon}$. The shape, intensity and positon of each absorption signal is dependent on the molecular structure and the position of functional groups within the structure. The spectrum is a result of the energy needed to cause each atom to vibrate in one or more vibrational modes and is further influenced by the mass of the vibrating species and the respective intramolecular bonding strength. A number of vibrational modes have been identified: symmetric or antisymmetric stretching, scissoring, wagging, rocking and twisting. The degrees of vibrational modes of a molecule, also referred to as the vibrational degrees of freedom, are determined by the molecule's linearity and the number of atoms, N. Linear molecules have 3N-5 vibrational degrees of freedom while non-linear molecules are restricted to 3N-6 degrees of freedom.

Each vibrational mode of each functional group can be identified separately as a specific signal at a certain wavenumber in the IR spectrum. The combination of all signals allows the identification of the complete molecule. The fingerprint region below 800 cm^{-1} in particular contains unique information about the molecular structure.

FTIR spectroscopy was performed on a Varian 600 IR. 1.5-3 mg BDP was ground with 110-120 mg potassium bromide (KBr) and pressed into a disc. After measuring the background

(pure KBr disc, 64 scans), the IR spectra were recorded at 500-4000 cm^{-1} (64 scans). The resolution was set at 4 cm^{-1}.

2.1.2 X-ray Powder Diffraction

X-ray Powder Diffraction (XRPD), a powerful method to assess the crystallinity of a sample, to distinguish crystalline structures and to identify polymorphs (Borchardt-Ott, 2011), is based on the scattering of X-rays on a crystal lattice (Friedrich et al., 1912). As described by Bragg's law (Equation 2-1) the constructive interference of deflected X-rays gives a sample specific pattern of different intensities (Bragg and Bragg, 1949, Bragg and Bragg, 1913). The strongest intensities can be observed if the following condition is fulfilled.

$$2d\,sin\,\theta = n\lambda \tag{2-1}$$

This equation includes the distance between the crystal planes, *d*, the incident angle, θ, at which the X-ray is deflected, the wavelength, λ, and an integer, *n*, and shows that the path difference between the interfering scattered X-rays is an integer multiple of their wavelength. Crystalline structures consist of a neatly ordered long-range atomic lattice with defined spacing which is mirrored in characteristic XRPD patterns.

XRPD was carried out using a Stoe Stadi MP PowderXRD (STOE, Germany) in transmission mode (Cu Kα source) at 40 kV and 40 mA over a range of 5 - 40° 2θ rotating at a step size of 0.008° 2θ.

2.1.3 Dynamic Vapour Sorption

Dynamic vapour sorption (DVS) is used to analyse the relative weight change of a sample upon exposure to solvent vapour, generally water, over defined periods of time. The concentration of the surrounding water or solvent vapour is programmed to change gradually, either continuously or in a series of controlled steps under usually isothermal conditions while the relative or absolute weight change is recorded. Exposing a sample to controlled levels of humidity is a common technique to determine its hygroscopic properties and to assess the performance and stability of the material under defined conditions.

The samples were analysed at 25 °C using a SMS DVS Intrinsic 1 (Surface Measurement Systems, UK). After stabilisation at 20 % relative humidity (RH), the RH was increased in 10 % increments to 100 % before lowering the RH first to 50 % in 5 % steps, then to 20 % in 10 % steps. The equilibration times were set at 2 h per step. In a separate experiment, the RH was held constant at 100 % for 3 h.

2.1.4 Thermogravimetric Analysis

Thermogravimetric analysis (TGA) is a method to assess the weight change of a compound upon exposure to a defined temperature programme, usually either a temperature ramp or an isothermal hold. The resulting curve, showing the absolute or relative mass of the sample as a function of time or temperature, can be used to determine the melting point or degradation of the compound, kinetic stability and reaction enthalpies. In addition, oxidation, sublimation and evaporation processes can be observed and the data can serve as a basis for calculating moisture, solvent or filler contents (Haines, 2002, Schubnell, 2005).

The samples were analysed at a heating rate of 10 °C per minute up to 500 °C using a Q50 analyser (TA Instruments, UK).

2.1.5 Dynamic Scanning Calorimetry

Differential scanning calorimetry (DSC) uses thermal effects in a material to characterise its physicochemical properties. The technique can be applied to identify materials based on their specific behaviour such as transition, polymerisation and melting. In pharmaceutical applications, DSC is often used to assess the purity of an API, to learn about its degree of crystallinity and to investigate the stability of the compound (Höhne et al., 2013). DSC is especially useful in combination with TGA. Comparing corresponding temperature profiles enables the distinction of desolvation processes from phase transitions and melting.

In a common DSC experiment, the heat flow through a sample within a (sealed) pan is measured in comparison to an empty reference pan while applying a defined heating programme. The difference is shown as an endothermic (heat consumption) or exothermic (heat production) signal with characteristic enthalpies (ΔH). In the most basic setup, the sample is monitored while increasing the temperature at a constant heating rate. Thermal events are recorded as either a positive or a negative difference to the reference sample. To assess the reversibility of events and to investigate the stability of a compound, several heating and cooling cycles can be run consecutively.

Sample preparation is crucial in DSC as the sample mass and the choice of pan and lid affect the results. Hermetically sealed pans are useful to assess material characteristics such as melting point and phase transition. Dehydration and desolvation, however, would not be visible on the thermogram as the vapour is kept within the pan. DSC curves obtained from open pans, in contrast, would indicate the loss of loosely bound solvent as a flat endothermic signal while the sudden release of neatly incorporated solvent would show as a sharp peak. The use of open pans, however, may cause the contamination of the DSC heating chamber due to sample degradation and overflowing pans. To prevent this, pin holed pans are commonly used. This complicates

interpretation since the size, position and number of pin holes significantly affects the shape and onset of desolvation peaks (Höhne et al., 2013).

3-5 mg of BDP was filled into Tzero Hermetic pans (TA Instruments, UK). The pans were sealed and a paper clip was used to make three pin holes into the lid to prevent bursting. The DSC scans were carried out on a Q2000 calorimeter (TA Instruments, UK) with the nitrogen feed set to 50 mL/min. The calorimeter was calibrated using the indium calibration standard supplied by TA Instruments. After equilibration at -10 °C, the samples heated at a rate of 10 °C/min to 220 °C.

2.1.6 Gas Sorption

Gas sorption is based on the gradual ad- and desorption of an inert gas such as krypton, helium or nitrogen onto and from the sample surface under varying pressure within a closed system at 77 K (Storey and Ymen, 2011). This results in two isotherms (adsorption and desorption, often showing a hysteresis) based on which the presence and shape of pores can be predicted and which are used to calculate the specific surface area of a sample (Brunauer et al., 1938), to evaluate the affinity between adsorbent and adsorbate (Brunauer et al., 1938) and, in the case of a porous sample, to determine the pore size distribution (Barrett et al., 1951). While increasing the pressure relative to the saturated vapour pressure of the gas, the gas molecules adsorb onto the adsorbent at the gas/solid interface in a monolayer. Increasing the relative pressure usually leads to the formation of multiple layers. The quantity of adsorbate covering the adsorbent in a monolayer is used to calculate the specific surface area of the sample according to Brunauer, Emmet, Teller (Brunauer et al., 1938) who are the name patrons of the BET equation (Equation 2-2).

$$\frac{V}{V_m} = \frac{C\frac{p}{p_0}}{\left(1-\frac{p}{p_0}\right)\left(1+C-\frac{p}{p_0}\right)} \tag{2-2}$$

This calculation includes the volume of adsorbate in adsorbed state, V, the volume of adsorbate adsorbed in a monolayer, V_m, the C factor (BET constant), C, and the pressure relative to the vapour pressure of nitrogen, $^{p}/_{p_0}$. The C factor, depending on the enthalpy of adsorption and the enthalpy of condensation is related to the affinity between adsorbate and adsorbent and therefore a useful value to compare the surface energetics of adsorbents.

The specific surface area is calculated from the linear range of the isotherm at relative pressures between 0.05 and 0.3 and takes size and molar volume of the adsorbate and the mass of the adsorbent into account. Despite the theoretical assumption of an energetically homogeneous surface it has to be acknowledged that the occupation of free sites is controlled by the presence of high and low energy areas on the adsorbent. It has been found that the optimal balance

between the completion of a monolayer and the development of further layers falls within the above mentioned range where all high energy sites seem to be occupied (Lowell et al., 2012).

Nitrogen sorption was used to investigate the as-received BDP. The measurements were performed on a Gemini VI 2385C (Micromeritics) at 77 K. 500 mg BDP was degassed under nitrogen at 50 °C for 24 h prior to measurement. The sample was evaporated at 25.0 mmHg/min at an evaporation time of 0.5 min.

2.1.7 Particle Size Analysis

The particle size distribution (PSD) is generally determined using laser diffraction (LD) or dynamic light scattering (DLS). BDP does not readily disperse or dissolve in water but is soluble in most common solvents and the particle diameter exceeded the maximum size suitable for DLS (max. 3 µm). Dry powder LD was therefore used to analyse the PSD of as-received BDP. Particle size analysis through LD is based on the assumption of ideally spherical particles. The calculation of the PSD is less accurate when irregular shaped particles or particles with high aspect ratios are analysed. In such cases, the results give a good estimation of the true PSD but should be complemented by the optical counting methods or visually where possible.

The PSD was determined on a Mastersizer 2000 laser diffraction particle size analyser (Malvern Instruments, UK). Prior to analysis, the powder samples were mixed with a spatula and shaken on a Vortex Mixer (Vortex Genie2) to break up loose agglomerates. The dry powder compartment (Scirocco 2000 Dry Powder Feeder, Malvern Instruments UK), equipped with a micro volume dry sample tray, was filled with about 1 mg. The powder was dispersed at an air pressure of 3 mbar and 50 – 100 % vibration to reach an obscuration of at least 3 %. The refractive index was set at 1.564 (Ooi et al., 2014). Sand was used to clean the sample compartment between measurements.

2.1.8 Scanning Electron Microscopy

The shape and average size of the particles was further examined under the scanning electron microscope (SEM) This technique relies on a focussed electron beam scanning across the sample. The interaction of the atoms on the surface and the top layers of the sample leads to the emission of secondary electrons, the generation of backscattered electrons and X-rays. Depending on the sample material, its density and the accelerating voltage the electron beam can penetrate the first top layers up to a depth of a few µm.

SEM images of anhydrous BDP were obtained in vacuum using a Hitachi S-2460N equipped with a secondary electron detector. The accelerating voltage was set to 22 kV. To prevent charging, the samples were gold-coated with an Emitech sputter coater prior to imaging.

2.1.9 Atomic Force Microscopy

AFM is an advanced technique for surface characterisation studies (Wu et al., 2010) which relies on the physical interaction between a probe and the surface of a substrate fixed onto a motorised stage (Figure 2-2). The probe consists of a sharp tip at the free end of a cantilever attached to a chip. The most common materials are silicon (Si) and silicon nitride (Si_3N_4). Piezoelectric elements, either included in the scan head or the AFM stage, ensure precise motion in the nanoscale. As the probe scans across the sample surface, a laser beam is directed onto the cantilever surface and reflected back onto a four-quadrant photodiode. Upon meeting a resistance on the scanned surface the cantilever twists and bends, causing the beam to reflect at different angles. These deflections are recorded through the four-quadrant photodiode and analysed by the feedback controller. The signal is used to adjust the stage height to control the force exerted by the probe onto the sample, to maintain a certain distance between tip and specimen surface and to reconstruct an image of the surface topography from the corrective factors or error signals (Eaton and West, 2010). Such three-dimensional height images, which can reach resolutions within the atomic range (Giessibl, 2005, Binnig et al., 1987, Gan, 2009), can be evaluated quantitatively (Lamprou and Smith, 2014, Eaton and West, 2010).

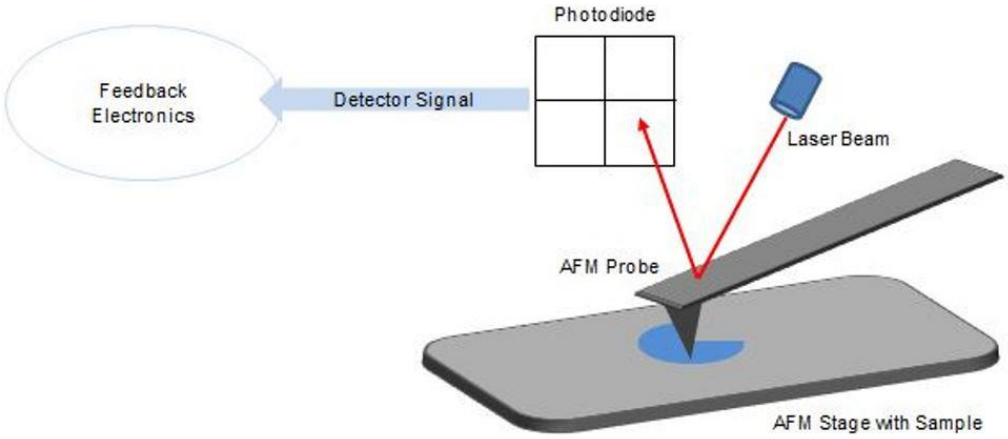

Figure 2-2. Schematic overview of AFM measurements (Weiss et al., 2015).

The sample is scanned by an AFM probe onto which a laser beam is directed and reflected onto a four-quadrant photodiode. The signal from the photodiode is then evaluated by the feedback controller. Piezoelectric elements are included in the scan head or the AFM stage to ensure precise motion in the nanoscale.

Data can be generated using a number of different AFM modes. The preferred modes for the acquisition of height maps are contact, non-contact and intermittent contact mode but AFM also offers a number of more specific modes of operation, such as force spectroscopy and mechanical property mapping; electric, lateral and magnetic force spectroscopy; tunnelling atomic force microscopy, Kelvin probe force microscopy and more (Eaton and West, 2010).

To image anhydrous BDP, AFM measurements were performed on a Bruker Dimension Icon ScanAsyst AFM using Bruker equipment inside a glovebox where the water and oxygen levels were below 0.1 ppm each. Each AFM probe was calibrated before starting the measurement. The spring constant was determined using the thermal tuning option provided by the software (NanoScope, Bruker) and the average deflection sensitivity was calculated from three force curves (sapphire substrate, ramp size 500 nm, ramp rate to 0.5 Hz, trig threshold to 0.5 V).

The anhydrous BDP was glued onto a silicon wafer (Wacker Chemie AG) with Tempfix mounting adhesive (Agar Scientific, UK) and the surface was scanned in soft-tapping mode using a ScanAsyst Air probe (0.4 N/m, 70 kHz) (Bruker Nano, CA, USA).

2.2 Results

2.2.1 Fourier Transform Infrared Spectroscopy

As outlined in the European Pharmacopoeia (Ph. Eur. 5.0, 1055), FTIR is one of two techniques to identify BDP. The FTIR spectrum of anhydrous BDP as-received (Figure 2-3) shows a broad peak at 3275 cm^{-1} caused by the hydroxyl group in the C_{11} position (Figure 2-1). The sharp bands at 1755 cm^{-1}, 1730 cm^{-1}, 1659 cm^{-1} and 1614 cm^{-1}, characteristic of the stretching of the ester carbonyl group of the propionate branches (1755 cm^{-1}), the non-conjugated and the conjugated carbonyl groups (1730 cm^{-1}, 1659 cm^{-1}) and the carbon-carbon double bonds (1614 cm^{-1}) (Sahib et al., 2012) (Nachiengtung, 1997).

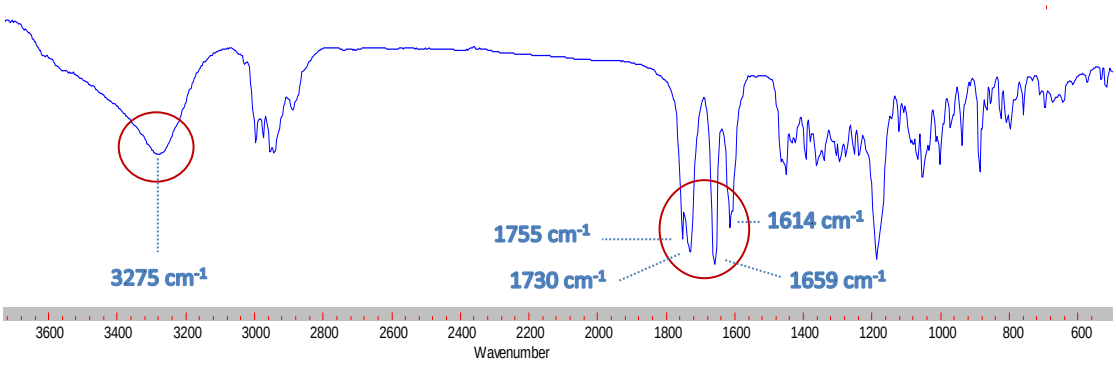

Figure 2-3. FTIR of anhydrous BDP as-received with characteristic signals (marked) at 1755 cm^{-1}, 1730 cm^{-1}, 1659 cm^{-1} and 1614 cm^{-1} and a broad band at 3275 cm^{-1} (Sahib et al., 2012).

2.2.2 X-ray Powder Diffraction

The XRPD analysis of anhydrous BDP as-received was well resolved (Figure 2-4) and the signals characteristic of anhydrous BDP (Nachiengtung, 1997, Wang et al., 2007) were identified at the expected positions (Table 2-1).

Table 2-1. XRPD signals at 2Θ and relative intensities (I/I_{100}) of anhydrous BDP as-received.

2θ	I/I_{100}	2θ	I/I_{100}	2θ	I/I_{100}
9.32	26	14.45	54	16.97	20
9.50	72	14.54	47	18.41	49
9.59	100	14.81	54	18.50	45
9.68	64	14.90	56	20.12	23
11.30	57	15.53	57	22.82	24
11.39	47	15.62	50		

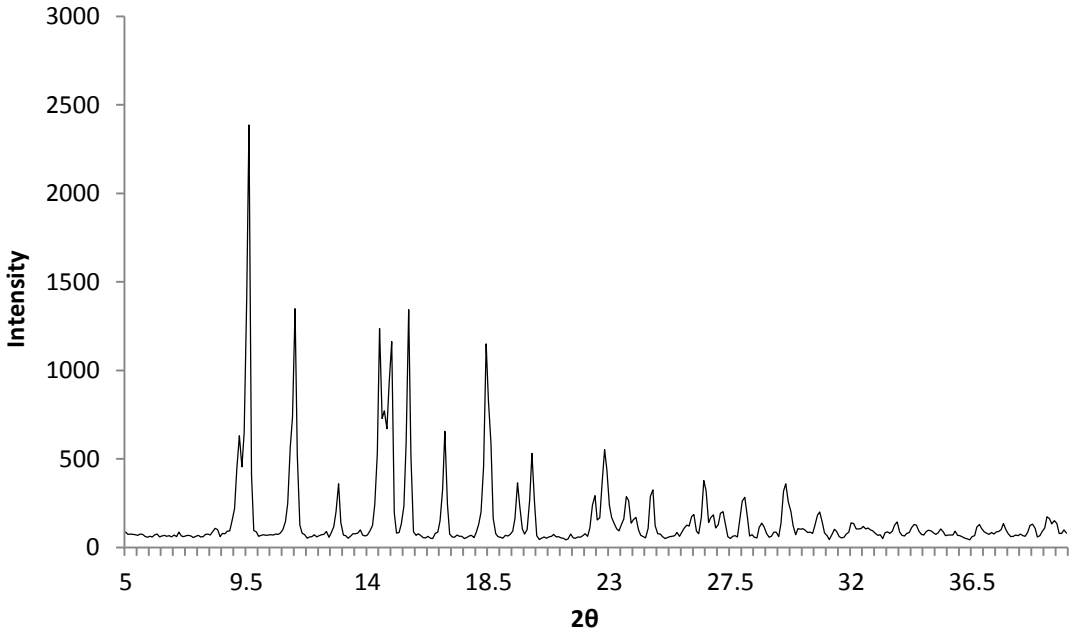

Figure 2-4. XRPD signals of anhydrous BDP as-received.

2.2.3 Dynamic Vapour Sorption

DVS was carried out to investigate the hygroscopicity of BDP and the material's behaviour at high levels of humidity.

The mass increase immediately in response to the increasing humidity up to 90 % RH (Figure 2-5). At higher levels of humidity, the sample mass rose significantly. This behaviour was mirrored when lowering the RH where the mass dropped drastically until reaching 90 % RH and synchronising with stepwise decrease of humidity. The initial and final masses corresponded to each other and only a narrow hysteresis was visible between adsorption and desorption isotherms during the experiment (Figure 2-6). This suggested that the as-received anhydrous BDP was in its crystalline state and that no phase transitions were caused in such conditions.

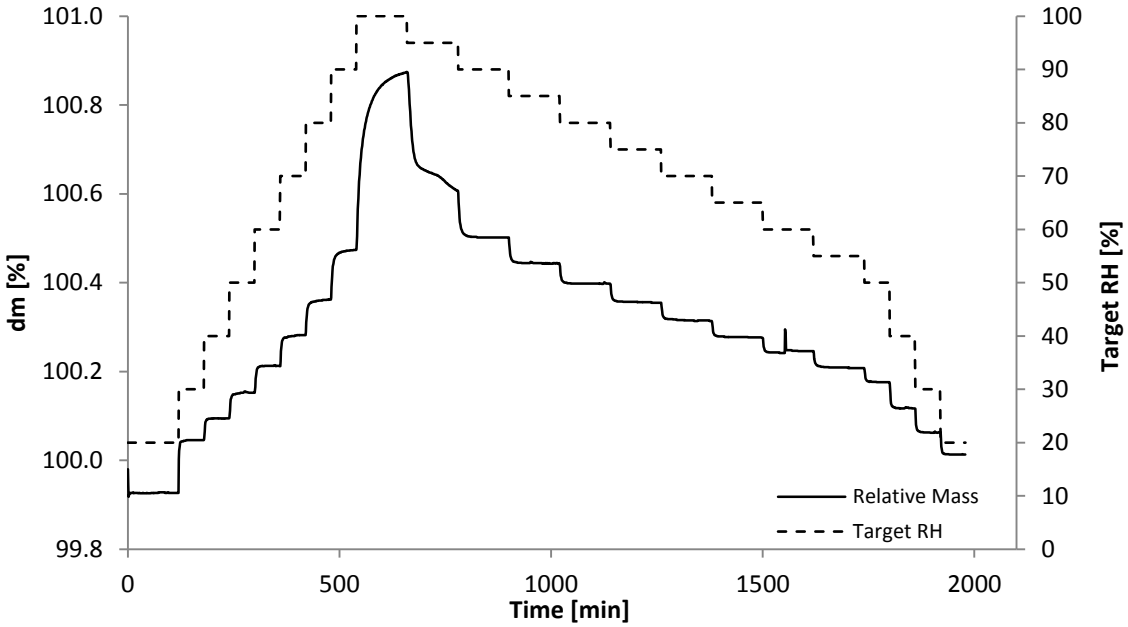

Figure 2-5. DVS (H_2O) at 25 °C showing the relative mass change of anhydrous BDP as a function of time and changing relative humidity (RH).

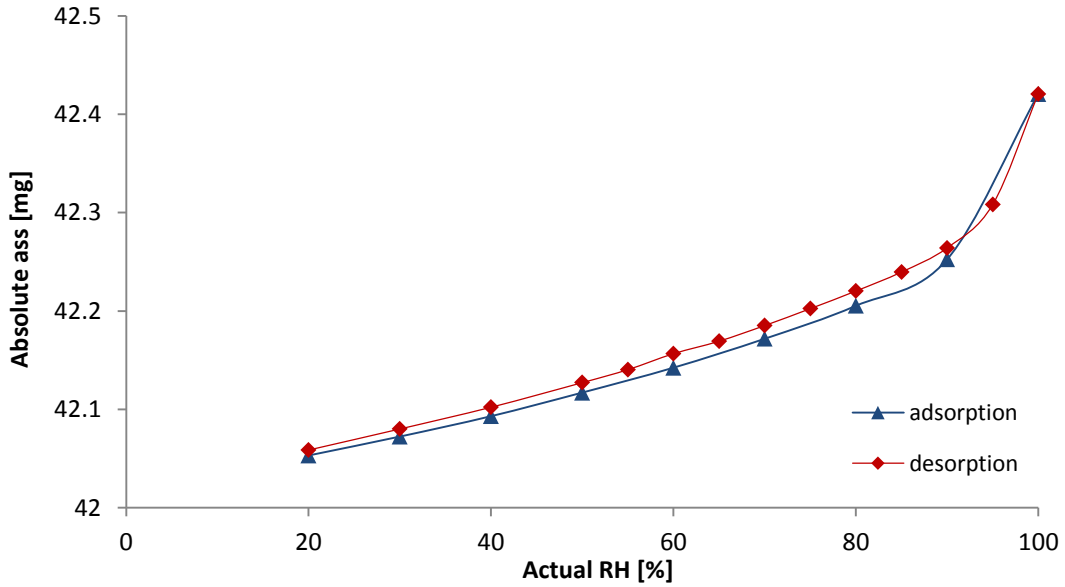

Figure 2-6. DVS (H_2O) at 25 °C, absolute mass of anhydrous BDP as a function of relative humidity (absorption vs. desorption).

2.2.4 Thermal Analysis

DSC analysis (Figure 2-7), used to evaluate the thermal behaviour of anhydrous BDP, showed a sharp endothermic signal at an onset temperature of 209 °C (extrapolated onset temperature of 212.77 ± 0.18 °C and an enthalpy of 75.64 ± 31.62 Jg^{-1} (n = 4). At the same temperature, the weight of BDP started decreasing (seen in the slope of the first derivative, Figure 2-7) and it

dropped significantly from approx. 219 °C. This is characteristic of anhydrous BDP which melts at around 210 °C (Ph. Eur. 5.0, 1055) and subsequently degrades (Nachiengtung, 1997).

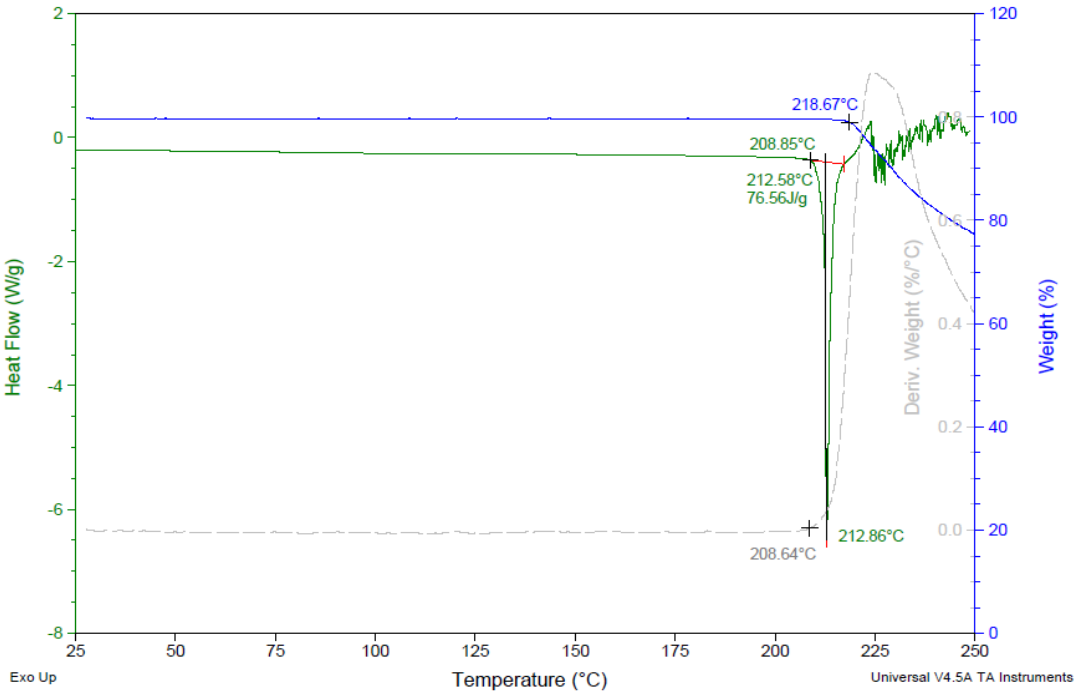

Figure 2-7. Thermal analysis (DSC, green, and TGA, blue: weight change, silver: first derivative) of anhydrous BDP. Melting at 212.58 °C (extrapolated onset temperature) followed by degradation. Exo up.

Anhydrous BDP was kept at 100 % RH for 3 h to evaluate the material's hygroscopic properties. The mass increase caused by adsorbed water amounted to only 0.86 % of the initial samples mass which was indicative of the hydrophobic properties of anhydrous BDP. The sample was then immediately analysed using DSC which showed a broad endothermic signal below 100 ºC characteristic of the evaporation of surface moisture with an extrapolated onset temperature close to room temperature (Figure 2-8). Melting started at 210.16 °C.

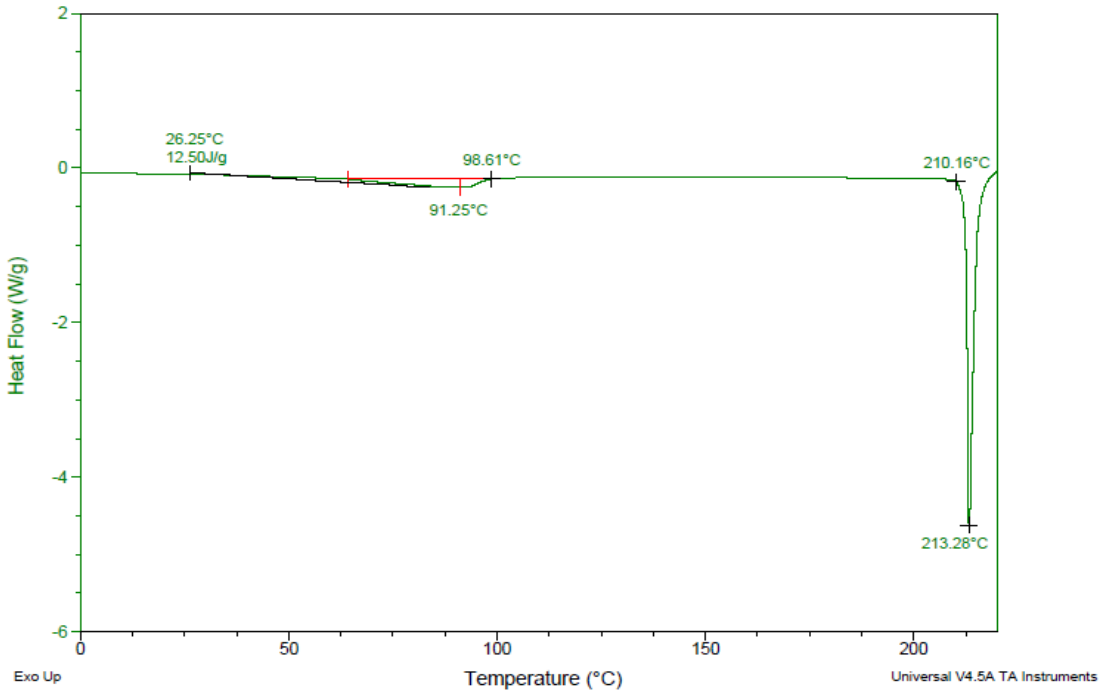

Figure 2-8. DSC of anhydrous BDP after 3 h at 100 % RH. Broad endothermic signal indicating evaporation of surface moisture below 100 °C and melting at 210.16 °C (extrapolated onset temperature). Exo up.

2.2.5 Gas Sorption and Particle Size Analysis

The BET specific surface area was 2.22 ± 0.04 m^2g^{-1}, the C factor was 35.22 ± 0.41 (n = 3).

Dry particle size analysis showed a broad particle size distribution (PSD) (Table 2-2) and a calculated BET surface area of 1.15 ± 0.02 m^2/g (n = 3).

Table 2-2. PSD (percentile values d_{10}, d_{50}, d_{90}) of anhydrous BDP as-received (n = 3).

d_{10} [µm ± StDev]	d_{50} [µm ± StDev]	d_{90} [µm ± StDev]
2.13 ± 0.02	10.39 ± 0.32	60.89 ± 3.82

2.2.6 Scanning Electron and Atomic Force Microscopy

The anhydrous BDP sample appeared to consist of characteristically irregularly shaped particles (Nachiengtung, 1997) under the SEM (Figure 2-9a) with an uneven surface as shown under the AFM (Figure 2-9b).

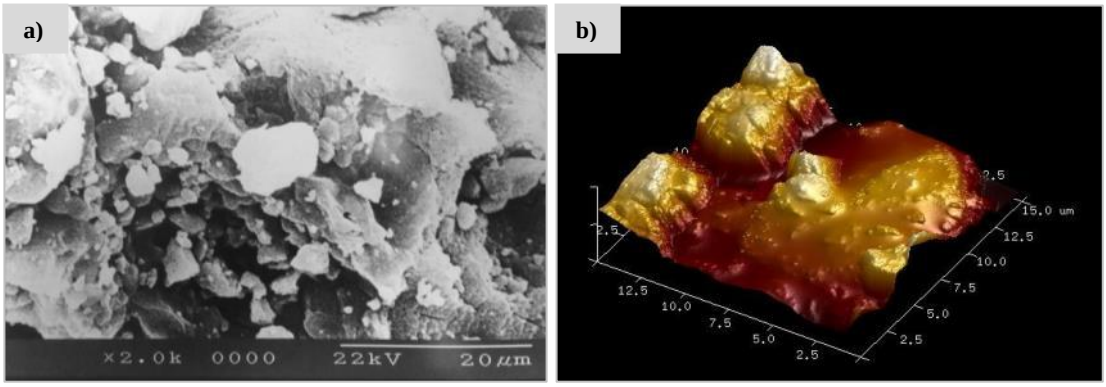

Figure 2-9. Anhydrous BDP as-received under the a) SEM (x 2,000) and b) AFM, scale given on image.

2.3 Discussion

FTIR and XRPD matched reported results (Sahib et al., 2012, Nachiengtung, 1997, Wang et al., 2007, Ooi et al., 2014), thus confirming the crystalline structure. The material showed the thermal behaviour characteristic of anhydrous BDP (Nachiengtung, 1997, Ooi et al., 2014) and, as expected, did not transform into the monohydrate when exposed to high levels of humidity (Nachiengtung, 1997). Moisture appeared to condense on the particle surface at humidity levels exceeding 90 %. This suggested the presence of pores or a high surface roughness with indentations where water could condense and accumulate. Pores would have led to a noticeable hysteresis between the sorption isotherms which was not the case (Figure 2-6). The low specific surface area of 2.22 ± 0.04 m^2/g further confirmed the lack of pores.

AFM topographical mapping indicated an uneven particle surface (Figure 2-9b) with irregular protrusions and indentations. The particles appeared to be of irregular shape which is characteristic of anhydrous BDP (Nachiengtung, 1997). Considerable size differences were visible (Figure 2-9a) which was reflected in the broad PSD (d_{90} = 60.89 ± 3.82 µm).

2.4 Conclusions

Anhydrous BDP as received was analysed and the results, matching reported data, served as basis for further experimental work. The particle size exceeded the size range recommended for respiratory drug delivery and milling or similar high-energy processes would be necessary to reduce the PSD of the as-received anhydrous BDP. However, such processes potentially lead to surface defects and the generation of amorphous content which in turn could affect the stability and performance of a DPI formulation, mainly due to spontaneous recrystallisation. An alternative processing method that excludes the need to use high-energy micronisation would be beneficial for the preparation of DPI formulation.

In this study, the use of BDP solvates as precursors for anhydrous BDP was investigated. BDP were crystallised from solution and characterised using the methods outlined in Chapter 2 unless otherwise stated.

2.5 References

Barrett, E. P., Joyner, L. G. & Halenda, P. P. 1951. The determination of pore volume and area distributions in porous substances. I. Computations from nitrogen isotherms. *Journal of the American Chemical society,* 73**,** 373-380.

Binnig, G., Gerber, C., Stoll, E., Albrecht, T. & Quate, C. 1987. Atomic resolution with atomic force microscope. *EPL (Europhysics Letters),* 3**,** 1281.

Borchardt-Ott, W. 2011. *Crystallography: an introduction*, Springer Science & Business Media.

Bragg, L. & Bragg, W. H. 1949. *The crystalline state: a general survey*, Bell.

Bragg, W. H. & Bragg, W. L. 1913. The reflection of X-rays by crystals. *Proceedings of the Royal Society of London. Series A, Containing Papers of a Mathematical and Physical Character,* 88**,** 428-438.

Brunauer, S., Emmett, P. H. & Teller, E. 1938. Adsorption of gases in multimolecular layers. *Journal of the American Chemical Society,* 60**,** 309-319.

Christopher, E. A. 1993. *Solid-state NMR study of polymorphism in pharmaceuticals.* Durham University.

Eaton, P. J. & West, P. 2010. *Atomic force microscopy*, Oxford University Press Oxford.

Foe, K., Cheung, H. A., Tattam, B. N., Brown, K. F. & Seale, J. P. 1998. Degradation products of beclomethasone dipropionate in human plasma. *Drug metabolism and disposition,* 26**,** 132-137.

Friedrich, W., Knipping, P. & Laue, M. 1912. Interferenz-Erscheinungen bei Röntgenstrahlen Sitzungsber. *Kgl. Bayer: Akad. Wiss*, 303.

Gan, Y. 2009. Atomic and subnanometer resolution in ambient conditions by atomic force microscopy. *Surface Science Reports,* 64**,** 99-121.

Giessibl, F. J. 2005. AFM's path to atomic resolution. *Materials Today,* 8**,** 32-41.

Haines, P. J. 2002. *Principles of thermal analysis and calorimetry*, Royal society of chemistry.

Hesse, M. & Meier, H. 2014. *Spektroskopische Methoden in der organischen Chemie, 8. überarb. Auflage 2011*, Georg Thieme Verlag.

Höhne, G., Hemminger, W. F. & Flammersheim, H.-J. 2013. *Differential scanning calorimetry*, Springer Science & Business Media.

Lamprou, D. & Smith, J. R. 2014. Applications of AFM in pharmaceutical sciences. *In:* Rades, T., Mullertz, A., Perrie, Y. (ed.) *Analytical techniques in pharmaceutical sciences.* Springer.

Lowell, S., Shields, J. E., Thomas, M. A. & Thommes, M. 2012. *Characterization of porous solids and powders: surface area, pore size and density*, Springer Science & Business Media.

Millard, J. W. & Myrdal, P. B. 2002. Anhydrous beclomethasone dipropionate. *Acta Crystallographica Section E: Structure Reports Online,* 58**,** o712-o714.

Nachiengtung, N. 1997. Solid-state characterization of beclomethasone dipropionate solvates and polymorphs. PhD Thesis, Purdue University, IN, USA.

Ooi, J., Gaisford, S., Boyd, B. J., Young, P. M. & Traini, D. 2014. Isothermal calorimetry: A predictive tool to model drug-propellant interactions in pressurized metered dose systems. *International journal of pharmaceutics,* 461**,** 301-309.

Othman, A., Harris, R. K., Hodgkinson, P., Christopher, E. A. & Lancaster, R. W. 2008. Structural characterisation of two pharmaceutically important steroids by solid-state NMR. *New Journal of Chemistry,* 32**,** 1796-1806.

Sahib, M. N., Abdulameer, S. A., Darwis, Y., Peh, K. K. & Tan, Y. T. F. 2012. Solubilization of beclomethasone dipropionate in sterically stabilized phospholipid nanomicelles (SSMs): physicochemical and in vitro evaluations. *Drug design, development and therapy,* 6**,** 29.

Schubnell, M. 2005. Methodenentwicklung in der thermischen Analyse. UserCom.

Schwedt, G. 1997. *The essential guide to analytical chemistry*, John Wiley & Sons Inc.

Storey, R. A. & Ymen, I. 2011. *Solid state characterization of pharmaceuticals*, Wiley Online Library.

Wang, Z., Chen, J.-F., Le, Y., Shen, Z.-G. & Yun, J. 2007. Preparation of ultrafine beclomethasone dipropionate drug powder by antisolvent precipitation. *Industrial & engineering chemistry research,* 46**,** 4839-4845.

Weiss, C., McLoughlin, P. & Cathcart, H. 2015. Characterisation of dry powder inhaler formulations using atomic force microscopy. *International journal of pharmaceutics,* 494**,** 393-407.

Wu, X., Li, X. & Mansour, H. M. 2010. Surface analytical techniques in solid-state particle characterization for predicting performance in dry powder inhalers. *KONA Powder and Particle Journal,* 28**,** 3-19.

CHAPTER 3

PROTON NMR ANALYSIS OF ANHYDROUS BECLOMETHASONE DIPROPIONATE

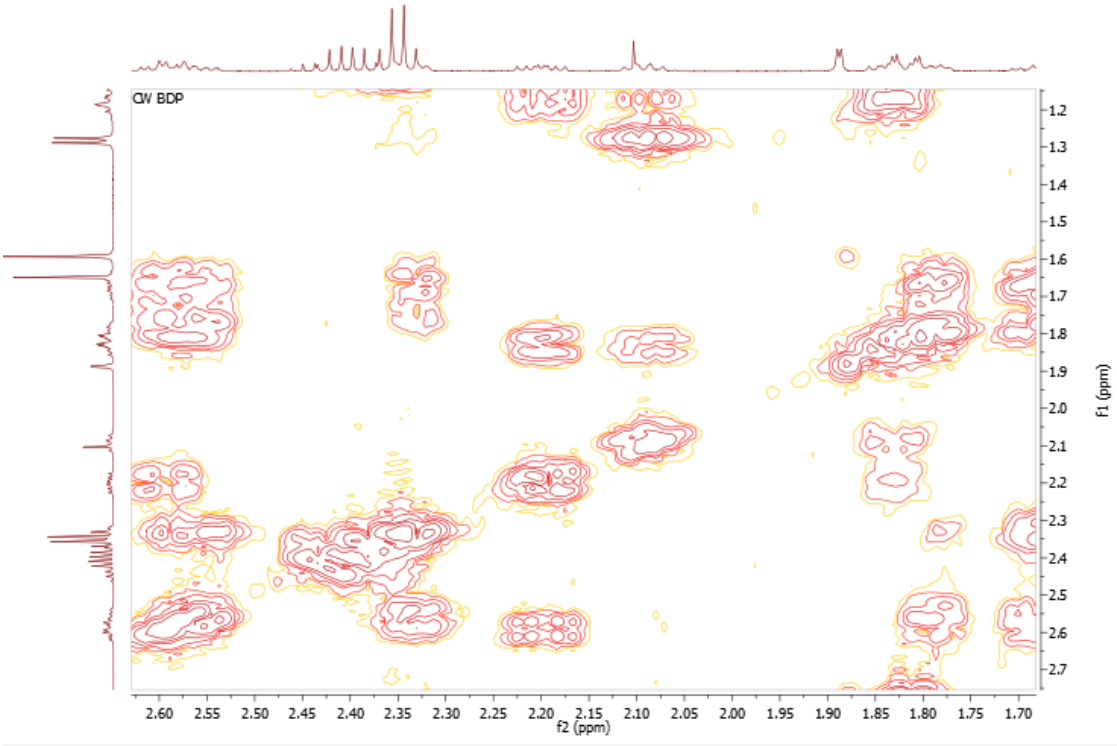

Figure 3. ^{1}H COSY spectrum of anhydrous beclomethasone dipropionate.

3 Proton NMR Analysis of Anhydrous Beclomethasone Dipropionate

NMR spectroscopy is one of the standard techniques used in chemistry, pharmaceutical science and related fields and is a valuable technique to analyse marginal changes in molecular structures. Yet in order to identify the molecular structure, all protons of anhydrous BDP need be assigned to the signals seen in the corresponding ^{1}H NMR spectrum. While the ^{13}C NMR spectrum for BDP has been solved completely (Christopher, 1993, Othman et al., 2008), the more important ^{1}H NMR spectrum has only been analysed partially (Foe et al., 1998).

In order to be able to distinguish potential differences in the crystalline structure and possible intermolecular interactions between the BDP and different solvents, the ^{1}H NMR spectrum of anhydrous BDP was analysed for comparison.

3.1 Materials and Methods

Anhydrous BDP was supplied by Intatrade Chemicals GmbH, Germany, and dissolved in deuterated chloroform ($CDCl_3$) supplied by Sigma Aldrich, UK.

3.1.1 Preparation of BDP Monohydrate

BDP monohydrate was prepared by antisolvent crystallisation (Wang et al., 2007) for comparison. 3 g of BDP were dissolved in 100 mL acetone while stirring at 300 rpm for 2 h at room temperature. The clear solution was filtered through a 0.45 µm filter (Millipore) to remove undissolved residues. The filtrate was poured into 500 mL ultra-pure water at a rate of 100 mL/min while sonicating. Precipitation occurred immediately. The white precipitate was filtered off and freeze-dried at -46° C for 24 h. The BDP monohydrate was stored in closed, Parafilm-sealed glass vials at 4 °C.

3.1.2 Nuclear Magnetic Resonance Spectroscopy

NMR spectroscopy is based on the magnetic properties of atomic nuclei, consisting of protons and neutrons with specific intrinsic spins (Field et al., 2012). Each nucleus with a spin quantum number I can assume $2I+1$ different orientations relative to the external magnetic field. In spin ½ nuclei, the two possible spin states in presence of an external magnetic field are defined as spin up and spin down, or + ½ and - ½. The overall spin of a nucleus is described by a characteristic spin quantum number I. Nuclei with $I = 0$ have an even number of protons and neutrons and are not NMR active. The spins cancel each other out. Nuclei with $I > ½$ are NMR active but, on account of an electric quadrupole, give broad signals which are more difficult to analyse. The sharpest signals are obtained from nuclei with $I = ½$ and the most common NMR experiments are based on the NMR active ^{1}H and ^{13}C isotopes ($I = ½$ for ^{1}H and ^{13}C). Not all nuclei occur equally in nature and low natural abundance can result in a weak signal. This is usually not an issue in ^{1}H NMR spectroscopy (natural abundance of ^{1}H: 99.98 %) but needs to

be considered when carrying out ^{13}C NMR experiments (natural abundance of ^{13}C:1.108 %) (Field et al., 2012).

Quantised in an external magnetic field, B_0, the spins can transition from one state into the other. The strength of the external magnetic field determines the energetic difference, ΔE, between the spin states (Equation 3-1).

$$\Delta E = \gamma \hbar B_0 \tag{3-1}$$

Equation 3-1 shows the direct relation between ΔE and B_0, γ is the gyromagnetic ratio, a nucleus specific constant, $\hbar$ is the reduced Planck constant. The energy difference corresponds directly to a nucleus specific resonance frequency when magnetic resonance absorption occurs. It can be identified by applying the exact same radio frequency to the nucleus, thus causing spin transition. To obtain an NMR spectrum, a constant magnetic field and radio frequency pulses are applied to the sample. The subsequent emission of radio frequency from the excited nuclei is then monitored (free induction decay, FID) and converted into the NMR spectrum using Fourier transformation. The results are standardised to the reference compound tetramethylsilane (TMS) as signals on a ppm scale.

Electrons surrounding a nucleus create weak magnetic fields opposing the external magnetic field, thus shielding the nucleus from the latter. This results in a chemical shift to lower frequencies (upfield shift). In contrast, electron withdrawing groups on nearby atoms within the molecule decrease the electron density around the nucleus, resulting in deshielding and a downfield shift. Chemical shifts therefore give information about the distribution of electron density within a molecule.

3.1.2.1 One dimensional solution state NMR

To identify all signals in a spectrum, one dimensional (1D) solution state ^{1}H and ^{13}C NMR is generally the first approach. The position, intensity and multiplicity of the signals in ^{1}H NMR are used to analyse a chemical compound (Field et al., 2012). While the position of a signal is defined by the electron density around the nucleus, the relative intensity of the signal depends on the number of protons responding to the same frequency. It is possible to determine the relative number of protons by integrating the area under each peak. Spin-spin coupling between adjacent nuclei results in symmetrically split signals which are created by the magnetic interaction of chemically equivalent but magnetically inequivalent nuclei. The degree of splitting depends on the number of neighbouring nuclei. The multiplicity of the signal and the magnitude of the coupling constant are used to characterise the chemical compounds. In rigid molecular structures where rotational movements are very constrained, the coupling constant is determined by the angle between the interacting protons. The correlation of angle and coupling constant is

described by the Karplus curve and has proven useful in the determination of axially and equatorially aligned protons in cyclic compounds (Richards and Hollerton, 2010).

The analysis of a regular ^{13}C NMR spectrum is based only on the position and chemical shift of the signals. Each signal consists of only a single peak and the intensity does not allow any conclusions about the number of ^{13}C nuclei involved.

For this reason, advanced ^{13}C NMR spectroscopy such as distortionless enhancement by polarisation transfer (DEPT) experiments are often used to support the information gained from a ^{13}C NMR spectrum. DEPT allows the distinction of ^{13}C based on their multiplicity. The phase of the respective signal depends on the number of protons directly bonded to the ^{13}C nucleus. Odd ^{13}C nuclei (CH, CH_3) are shown as positive signals (pointing upwards) while CH_2 groups can be distinguished by signals in the opposite direction when using a 90° pulse (DEPT-90). ^{13}C without any covalent C-H bonds do not show up in the spectrum.

3.1.2.2 Two dimensional solution state NMR

Complicated structures such as steroids can often not be solved by 1D NMR alone. Two dimensional (2D) NMR gives additional information about the spatial proximity of nuclei and the coupling of nuclei via up to four chemical bonds. A variety of 2D NMR experiments can be used to examine H-H and C-H coupling across chemical bonds and between spatially close nuclei.

The signals in a 2D NMR spectrum are a function of two frequencies of two pulses. These two frequencies can be applied consecutively, separated by a certain time, the evolution period t_1, during which the excited nuclei can interact with each other. The second pulse is applied after t_1 to record the regular FID of the nuclei in the sample. This process is repeated systematically with a slightly increasing t_1 ($t_1 + 0$, $t_1 + x$, $t_1 + 2x$, …, $t_1 + nx$). The result of the first time dimension is then transformed into a 1D spectrum via Fourier transformation and the 2D spectrum is obtained by a Fourier transformation of the second time dimension.

More advanced 2D experiments require the application of more than just two frequencies. Nevertheless, the principle remains the same: In all cases, the nuclei are excited in the preparation sequence, then either evolve at their own resonance frequency or interact with each other for t_1, followed by a mixing sequence – the parameters of which depend on the type of 2D NMR carried out – and signal detection during t_2 (Field et al., 2012). The results are plotted against each other on two axes based on the frequencies detected in t_1 (F_1 axis) and the signals detected in t_2 (F_2 axis).

Correlation Spectroscopy

Multiplets and overlapping signals can often be analysed with correlation spectroscopy (COSY) which captures spin-spin coupling of protons over chemical bonds (Field et al., 2012). A single pulse is applied in the preparation sequence and a second single pulse is applied after t_1 in the mixing period. This is when magnetisation can be transferred between the protons. Thus, two frequencies are acquired of each proton: the resonance frequency and the frequency that results from spin-spin coupling due to scalar interaction via chemical bonds. The most common COSY experiment is the COSY-90 where the first pulse turns the nuclear spin by 90°.

The 2D spectrum is symmetrical about a diagonal consisting of strong signals. Since the frequencies of the identical isotope (^{1}H) are plotted against each other on the F_1 an F_2 axis, signals that are in the same position on both axes overlap along this diagonal line. Signals with different coordinates on each axis overlap on either side of the diagonal in a symmetrical fashion. These signals show where scalar spin-spin coupling, i.e. magnetisation transfer, occurs. In general, spin-spin coupling can be detected over up to four chemical bonds.

Nuclear Overhauser Effect Spectroscopy

Nuclear Overhauser effect spectroscopy (NOESY) is similar to COSY – the pulsing sequence is based the same principle and the NOESY spectrum shows homonuclear interaction occurring during the mixing period – but the interaction is based on spin-lattice relaxation through space instead of spin-spin coupling through chemical bonds (Field et al., 2012). Magnetisation is transferred between spatially close nuclei in the same molecule via cross-relaxation (nuclear Overhauser effect, NOE). This effect has been successfully used to study the stereochemistry of cyclic compounds including steroids (Stonehouse et al., 1994) and is a very powerful tool to analyse the structure of large organic molecules such as proteins (Herrmann et al., 2002, Parsons et al., 2015).

The frequencies of identical isotopes are plotted against each other and the spatial nuclear interactions are shown by cross-peaks which are arranged symmetrically above and below a diagonal line. The intensity of the cross-peaks is related to the distance between the interaction nuclei.

Heteronuclear Single Quantum Coherence

Heteronuclear single quantum coherence (HSQC) spectroscopy is based on the spin-spin coupling between a ^{13}C nucleus and all attached protons (Field et al., 2012). The pulse sequence consists of a series of 90° and 180° pulses to excite the nuclei. Magnetisation is first transferred from each proton to the chemically bonded ^{13}C before being transferred back from each ^{13}C nucleus to all directly bonded protons after t_1.

The acquired signals (F_2 axis) are then plotted against a regular ^{13}C spectrum (F_1 axis) to obtain the 2D HSQC spectrum. In contrast to homonuclear 2D NMR spectroscopy, heteronuclear spectra are not symmetrical about a diagonal. The spin-spin couplings between the chemically bonded ^{1}H and ^{13}C nuclei are seen single cross-peaks.

Heteronuclear Single Quantum Coherence – Total Correlation Spectroscopy

Heteronuclear single quantum coherence – total correlation spectroscopy (HSQC-TOCSY) is similar to regular TOCSY experiment which shows proton –proton coupling of all spins within one spin system (Field et al., 2012). This is particularly useful when identifying overlapping signals as in the case of steroid derivatives. In contrast to TOCSY, however, these couplings are not shown at the frequency of the protons but appear as cross peaks at the frequency of the protons of one spin system (F_2 axis) and the ^{13}C (F_1 axis) in a HSQC-TOCSY spectrum (Kövér et al., 1997).

Heteronuclear Multiple Bond Correlation

Heteronuclear multiple bond correlation (HMBC) is similar to HSQC but shows the magnetisation transfer between ^{13}C and protons that are coupled via more than one bond – excluding all single bond couplings. The long-range heteronuclear interactions across two or three bonds give strong signals. In some cases the coupling of nuclei separated by four bonds can be detected if the molecular structure is rigid enough (Field et al., 2012). Since couplings via quaternary carbons and through heteroatoms such as oxygen can be observed, correlations between different spin systems can be identified as cross peaks between protons (F_2 axis) and ^{13}C nuclei (F_1 axis).

3.1.3 Solution NMR spectroscopy

BDP was dissolved in $CDCl_3$ for solution NMR spectroscopy. A Bruker AVANCE-600 spectrometer was used to acquire ^{1}H and ^{13}C 1D (including DEPT-90) and 2D spectra (HSQC, HSQC-TOCSY, HMBC, COSY, NOESY; 600 MHz).

3.2 Results

The ^{1}H and ^{13}C NMR spectra of BDP were reported in previous studies (Christopher, 1993, Othman et al., 2008, Foe et al., 1998) but due to poor resolution and multiplets between 1.70 ppm and 2.70 ppm, not all protons could be assigned. To improve resolution, solution NMR spectroscopy of anhydrous BDP as-received was carried at 600 MHz. BDP is soluble in chloroform (Christopher, 1993, Othman et al., 2008, Foe et al., 1998), therefore $CDCl_3$ was used to prepare the samples. For data analysis, the protons were labelled in relation to the directly bonded carbons as shown in Figure 3-1.

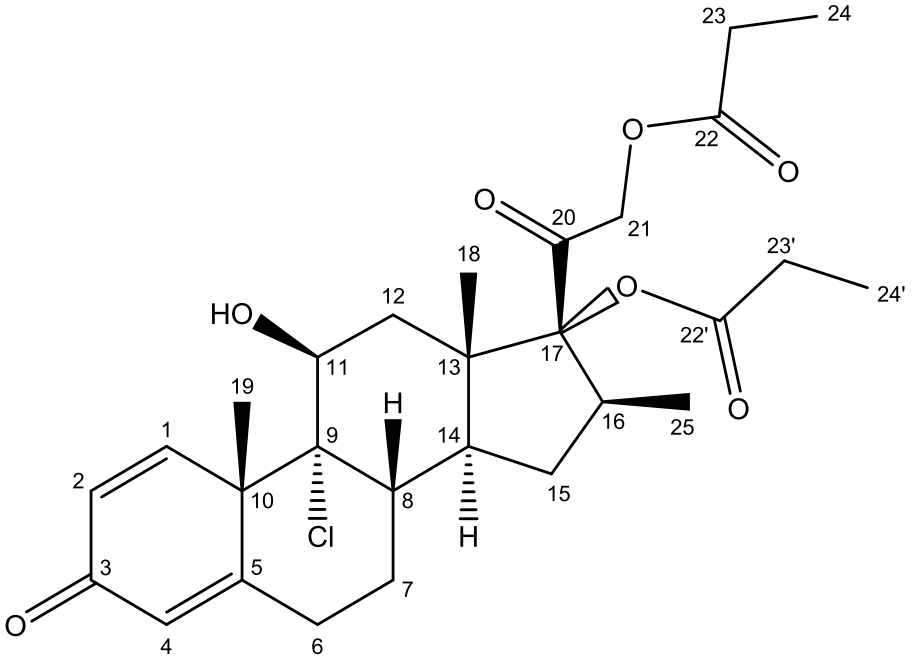

Figure 3-1. Structure of BDP. Carbon atoms labelled as referred to in NMR analysis.

The 1D ^{1}H NMR spectrum of anhydrous BDP (Figure 3-2) was analysed first. All previously assigned ^{1}H signals (Christopher, 1993, Othman et al., 2008, Foe et al., 1998) were found at the expected positions with matching coupling constants (Table 3-1).

Similarly, all previously reported ^{13}C signals (Foe et al., 1998, Christopher, 1993) could be matched to the signals shown in Figures 3-3 (^{13}C NMR) and Figure 3-4 (DEPT-90) . The results (Table 3-2) confirmed that the as-received BDP was pure anhydrous BDP and the data could be used as reference for additional NMR experiments.

To separate the multiplets in the region between 1.70 ppm and 1.80 ppm and to accurately assign all ^{1}H NMR signals, additional heteronuclear and homonuclear spectra (HSQC, HSQC-TOCSY, HMBC, COSY, NOESY, Figures 3-5 to 3-9) were analysed.

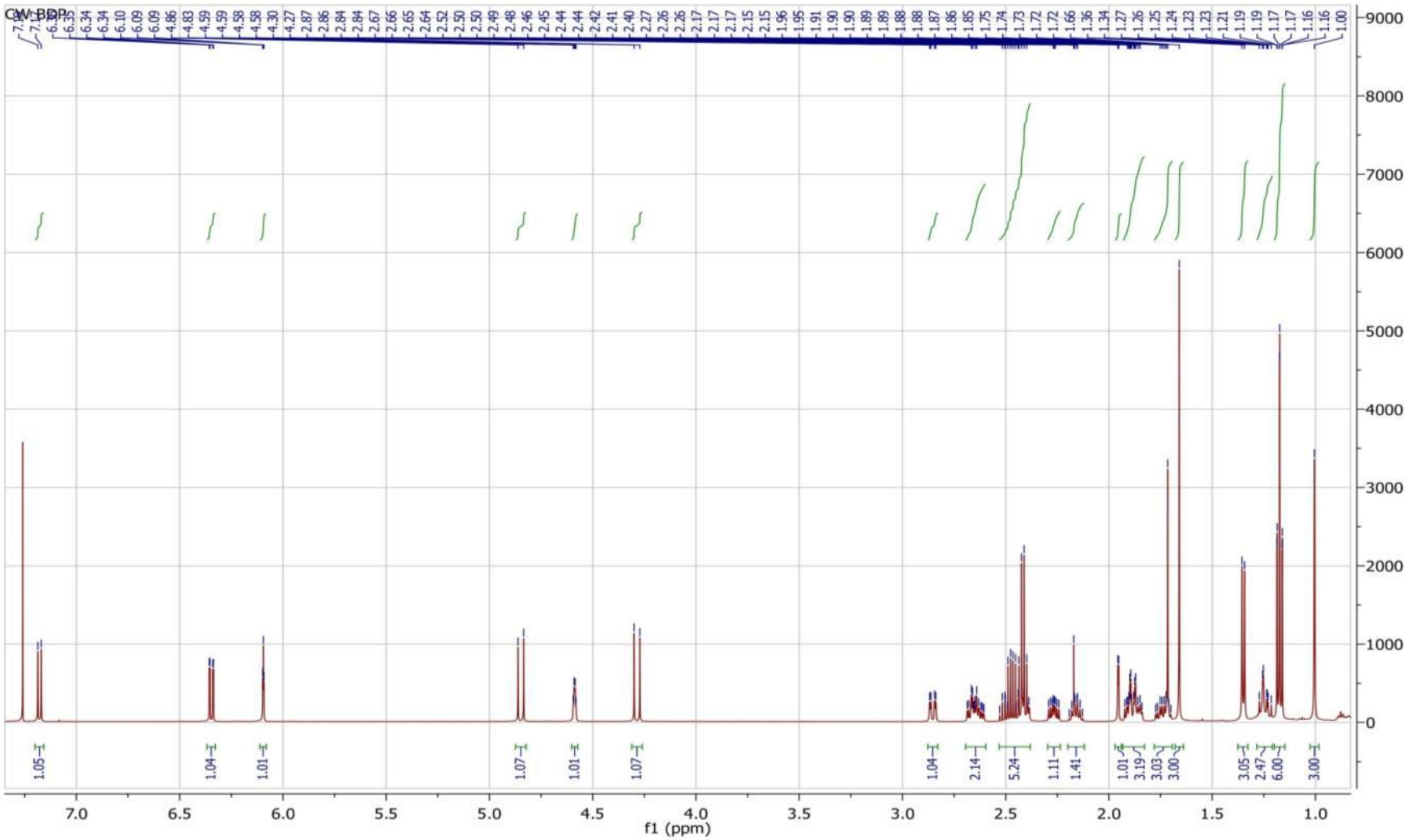

Figure 3-2. ^{1}H NMR (600 MHz, $CDCl_3$) of anhydrous BDP. Chemical shifts and additional signals marked.

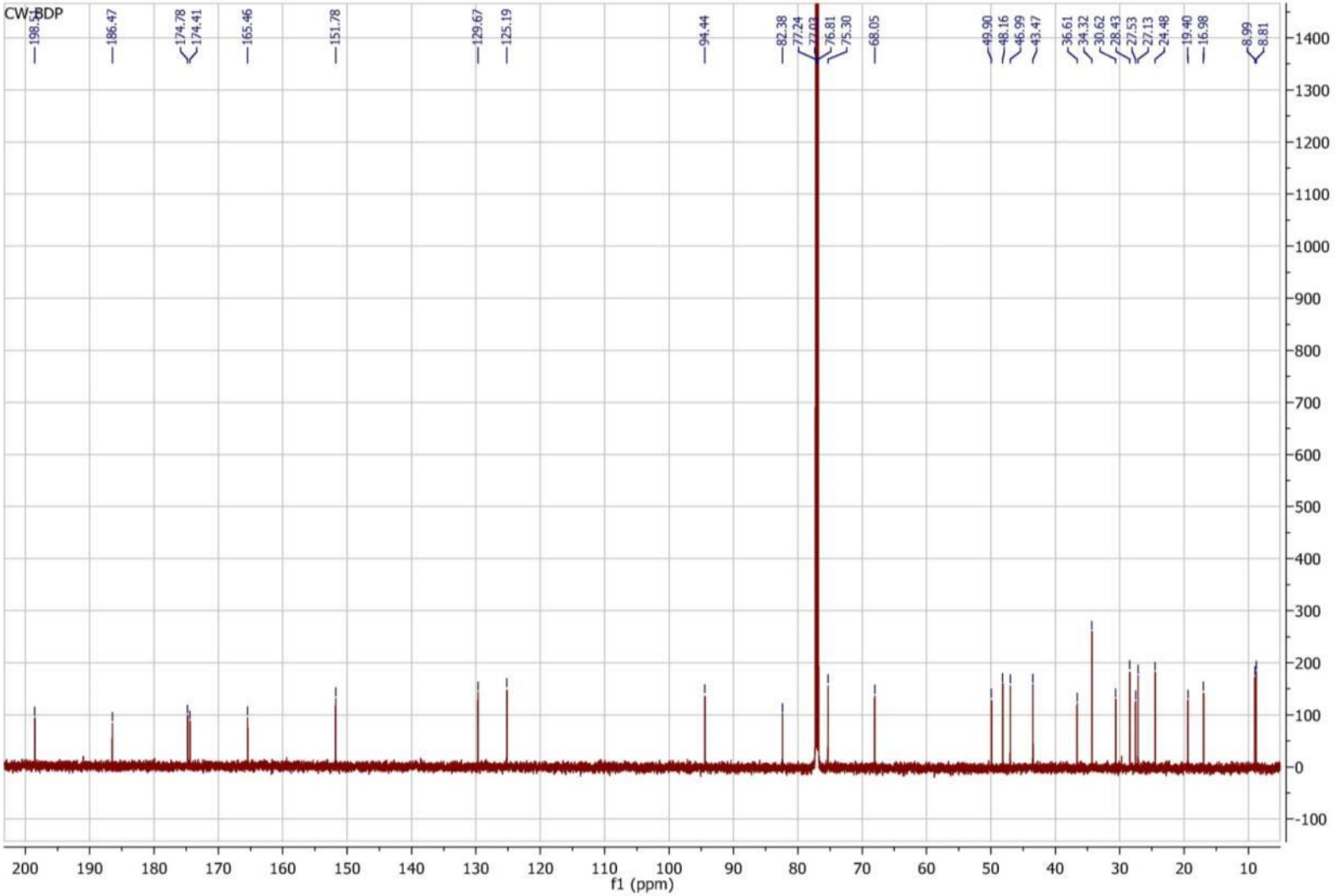

Figure 3-3. ^{13}C NMR (600 MHz, $CDCl_3$) of anhydrous BDP.

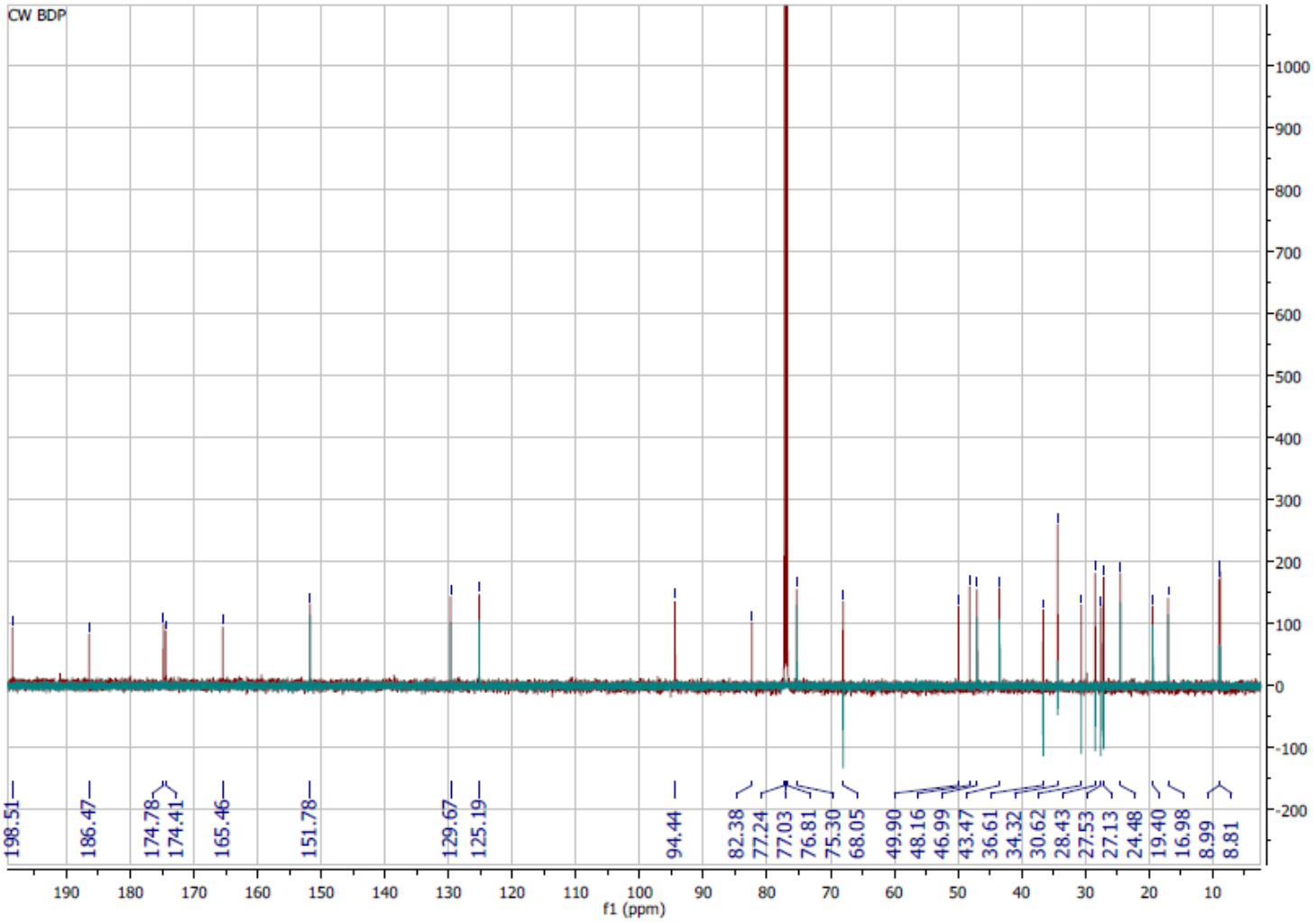

Figure 3-4. Overlay of ^{13}C NMR and DEPT (600 MHz, $CDCl_3$) of anhydrous BDP. CH and CH_3 are positive, CH_2 are negative, C are not shown.

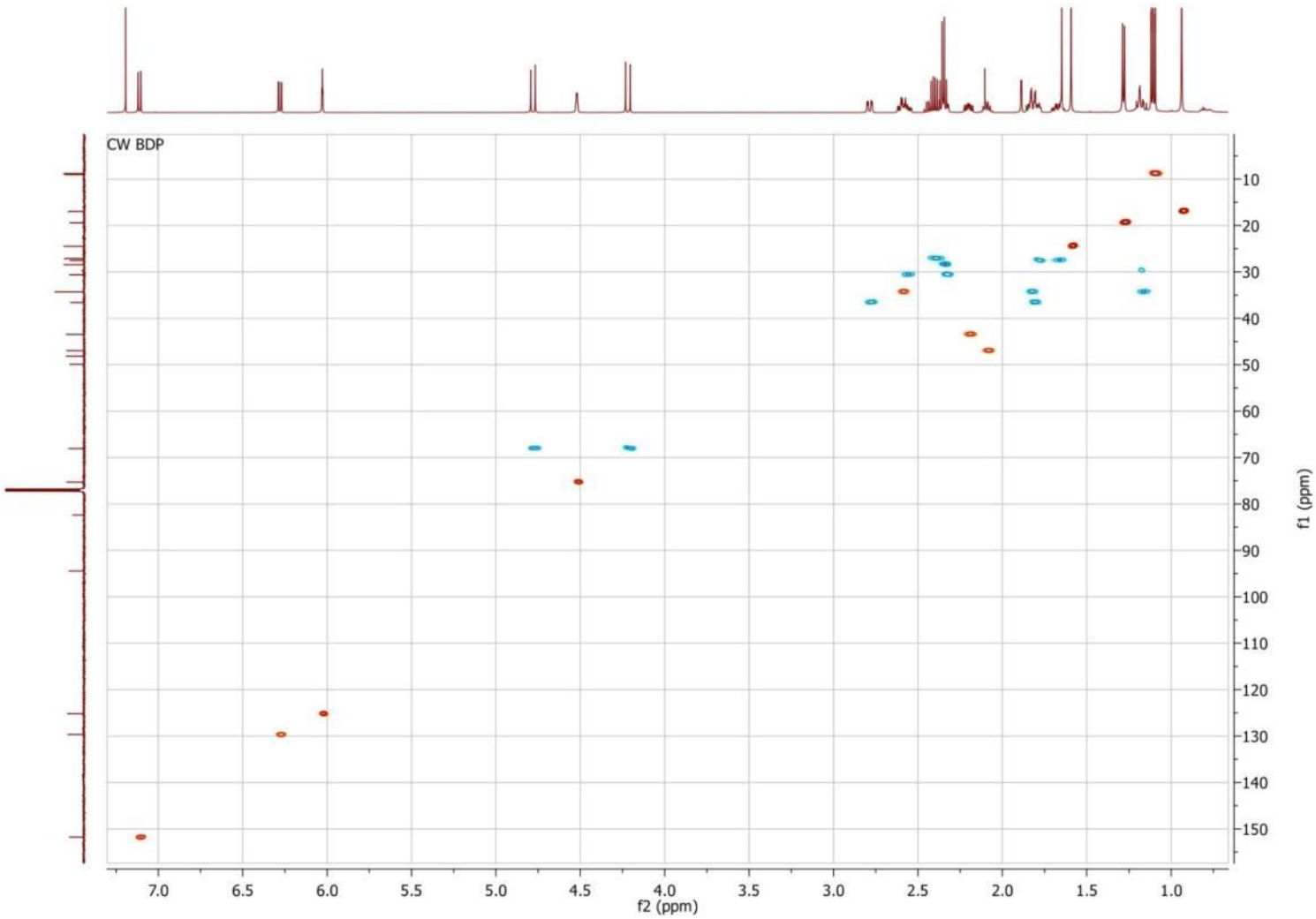

Figure 3-5. HSQC NMR (600 MHz, $CDCl_3$) of anhydrous BDP.

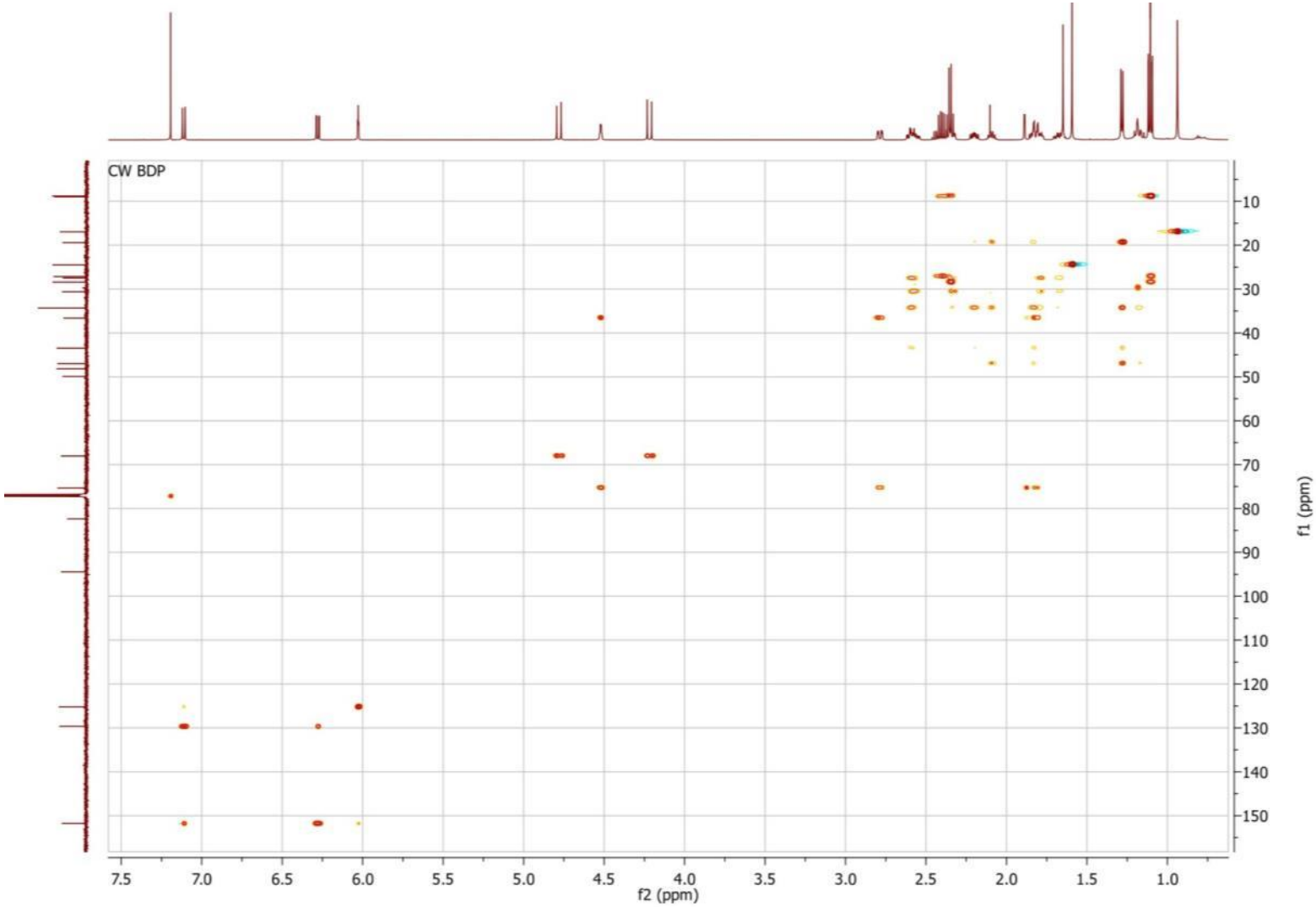

Figure 3-6. HSQC-TOCSY NMR (600 MHz, $CDCl_3$) of anhydrous BDP.

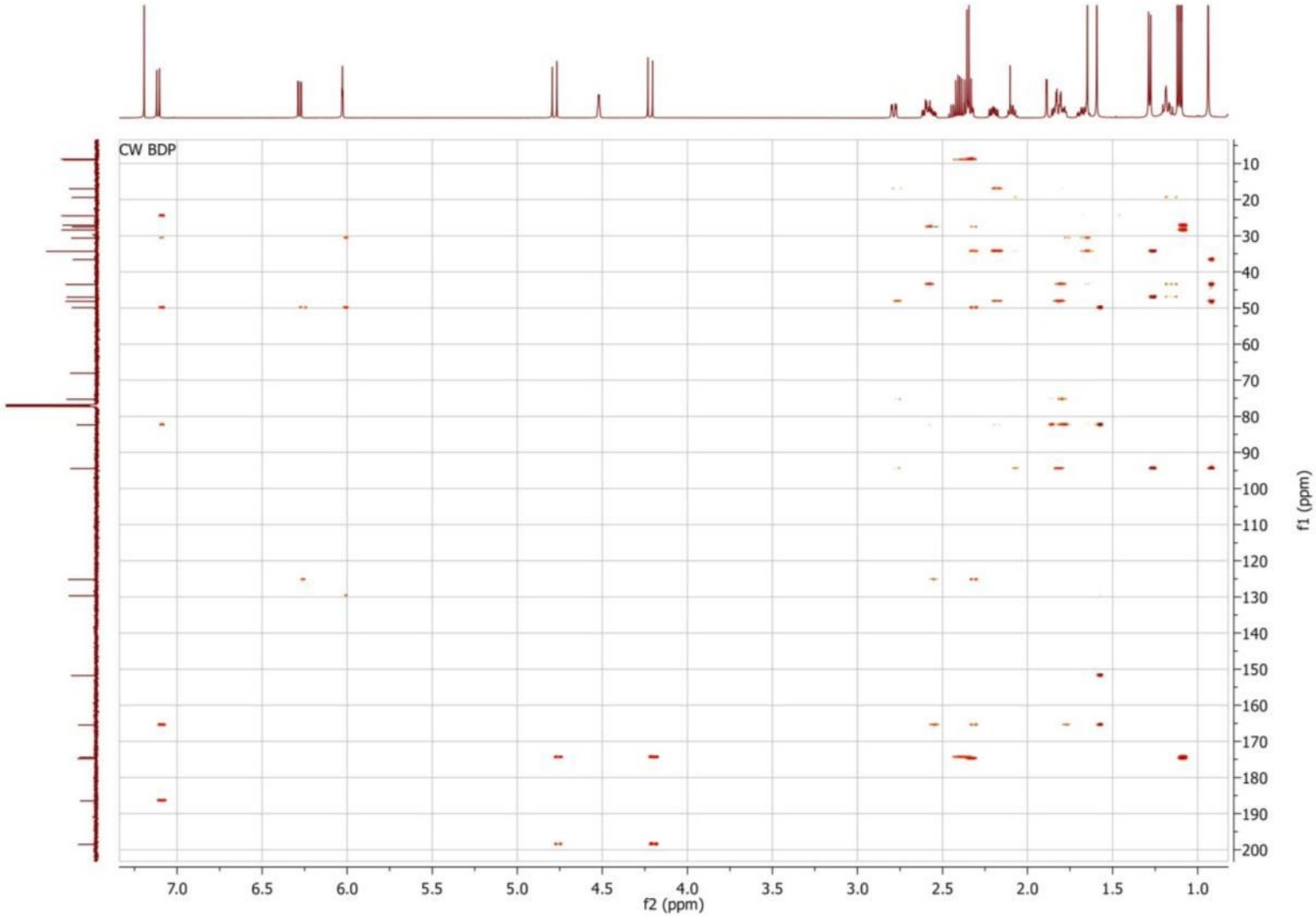

Figure 3-7. HMBC NMR (600 MHz, $CDCl_3$) of anhydrous BDP.

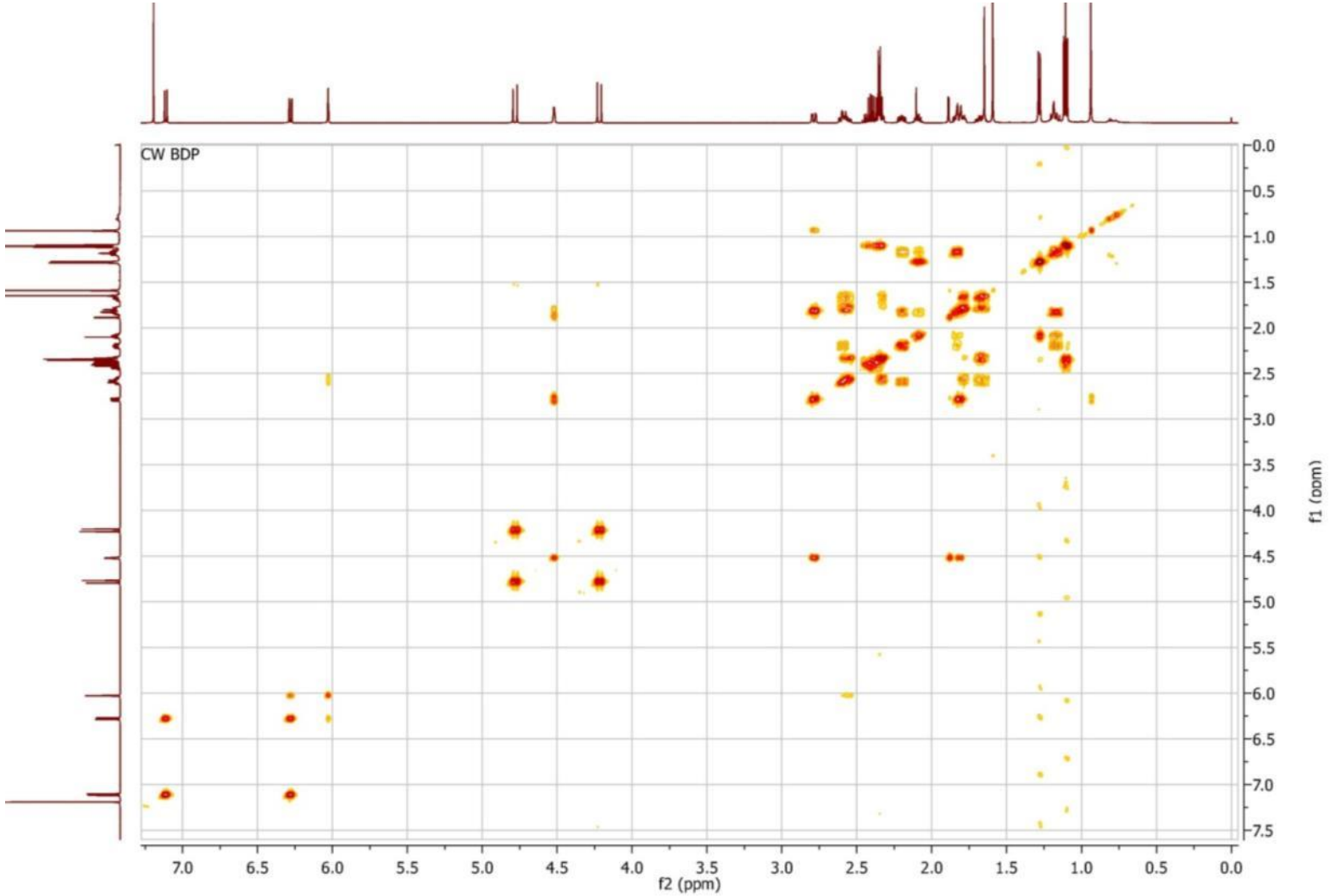

Figure 3-8. COSY NMR (600 MHz, $CDCl_3$) of anhydrous BDP.

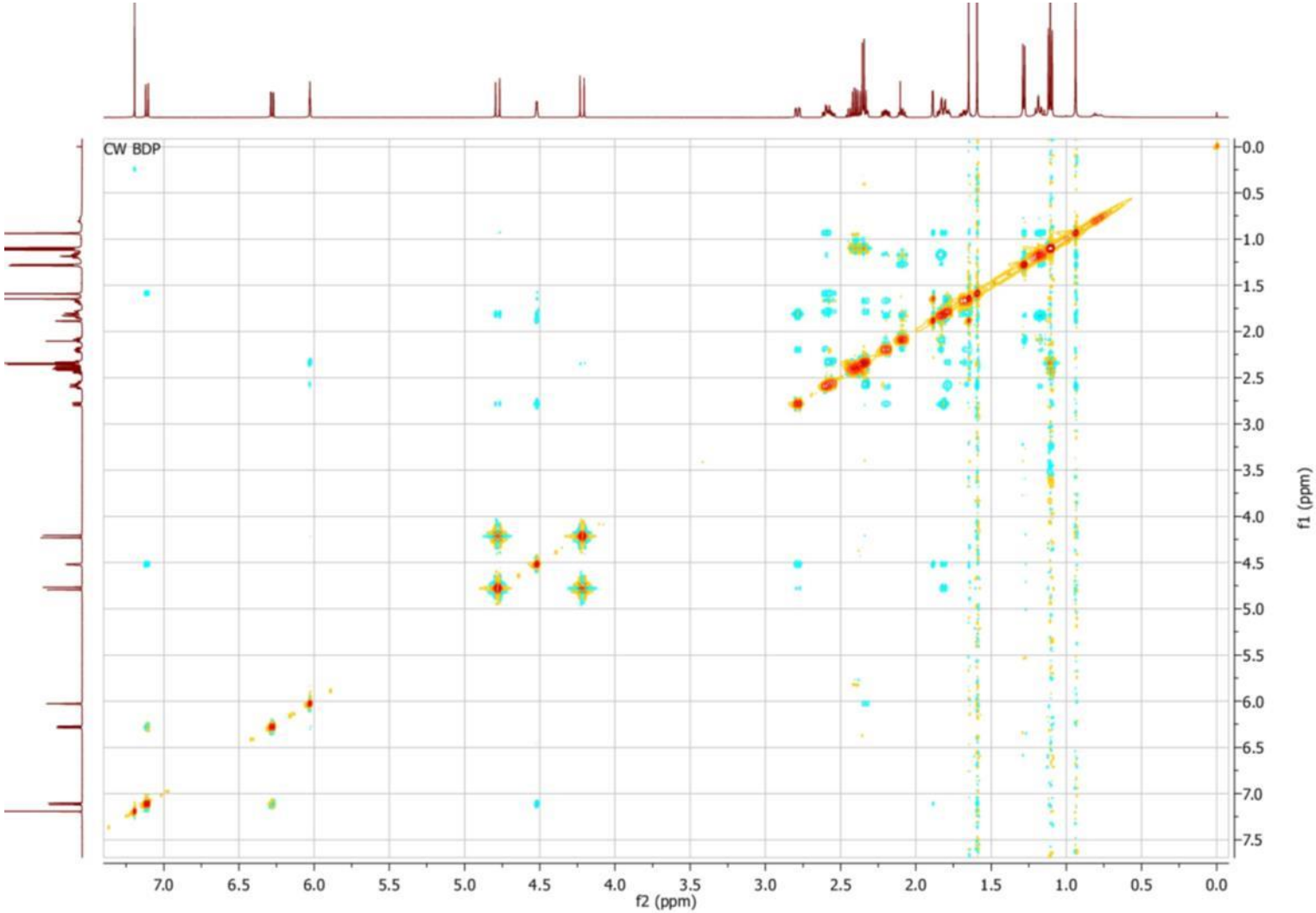

Figure 3-9. NOESY NMR spectrum (600 MHz) of anhydrous BDP.

3.3 Discussion

The structure of the sterically complex BDP molecule is based on a steroid (Figure 3-10) with only the two cyclohexane rings B and C existing in the preferred low energy chair form while ring A is planar due to conjugation (Rohrer and Duax, 1977).

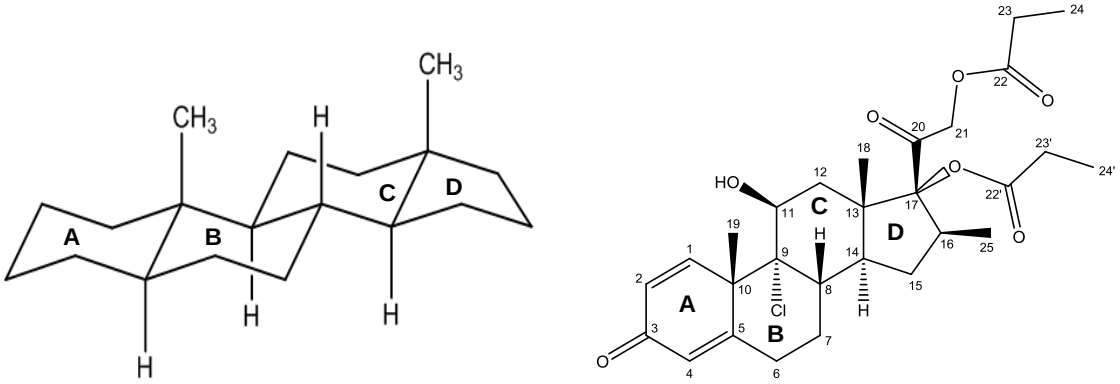

Figure 3-10. Molecular structure of a) a steroid in its preferred conformation and b) BDP. Corresponding rings A, B, C and D labelled in each structure.

Ring A, containing two double bonds and a carbonyl group, can be easily identified using ^{1}H NMR. The protons H_1, H_2 and H_4 have been assigned in previous studies (Christopher, 1993, Foe et al., 1998) and were found in the same positions with identical multiplicities and similar coupling constants (Table 3-1).

Table 3-1. ^{1}H NMR (600 MHz, $CDCl_3$) of anhydrous BDP. Chemical shifts, δ (ppm), multiplicity, coupling constants, J (Hz) and integrated intensities, I. Known data included for validation (Foe et al., 1998).

Position	^{1}H NMR				BDP
	δ [ppm]	I	multiplicity	J [Hz]	(Foe et al., 1998)
H_1	7.18	1.05	d	10.1	7.18 (d 10.2)
H_2	6.34	1.04	dd	10.1, 1.9	6.34 (dd 10.1, 2.0)
H_4	6.09	1.01	s	-	6.09 (bs)

Rings B and C cannot switch into another conformation and the protons are fixed in their positions. This leads to complex spin-spin couplings, resulting in partly overlapping multiplets in the ^{1}H NMR spectrum (Figure 3-2). The multiplets were separated using heterogeneous 2D NMR spectroscopy. The analysis of the orientation of each proton was based on their respective coupling constants and NOESY.

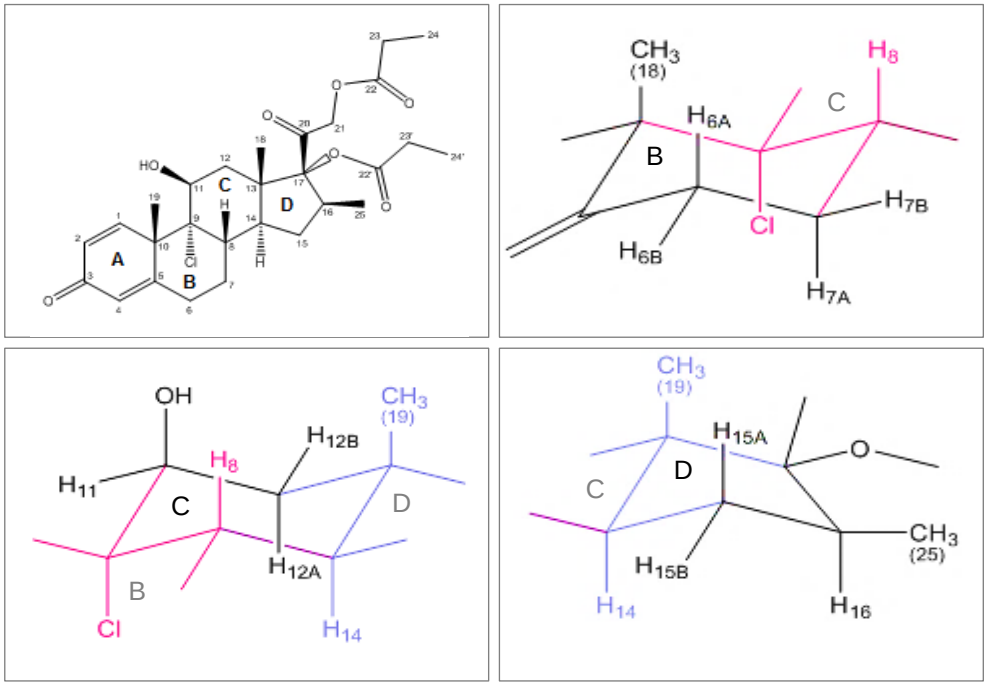

Figure 3-11. Axially and equatorially aligned protons in BDP steroid rings B, C and D (black; neighbouring rings marked with grey letters). Colours indicate parts of the structure shared between the rings.

H_{16}, H_{14} and H_8 were shown as broad multiplets (Figure 3-2). Since the chemical shifts of C_{16}, C_{14} and C_8 were known (Christopher, 1993, Othman et al., 2008) the proton signals were identified using HSQC and NOESY spectroscopy (Figures 3-12, 3-13; Tables 2-3, 3-3).

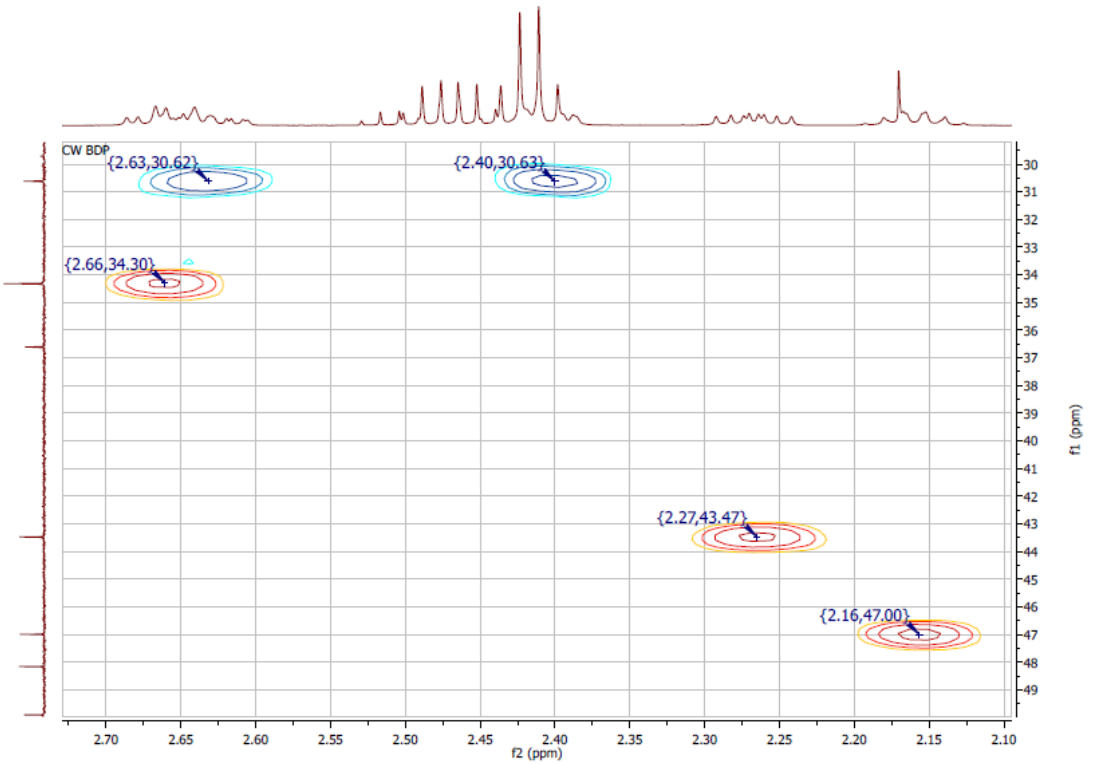

Figure 3-12. HSQC (600 MHz, $CDCl_3$) showing coupling between C_8 and H_8, C_{14} and H_{14} and C_{16} and H_{16}.

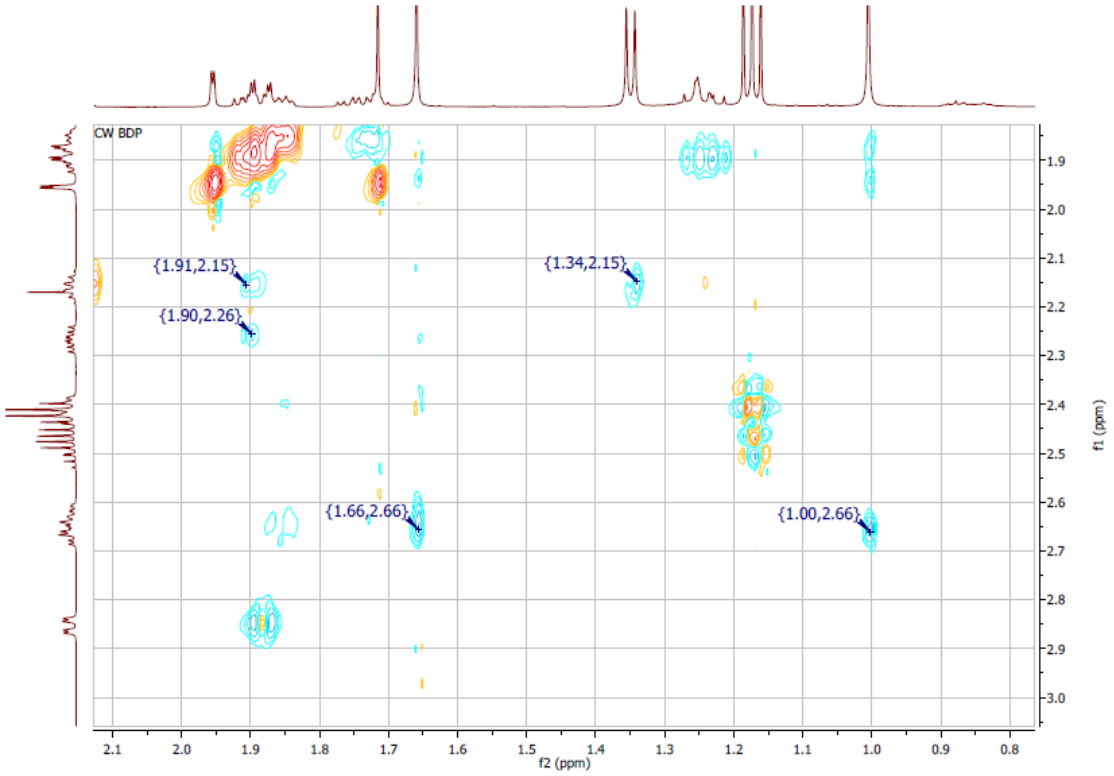

Figure 3-13. NOESY (600 MHz, $CDCl_3$) showing spatial coupling of H_8, H_{14} and H_{16}.

Table 3-2. Assignment of ^{1}H NMR signals through H-C coupling (HSQC, Figure 3-12).

^{13}C NMR		HSQC		^{1}H NMR			
δ [ppm]		δ [ppm]		δ [ppm]	I	multiplicity	J [Hz]
C_8	34.3	H_8	2.66	2.64 – 2.69	1.12[1]	m	-
		H_{15B}	1.90[2]	-	-	-	-
		H_{15A}	1.24[2]	-	-	-	-
C_{14}	43.5	H_{14}	2.27	2.26	1.11	ddd	13.3, 11.0, 5.9
C_{16}	47.0	H_{16}	2.16	2.15	1.41	ddq	16.6, 15.4, 7.6

[1] Estimated integrated intensity based on two overlapping multiplets (2.60-2.69 ppm, assigned to H_{6B} and H_8) with total integrated intensity of 2.14.
[2] Assigned to $H_{15A/B}$ based on NOESY as shown in Table 3-3, Figures 3-13, 3-14.

Table 3-3. Assignment of ^{1}H NMR signals through H-H coupling across space (NOESY, Figure 3-13).

^{1}H NMR		NOESY			
δ [ppm]		δ [ppm]		δ [ppm]	
H_8	2.64-2.69	H_{19}	1.66	H_{18}	1.00
H_{14}	2.26	H_{15B}	1.90		
H_{16}	2.15	H_{15B}	1.91	H_{25}	1.34

H_{16}, a doublet of doublet of quartets (ddq) due to coupling with the axial and the equatorial H_{15} ($^3J_{HH}$ = 16.6 MHz, $^3J_{HH}$ = 15.4 MHz) and the methyl group H_{25} ($^3J_{HH}$ = 7.6 MHz), was found at 2.15 ppm. NOESY (Figure 3-13, Table 3-3) showed spatial coupling to H_{25} (1.34 ppm) and H_{15B} (1.89-1.92 ppm). Integration gave 1.41 with the excess 0.41 being due to an acetone impurity overlapping at 2.17 ppm (Gottlieb et al., 1997).

H_{14}, in axial alignment, had a chemical shift to 2.26 ppm where the signal is split up into a doublet of doublet of doublets (ddd) by the axial and the equatorial H_{15} ($^3J_{HH}$ = 13.3 Hz, $^3J_{HH}$ = 5.9 Hz) and the axial H_8 ($^3J_{HH}$ = 11.0 Hz). The coupling constant $^3J_{HH}$ between vicinal axially aligned protons of cyclohexane in a motionally constrained chair conformation is larger than $^3J_{HH}$ between two equatorially aligned protons or an axially and an equatorially aligned proton (Richards and Hollerton, 2010). Across space (NOESY, Figure 3-13, Table 3-3) H_{14} interacted with H_{15B} (1.88-1.92 ppm) and H_8 coupled to the axially aligned H_{18} (1.00 ppm) and H_{19} (1.65 ppm). H_{14} and H_8 were therefore found to be in axial position. H_8 was assigned to the multiplet at 2.64 – 2.69 ppm but could not be analysed further.

As part of the rigid steroid structure, the protons attached to C_{15}, C_{12}, C_7 and C_6 were identified using HSQC (Figure 3-14, Table 3-4) and distinguished with regard to their sterical alignment. Geminal protons in axial and equatorial orientations have a larger coupling constant compared to the smaller coupling constant of an axial and an equatorial proton in vicinal position.

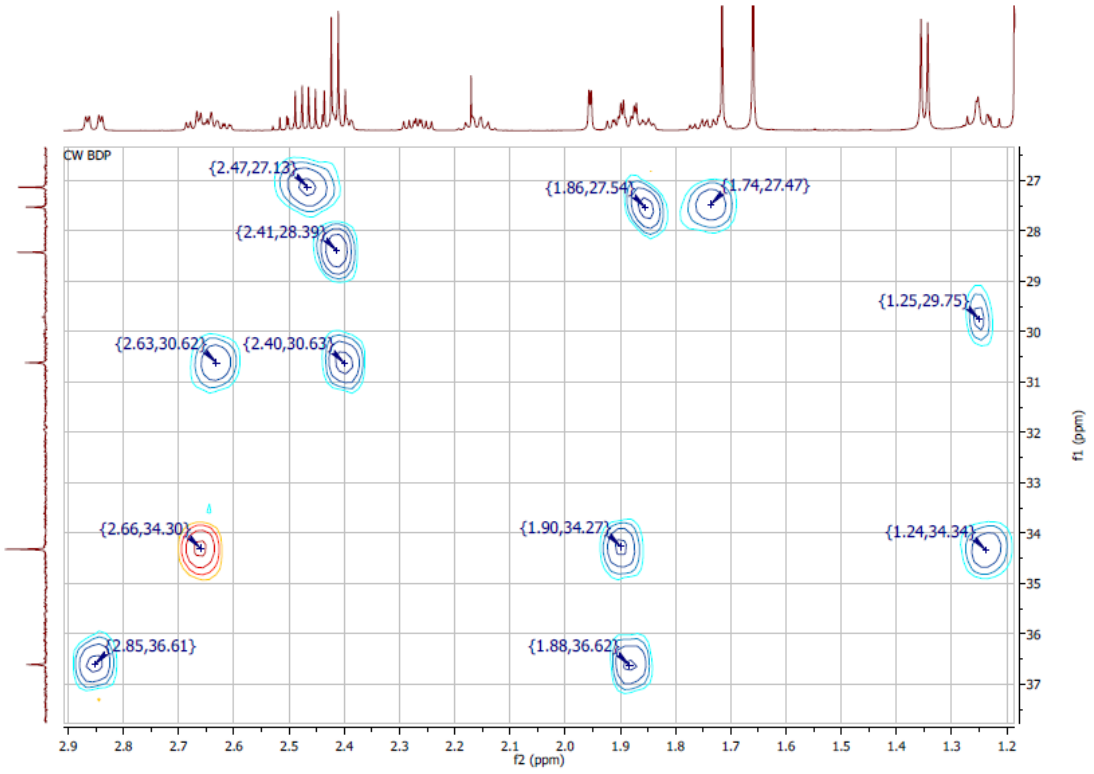

Figure 3-14. HSQC (600 MHz, $CDCl_3$) showing coupling between C_6 (30.6 ppm) and H_6, C_7 (27.5 ppm) and H_7, C_{12} (36.6 ppm) and H_{12} and C_{15} (34.3 ppm) and H_{15}.

Table 3-4. Assignment of ^{1}H NMR signals through H-C coupling (HSQC, Figure 3-13).

^{13}C NMR		HSQC		^{1}H NMR			
δ [ppm]		δ [ppm]		δ [ppm]	I	multiplicity	J [Hz]
C_6	30.6	**H_{6A}**	2.40	2.38-2.42	1.05[1]	m	-
		H_{6B}	2.63	2.60-2.64	1.12[2]	m	-
C_7	27.5	**H_{7A}**	1.74	1.70-1.77	3.03[3]	m	-
		H_{7B}	1.86	1.84-1.86	1.06[4]	m	-
C_{12}	36.6	**H_{12A}**	2.85	2.85	1.04	dd	14.1, 3.5
		H_{12B}	1.88	1.89	1.06[4]	dd	14.3, 2.6
C_{15}	34.4	**H_{15B}**	1.90	1.88-1.92	1.06[4]	m	-
		H_{15A}	1.24	-	-	-	-
		H_8	2.66[3]	-	-	-	-

[1] Estimated integrated intensity based on overlapping signals (2.38-2.53 ppm, assigned to H_{6B}, H_{23} and H_{23}') with a total integrated intensity of 5.24.
[2] Estimated integrated intensity based on two overlapping multiplets (2.60-2.69 ppm, assigned to H_{6B} and H_8) with a total integrated intensity of 2.14.
[3] Overlapping impurity (H_2O, 1.72 ppm, s, downfield shift caused by interaction with OH and Cl groups) with total integrated intensity of 3.03. Partial integration with exclusion of single signal was 0.97.
[4] Assigned to H_8 (Table 3-2).

H_{12B}, split into a doublet of doublets (dd) at 2.85 ppm, was also identified through its coupling constants with the geminal H_{12A} ($^{2}J_{HH}$ = 14.1 Hz) and the vicinal H_{11} ($^{3}J_{HH}$ = 3.5 Hz). The geminal H_{12A} at 1.89 ppm (dd) coupled with H_{12B} ($^{2}J_{HH}$ = 14.3 Hz) and H_{11} ($^{3}J_{HH}$ = 2.6 Hz). H_{12A} (1.89 ppm) was found to interact across space (NOESY, Figure 3-15) with H_{12B} (2.85 ppm), $H_{11(OH)}$ (1.95 ppm), H_{21A} (4.85 ppm), H_{7A} (1.74 ppm, weak) and H_{18} (1.00 ppm, weak) whereas H_{12B} (2.85 ppm) appeared to only couple with H_{12A} (1.89 ppm). Together with the spatial coupling of $H_{11(OH)}$ (d) at 1.95 ppm with H_{11} (4.58 ppm) and H_{18} (1.00 ppm), this confirmed the equatorial alignment of H_{11} and the axial orientation of $H_{11(OH)}$ (Figure 3-16).

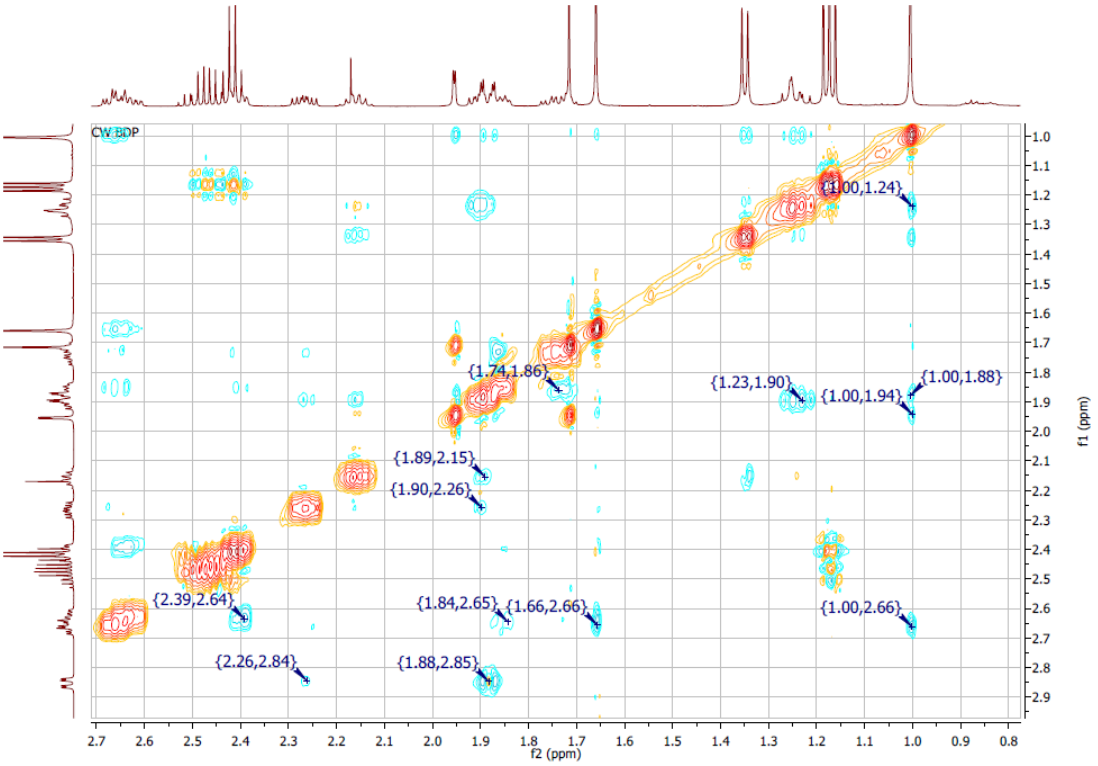

Figure 3-15. NOESY (600 MHz, $CDCl_3$) showing spatial coupling of H_6, H_7, H_{12} and H_{15}.

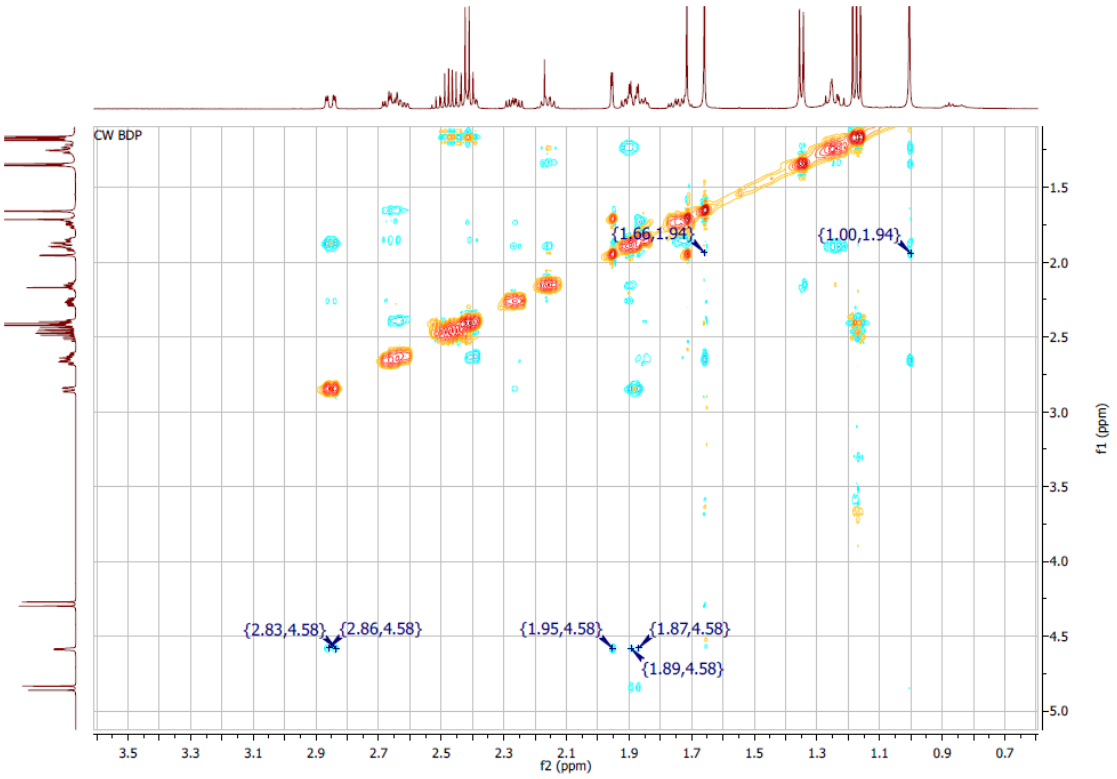

Figure 3-16. NOESY (600 MHz, $CDCl_3$) showing spatial coupling of H_{11} and $H_{11(OH)}$.

The multiplicity of H_6 and H_7 could not be resolved due to the overlapping signals masking each other, thus appearing as broad irregular multiplets (Figure 3-2). NOESY, however, showing magnetisation transfer between spatially close protons (Figure 3-15, Table 3-5), allowed the distinction of H_{6A}/H_{6B} and H_{7A}/H_{7B}. H_{6A} (2.38 – 2.42 ppm) experienced magnetisation transfer from/to the nearest axially aligned proton, H_{8A} (2.64 – 2.69 ppm) and H_4 (6.09 ppm) and was the only coupling partner of the geminal H_{6B} (2.60 – 2.64 ppm). Correspondingly, H_{7A} (1.70 – 177 ppm) coupled across space with H_{12A} (1.89 ppm) and was the only proton coupling with H_{7B} (1.84 – 1.86 ppm).

H_{15A} and H_{15B} were analysed through their direct coupling to C_{15}. H_{15A} was assigned to a signal (ddd) at 1.23 ppm which showed coupling to H_{14} (2.26 ppm, $^3J_{HH}$ = 13.3 Hz) and could thus be identified as the axially aligned proton. H_{15A} coupled to the geminal H_{15B} at 1.88 – 1.92 ppm ($^2J_{HH}$ = 11.8 Hz), H_{16} (2.15 ppm, $^3J_{HH}$ = 9.5 Hz) and across space to H_{12A} (1.89 ppm) and H_{18} (1.00 ppm). The multiplet at 1.88 – 1.92 ppm representing the equatorial H_{15B} could not be resolved but was found to interact spatially with H_{16} (2.15 ppm) and H_{18} (1.00 ppm).

Table 3-5. Assignment of ^{1}H NMR signals through H-H coupling across space (NOESY, Figures 3-15, 3-16)

^{1}H NMR		**NOESY**							
δ [ppm]		**δ [ppm]**		**δ [ppm]**		**δ [ppm]**		**δ [ppm]**	
H_{6A}	2.38-2.42	**H_4**	6.09	**H_{6B}**	2.64				
H_{6B}	2.60-2.64	**H_{6A}**	2.39						
H_{7A}	1.70-1.77	**H_{7B}**	1.86						
H_{7B}	1.84-1.86	**H_8**	2.65	**H_{7A}**	1.74				
H_8	2.64-2.69	**H_{19}**	1.66	**H_{18}**	1.00				
H_{11}	4.59	**H_{12A}**	2.85	**$H_{11(OH)}$**	1.95	**H_{12B}**	1.88		
$H_{11(OH)}$	1.95	**H_{11}**	4.58	**H_{19}**	1.66	**H_{18}**	1.00		
H_{12A}	2.85	**H_{11}**	4.59	**H_{14}**	2.26	**H_{12B}**	1.88		
H_{12B}	1.89	**H_{21A}**	4.85	**H_{11}**	4.59	**H_{12A}**	2.85	**H_{18}**	1.00
H_{15A}	1.23	**H_{15B}**	1.90	**H_{18}**	1.00				
H_{15B}	1.88-1.92	**H_{14}**	2.26	**H_{16}**	2.15	**H_{15A}**	1.23		

While the propionate branches could not be distinguished in previous studies (Othman et al., 2008, Christopher, 1993, Foe et al., 1998), the combination of HMBC (Figure 3-17) and HSQC-TOCSY (Figure 3-18) allowed the differentiation between the two spin systems.

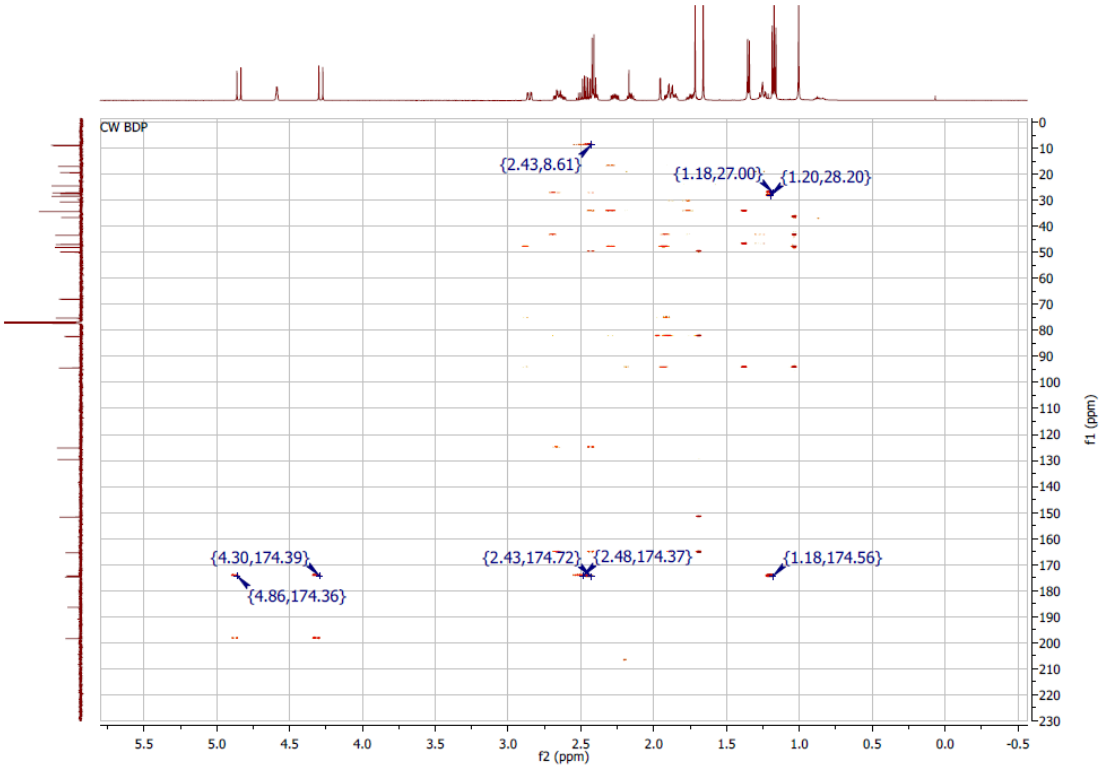

Figure 3-17. HMBC (600 MHz, $CDCl_3$) showing heteronuclear coupling across several bonds.

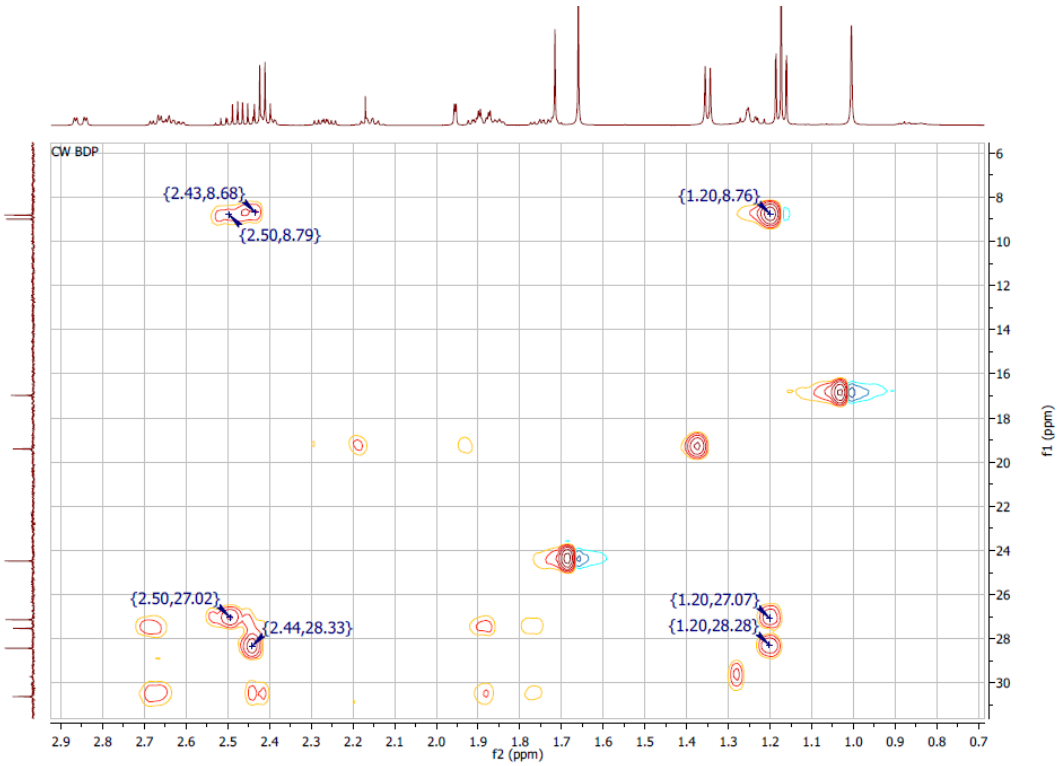

Figure 3-18. HSQC-TOCSY (600 MHz, $CDCl_3$) showing heteronuclear coupling in separate spin systems.

HMBC analysis showed multiple bond coupling between H_{21} ($H_{21A/B}$ at 4.83 ppm and 4.27ppm), H_{23}, H_{24} and C_{22} at 174.4 ppm (Figure 3-17).

HSQC-TOCSY showed that the signals at 27.1 ppm and 8.8 ppm belong to one spin system together with the protons appearing at 2.50 ppm and 1.20 ppm (Figure 3-18). By exclusion, the carbon nuclei at 28.4 ppm and 9.0 ppm must belong to the second system, i.e. the other propionate branch. Together with these results it was possible to assign C_{23} to 27.1 ppm, H_{23} to 2.46 ($^2J_{HH}$ = 7.5 Hz) and C_{24} to 9.0 ppm. C_{22}' was found at 174.8 ppm and C_{23}' at 28.4 ppm with H_{23}' at 2.41 ppm ($^2J_{HH}$ = 7.6 Hz) and C_{24}' at 8.8 ppm. H_{24} and H_{24}' could not be distinguished. Integration of the triplet at 1.17 ppm ($^2J_{HH}$ = 7.6 Hz) indicated that all six protons resonated at the same frequency.

Due to the signals being very close to each other, it was not possible to separate the protons coupling with C_{24} and C_{24}' (Table 3-6).

Table 3-6. Assignment of ^{13}C and ^{1}H NMR signals using heteronuclear coupling (HMBC, HSQC-TOCSY, Figures 3-17 and 3-18).

^{13}C NMR	HMBC				HSQC-TOCSY	
δ [ppm]	δ [ppm]	δ [ppm]	δ [ppm]	δ [ppm]	δ [ppm]	δ [ppm]
C_{22} 174.4	**H_{21A}** 4.86	**H_{21B}** 4.30	**H_{23}** 2.48	**H_{24}** 1.18		
C_{22}' 174.8	**H_{23}'** 2.43	**H_{24}'** 1.18				
C_{23} 27.1	**H_{24}** 1.20				**H_{23}** 2.50	**H_{24}** 1.20
C_{23}' 28.4	**H_{24}'** 1.18				**H_{23}'** 2.44	**H_{24}'** 1.20
C_{24} 9.0	**H_{23}/H_{23}'** 2.43			**C_{24}**	**H_{23}/H_{23}'** 2.43, 2.50	
C_{24}' 8.8				**C_{24}'**	**H_{24}/H_{24}'** 1.20	

To complete the analysis, the COSY spectrum (Figure 3-8) was analysed. The expected signals caused by homonuclear proton-proton coupling matched the signals seen in the spectrum, thus confirming the results. The complete assignment of all ^{13}C and ^{1}H signals is summarised in Tables 3-8 and 3-9. Literature data was included for comparison

Table 3-7. ^{13}C-NMR and DEPT (600 MHz, $CDCl_3$) of anhydrous BDP (BDP) compared to signals reported in literature (BDP_{lit}) (Christopher, 1993).

Position	Group	BDP^1_{lit}	BDP	DEPT signal
C_1	CH	152.0	151.8	CH/CH_3
C_2	CH	129.5	129.7	CH/CH_3
C_3	C	186.4	186.5	-
C_4	CH	125.1	125.2	CH/CH_3
C_5	C	165.6	165.5	-
C_6	CH_2	30.6	30.6	CH_2
C_7	CH_2	28.4	27.5	CH_2
C_8	CH	34.4	34.3	$CH/CH_3/CH_2$
C_9	C	82.6	82.4	-
C_{10}	C	50.0	49.9	-
C_{11}	CH	75.2	75.3	CH/CH_3
C_{12}	CH_2	36.5	36.6	CH_2
C_{13}	C	48.2	48.2	-
C_{14}	CH	43.5	43.5	CH/CH_3
C_{15}	CH_2	34.4	34.3	$CH/CH_3/CH_2$
C_{16}	CH	47.0	47.0	CH/CH_3
C_{17}	C	94.5	94.4	-
C_{18}	CH_3	16.9	17.0	CH/CH_3
C_{19}	CH_3	24.4	24.5	CH/CH_3
C_{20}	C	198.4	198.5	-
C_{21}	CH_2	67.8	68.1	CH_2
C_{22}	C	174.6	174.4	-
C_{22}'	C	174.1	174.8	-
C_{23}	CH_2	27.5	27.1	CH_2
C_{23}'	CH_2	27.1	28.4	CH_2
C_{24}	CH_3	8.9	9.0	CH/CH_3
C_{24}'	CH_3	8.7	8.8	CH/CH_3
C_{25}	CH_3	19.3	19.4	CH/CH_3

[1] Assignments for propionate chains (C_{22}-C_{24}, C_{22}'-C_{24}') are uncertain (Christopher, 1993).

Table 3-8. ^{1}H-NMR signals of BDP. Comparison of signals reported in literature (BDP_{lit}) (Foe et al., 1998) and new assignments based on 1D (BDP^{1}) and 1D together with 2D spectra (BDP^{2}).

Position	^{1}H-NMR: Chemical shifts [ppm], multiplicity, coupling constants [Hz]		
	BDP_{lit}	BDP^{1}	BDP^{2}
H_1	7.18 (d; 10.2)	7.18 (d; 10.1)	
H_2	6.34 (dd; 10.1, 2.)	6.34 (dd; 10.1, 1.9)	
H_4	6.09 (bs)	6.09 (s)	
H_{6A}			2.38-2.42 (m)
H_{6B}			2.60-2.64 (m)
H_{7A}			1.70-1.77 (m)
H_{7B}			1.84-1.86 (m)
H_8			2.64-2.69 (m)
$H_{11(OH)}$	2.2 (d; 2.0)	1.95 (d; 2.3)[3]	
H_{11}	4.57 (bs)	4.58 (dd; 5.4, 2.5)[4]	
H_{12A}			2.85 (dd; 14.1, 3.5)
H_{12B}			1.89 (dd; 14.3, 2.6)
H_{14}			2.26 (ddd; 13.3, 11.0, 5.9)
H_{15A}			1.23 (ddd; 13.3, 11.8, 9.5)
H_{15B}			1.88-1.92 (m)
H_{16}			2.15 (ddq; 12.2, 7.6, 6.4)
H_{18}	0.99 (s)	1.00 (s)	
H_{19}	1.65 (s)	1.65 (s)	
H_{21A}	4.27 (d; 16.3)	4.27 (d; 16.4)	
H_{21B}	4.85 (d 16.3)	4.83 (d 16.4)	
H_{23}	2.41 (q 7.6)	2.46 (q 7.5)	
H_{23}'	2.41 (q 7.6)	2.41 (q 7.6)	
H_{24} / H_{24}'	1.16 (t 7.6)	1.17 (t 7.6)	
H_{25}	1.34 (d 7.4)	1.34 (d 7.3)	

[1] Based on 1D ^{1}H NMR data.
[2] Derived from combination of 1D and 2D NMR analysis.
[3] Chemical shift of OH proton may vary due to presence of impurities and strength of interaction (Bruice, 2011).
[4] Broad singlet at 300 MHz, doublet of doublet at 600 MHz. Coupling of two protons (H_{12} axial and equatorial).

3.4 Conclusions

The complete structure of BDP in its anhydrous form has been assigned to the signals seen in the ^{1}H NMR spectrum for the first time. This was based on a combination of 1D ^{1}H and ^{13}C NMR including DEPT and COSY, NOESY, HMBC, HSQC and HSQC-TOCSY. It was possible to distinguish between axially and equatorially aligned protons.

Solving the proton NMR spectrum of anhydrous BDP made it possible to use NMR titration to evaluate the intermolecular interactions between BDP and different solvents (Chapter 5). The chemical shifts observed when adding a solvent to a solution of BDP in deuterated chloroform were assigned to specific protons of the BDP molecule which allowed predictions about the impact of intermolecular interactions between certain functional groups on solvate formation.

3.5 References

Bruice, P. Y. 2011. *Organische Chemie: studieren kompakt*, Pearson Deutschland GmbH.

Christopher, E. A. 1993. *Solid-state NMR study of polymorphism in pharmaceuticals*. Durham University.

Field, L. D., Sternhell, S. & Kalman, J. R. 2012. *Organic structures from spectra*, John Wiley & Sons.

Foe, K., Cheung, H. A., Tattam, B. N., Brown, K. F. & Seale, J. P. 1998. Degradation products of beclomethasone dipropionate in human plasma. *Drug metabolism and disposition,* 26**,** 132-137.

Herrmann, T., Güntert, P. & Wüthrich, K. 2002. Protein NMR structure determination with automated NOE assignment using the new software CANDID and the torsion angle dynamics algorithm DYANA. *Journal of molecular biology,* 319**,** 209-227.

Gottlieb, H. E., Kotlyar, V. & Nudelman, A. 1997. NMR chemical shifts of common laboratory solvents as trace impurities. *The Journal of organic chemistry,* 62**,** 7512-7515.

Kövér, K. E., Hruby, V. J. & Uhrín, D. 1997. Sensitivity-and gradient-enhanced heteronuclear coupled/decoupled HSQC–TOCSY experiments for measuring long-range heteronuclear coupling constants. *Journal of Magnetic Resonance,* 129**,** 125-129.

Othman, A., Harris, R. K., Hodgkinson, P., Christopher, E. A. & Lancaster, R. W. 2008. Structural characterisation of two pharmaceutically important steroids by solid-state NMR. *New Journal of Chemistry,* 32**,** 1796-1806.

Parsons, I. C., Lansing, J., Bosques, C. J. & Beccati, D. 2015. *Comparative analysis of protein conformations by using 2D NOESY NMR spectra*.

Richards, S. A. & Hollerton, J. C. 2010. *Essential practical NMR for organic chemistry*, John Wiley & Sons.

Rohrer, D. & Duax, W. 1977. 9α fluoro-16α-methyl-11β, 17α, 21-trihydroxy-1, 4-pregnadiene-3, 20-dione (dexamethasone)(C22H29FO5). *Cryst Struct Commun,* 6**,** 123-126.

Stonehouse, J., Adell, P., Keeler, J. & Shaka, A. 1994. Ultrahigh-quality NOE spectra. *Journal of the American Chemical Society,* 116**,** 6037-6038.

Wang, Z., Chen, J.-F., Le, Y., Shen, Z.-G. & Yun, J. 2007. Preparation of ultrafine beclomethasone dipropionate drug powder by antisolvent precipitation. *Industrial & engineering chemistry research,* 46**,** 4839-4845.

CHAPTER 4

PREPARATION AND CHARACTERISATION OF CRYSTALLINE BECLOMETHASONE DIPROPIONATE FROM ALCOHOL AND ACETONE SOLUTIONS

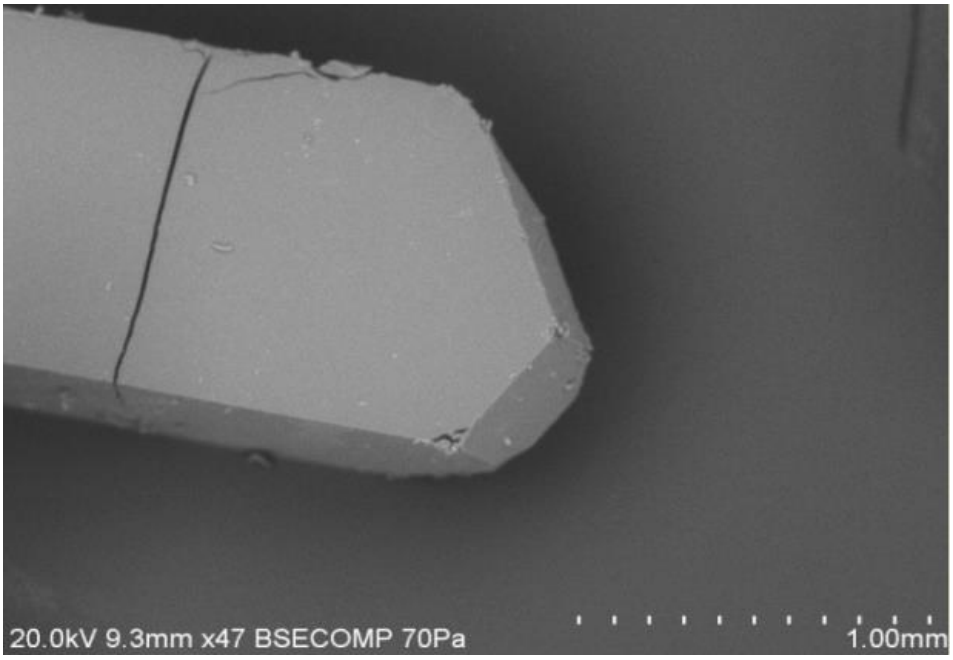

Figure 4. BDP ethanol solvate under the SEM.

4 Preparation and Characterisation of Crystalline Beclomethasone Dipropionate from Alcohol and Acetone Solutions

BDP is known to readily form monohydrates (Nachiengtung, 1997, Hunt and Padfield, 1989, Wang et al., 2007), ethanol solvates (Kuehl et al., 2003, Jinks, 1989, Bouhroum et al., 2010), ethyl acetate solvates (Othman et al., 2008) and di-isopropyl ether solvates (Page and Heggie, 1990) with the solvent molecules incorporated in channel structures within the host crystal. The structure of these channels depends on the solvent they contain. In the BDP monohydrate, hydrogen bonding occurs between the water molecules and the BDP. Each water molecule develops three hydrogen bonds and bridges two BDP molecules which helps maintain the channel structure (Hunt and Padfield, 1989). In contrast, in the BDP ethanol and ethyl acetate solvates, the channels are constructed by hydrogen bonding between two BDP molecules (Othman et al., Kuehl et al., 2003) and the solvent molecules are highly mobile within the channels (Kuehl et al., 2003, Othman et al.). The incorporation of the solvent molecules either as part of the crystalline structure or merely as guests within the channels affects the stability of the compound. Solvent-based structures are less stable and the solvent may be gradually released or substituted by water over time to form a more stable compound (Morissette et al., 2004). Solvent removal may lead to the rearrangement of the crystalline structure or even cause the crystal to collapse into an amorphous form (Bouhroum et al., 2010). The BDP monohydrate is known to be stable enough to be used in drug formulations (Hunt and Padfield, 1989). However, contradictory results were reported for the BDP ethanol solvate. One group specified the need to operate under sub-ambient conditions at -71.15 °C to prepare the channel solvate (Kuehl et al., 2003). Others found the BDP ethanol solvate to be stable over six months in a CFC propellant (Jinks, 1989). In addition, a stable BDP solvate containing freely moving ethanol and HFA 134a was discovered (Harris et al., 2003). The di-isopropyl ether solvate was also found to be bulk stable over time and suitable for use in aerosol formulations (Page and Heggie, 1990). Alcohol-based BDP solvates (methanol, ethanol, 1-propanol, 2-propanol, allyl alcohol, 1-butanol, 2-methyl-1-propanol) were identified (Jinks, 1989) and their particle size was shown to change only minimally over six months when kept in a CFC propellant. However, other physicochemical characteristics were not determined (Jinks, 1989).

To gain a better understanding of the nature of BDP solvates, their stability and the mechanisms leading to solvate formation and the inclusion of solvent molecules, BDP was crystallised from methanol, ethanol, 1-propanol, 2-propanol, 1-butanol, 1-pentanol and acetone. BDP is soluble in acetone and in short-chain alcohols (C1 to C5), ethyl acetate, esters, chloroform and dichloromethane and partly soluble in alkanes (C5 to C8) (Wang et al., 2007, Neale and Taylor, 1997, Page and Heggie, 1990, Jinks, 1989, Finckenor, 1980) and therefore well suited for precipitation from supersaturated solution.

4.1 Materials and Methods

Anhydrous BDP was supplied by Intatrade Chemicals GmbH, Germany. All solvents, purchased from Sigma Aldrich, UK, were of analytical grade and used as received. Demineralised water was purified using an Ultra Clear System (Evoqua GmbH, Germany).

4.1.1 Crystallisation of BDP Solvates

Crystalline BDP was prepared from solutions of acetone, methanol, ethanol, 1-propanol, 2-propanol, 1-butanol and 1-pentanol (Table 4-1).

Table 4-1. Solvents used, their structure and their properties: molar weight (M), boiling point (T_B) and relative polarity (relative to water: relative polarity$_{H2O}$ = 1).

Solvent	Structure	M [g/mol]	Bp [°C]	Rel. polarity
Methanol		32.04	64.6	0.762
Ethanol	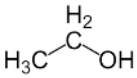	46.07	78.5	0.654
1-Propanol	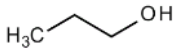	60.10	97.0	0.617
2-Propanol	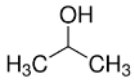	60.10	82.4	0.546
1-Butanol	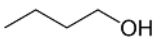	74.12	117.6	0.586
1-Pentanol	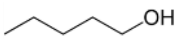	88.15	138.0	0.568
Acetone	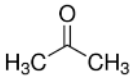	58.08	56.2	0.355

3 g of BDP was dissolved in 60 mL of solvent while stirring at 300 rpm for 2 h. The alcohol solutions were stirred at 75 – 90 °C, while the acetone-based solution was stirred at room temperature. The solutions were filtered through a 0.45 µm nylon filter (Millipore) to remove any undissolved material and then reheated to 75 °C to ensure complete dissolution of the BDP and to obtain comparable starting conditions.

The concentration of each solution was determined at approximately 75 °C (Table 4-1) using UV-Vis spectrometry. Due to the concentrations being too high to be measured directly, the solutions were diluted before UV-Vis spectrometry was carried out.

The solutions were cooled to 4 °C and stirred at 300 rpm for 24 h, causing an increase in supersaturation (Table 4-2) and facilitating nucleation and crystal growth.

Table 4-2. Sample preparation: temperature used to dissolve the BDP prior to crystallisation (T_{dis}), concentration at this temperature (C_0), at crystallisation temperature of 4 °C (C_{sat}), and degree of supersaturation at 4 °C (S). Stirred at 300 rpm during crystallisation for 24 h at 4 °C.

Solvent	Sample preparation			
	T_{dis} [°C]	C_0 [mmol/L]	C_{sat} [mmol/L]	S
Methanol	75	113.16	4.70	24.07
Ethanol	75	130.57	22.70	5.75
1-Propanol	75	111.93	33.15	3.38
2-Propanol	75	180.19	22.86	7.88
1-Butanol	75	124.86	51.93	2.40
1-Pentanol	75	101.62	92.34	1.10
Acetone	25	111.44	106.68	1.04

The degree of supersaturation, *S*, was calculated (Equation 4-1) based on the saturation concentration of BDP in each solvent at 4 °C, C_{sat}, and the initial concentration after dissolution at 75 °C, C_0:

$$S = \frac{C_0}{C_{sat}} \tag{4-1}$$

Vacuum filtration was used to collect the crystalline BDP (0.45 µm nylon filter, Millipore) which was dried for 3 h at 37 °C to remove excess solvent and stored in closed, Parafilm-sealed glass vials at 4 °C.

4.1.2 Preparation of BDP Monohydrate

BDP monohydrate was prepared using anti-solvent precipitation as described in Chapter 2.

4.1.3 Fourier Transform Infrared Spectroscopy

FTIR was carried out as described in Chapter 2.

4.1.4 X-ray Powder Diffraction

XRPD in transmission mode was used to collect crystallograhpic data. The experimental work was carried out on an X'Pert MPD PRO (PANalytical, The Netherlands) using a Cu Kα source at 40 kV and 40 mA. The samples were scanned in transmission mode from (5- 50° 2θ) and rotated at a step size of 0.017° 2θ. The scan step time was set to 40 s.

4.1.5 Thermal Analysis

Thermal analysis was carried out as described in Chapter 2. Each TGA measurement was repeated three times (n = 3), the sample crystallised from acetone was measured five times (n = 5). The DSC measurements were repeated three times (n = 3), the sample crystallised from

acetone was measured six times (n = 6). The samples were cooled to -10 °C and a second heating cycle was run using identical parameters.

4.1.6 Headspace Gas Chromatography with Mass Spectrometry

The solvents released from the solvates were analysed using headspace gas chromatography with mass spectrometry (GC-MS, Varian 450 GC; Varian 220 Ion Trap MS, helium). After agitating 0.05 g samples in sealed glass vials (10 mL) for 10 min at 120 °C, 250 µL of headspace vapour was collected. The syringe temperature was set to 150 °C. Each sample was injected and focused on a polydimethylsiloxane column at 40 °C, using a split ratio of 200. The oven temperature was ramped at 10 °C/min to 250 °C to separate the analytes by their boiling points. The analytes were detected using MS (m/z 40 – 350).

4.1.7 Scanning Electron Microscopy

The samples were imaged at 70 Pa using a Hitachi S-3000N VP (Hitachi, Japan) equipped with a secondary electron detector. To enable rapid imaging after preparation and to reduce degradation as observed under high vacuum and during gold coating, the samples were not gold-sputtered but used as synthesised. Despite these precautions, SEM images had to be captured without delay since long exposure to low vacuum and accelerated electrons appeared to lead to the crystals cracking and crumbling (Figure 4-1).

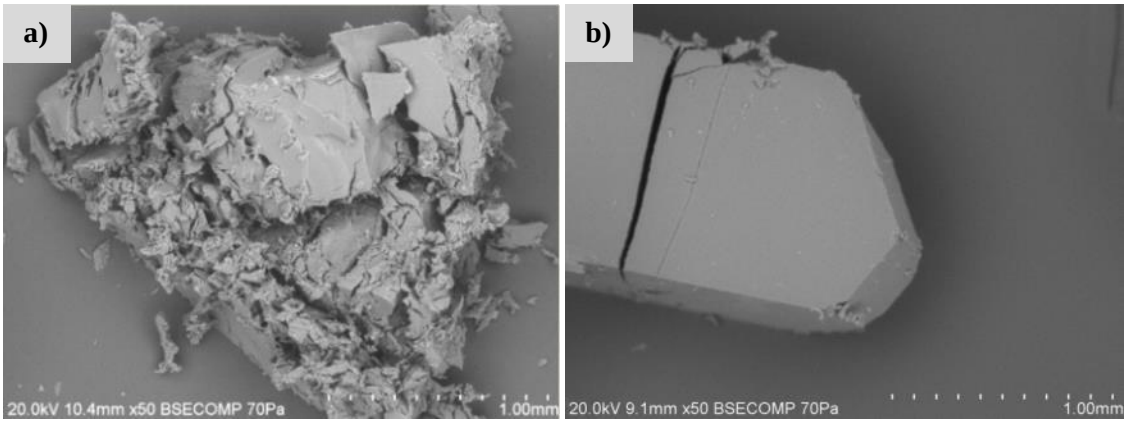

Figure 4-1. BDP crystals cracking under the electron beam (accelerating voltage 20 kV) at 70 Pa: a) BDP grown from methanol solution, b) BDP grown from ethanol solution.

4.1.8 Morphologi Image Analyser

The aspect ratio of BDP prepared from ethanol, 1-propanol and 2-propanol was measured using a Morphologi G3 microscope (Malvern Panalytical). Small aliquots of materials were filled into an Eppendorf tube which was then tumbled to achieve dispersion. A precise volume aliquot was extracted and dispersed by the Morphologi G3 accessory under air pressure (1 bar) onto a clear dry glass plate.

The resulting dispersions appeared to have well-separated particles. They were scanned with a 5X objective over a small central area, which viewed and measured 19960, 17455 and 10195 particles respectively.

4.1.9 Atomic Force Microscopy

Atomic force microscopy (AFM) was used to evaluate the surface roughness of the BDP particles. Crystals were selected for analysis based on their size and visual appearance such that the chosen particles were representative of the sample.

All measurements were performed on a Bruker Dimension Icon ScanAsyst AFM (Bruker Nano, CA, USA) inside a glovebox under nitrogen. The water and oxygen levels were both below 0.1 ppm. These conditions were found to cause the desolvation of the BDP solvates. As soon as the AFM probe scratched the surface of a BDP ethanol solvate particle (ethanol solvate confirmed using FTIR and thermal analysis), the initially clear crystal became opaque and eventually collapsed into white powder (Figure 4-2) which was identified as the anhydrous form (FTIR).

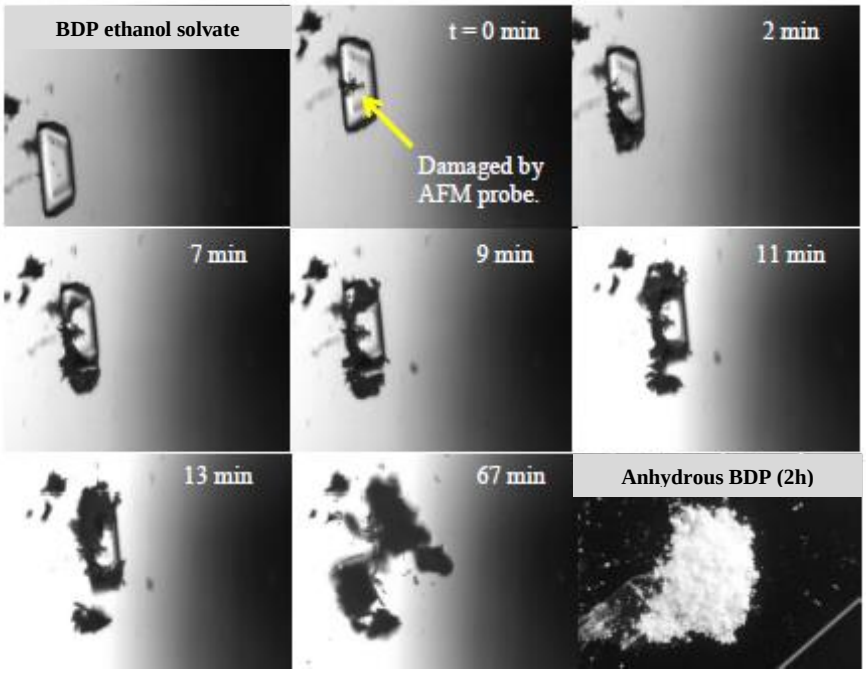

Figure 4-2. Desolvation of damaged BDP ethanol solvate and phase transition into anhydrous BDP within 2h. The sample was monitored under the AFM camera for 67 minutes. An external camera was used to capture the sample after 2h.

To avoid this, all measurement parameters were pre-set before starting the acquisition of any topographical AFM images. In addition, the scanning process was monitored visually until completion. As soon as the sample under investigation appeared to change, the AFM probe was removed to prevent the uptake of particulate matter and further damage. Where image acquisition was not possible under nitrogen, the topography was scanned in iso-octane using the Bruker liquid cell set up. IR spectroscopy before and after immersion in iso-octane for a

maximum of 1 h did not show any changes in the sample so that iso-octane was considered a suitable solvent to be used in liquid cell AFM set-up.

For AFM measurements carried out under dry conditions, the samples were glued onto a silicon wafer (Wacker Chemie AG, Germany) using Tempfix (Agar Scientific, UK), a thermoplastic adhesive, and the particle surfaces was scanned in soft-tapping mode. For measurements carried out in the liquid cell set up, the BDP solvates were attached to a silicon wafer in the same way and immersed into a 3 mm layer of iso-octane in a petri dish. The immersed sample was monitored visually at all times and no physical change was noted.

4.2 Results

The BDP particles crystallised from acetone and alcohol solutions were characterised and the influence of the respective solvents on different material characteristics was investigated.

4.2.1 FTIR

FTIR was used to distinguish between BDP in its solvated and anhydrous forms. For comparison, FTIR spectroscopy was also carried out using BDP monohydrate (Figure 4-3).

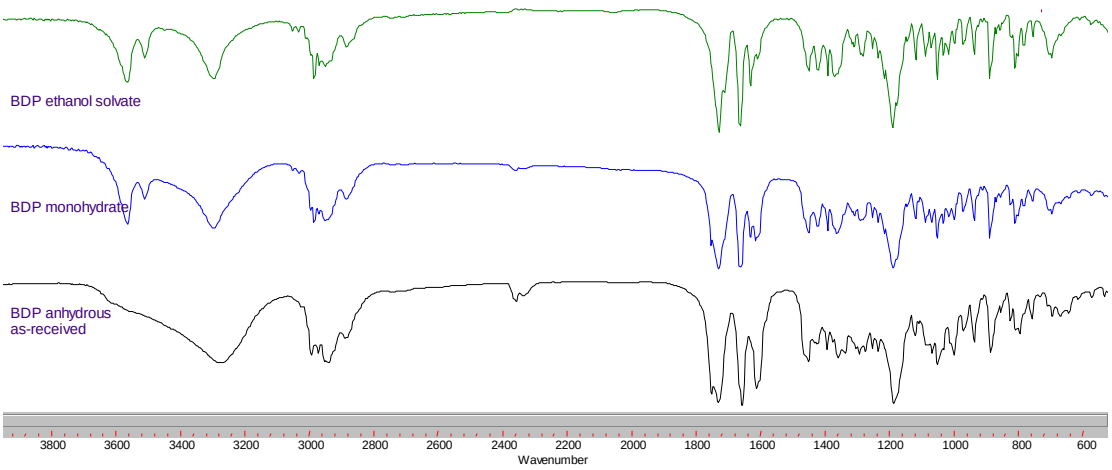

Figure 4-3. FTIR spectra (KBr, 64 scans, resolution 4 cm^{-1}) of the BDP ethanol solvate (top), BDP monohydrate (centre) and as–received anhydrous BDP (bottom).

The spectra of the BDP samples prepared from supersaturated solutions as outlined above differed from that of anhydrous BDP in noticeable peak shifts and peak broadening similar to those observed in crystalline BDP monohydrate (Hunt and Padfield, 1989). Additional broad signals, assigned to the hydroxyl groups of the solvent, appeared between 3450 cm^{-1} and 3600 cm^{-1} in all cases where alcohol was used.

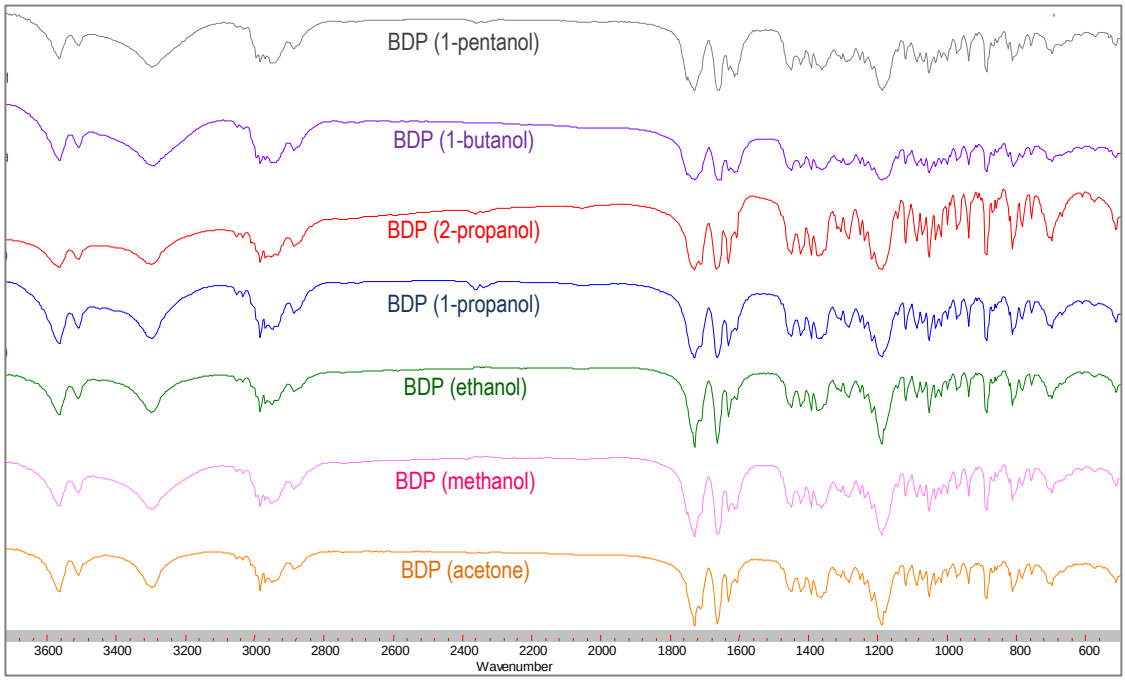

Figure 4-4. FTIR spectroscopy (KBr, 64 scans, resolution 4 cm^{-1}) of BDP crystallised from solution. The solvents used to prepare the respective samples are indicated below the FTIR signals.

The sharp signals defining the BDP carbon-carbon double bonds at 1614 cm^{-1} appeared to have shifted to 1631 cm^{-1}. The electron density in the double bonds was increased by the intermolecular bonding of the conjugated carbonyl group in C_3 position.

The signal at 1755 cm^{-1} had disappeared in all cases, indicating bonding to the ester carbonyl groups of BDP with an expected shift to smaller wavenumbers as reported for the BDP monohydrate (Hunt and Padfield, 1989). Similarly, intermolecular bonding to the BDP non-conjugated and conjugated carbonyl groups would lead to the signals at 1730 cm^{-1} shifting to lower and the peak at 1659 cm^{-1} to higher wavenumbers. These assumptions were again based on data reported for the BDP monohydrate (Hunt and Padfield, 1989). The BDP monohydrate crystallises in a different structure than the characterised BDP solvates (Kuehl et al., 2003, Harris et al., 2003, Othman et al.) but the same functional groups are involved in hydrogen bonding albeit in different intermolecular bonding.

All BDP samples showed slightly broadened peaks at 1730 cm^{-1}, yet only the samples prepared from methanol, ethanol, 1-propanol, 2-propanol and acetone solution had signals at 1713 cm^{-1} and 1665 cm^{-1}. These were not observed in the BDP prepared from longer alcohols, 1-butanol and 1-pentanol suggesting the formation of anhydrous BDP rather than solvates (Table 4-3).

Table 4-3. FTIR spectroscopy: Comparison of relevant signals (cm^{-1}).

Sample (solvent)	FTIR signals [cm^{-1}]						
BDP anhydrate	1614		1659			1730	1755
BDP monohydrate		1631		1665	1712	1730	
BDP (methanol)	1616	1631		1664		1730	
BDP (ethanol)		1631		1665	1713	1730	
BDP (1-propanol)		1632		1665	1714	1730	
BDP (2-propanol)		1632		1665	1713	1730	
BDP (1-butanol)	1616	1631	1660			1728	
BDP (1-pentanol)	1616	1631	1661			1730	
BDP (acetone)		1631		1665	1713	1730	

4.2.2 Thermal Analysis and Headspace GC-MS

DSC and TGA were used to investigate the effect of heating on the samples. As expected (Nachiengtung, 1997), the monohydrate (Figure 4-5) only showed the expected endothermic signal at approximately 100 °C coinciding with a mass loss of about 3.3 % (Figure 4-6). This indicated the release and evaporation of crystalline water which was followed by an exothermic phase transition (T_{onset} = 126.61 ºC, T_{max} = 132.30 °C) into the anhydrous form and melting starting at 212.65 °C (extrapolated onset temperature).

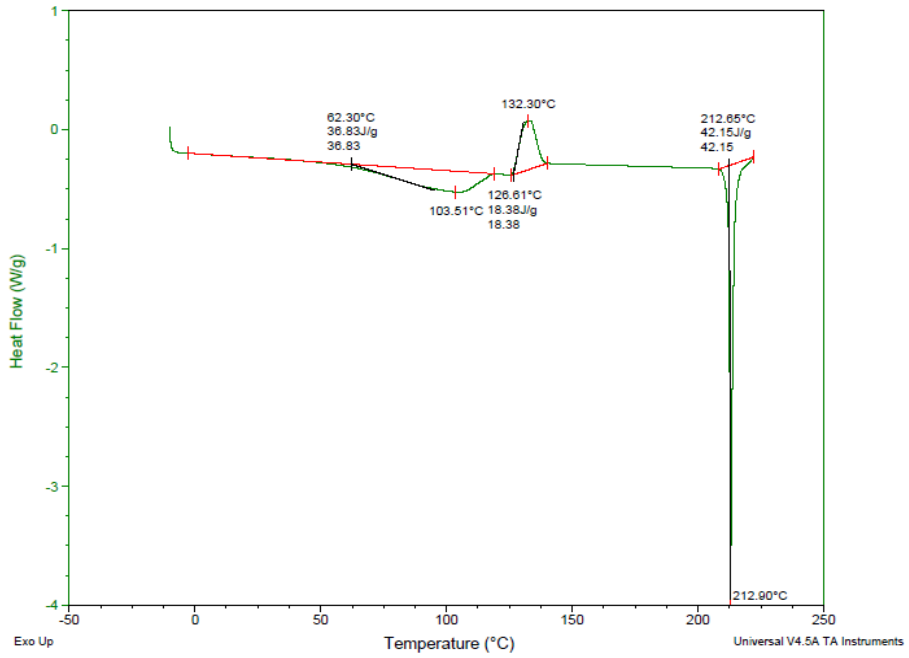

Figure 4-5. DSC analysis (10 °C/min) of BDP monohydrate showing the endo- and exothermic signals characteristic of BDP monohydrate (Nachiengtung, 1997).

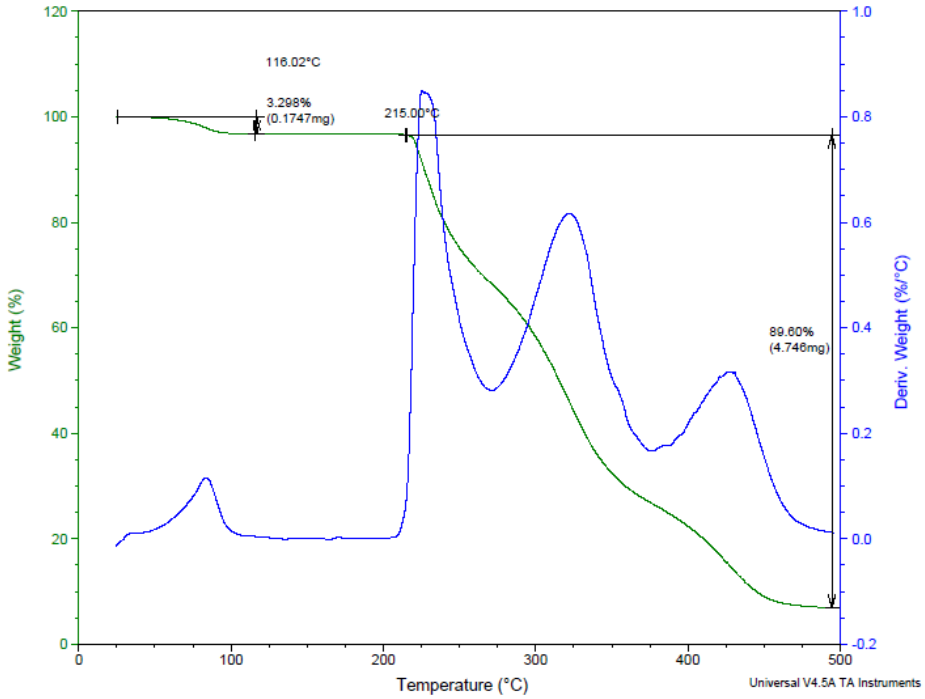

Figure 4-6 DSC analysis (10 °C/min) of BDP monohydrate showing the endo- and exothermic signals characteristic of BDP monohydrate (Nachiengtung, 1997)

In contrast, the DSC thermograms of all other BDP samples showed the gradual onset of an endothermic signal at lower temperatures (Table 4-4) which coincided with a reduction in mass (Table 4-5; Figures 4-7, 4-8, 4-9).

Table 4-4. Thermally induced desolvation calculated from DSC (extrapolated onset temperature, T_{on}). DSC indicated evaporation of excess solvent at low temperatures (Figures 4-7, 4-8, 4-9); n = 3, BDP-AC: n =6.

Sample (solvent)	Desolvation – extrapolated onset temperatures		
	1st T_{on} [°C]	2nd T_{on} [°C]	3rd T_{on} [°C]
BDP (methanol)	76.8 ± 3.1	-	-
BDP (ethanol)	96.1 ± 0.8	-	-
BDP (1-propanol)	108.3 ± 0.6	-	-
BDP (2-propanol)	107.0 ± 0.3	-	-
BDP (1-butanol)	71.6 ± 0.5	-	-
BDP (1-pentanol)	73.8 ± 1.0	-	-
BDP (acetone)[1]	83.5 ± 4.1	86.5 ± 2.8	-
BDP (acetone)[2]	67.0 ± 7.3	82.3 ± 0.9	104.1 ± 1.6

[1] BDP prepared from acetone with two endothermic signals.
[2] BDP prepared from acetone with three distinct endothermic signals separated by exothermic signals.

Table 4-5. Mass loss (TGA, Figures 4-7, 4-8, 4-9); n = 3, BDP-AC: n = 5.

Sample (solvent)	Mass loss due to desolvation		
	1st mass loss [%]	2nd mass loss [%]	3rd mass loss [%]
BDP (methanol)	1.3 ± 0.3	-	-
BDP (ethanol)	10.5 ± 0.2	-	-
BDP (1-propanol)	8.5 ± 0.9	5.4 ± 0.9	-
BDP (2-propanol)	6.6 ± 0.5	6.7 ± 0.6	-
BDP (1-butanol)	0.9 ± 0.3	-	-
BDP (1-pentanol)	-	-	-
BDP (acetone)[1]	14.4 ± 1.3	2.9 ± 0.1	-
BDP (acetone)[2]	11.6 ± 0.2	0.8 ± 0.1	0.2 ± 0.1

[1] BDP prepared from acetone showing two distinct mass loss signals.
[2] BDP prepared from acetone showing three distinct mass loss signals.

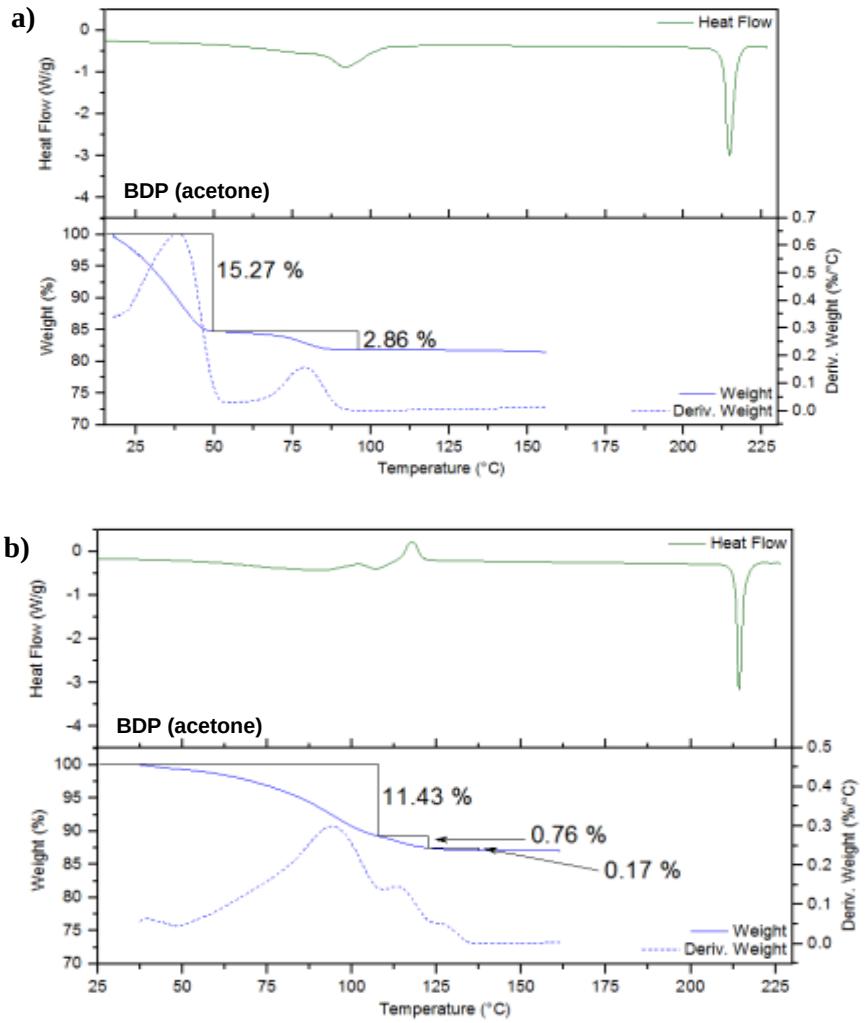

Figure 4-7. Thermal analysis (representative examples) of BDP prepared from acetone solution, showing a) two steps and b) three steps of desolvation. Top in green: DSC, 10 °C/min; bottom in blue: TGA, 10 °C/min, weight loss (in %) shown on images, dashed: first derivative; n = 5 (TGA), n = 6 (DSC). Exo up.

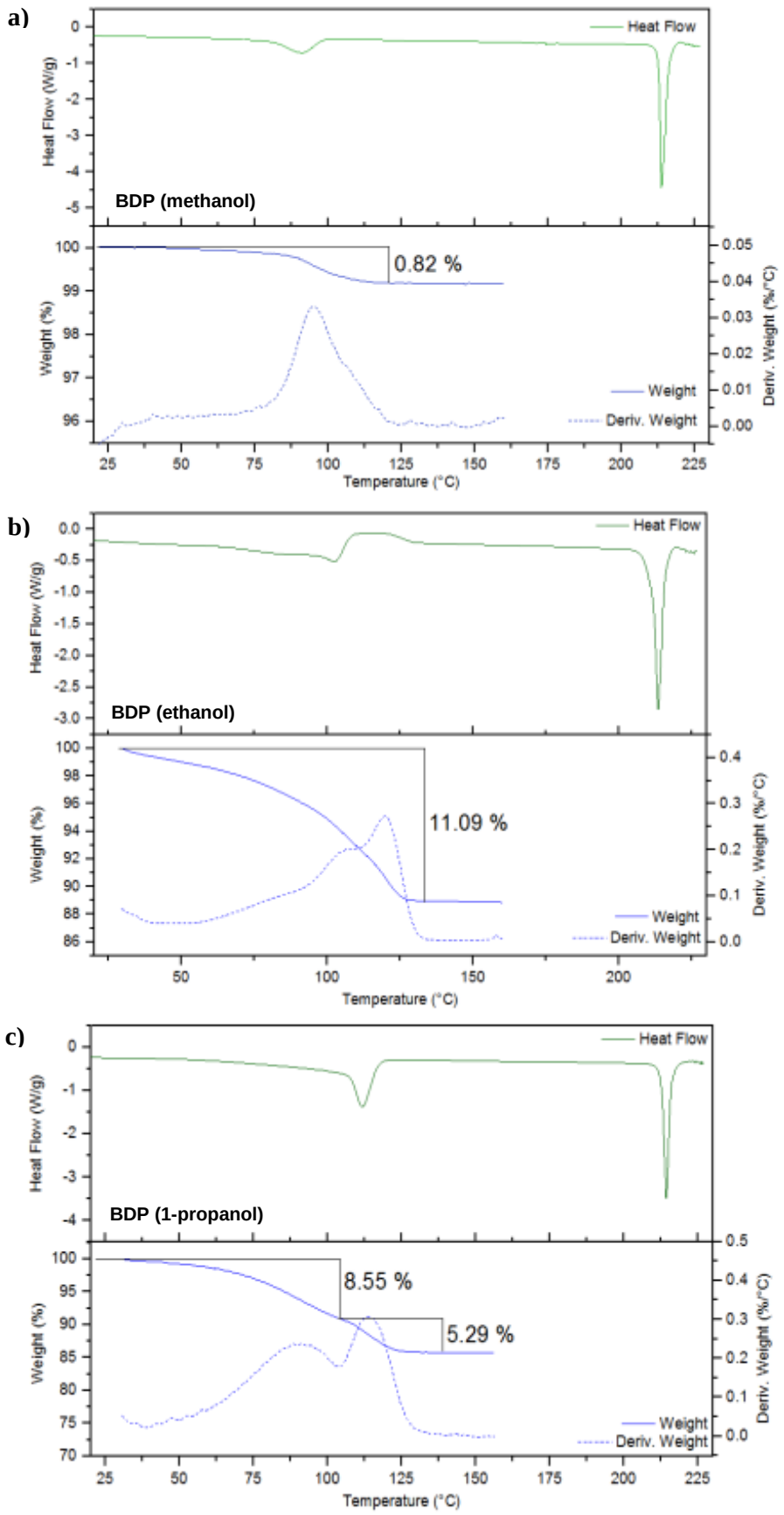

Figure 4-8. Thermal analysis (representative examples) of BDP prepared from solutions of a) methanol, b) ethanol c) 1-propnaol. Top in green: DSC, 10 °C/min; bottom in blue: TGA, 10 °C/min, weight loss (in %) shown on images, dashed: first derivative; n = 3. Exo up.

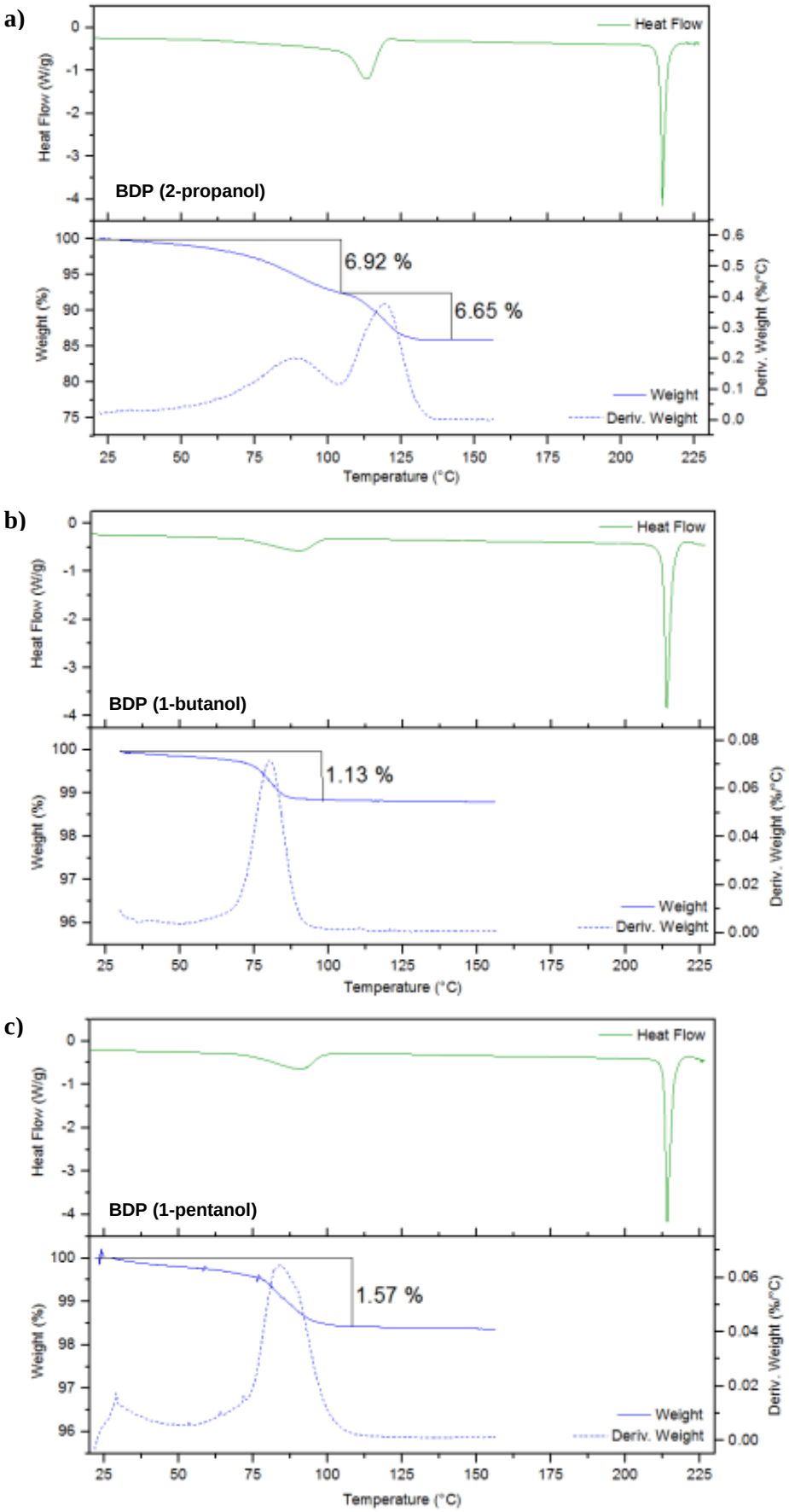

Figure 4-9. Thermal analysis (representative examples) of BDP prepared from solutions of a) 2-propanol, b) 1-butanol, c) 1-pentanol. Top in green: DSC, 10 °C/min; bottom in blue: TGA, 10 °C/min, weight loss (in %) shown on images, dashed: first derivative; n = 3. Exo up.

To analyse the origin of the endothermic signal, headspace GC-MS was carried out where the separation of the analytes is based on their respective vapour pressure/boiling point and their interaction with the separation column.

Mass spectrometry (MS) was used to identify the analytes (Table 4-6). The characteristic signal at m/z 31, often used to identify linear alcohols, was not visible on account of the MS cut-off at m/z 40. This threshold also made it impossible to detect methanol and ethanol.

Table 4-6. Headspace GC-MS results including retention times (tr) and m/z signals (limited to ≥ 40 m/z).

Sample (solvent)	Headspace GC-MS	
	t_r [min]	m/z
BDP (methanol)	-	-
BDP (ethanol)	-	-
BDP (1-popanol)	1.909	59, 43, 42, 41
BDP (2-popanol)	1.711	45, 43, 41.1
BDP (1-butanol)	2.555	56.8, 55.9, 55, 43, 41.9, 40.9
BDP (1-pentanol)	3.678	70.8, 70, 68.8, 56.9, 56, 55, 43, 42, 41
BDP (acetone)	1.71	42.8, 41.8

Headspace GC-MS (Table 4-6) confirmed the release of the solvent over the respective temperature range and FTIR analysis (Table 4-3) proved the conversion into anhydrous BDP. These findings suggested that the endothermic signal was either caused by the desolvation of a solvate or by the evaporation of residual surface solvent.

Despite not all samples showing an exothermic signal indicative of phase transition, the mutual melting point at 213 °C suggested that anhydrous BDP had been formed at some stage during the process. In all cases, the second heating cycle matched the DSC graph (Figure 2-7) obtained from as-received anhydrous BDP which further confirmed the conversion into anhydrous BDP.

The endothermic signals seen in the DSC graphs of the samples prepared from ethanol, 1-propanol, 2-propanol and acetone indicated solvent evaporation. In addition, an exothermic signal (Figures 4-7, 4-8b, c, 4-9a; Table 4-7) was observed after the desolvation peak, indicating that a transformation had occurred.

Table 4-7. Phase transition based on DSC, exothermic signals (extrapolated onset temperature, T_{trans}); n = 3, BDP (acetone): n = 6.

Sample (solvent)	Desolvation – extrapolated onset temperatures	
	1st T_{trans} [°C]	2nd T_{trans} [°C]
BDP (ethanol)	108.1 ± 1.6	-
BDP (1-propanol)	120.5 ± 0.2	-
BDP (1-propanol)	119.3 ± 0.2	-
BDP (acetone)[1]	113.1 ± 0.9	-
BDP (acetone)[2]	101.2 ± 1.2	113.1 ± 1.9

Based on their thermal behaviour, the BDP samples prepared from solution were divided into three groups. The same grouping had been observed in FTIR analysis (Table 4-3).

BDP prepared from 1-butanol and 1-pentanol

In these two samples, the solvent was released below the boiling point of their respective solvents (Figure 4-7, Table 4-3). BDP-BU exhibited minimal mass loss (≤ 1 %), while the mass loss from BDP-PE varied considerably from sample to sample between 1.6 % and 8.5 % (Table 4-4). Neither sample displayed any exothermic transition signal prior to melting which occurred at 213 °C, the characteristic melting point of the anhydrous form of BDP (Nachiengtung, 1997, Bouhroum et al., 2010). These results suggest that the BDP crystallised in its anhydrous form from these solvents and that the mass loss at low temperatures was residual surface solvent evaporation. The same samples showed FTIR signals matching the signals characteristic of anhydrous BDP at 1616 cm^{-1}, 1631 cm^{-1},1660 cm^{-1} and 1728 cm^{-1} (Table 4-3).

BDP prepared from ethanol, 1-propanol, 2-propanol and acetone

In these four samples, the solvent was released at temperatures above the boiling points of their respective solvents (Table 4-3), suggesting that it was due to desolvation rather than residual solvent evaporation. These samples all exhibited significant mass loss between 11 % and 24 % during this event (Table 4-4). All four samples then showed an exothermic signal without any simultaneous mass loss between 110 °C and 120 °C (Figures 4-7, 4-8b, c, 4-9a; Table 4-7), which is characteristic of a phase transition. In contrast to BDP prepared from ethanol, 1-propanol and 2-propanol, however, BDP prepared from acetone exhibited either two or three mass loss events divided by an exothermic signal (Figure 4-7; Tables 4-5, 4-6, 4-7). In this temperature region. In both cases, the mass loss was followed by a phase transition at ~113 °C and the samples melted at ~213 °C. Yet acetone is likely to interact in a different way with the BDP host due to its different functionality and was found to evaporate in either two or three steps with one or two phase transitions occurring before melting at the temperature characteristic of anhydrous BDP (Nachiengtung, 1997, Wang et al., 2007). This was possibly due to the solvent

molecules being more or less strongly retained within the BDP host or to an intermediate form forming in between.

DSC analysis was also performed on the samples using hermetically sealed DSC (data not shown). In all cases, the initial broad endothermic peak disappeared showing that it could be fully attributed to desolvation rather than concurrent desolvation and melting. Thus, the exothermic peaks marked a monotropic solid-solid exothermal transition (Nachiengtung, 1997) rather than recrystallisation following a melt. Observations of BDP solvates crumbling and forming anhydrous BDP under nitrogen conditions (Figure 4-2) further supported monotropic solid-solid transition.

BDP prepared from ethanol, 1-propanol, 2-propanol and acetone showed matching FTIR spectra with the signals at 1632 cm^{-1}, 1665 cm^{-1}, 1713 cm^{-1} and 1730cm^{-1} (Table 4-3) indicating solvate formation.

BDP prepared from methanol

This sample displayed mixed behaviour. The onset of the solvent release was well above the boiling point of methanol, suggesting that it was not simply evaporation of residual solvent (Figure 4-7, Table 4-4). However, the mass loss was quite low (1.3 ± 0.3%) and no exothermic transformation peak was observed (Figure 4-8a, Table 4-7). The sample melted at the characteristic temperature of anhydrous BDP (Nachiengtung, 1997). It is possible that the BDP prepared from methanol initially formed as a very unstable solvate, which desolvated during handling, returning to a predominantly anhydrous form. The observed mass loss was due to small amounts of solvated BDP in the sample which had not yet transformed. This would account for the high onset temperature. However, as there was very little solvated BDP remaining in the sample, the mass loss was very low and the transformation peak was too small to be observed by DSC.

FTIR data (Table 4-3) also showed signals both characteristic of anhydrous BDP (1616 cm^{-1}, 1730 cm^{-1}) and indicative of the solvated form (1631 cm^{-1}, 1664 cm^{-1}).

4.2.3 X-ray Powder Diffraction

XRPD (Figures 4-10, 4-11) was used to distinguish solvated BDP from anhydrous BDP and to investigate possible differences between the BDP ethanol solvate (Figure 4-11), a known channel solvate (Kuehl et al., 2003), and the BDP crystals which were prepared from other solvents.

Modelled XRPD spectra (Mercury 3.3) of the anhydrous form (Figure 4-9, grey) (Millard and Myrdal, 2002) and the BDP ethanol solvate (Figure 4-11, grey) (Kuehl et al., 2003) along with

the XRPD pattern of as-received anhydrous BDP (black in Figures 4-10, 4-11) were used as references.

It should be noted that the actual XRPD pattern characterising the as received anhydrous BDP differed from the predicted one. However, all differences were found to be within an acceptable range (± 0.2 °2θ of the ten strongest signals according to 1995 USP 23/NF).

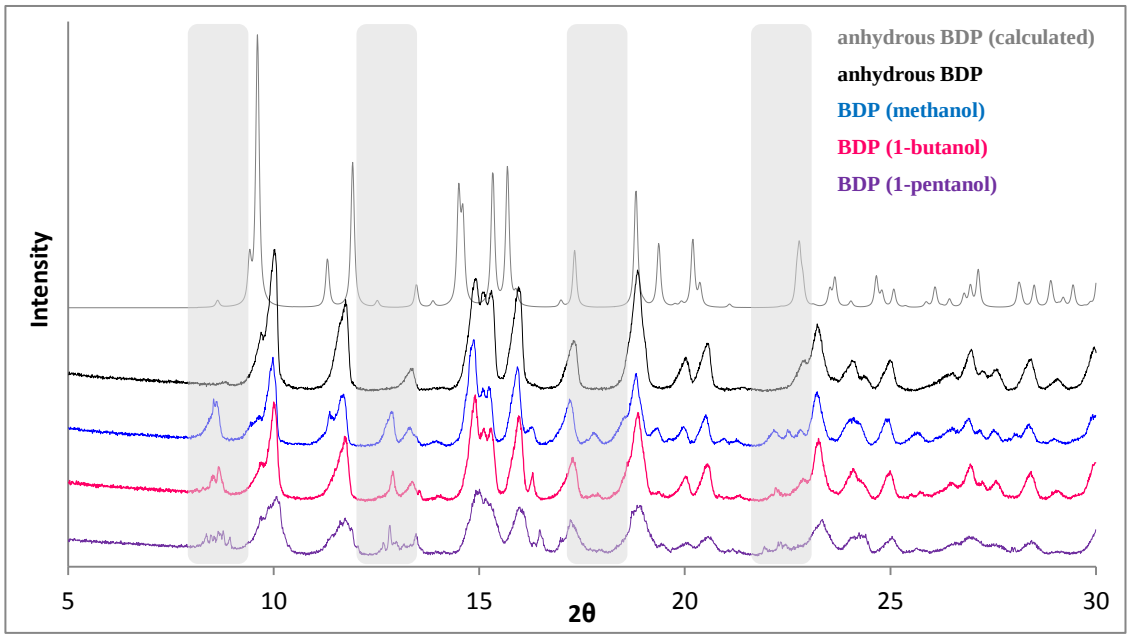

Figure 4-10. XRPD of anhydrous BDP (modelled, Mercury 3.3 Crystal Structure Visualisation Software, and as-received) and BDP prepared from methanol, 1-butanol and 1-pentanol as indicated in the legend. Differences to the as-received anhydrous form (black) are highlighted in grey.

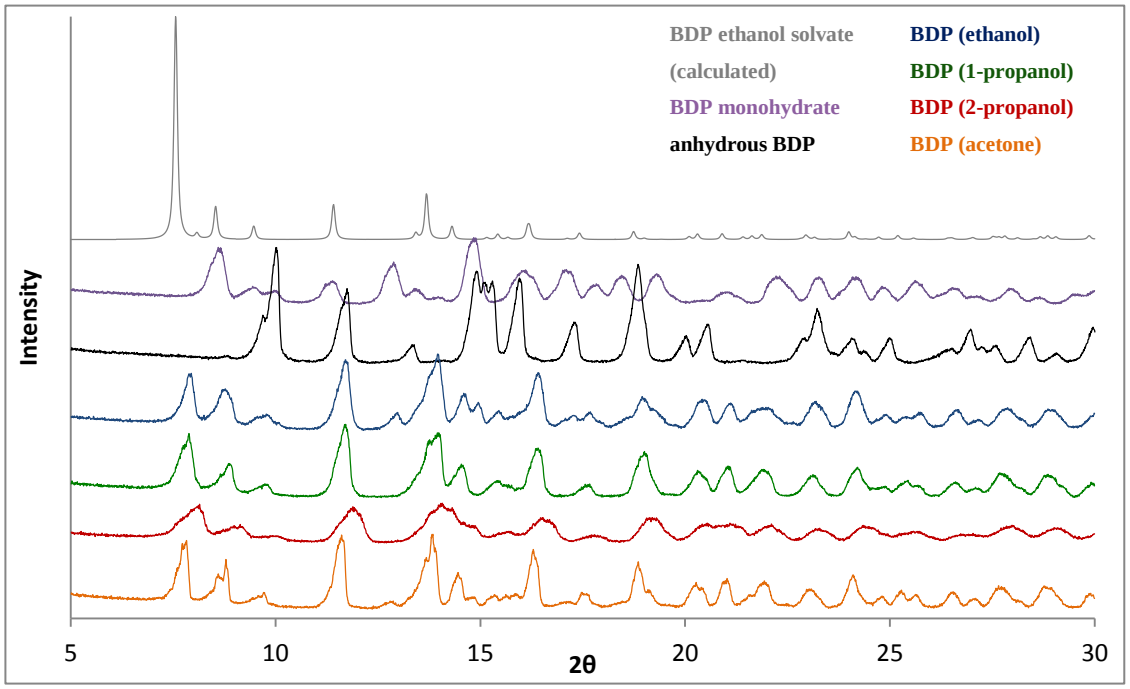

Figure 4-11. XRPD of BDP ethanol solvate (modelled, Mercury 3.3 Crystal Structure Visualisation Software) and BDP prepared from ethanol, 1-propanol, 2-propanol and acetone as indicated in the legend. Anhydrous BDP and BDP monohydrate included for comparison.

The results showed that the recrystallisation of BDP in alcohol and acetone as described above led to the formation of different compounds which were divided in two groups. One group showed distinctive thermal behaviour and the compounds were found to have XRPD patterns similar to the anhydrous form. The other group appeared to form solvates similar to the BDP ethanol solvate (Kuehl et al., 2003).

BDP prepared from methanol, 1-butanol and 1-pentanol

The XRPD spectra of BDP prepared from methanol, 1-butanol and 1-pentanol were similar to as-received anhydrous BDP (Figure 4-10, 4-11) but differences in peak intensities at 8.5 °2θ and several additional signals were noted (Figure 4-10, highlighted in grey). The as-received anhydrous BDP had a single low intensity signal at 8.5 °2θ whereas the BDP prepared from methanol, 1-butanol and 1-pentanol displayed signals of higher relative intensity and with an increasing number of peaks in this range. At 11.8 °2θ, BDP (methanol) showed two peaks. This split was not observed in any other sample. The single peak at 13.4 2θ seen in the spectrum of the as-received anhydrous BDP, however, was split into two or more signals in all BDP samples prepared from methanol, 1-butanol and 1-pentanol. Additional signals, not present in the as-received anhydrous form, appeared at 16.3 °2θ, 17.9 °2θ, 19.4 °2θ and, less pronounced, at higher °2θ values.

Such variations to the underlying spectrum suggested that impurities or small amounts of solvated BDP were present in the samples. TGA showed a small mass loss of approx. 1 % at low temperatures (Table 4-5). In XRPD, this would produce additional signals and decrease the overall resolution as seen in Figure 4-10.

BDP prepared from ethanol, 1-propanol, 2-propanol and acetone

The XRPD patterns of BDP prepared from ethanol, 1-propanol, 2-propanol and acetone solution corresponded to the modelled pattern (Mercury 3.3 Crystal Structure Visualisation Software) of the BDP ethanol solvate (Figure 4-11, grey) (Kuehl et al., 2003) rather than that of the anhydrous form (Figure 4-10, black), confirming the presence of BDP solvates. Apart from showing differences in resolution and peak intensity, signals were found in slightly varying positions. The signal at 8.7 °2θ, present in all XRPD spectra, split into two signals in BDP (1-propanol) and BDP (acetone) (Figure 4-7). The same appeared to happen to the peak at 14.5 °2θ. Additional signals were seen in BDP (ethanol) and BDP (acetone) at 12.9 °2θ and 14.9 °2θ which were not present in BDP (1-propanol) and BDP (2-propanol). The BDP prepared from ethanol solution had an additional signal at 17.5 °2θ.

Any differences in resolution and intensity may be explained by the presence of particles in various states of desolvation. As reported previously, the BDP ethanol solvate may not be stable under standard conditions (Kuehl et al.,2003). This was also observed when carrying out SEM

analysis at low pressure (Figure 4-1) and AFM imaging under nitrogen (Figure 4-2). The gradual evaporation of solvent would be expected to destabilise the channel structure and cause the formation of anhydrous BDP during the XRPD measurement. In addition, the gradual desolvation may have added to the strain acting on the crystalline structure, thus leading to small changes within the lattice parameters of the affected crystals. This would in turn explain the differences in the peak intensity and peak broadening and may also have led to slightly shifted peak positions (Jenkins and Snyder, 1996).

4.2.4 Microscopic Analysis

Microscopy, SEM and topographical AFM, were used to image the particles, to visually examine their shape and to quantify their surface roughness.

The particles could be roughly divided into two groups based on shape and ruggedness (Figures 4-12, 4-13).

BDP prepared from acetone, methanol, 1-butanol, 1-pentanol

This group appeared to consist of particles of more irregular shape including flakes, rugged fragments and larger particles with a seemingly smoother surface. This was attributed to the presence of anhydrous BDP and BDP in various states of desolvation as indicated by thermal analysis and XRPD for BDP prepared from methanol, 1-butanol and 1-pentanol.

While BDP prepared from acetone appeared to have a rough surface and irregular shape too (Figure 4-12d), thermal analysis and XRPD indicate that a solvate was formed. Yet acetone is likely to interact in a different way with the BDP host due to its different functionality and was found to evaporate in several steps, possibly while forming an intermediate form in between.

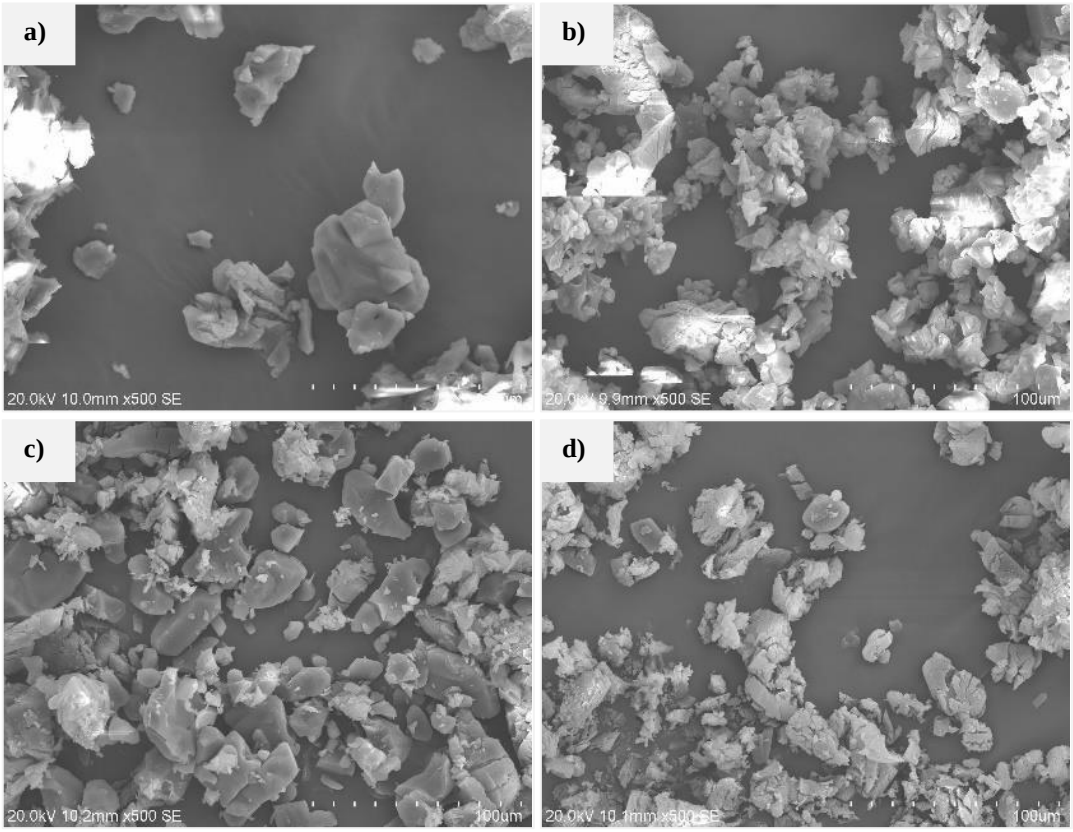

Figure 4-12. SEM images (x500) of BDP prepared from a) methanol, b) 1-butanol, c) 1-pentanol and d) acetone.

BDP prepared from ethanol, 1-propanol and 2-propanol

In contrast, the samples prepared from ethanol, 1-propanol and 2-propanol resulted in the formation of more regularly shaped crystals with increased elongation (Figure 4-13). While the sample prepared from 1-propanol appeared to have a less distinctive elongation compared to BDP prepared from ethanol and 2-propanol, all three samples were found to have a similar aspect ratio between 0.693 and 0.710 and a mean elongation of about 300 (Figure 4-14). This matched the already reported and filed BDP ethanol solvate that has a characteristically elongated hexagonal unit cell (Kuehl et al., 2003).

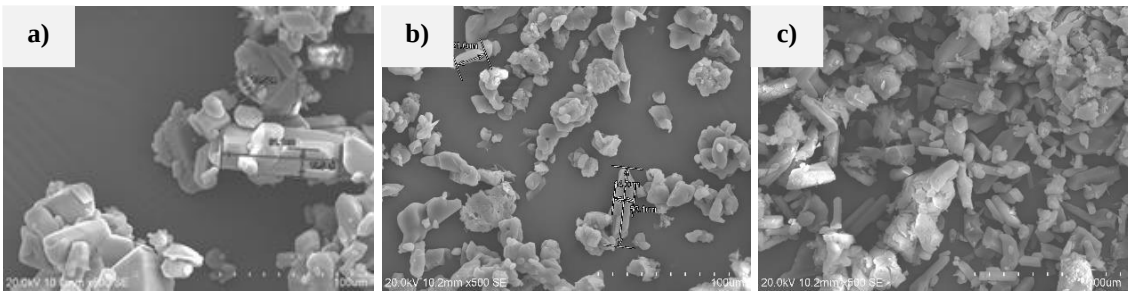

Figure 4-13. SEM images (x500) of BDP prepared from a) ethanol, b) 1-propanol and c) 2-propanol.

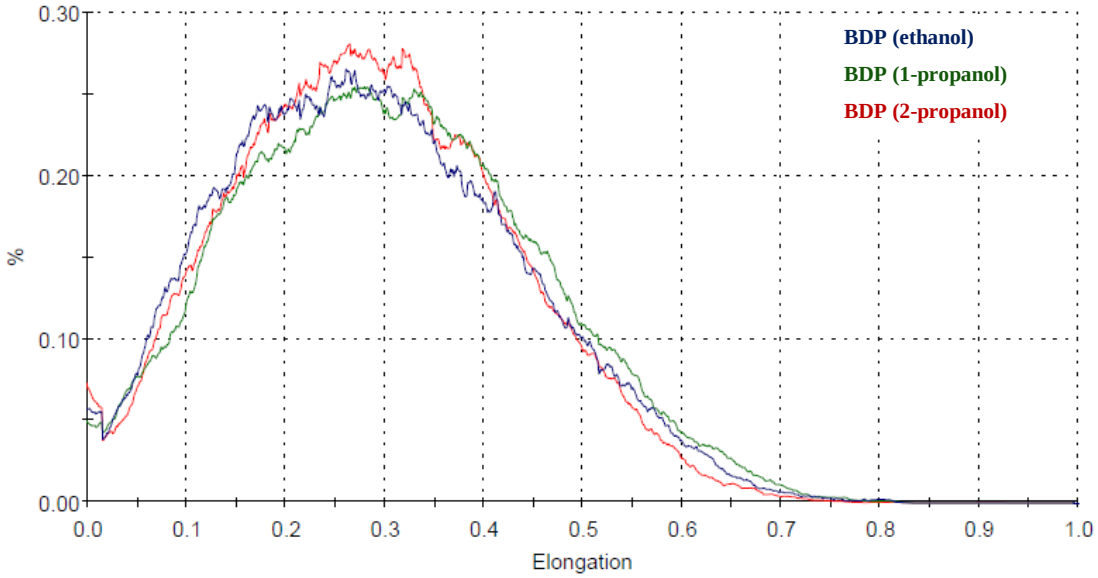

Figure 4-14. Elongation of BDP prepared from ethanol (blue), 1-propanol (green) and 2-propanol (red) based on Morphologi G3 image analysis.

Large crystals had been selected from each group as representative examples for AFM. BDP prepared from methanol (Figure 4-15), representative of the first group, appeared to have a more irregular shape than BDP prepared from ethanol (representing the second group, Figure 4-16) which formed an elongated smooth crystal. In addition, the BDP ethanol crystal was more resistant to low pressure and electron bombardment under the SEM. Cracking and crumbling occurred at a slower pace (Figures 4-15, 4-16).

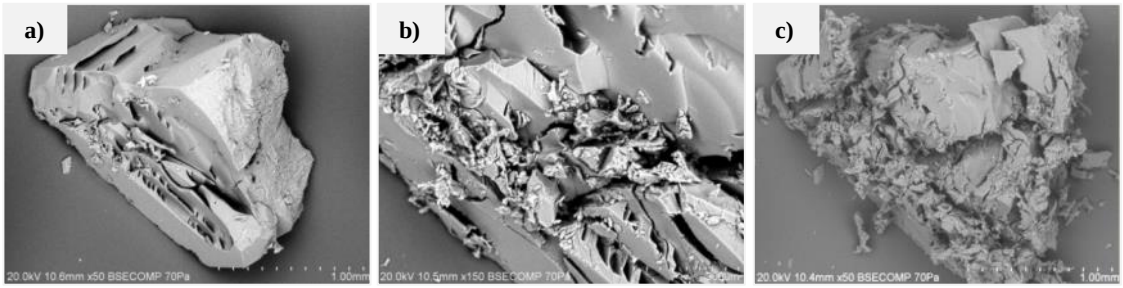

Figure 4-15. Gradual cracking of BDP crystallised from methanol solution (SEM, x50, 70 Pa, 20 kV).

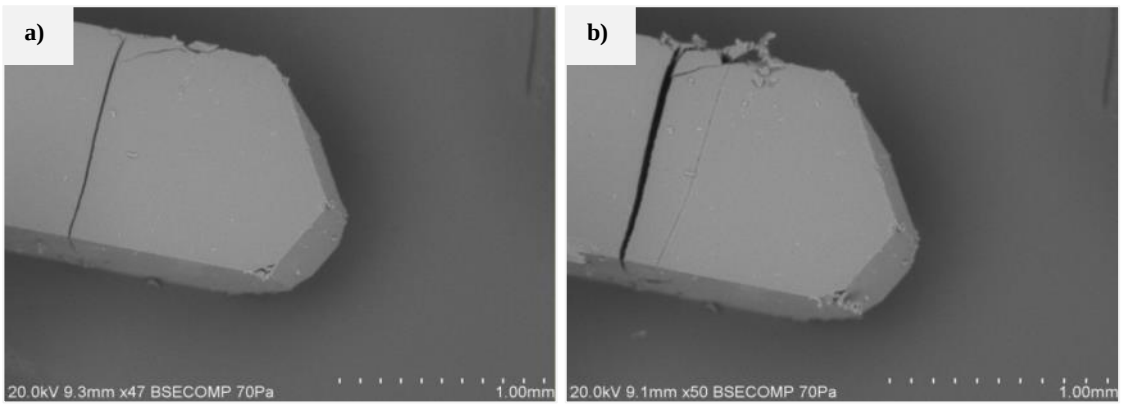

Figure 4-16. Gradual cracking of BDP crystallised from ethanol solution (SEM, x50, 70 Pa, 20 kV).

AFM was used to acquire topographical maps of each sample. These maps (representative maps: Figure 4-17) were evaluated quantitatively and ten roughness measurements were carried out on randomly chosen spots (spot size of 1 μm^2) on each height map to obtain an average value representative of the sample surface. Two values are commonly reported when comparing surface roughness: the root mean square roughness, R_q, (Equation 4-1) where Z_i is the peak-to-valley height difference within the selected area (1 μm^2) and N represents the number of data points within that area and the arithmetic average roughness, R_a, (Equation 4-2) which represents the arithmetic average of the absolute surface height deviations, Z_j, from the mean plane of the selected area (1 μm^2).

$$R_q = \sqrt{\frac{\sum Z_i^2}{N}} \tag{4-1}$$

$$R_a = \frac{1}{N}\sum_{i=1}^{N}|Z_j| \tag{4-2}$$

The roughness measurements (Table 4-8) confirmed the exceptional smoothness of BDP prepared from ethanol (Figure 4-13a, 4-17a) and 1-propanol (Figure 4-13b). Quantitative analysis of the surface of BDP prepared from 2-propanol (Table 4-8) showed a surprisingly rough surface compared to the visual impression from SEM imaging (Figure 4-13c). The irregular surface texture of BDP prepared from 1-pentanol solution (Figures 4-12c, 4-17b) was reflected in AFM based quantitative evaluation (Table 4-8).

Table 4-8. Surface roughness of BDP prepared from solution: root mean square, R_q, and arithmetic average R_a, both based on n = 10 areas of 1x1 μm^2 (AFM height maps).

Sample (solvent)	R_q [nm]	R_a [nm]
BDP (methanol)	52.8 ± 23.6	41.7 ± 19.6
BDP (ethanol)	13.1 ± 8.4	10.1 ± 6.9
BDP (1-propanol)	17.0 ± 7.2	5.7 ± 3.1
BDP (2-propanol)	67.2 ± 25.4	53.0 ± 18.3
BDP (1-butanol)	65.0 ± 25.3	50.8 ± 20.7
BDP (1-pentanol)	150.2 ± 65.5	123.6 ± 55.3
BDP (acetone)	92.8 ± 23.1	76.9 ± 18.9

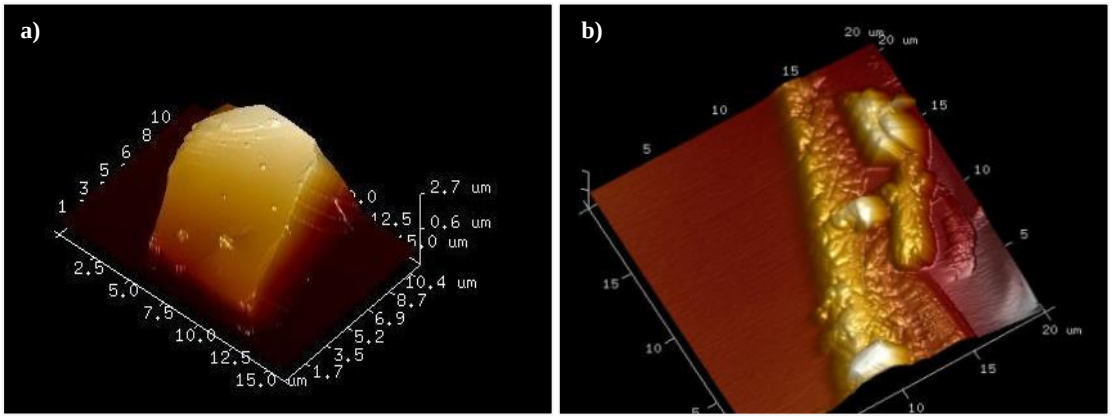

Figure 4-17. AFM topographical mapping of BDP prepared from a) ethanol (R_q = 13.1 ± 8.4 nm) and b) 1-pentanol (R_q = 150.2 ± 65.5 nm); n = 10.

4.2.5 Particle Size Analysis

The PSD obtained from dry powder particle size analysis (Table 4-9) gave a good estimation of the PSD of BDP prepared as described in paragraph 4.4.1 and were used as a reference for further studies. As seen from SEM imaging, the BDP solvates formed either irregular flakes or slightly elongated particles. Depending on the alignment of each particle at the time of the measurement, the algorithm uses either the long or the short side to calculate the PSD.

Table 4-9. PSD (µm, percentile d10, d50, d90) of BDP prepared from solution as indicated in brackets.

Sample (solvent)	d_{10} [µm]	d_{50} [µm]	d_{90} [µm]
BDP (methanol)	2.98	7.71	17.74
BDP (ethanol)	3.18	10.29	25.55
BDP (1-propanol)	2.84	10.89	32.09
BDP (2-propanol)	2.97	9.02	21.49
BDP (1-butanol)	3.14	11.03	40.18
BDP (1-pentanol)	3.68	12.65	39.27
BDP (acetone)	4.09	20.13	69.77

4.3 Discussion

The shape, thermal stability, and structure of crystalline BDP appeared to depend on the solvent used in the process of crystallisation. XRPD indicated that the use of methanol, 1-butanol and 1-pentanol resulted in predominantly anhydrous BDP whereas using ethanol, 1-propanol, 2-propanol and acetone led to the formation of BDP solvates with solvent molecules being incorporated within a channel structure. Based on XRPD, the crystalline structure was assumed to be similar to that of the known BDP ethanol solvate (Kuehl et al., 2003) but specific solvent properties such as size and polarity may influence the host-guest interactions and the arrangement of the molecules within the unit cell. The development of hydrogen bonds has an

impact on the stoichiometry and, together with the length of the solvent molecule and the degree of branching, affects the channel volume (Suitchmezian et al., 2006, Chavez et al., 2010). In addition, the degree of supersaturation is known to influence the probability of nucleation. Increased supersaturation reduces the energy barrier and critical size that control the kinetics of nucleation and need to be overcome before a nucleus becomes stable and crystal growth can set in. Crystal growth, too, is facilitated by higher supersaturation due to more solute molecules being available for crystallisation. The solvent molecules in turn may act as a barrier and facilitate or hinder the solute from accessing certain faces or sites on the growing crystal. This may lead to a preferred growth direction, thus giving the crystal its unique shape. Solvate formation occurs when the free energy of the solvate is lower than that of the crystal without any guest molecules (De Yoreo and Vekilov, 2003). It was therefore assumed that the solvent molecules were oriented along the crystal, possibly forming weak bonds to the BDP host molecule. The BDP molecules appeared to arrange themselves around the solvent so that host-guest compounds are formed which was suggested to lead to the formation of a BDP clathrate structure where the solvent is highly mobile within the channel structure of the crystal (Kuehl et al., 2003, Othman et al., 2008).

TGA and DSC suggested the formation of channel solvates with ethanol, 1-propanol, 2-propanol and acetone guest molecules forming a crystalline structure with the BDP host. The solvent molecules were incorporated within the channels and desolvation only occurs at temperatures above the boiling points of the solvents (Figures 4-7, 4-8b, c, 4-9a). On account of the similarities between the modelled and the actual XRPD pattern (Figure 4-11) it can be assumed that the solvent is present within a channel structure. Host-guest interactions such as hydrogen bonding may occur, the size and flexibility of the guest compound and the position of the functional group may have an impact on the arrangement of the molecules relative to each other and on the binding strength between host and guest. In addition, these factors may influence the volume of the channels slightly (Suitchmezian et al., 2006, Chavez et al., 2010). This would manifest itself in slightly varying lattice parameters, thus also in shifted XRPD signals while the overall pattern and relative peak positions would still be the same. Peak broadening and peak intensity are affected by preferred orientation, amorphous content, size distribution and residual stress and strain acting on the crystal during the measurement (Jenkins and Snyder, 1996).

The samples prepared from BDP ethanol, 1-propanol, 2-propanol and acetone solution appeared to be similar in that they are the only compounds that were found to form solvates as shown in FTIR (Table 4-3), thermal analysis (Figures 4-7, 4-8b, c, 4-9a) and XRPD (Figure 4-11). BDP prepared from ethanol, 1-propanol and 2-propanol had a regular, slightly elongated shape in agreement with reported crystalline data of the BDP ethanol solvate (Kuehl et al., 2003) with BDP prepared from ethanol and 1-propanol) also having a significantly smoother surface than

the other samples (Table 4-8). This might be due to solvent inclusion. The incorporation of solvent molecules is known to have an impact on the host-guest compound and the impact increases with an increasing solvent content (Chavez et al., 2010).

The stoichiometric ratio of solvent to BDP molecules (molar ratio r_{mol}) was calculated for the samples from the TGA percentage mass loss (Table 4-5) using equations 4-3 and 4-4 where *MW* stands for molecular weight.

$$mass\ loss\ (\%) = \frac{r_{mol} \cdot MW_{solvent}}{r_{mol} \cdot MW_{solvent} + MW_{BDP}} \quad (4\text{-}3)$$

$$r_{mol} = \frac{mass\ loss\ (\%) \cdot \frac{1}{100} \cdot MW_{BDP}}{MW_{solvent} - mass\ loss\ (\%) \cdot \frac{1}{100} \cdot MW_{solvent}} \quad (4\text{-}4)$$

The calculations were based on the average mass loss from a minimum of three different batches. The combined mass loss was taken into account for BDP (1-propanol) and BDP (2-propanol). Due to large variations observed in the mass loss of BDP (1-pentanol) the stoichiometric ratio was not calculated for this sample. As before, two trends could be distinguished (Table 4-10) and the results were divided into two groups.

Table 4-10. Molar ratio (solvent:BDP) calculated from TGA (Table 4-5); n = 3, BDP-AC: n = 5.

Sample (solvent)	Molar ratio (solvent:BDP)
BDP (methanol)	0.22 ± 0.05
BDP (ethanol)	1.33 ± 0.02
BDP (1-propanol)	1.40 ± 0.08
BDP (2-propanol)	1.33 ± 0.05
BDP (1-butanol)	0.07 ± 0.02
BDP (1-pentanol)[1]	-
BDP (acetone)[2]	1.88 ± 0.06
BDP (acetone)[3]	1.30 ± 0.01

[1] BDP prepared from 1-pentanol: mass loss between 1.6 % and 8.5 %, BDP:1-pentanol ratio was not calculated.
[2] BDP prepared from acetone showing two distinct mass loss signals.
[3] BDP prepared from acetone showing three distinct mass loss signals.

BDP prepared from ethanol, 1-propanol, 2-propanol and acetone

BDP prepared from ethanol, 1-propanol, 2-propanol and acetone again formed one group. The samples were all found to incorporate similar stoichiometric amounts of solvent. The similarity of the stoichiometric ratio indicated that the accessible channel volume was independent of the solvent used and solely dependent on the host molecule.

BDP prepared from methanol and 1-butanol

The samples prepared from methanol and 1-butanol had a very low stoichiometric ratio which confirmed the assumption that only excess surface solvent evaporated during thermal analysis. The methanol molecules were too small to be retained within the channel where the solvent molecules are likely to be highly mobile (Kuehl et al., 2003, Harris et al., 2003) whereas 1-butanol was too large to penetrate the channels. Considering that the size of linear alcohols increases with increasing chain length, it was assumed that 1-pentanol, too, was too large to properly fit into the channels.

Within the crystalline structure of the first group, weak hydrogen bonding may occur between the hydroxyl proton of the alcohols and the keto and hydroxyl groups of the BDP host which would facilitate the alignment of the guest alcohol molecules along the direction of the channel within the host structure, thus stabilising the crystalline structure. Desolvation was found to occur gradually as seen by the broad endothermic peaks and appeared to destabilise the structure which then collapsed into the anhydrous form in a monotropic solid-solid transition. Yet the position of both the endothermic desolvation signal and the exothermic transition peak varied considerably. Differences regarding the width of the endothermic event were expected due to different rates of evaporation on account of the manually pierced lids covering the DSC pans (Gabbott, 2008). The shape, size and position of the pin holes has a considerable impact on the visible onset of desolvation and the shape of the broad endothermic peak as the pin holes restrict the evaporation of the solvent (Haines, 2002). Even though all pin holes were punched with the same sharp pin which was inserted to an equal depth in all cases, small variations cannot be ruled out and need to be taken into account when interpreting the data.

The gradual onset of desolvation may be the result of the evaporation of solvent from the channels due to slow migration of the solvent molecules along the host channels and towards the surface, followed by evaporation (Morissette et al., 2004). This is facilitated by only weak host-solvent interactions. The BDP ethanol solvate had previously been found to contain ethanol in a highly mobile, freely flowing state (Kuehl et al, 2003), similar to ethyl acetate in the ethyl acetate solvate (Othman et al., 2008). Desolvation therefore occurred gradually which in turn led to the gradual collapse of the solvent filled channels, thus maintaining the crystalline structure over a longer period of time. This might be the reason for the crystalline shape being translated from the solvate to the anhydrous form. The gradual phase transition, seen in the relatively broad exothermic DSC signal (Figures 4-7, 4-8b, c, 4-9a) was also beneficial for a reproducible and controlled process. A sudden collapse, in contrast, would have resulted in irregularly shaped particles and a large PSD.

Samples having a low solvent:BDP ratio such as seen in BDP prepared from methanol (0.22) and BDP prepared from 1-butanol (0.07) were irregular shaped and FTIR, XRPD and thermal analysis indicated the presence of anhydrous material in the samples. Particle shape is known to be strongly influenced by the interactions occurring between solvent and seeds during the growth process (De Yoreo and Vekilov, 2003). It was therefore expected that acetone and alcohols affect the crystalline shape in distinct ways. The strength of possible interactions due to the acidity of the alcohol hydrogen and the polarity of the solvent further impacted the crystal growth. In addition, the degree of supersaturation may have influenced the growth process. UV-Vis studies (Table 4-2) showed that the supersaturation, *S*, at 4 °C varied between 1.04 (acetone) and almost 25 (methanol). Crystal formation appeared to occur faster in acetone and alcohols with longer alkyl chains which are of lower polarity (Table 4-1), thus indicating that solvent polarity affects the growth process. In addition, possible weak BDP-solvent interactions within the channel solvate may be based on the solvent polarity. Methanol, however, despite having the highest polarity of all solvents used, appeared not to be incorporated within a BDP channel structure. This agrees with methanol being excluded from the list of clathrate forming solvents (Othman et al., 2008). A conclusive explanation has not yet been found to in literature. Further studies will be necessary to determine the nature and strength of any present host-guest interactions.

4.4 Conclusions

Taken as a whole, these results suggest that these samples initially crystallised as solvates which desolvated and transformed into the anhydrous form upon heating. The desolvation peak was very broad and the mass loss varied slightly from sample to sample. This is in keeping with previous reports from literature which show that BDP forms clathrates with weak BDP-solvent interactions and the solvent molecules being highly mobile within the channels (Kuehl et al., 2003, Harris et al., 2003, Bouhroum et al., 2010). As the clathrate is heated, the solvent gradually evaporates from open ends of the channels with more and more solvent molecules migrating out of the channel system, leading to the gradual desolvation of the host-guest system with a broad endothermic signal and mass loss occurring across a wider temperature range. As the solvent is removed, the crystal is destabilised leading to the collapse of the structure and transition into the thermodynamically more stable anhydrous form as observed under the AFM, SEM and during controlled desolvation.

Slight differences were observed in the behaviour of these four samples which may be related to differences in the size of the solvent molecules or differences in the strength of the solvent-BDP interactions due to variation in the polarity and/or hydrogen bonding for different solvents. Analysis of thermogravimetric data shows that BDP (1-propanol) and BDP (2-propanol) released solvent in two distinct steps. It is possible that the first step was a mixture of residual

solvent evaporation along with the desolvation of freely moving solvent molecules from the channels which are in a solvent-like environment (Höhne et al., 2013), while the second step was due to the release of solvent which was interacting with the BDP in the walls of the centre of the channels and thus required more energy to overcome solvent BDP interactions.

The BDP samples prepared from acetone were found to vary from batch to batch with either two or three distinct desolvation steps observed by both DSC and TGA. A varying number of exothermic peaks were also observed from sample to sample, showing that, in some samples, the transition occurred in several steps. The volatile acetone (bp 56.2 °C) may have been partially substituted by water from the air during handling allowing the BDP to partially convert into the more stable monohydrate which was reported to dehydrate above 100 °C and recrystallize into anhydrous BDP at about 130 °C (Nachiengtung, 1997, Hyvönen et al., 2005). Thus as the sample was heated, the solvent and/or water was released in several steps due to evaporation of residual surface acetone/water, desolvation of BDP solvate and dehydration of BDP monohydrate. Channel collapse and conversion into the anhydrate form would occur at different temperatures for the solvate and monohydrate leading to one or two exothermic peaks, depending on the composition of the particles.

Crystallisation from supersaturated solution appeared to lead to the formation of solvates when carried out using ethanol, 1-propanol, 2-propanol and acetone. These samples will be referred to as the BDP ethanol solvate, BDP 1-propanol solvate, BDP 2-propanol solvate and BDP acetone solvate in future studies. They were considered potential precursor solvates for the preparation of anhydrous BDP through desolvation. The formation of these solvates and their crystalline structure were analysed further. In addition, the desolvation process and the anhydrous BDP prepared from these samples were characterised.

A controlled desolvation process and accurate knowledge of the material characteristics of the resulting anhydrous BDP potentially support the development of tailored particulate BDP for pulmonary delivery. This in turn would be beneficial to the performance of the final product.

4.5 References

Bouhroum, A., Burley, J. C., Champness, N. R., Toon, R. C., Jinks, P. A., Williams, P. M. & Roberts, C. J. 2010. An assessment of beclomethasone dipropionate clathrate formation in a model suspension metered dose inhaler. *International journal of pharmaceutics,* 391**,** 98-106.

Chavez, K. J., Guevara, M. & Rousseau, R. W. 2010. Characterization of solvates formed by sodium naproxen and an homologous series of alcohols. *Crystal Growth & Design,* 10**,** 3372-3377.

De Yoreo, J. J. & Vekilov, P. G. 2003. Principles of crystal nucleation and growth. *Reviews in mineralogy and geochemistry,* 54**,** 57-93.

Finckenor, L. E. 1980. *Beclomethasone dipropionate-hexane solvate and aerosols prepared therefrom*. US Patent 4,225,597.

Gabbott, P. 2008. *Principles and applications of thermal analysis,* John Wiley & Sons.

Haines, P. J. 2002. *Principles of thermal analysis and calorimetry*, Royal society of chemistry.

Harris, J. A., Carducci, M. D. & Myrdal, P. B. 2003. Beclomethasone dipropionate crystallized from HFA-134a and ethanol. *Acta Crystallographica Section E: Structure Reports Online,* 59**,** o1631-o1633.

Höhne, G., Hemminger, W. F. & Flammersheim, H.-J. 2013. *Differential scanning calorimetry,* Springer Science & Business Media.

Hunt, J. H. & Padfield, J. M. 1989. *Micronised beclomethasone dipropionate monohydrate compositions and methods of use*. US Patent 4,866,051.

Hyvönen, S., Peltonen, L., Karjalainen, M. & Hirvonen, J. 2005. Effect of nanoprecipitation on the physicochemical properties of low molecular weight poly (L-lactic acid) nanoparticles loaded with salbutamol sulphate and beclomethasone dipropionate. *International journal of pharmaceutics,* 295**,** 269-281.

Jenkins, R. & Snyder, R. L. 1996. Diffraction theory. *Introduction to X-ray Powder Diffractometry, Volume 138***,** 47-95.

Jinks, P. A. 1989. *Physically modified beclomethasone dipropionate suitable for use in aerosols*. US Patent 4,810,488.

Kuehl, P. J., Carducci, M. D. & Myrdal, P. B. 2003. An ethanol solvate of Beclomethasone dipropionate. *Acta Crystallographica Section E: Structure Reports Online,* 59**,** 1888-1890.

Millard, J. W. & Myrdal, P. B. 2002. Anhydrous beclomethasone dipropionate. *Acta Crystallographica Section E: Structure Reports Online,* 58**,** o712-o714.

Morissette, S. L., Almarsson, Ö., Peterson, M. L., Remenar, J. F., Read, M. J., Lemmo, A. V., Ellis, S., Cima, M. J. & Gardner, C. R. 2004. High-throughput crystallization: polymorphs, salts, co-crystals and solvates of pharmaceutical solids. *Advanced drug delivery reviews,* 56**,** 275-300.

Nachiengtung, N. 1997. Solid-state characterization of beclomethasone dipropionate solvates and polymorphs. PhD Thesis, Purdue University, IN, USA.

Neale, P. J. & Taylor, A. J. 1997. *Medicaments for treating respiratory disorders*. US Patent 5,688,782.

Othman, A., Harris, R. K., Hodgkinson, P., Christopher, E. A. & Lancaster, R. W. 2008. Structural characterisation of two pharmaceutically important steroids by solid-state NMR. *New Journal of Chemistry,* 32**,** 1796-1806.

Page, P. R. & Heggie, W. 1990. *Preparation and use of new solvates of beclomethasone 17, 21-dipropionate*. US Patent 4,913,892.

Suitchmezian, V., Jeß, I. & Näther, C. 2006. Investigations on the polymorphism and pseudopolymorphism of triamcinolone diacetate. *International journal of pharmaceutics,* 323**,** 101-109.

Wang, Z., Chen, J.-F., Le, Y., Shen, Z.-G. & Yun, J. 2007. Preparation of ultrafine beclomethasone dipropionate drug powder by antisolvent precipitation. *Industrial & engineering chemistry research,* 46**,** 4839-4845.

CHAPTER 5

INVESTIGATION INTO BECLOMETHASONE DIPROPIONATE SOLVATE FORMATION

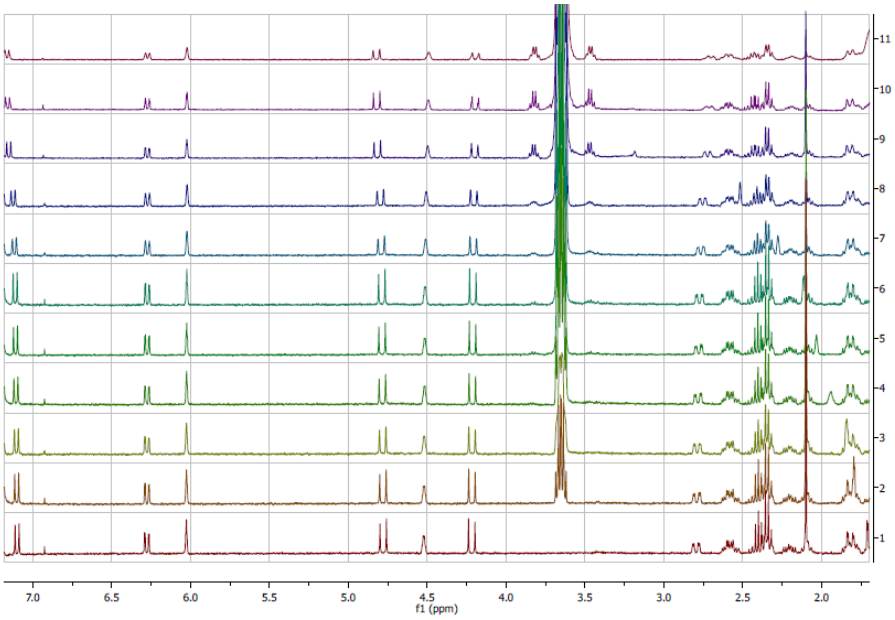

Figure 5. NMR titration of BDP ($CDCl_3$) using ethanol.

5 Investigation into Beclomethasone Dipropionate Solvate Formation

Understanding the forces acting between molecules during crystallisation is a prerequisite of controlling the growth of crystalline material and designing the crystallisation process. Such knowledge also improves the predictability of solvate formation. While BDP is known to form channels solvates with different organic solvents (Kuehl et al., 2003, Jinks, 1989, Othman et al., 2008, Harris et al., 2003, Page and Heggie, 1990), the reasons and mechanisms behind the formation of BDP clathrates containing organic solvent molecules has not yet been studied. Solvate formation affects only one propionate chain where molecular interaction occurs between the alcohol group in C_{11} position and the carbonyl oxygen in C_{22}' position which is part of the propionic ester at C_{17} (Kuehl et al., 2003). The second propionate branch reaches into the channel (Figure 5-1) and the functional groups at C_{20} and C_{22} are potentially available for hydrogen bonding with the solvent.

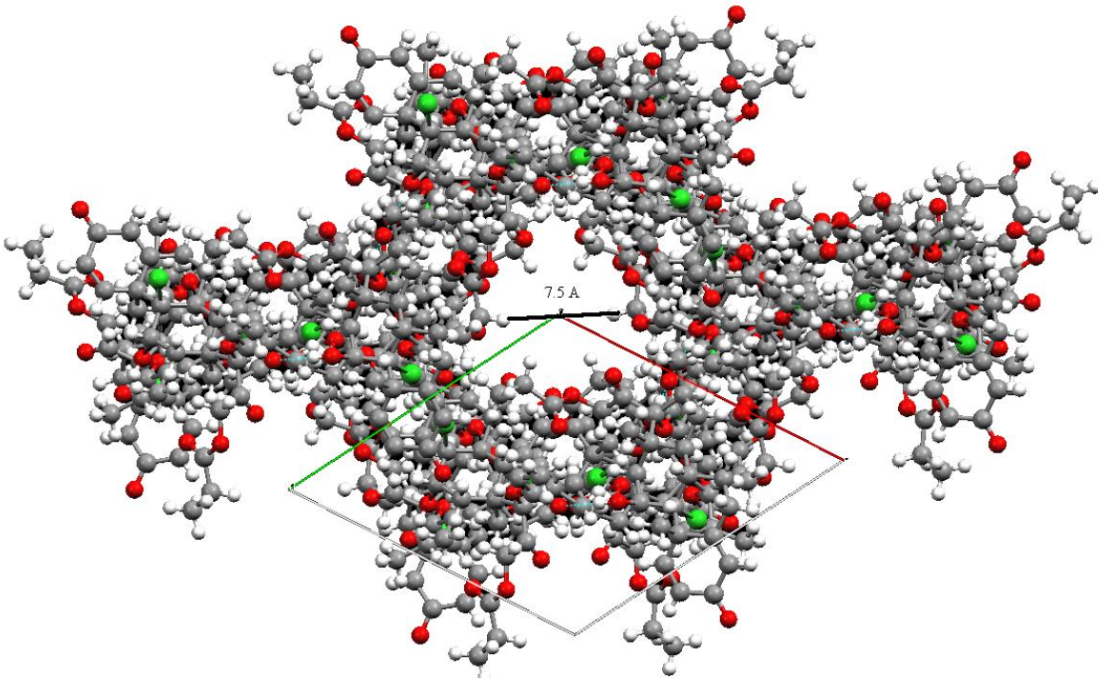

Figure 5-1. Molecular structure of the BDP ethanol solvate (Kuehl et al., 2003). White: hydrogen, grey: carbon, red: oxygen, green: chlorine.

Considering the polar nature of alcohols, it may be possible that weak interactions between the solvent and BDP during crystallisation from supersaturated solution control the formation of channel solvates and induce the encapsulation of solvent molecules within the voids.

NMR titration is a state-of-the-art technique which allows the determination of association constants and the analysis of the formation of intermolecular bonds. NMR titration is often used in the development of techniques such as molecular imprinting to analyse binding sites and to study host-guest complexation (Dudzik et al., 2017, Wierzbicka et al., 2017, dos Santos et al., 2016). Diffusion ordered spectroscopy (DOSY) was found to be complementary (Lamm et al.,

2014). Both methods were used in combination to identify the chemical shifts of nuclei in the propionate chains of anhydrous BDP, to explain the formation of BDP solvates and to analyse the strength of intermolecular interactions in BDP solvates. Understanding the mechanisms of solvate formation and how it is affected by specific solvent properties is necessary to ensure reproducibility. The techniques used could potentially be used as pre-screening method to predict the formation of (channel) solvates from different solutions and their stability.

5.1 Materials and Methods

Crystalline BDP was prepared from solution as outlined in Chapter 4.

$CDCl_3$, acetone, methanol, ethanol, 1-propanol, 2-propanol, 1-butanol and 1-pentanol, all used for NMR titration, were supplied by Sigma Aldrich, UK.

5.1.1 NMR titration

$CDCl_3$ was used to dissolve BDP for solution NMR spectroscopy. The ^1H titration experiments were carried out on a Bruker Auto-400 spectrometer (400 MHz, Bruker). 10.42 mg BDP (host) was dissolved in 10 mL $CDCl_3$ (0.002 M) and 0.5 M solutions of solvent (guest) in $CDCl_3$ were prepared in 5 mL volumetric flasks (Table 5-1).

300 µL host solution and increasing volumes of guest solution were mixed in an NMR tube to achieve different host-guest ratios (Table 5-2). $CDCl_3$ was added to a total volume of 600 µL.

Table 5-1. Amount (weight, m; volume, V) of solvent in $CDCl_3$ (5 mL total, 0.5 M); calculation based on solvent molecular weight, MW, and density, ρ.

Solvent	MW [g/mol]	ρ [g/mL]	m [mg]	V[mL]
Methanol	32.04	0.792	80.10	101.14
Ethanol	43.07	0.789	115.18	145.98
1-Propanol	60.10	0.803	150.25	187.11
2-Propanol	60.10	0.786	150.25	191.16
1-Butanol	74.12	0.810	185.30	228.77
1-Pentanol	88.15	0.811	220.38	271.73
Acetone	58.08	0.791	145.20	183.57

Table 5-2. NMR titration: volumes V (µL) and amount n (mmol) of solvent and BDP and molar ratio (solvent:BDP).

$V_{solvent/CDCl3}$ [µL]	$V_{BDP/CDCl3}$ [µL]	$n_{solvent}$ [mmol]	n_{BDP} [mmol]	n_{BDP}:n_{solven}
0	300	0.0000	0.0006	1:0.00
5	300	0.0025	0.0006	1:4.17
10	300	0.0050	0.0006	1:8.33
15	300	0.0075	0.0006	1:12.50
20	300	0.0100	0.0006	1:16.67
30	300	0.0150	0.0006	1:25.00
40	300	0.0200	0.0006	1:33.33
60	300	0.0300	0.0006	1:50.00
90	300	0.0450	0.0006	1:75.00
120	300	0.0600	0.0006	1:100.00
180	300	0.0900	0.0006	1:150.00
240	300	0.1200	0.0006	1:200.00
300	300	0.1500	0.0006	1:250.00

5.1.2 Diffusion Ordered Spectroscopy

Diffusion ordered spectroscopy (DOSY) is solution state NMR technique which relies on pulsed field gradients along the z-axis and different signal decay times of different molecules. Brownian molecular motion within a liquid leads to the gradual diffusion of the molecules in solution as described by the Stokes Einstein equation (equation 5-1).

$$D = \frac{k_B T}{6\pi\eta r} \tag{5-1}$$

The Stokes Einstein equation includes the Boltzmann constant k_B and explains how the translational diffusion coefficient D of an ideally spherical molecule depends on temperature T, viscosity η and the hydrodynamic radius r of the molecule in question (Einstein, 1905). The hydrodynamic radius, more generally speaking the molecular size, is reciprocally related to the translational diffusion of the molecule. Smaller molecules tend to diffuse faster than larger molecules which is recorded in a spatial separation in the pseudo 2D DOSY spectrum. This forms the basis of DOSY (Lamm et al., 2014, Choudhary, 2015).

DOSY is particularly useful for identifying reaction mechanisms and intermediate compounds (Schlörer et al., 2002) and for analysing aggregation and binding processes such as host-guest complexations (Choudhary, 2015, Lamm et al., 2014).

Here, the samples with the highest BDP:solvent ratio (1:250, Table 5-2) were used for DPSY NMR. The spectra were acquired on a Bruker AVANCE-600 spectrometer (600 MHz).

5.2 Results

The chemical shifts observed in NMR titration and the relative positions of BDP and the respective solvent molecule in DOSY were analysed based on the completely solved ^{1}H NMR spectrum of anhydrous BDP (Figure 3-2). The alcohol and acetone proton signals were identified through their characteristic spectra (Table 5-3).

Table 5-3. Characteristic ^{1}H NMR signals of alcohols and acetone in $CDCl_3$ (Yamaji et al., 2014) .

Solvent	Structure	δ_H [ppm]	δ_{OH}[ppm]
Methanol		3.15 (s)	3.97
Ethanol	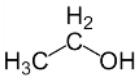	3.69 (q), 1.23 (t)	2.61
1-Propanol	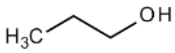	3.58 (t), 1.57 (tq), 0.94 (t)	2.26
2-Propanol	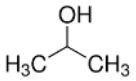	4.01 (qq), 1.20 (d)	2.16
1-Butanol	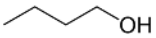	3.63 (t), 1.53 (tt), 1.39 (tq), 0.94 (t)	2.24
1-Pentanol	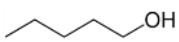	3.60 (t), 1.56 (tt), 1.34 (tt), 0.91 (t)	3.05
Acetone	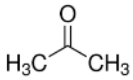	2.17 (s)	-

5.2.1 NMR Titration

NMR titration shows the chemical shift of certain signals in the host guest complex compared to the pure host compound. The chemical shift is a first indication of how the formation of a host guest system affects the electron density around the protons on the host molecule but does not necessarily correlate to the strength of interaction between the respective protons and functional groups. The chemical shift also depends on reaction kinetics and the speed of the formation of chemical bonds. To identify possible differences in the formation of BDP solvates, the chemical shifts were evaluated quantitatively (Thordarson, 2011) and the association constants (Figure 5-18) were calculated following Equation 5-2:

$$\Delta\delta_{max} = \Delta\delta \cdot \frac{\frac{1}{2}\left([H]_0+[G]_0+\frac{1}{Ka}\right)-\sqrt{\left([H]_0+[G]_0+\frac{1}{Ka}\right)^2+4[H]_0[G]_0}}{[H]_0} \qquad (5\text{-}2)$$

$\Delta\delta$ is the chemical shift (difference between of the host guest compound and the pure host), $\Delta\delta_{max}$ is the maximum chemical shift based on extrapolation to an infinite guest-to-host ratio,

$[H]_0$ and $[G]_0$ are the known (initial) concentrations of host and guest, respectively, and K_a is the association constant.

Equation 5-2 describes the specific case of a 1:1 host:guest equilibrium (Thordarson, 2011). The 1:1 ratio was chosen due to the assumption of the solvent molecules being highly mobile within the crystalline BDP structure. At any given point in time, one solvent molecule was assumed to in close proximity to the propionate BDP host so that (weak) bonding could occur. The solvate was found to be a channel like crystalline structure of BDP molecules interacting via hydrogen bonding with the solvent molecules being present in the channels, maintaining the structure by their presence and possibly interacting weakly with the BDP host (Kuehl et al., 2003, Othman et al., 2008) rather than a typical host guest complex with defined intermolecular interactions. Thermogravimetric analysis indicated a slightly higher host:guest ratio of 1:1.33 up to 1:1.40 based on BDP ethanol, 1-propanol and 2-propanol (Table 4-9). These values were taken as reference points while the BDP:acetone ratio of 1:1.80 (Table 4-9) was disregarded due to the titration with acetone not resulting in any chemical shifts, thus indicating the absence of any intermolecular interactions.

The increasing solvent:BDP ratio up to BDP:solvent 1:250 was clearly visible in the increasing intensity of all ^{1}H signals belonging to the solvents . It was noted that the ^{1}H signals assigned to the hydroxyl group of the alcohols were found at lower frequencies compared to their positions in their pure state in $CDCl_3$ (Yamaji et al., 2014) but then experienced a downfield shift at increasing solvent:BDP ratios (Table 5-4, Figures 5-2 to 5-8). Similarly, the signal assigned to the BDP alcohol group, $H_{11(OH)}$, was also found to have shifted upfield and subsequently moved to higher frequencies (Figures 5-3 to 5-8). In addition, the signals were first seen as multiplets before gradually reverting back into broad singlets (methanol, ethanol, 1-propanol, 2-propanol) or widening into a broad triplet (1-butanol, 1-pentanol) (Figures 5-3 to 5-8).

No chemical shift was observed for any other alcohol protons and the ^{1}H signal characteristic of acetone (Yamaji et al., 2014) also remained at the expected frequency (Figures 5-3 to 5-9). These results suggested that interaction occurs between the solvent hydroxyl group and the BDP. While being more shielded when initially interacting with BDP at a lower solvent content, the addition of larger volumes of alcohol led to a higher probability of the solvent molecules forming hydrogen bonds between each other. This resulted in a downfield shift $\Delta\delta$ towards the hydroxyl ^{1}H signal of the pure solvent in $CDCl_3$ (Table 5-4). Due to the change in electron density in the area. With the exception of methanol, the overall chemical shift towards the respective solvent's characteristic ^{1}H NMR signal (Yamaji et al., 2014) was found to increase with increasing solvent polarity (Figure 5-2).

Table 5-4. NMR Titration: Solvent polarity, ^{1}H-NMR signals δ_{OH} (ppm) of hydroxyl protons (alcohols) in solution (Gottlieb et al., 1997), ^{1}H-NMR signals δ_0 (ppm) at BDP:solvent 1:12.5; chemical shift $\Delta\delta$ (ppm) to higher frequencies δ_1 (ppm) observed in NMR titration (up to BDP:solvent 1:250).

Solvent	Polarity	δ_{OH} [ppm]	δ_0 [ppm]	$\Delta\delta$ [ppm][1]	δ_1 [ppm]
Methanol	0.762	3.97	0.93	0.27	1.20
Ethanol	0.654	2.61	1.20	0.28	1.48
1-Propanol	0.617	2.26	1.24	0.25	1.49
2-Propanol	0.546	2.16	1.26	0.18	1.44
1-Butanol	0.586	2.24	1.20	0.23	1.43
1-Pentanol	0.568	3.05	1.21	0.20	1.41
Acetone	0.355	-	-	-	-

[1] Downfield shift from position at BDP:alcohol ratio 1:12.5 with increasing alcohol concentration in NMR titration.

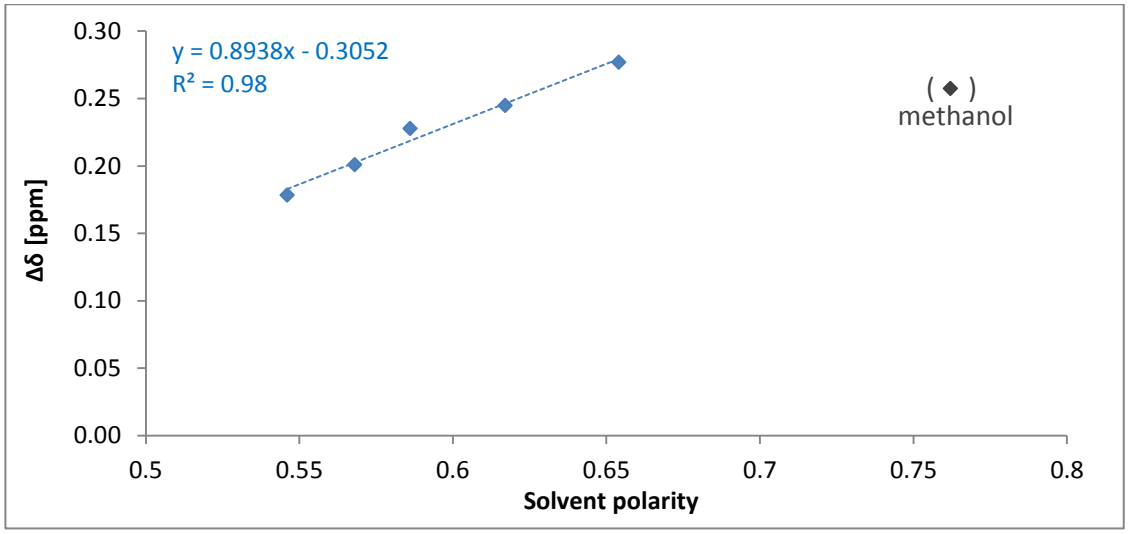

Figure 5-2. Linear relationship between solvent polarity (alcohols) and chemical shift of the signal $\Delta\delta$ (ppm) observed in NMR titration at a BDP:solvent ratio of 1:250.

The relative positions of the ^{1}H NMR signals of all alcohol hydroxyl protons at both the minimum and maximum BDP to solvent ratio compared to that of pure alcohol in $CDCl_3$ (Yamaji et al., 2014) were consistent. This also indicated that solvent-solvent interactions may have become stronger as more solvent was added to the mixture.

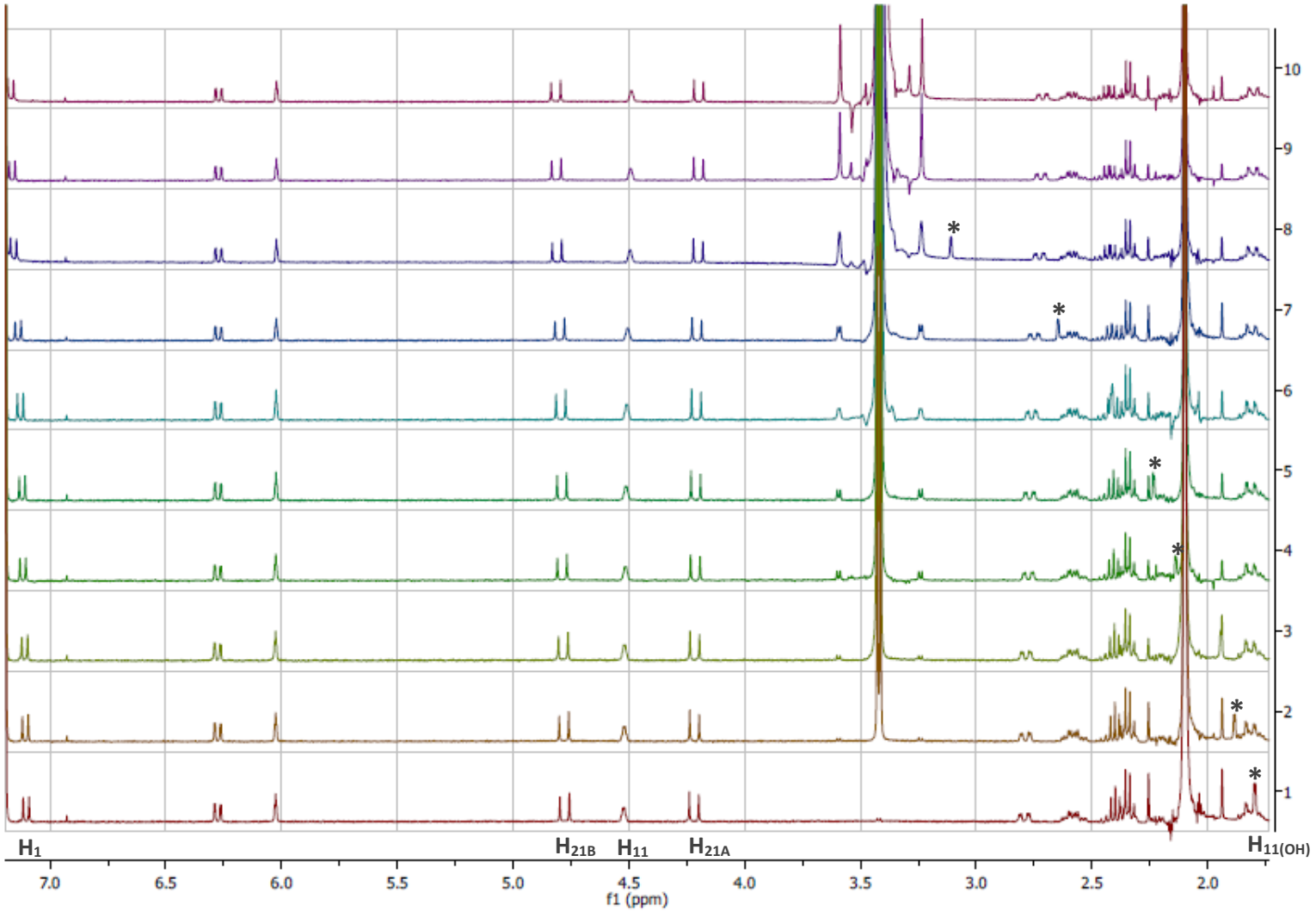

Figure 5-3. NMR titration (^{1}H, $CDCl_3$, 400 MHz) of BDP with methanol. Pure BDP (#1 on ordinate) up to a BDP:methanol ratio of 1:250 (#10 on the ordinate).

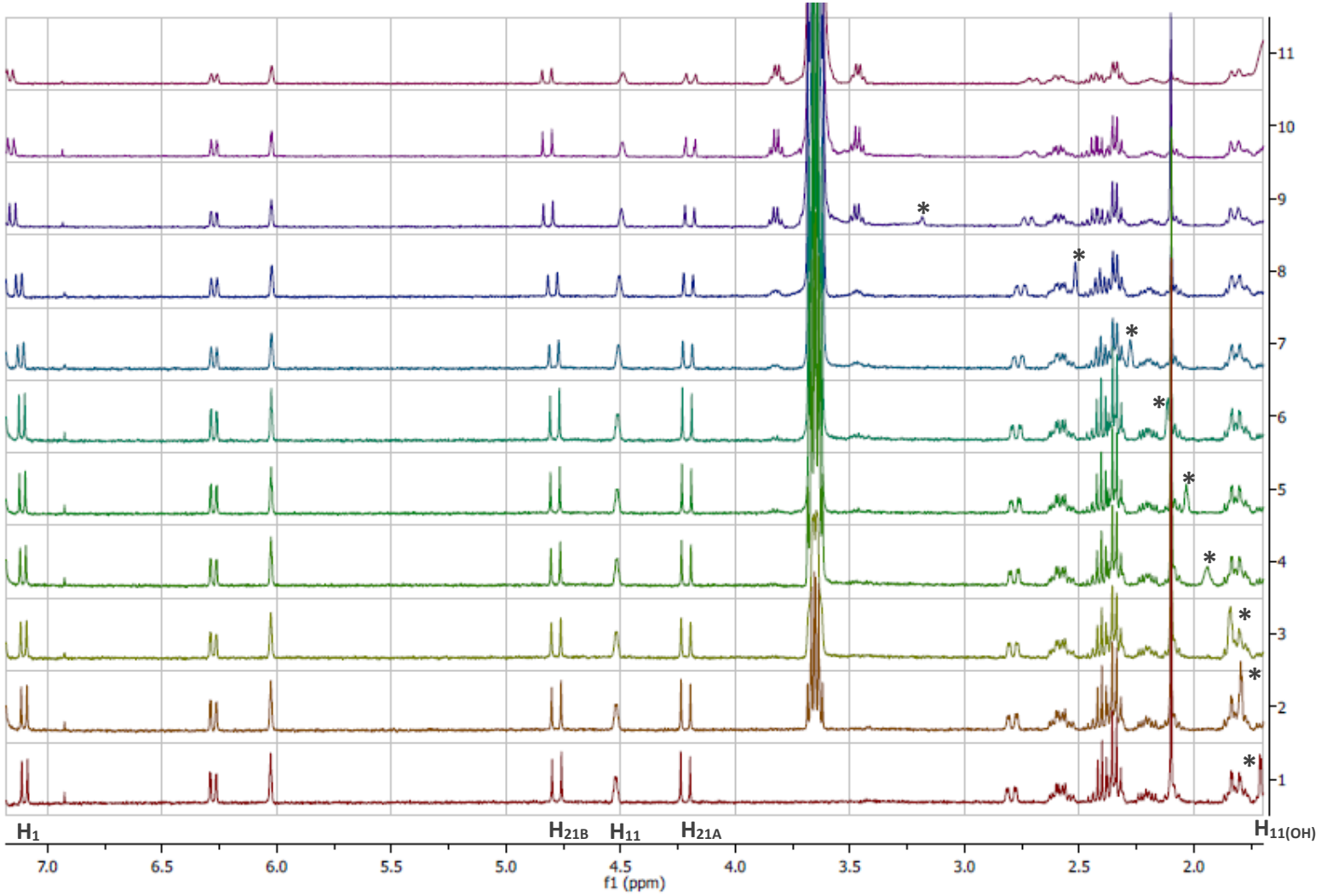

Figure 5-4. NMR titration (^{1}H, $CDCl_3$, 400 MHz) of BDP with ethanol. Pure BDP (#1 on ordinate) up to a BDP:ethanol ratio of 1:250 (#11). Asterisk: position of $H_{11(OH)}$.

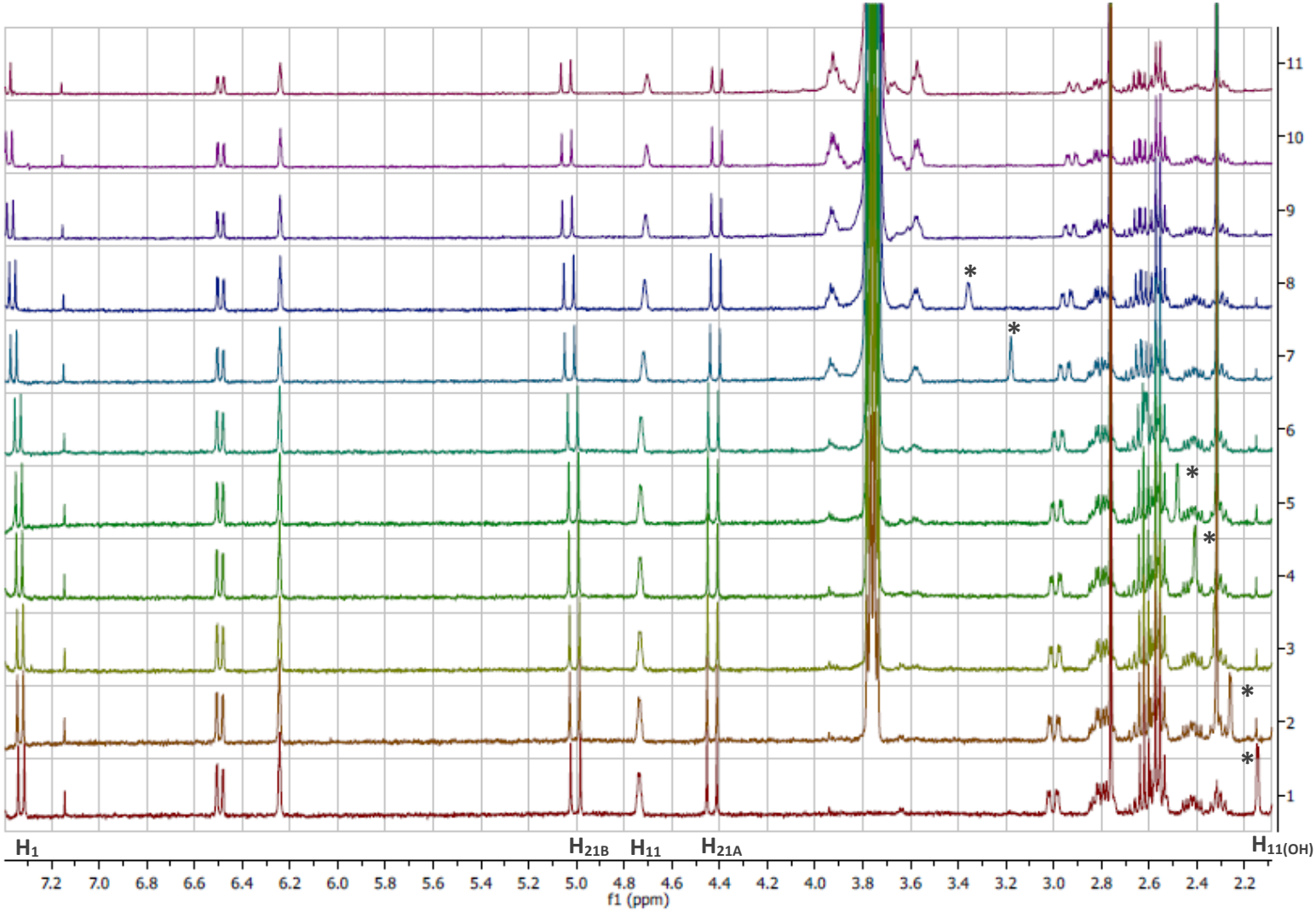

Figure 5-5. NMR titration (^{1}H, $CDCl_3$, 400 MHz) of BDP with 1-propanol. Pure BDP (#1 on ordinate) up to a BDP:1-propanol ratio of 1:250 (#11). Asterisk: position of $H_{11(OH)}$.

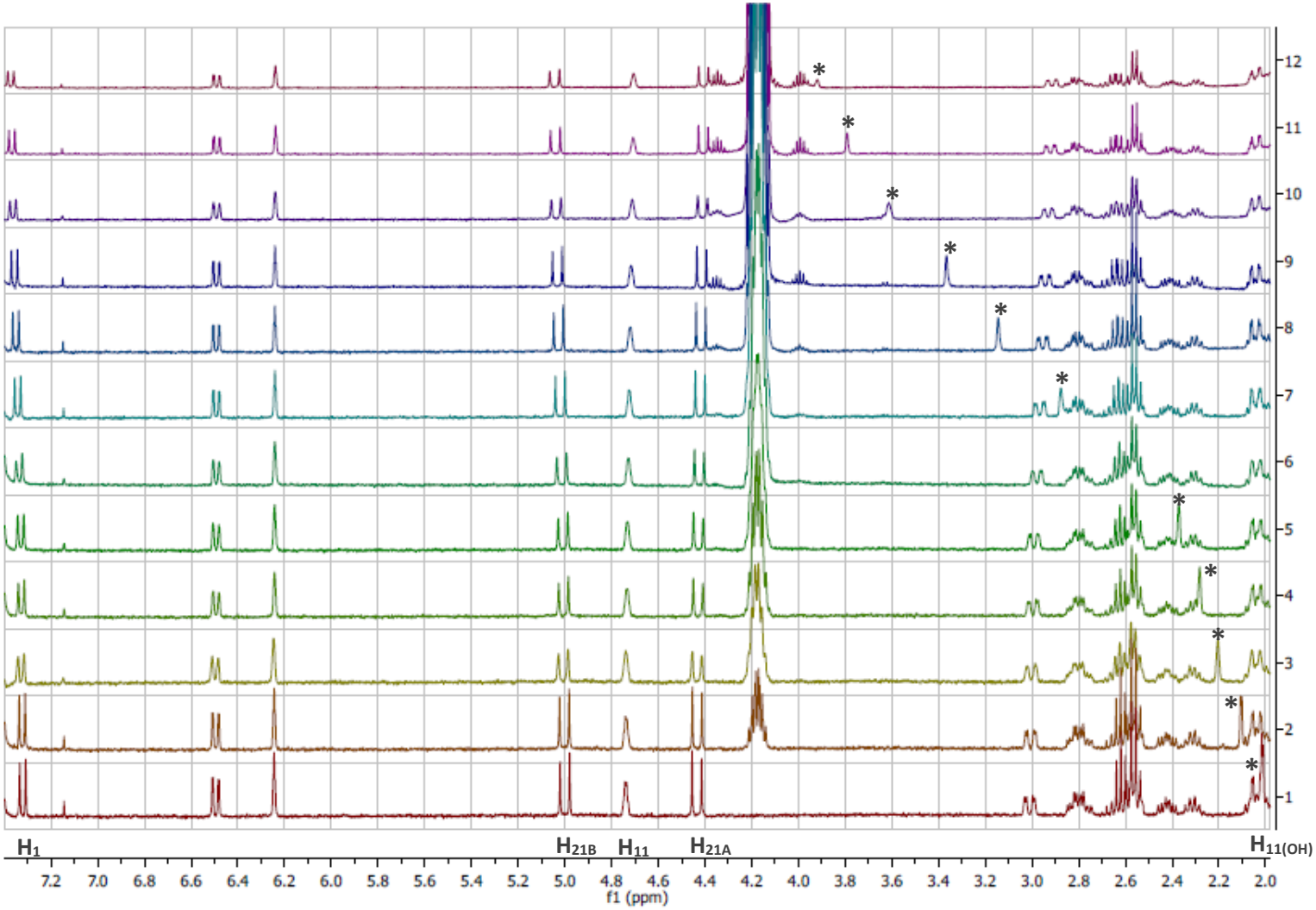

Figure 5-6. NMR titration (^{1}H, $CDCl_3$, 400 MHz) of BDP with 2-propanol. Pure BDP (#1 on ordinate) up to a BDP:2-propanol ratio of 1:250 (#12). Asterisk: position of $H_{11(OH)}$.

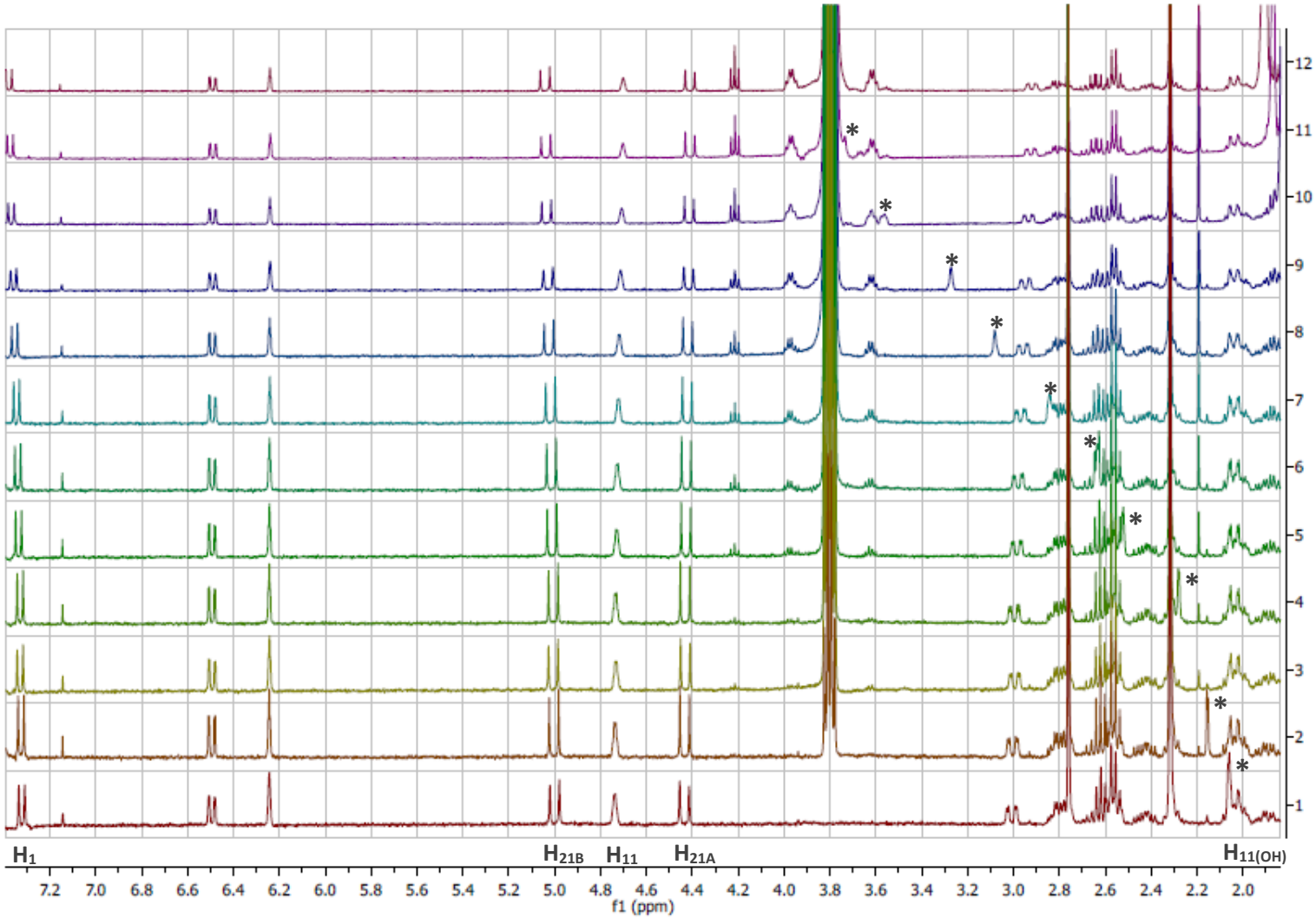

Figure 5-7. NMR titration (^{1}H, $CDCl_3$, 400 MHz) of BDP with 1-butanol. Pure BDP (#1 on ordinate) up to a BDP:1-butanol ratio of 1:250 (#12). Asterisk: position of $H_{11(OH)}$.

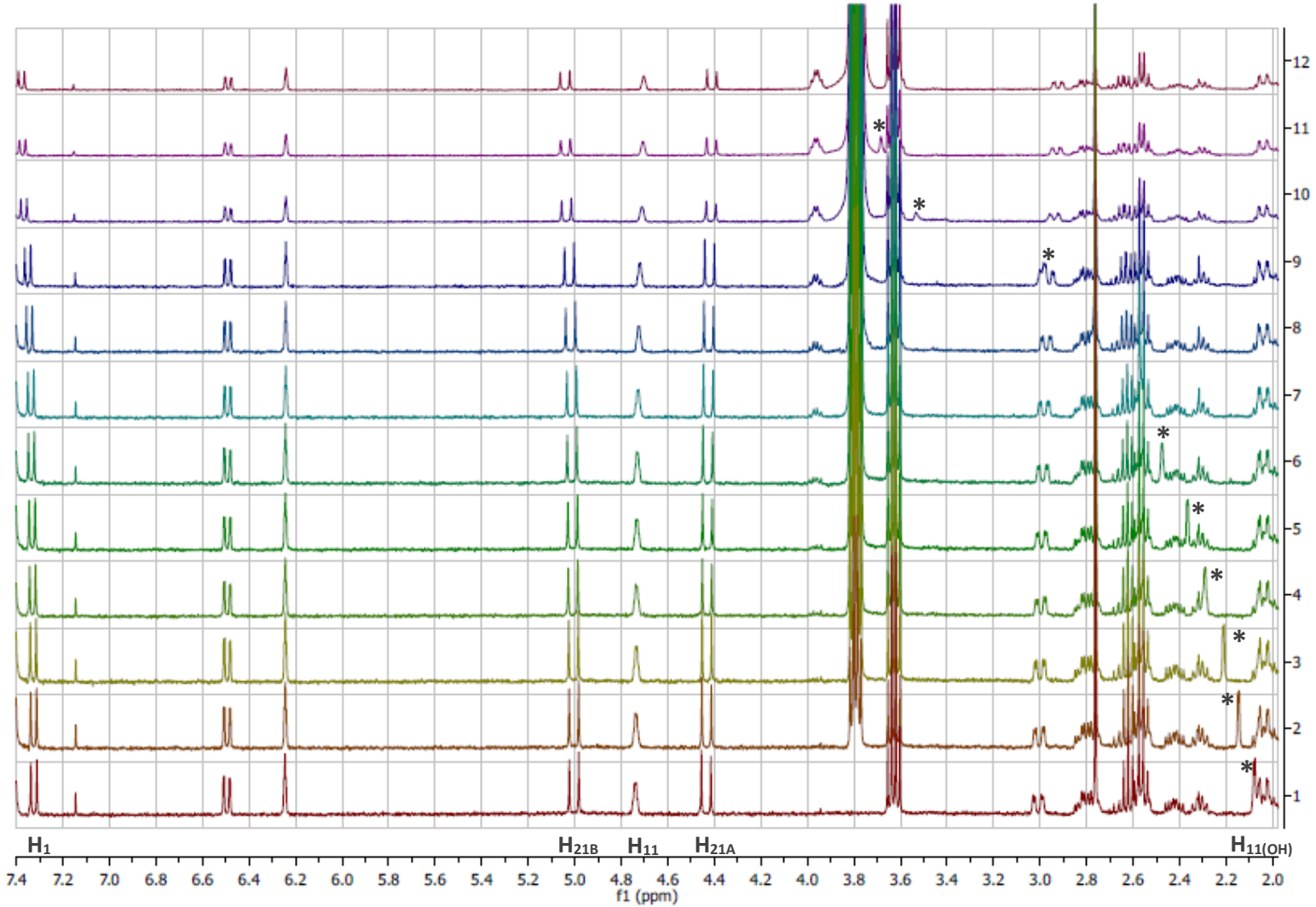

Figure 5-8. NMR titration (^{1}H, $CDCl_3$, 400 MHz) of BDP with 1-pentanol. Pure BDP (#1 on ordinate) up to a BDP:1-pentanol ratio of 1:250 (#12). Asterisk: position of $H_{11(OH)}$.

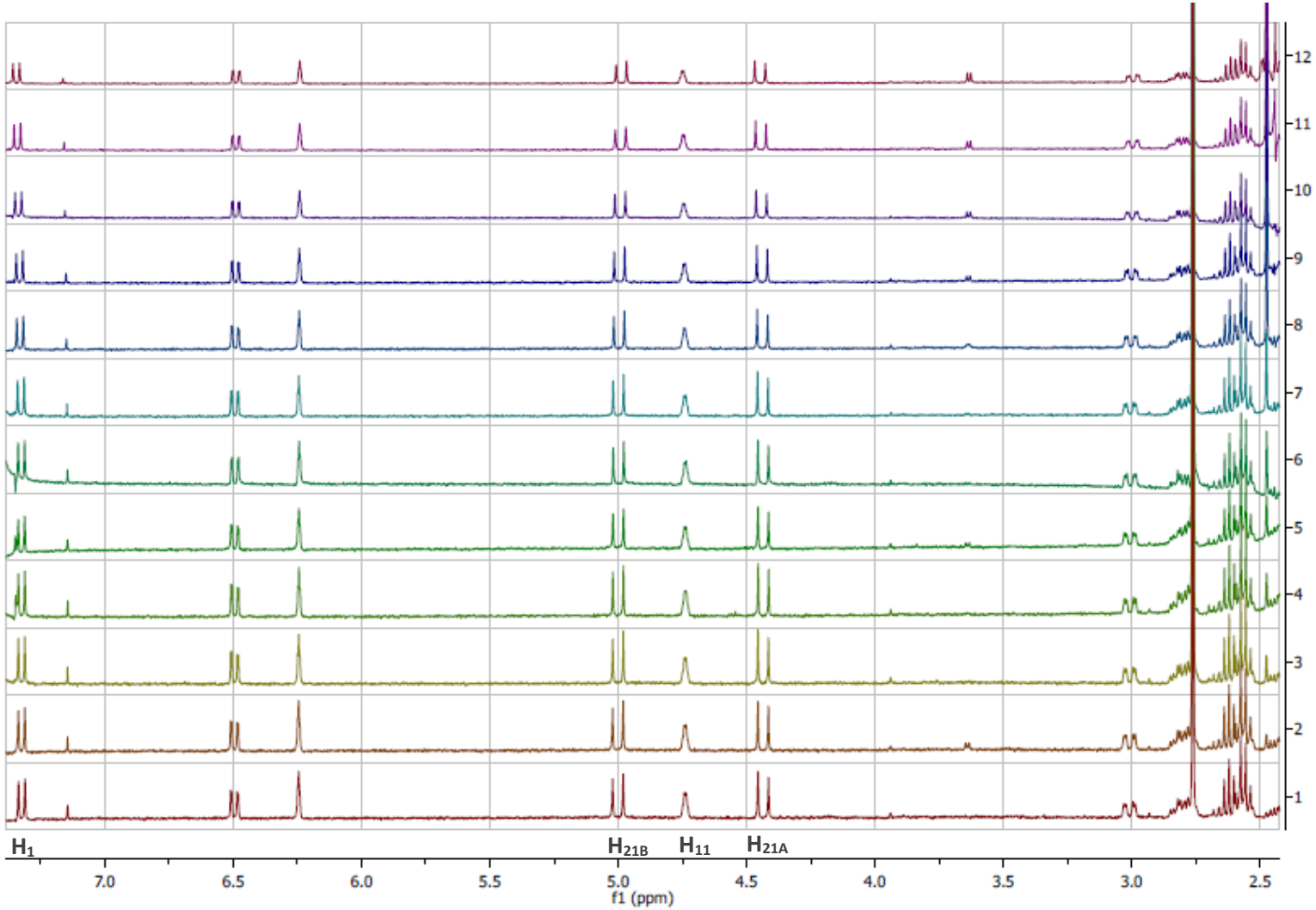

Figure 5-9. NMR titration (^{1}H, $CDCl_3$, 400 MHz) of BDP with acetone. Pure BDP (#1 on ordinate) up to a BDP:acetone ratio of 1:250 (#12).

Table 5-5. 1H-NMR: Chemical shifts [ppm] of pure BDP in $CDCl_3$ at 400 MHz, max. chemical shifts Δδ [ppm] observed in titration (molar ratio BDP:solvent = 1:250) and association constant K_a [M^{-1}] were based on Equation 5-2 using n = 10 to n = 13 values (± standard deviation).

^{1}H-NMR BDP	H_1	$H_{11(OH)}$[1]	H_{11}	H_{12A}	H_{21B}	H_{21A}	H_{23}/H_{23}'	H_{23}/H_{23}'
[ppm]	**7.18**	**1.95**	**4.58**	**2.85**	**4.83**	**4.27**	**2.49, 2.47, 2.45**	**2.49, 2.47, 2.45**
Methanol	downfield	downfield	upfield	upfield	downfield	upfield	downfield	upfield
Δδ [ppm]	0.07	1.31	0.03	0.08	0.04	0.02	0.03	0.02
K_a [M^{-1}]	5.3 ± 0.5	4.8 ± 0.5	5.5 ± 0.7	6.3 ± 0.6	8.5 ± 0.7	10.6 ± 0.4	7.6 ± 0.8	10.4 ± 1.3
Ethanol	downfield	downfield	upfield	upfield	downfield	upfield	downfield	upfield
Δδ [ppm]	0.06	1.47	0.03	0.09	0.04	0.02	0.03	0.02
K_a [M^{-1}]	5.5 ± 0.5	7.6 ± 0.7	12.3 ± 1.6	7.6 ± 0.5	7.9 ± 0.7	14.3 ± 2.3	3.9 ± 1.0	6.7 ± 1.0
n-Propanol	downfield	downfield	upfield	upfield	downfield	upfield	downfield	upfield
Δδ [ppm]	0.06	1.53	0.03	0.09	0.04	0.02	0.03	0.02
K_a [M^{-1}]	8.1 ± 0.5	9.4 ± 0.3	5.7 ± 1.0	8.2 ± 0.2	10.4 ± 1.3	10.8 ± 1.1	8.8 ± 0.5	14.0 ± 2.4
Butanol	downfield	downfield	upfield	upfield	downfield	upfield	downfield	upfield
Δδ [ppm]	0.06	1.50	0.04	0.09	0.04	0.03	0.03	0.02
K_a [M^{-1}]	7.3 ± 0.6	6.9 ± 0.9	7.0 ± 0.9	7.3 ± 0.6	10.0 ± 0.6	8.5 ± 1.3	7.3 ± 1.2	14.3 ± 3.5
Pentanol	downfield	downfield	upfield	upfield	downfield	upfield	downfield	upfield
Δδ [ppm]	0.05	1.45	0.04	0.09	0.04	0.03	0.02	0.02
K_a [M^{-1}]	5.3 ± 0.3	6.4 ± 3.1	5.3 ± 0.7	6.8 ± 0.3	6.3 ± 0.5	11.3 ± 0.7	3.5 ± 0.6	4.3 ± 0.5
iso-Propanol	downfield	downfield	upfield	upfield	downfield	upfield	downfield	upfield
Δδ [ppm]	0.05	1.90	0.04	0.10	0.04	0.03	0.03	0.02
K_a [M^{-1}]	6.8 ± 0.9	6.5 ± 1.4	9.7 ± 1.8	7.7 ± 0.8	7.8 ± 1.3	9.2 ± 1.0	5.3 ± 1.7	7.6 ± 1.8
Acetone	downfield	downfield	upfield	upfield	downfield	upfield	downfield	-
Δδ [ppm]	0.02	0.43	0.01	0.01	0.01	0.01	0.01	0.00
K_a [M^{-1}]	0.0 + 0.4	1.1 ± 0.2	-	1.9 ± 1.8	1.6 ± 0.5	0.0 + 0.4	3.0 ± 1.3	-

[1] Initial chemical shift of OH proton may vary due to presence of impurities and strength of interaction (Bruice, 2011).

In all cases where alcohol was used, differences between the ^{1}H peak positions of the pure BDP host in solution and the titration samples were observed (Table 5-5; Figures 5-3 to 5-8) with the most prominent shift affecting $H_{11(OH)}$ (downfield). Significant chemical shifts were also found at H_1 (downfield), H_{11} (upfield), H_{12} (upfield), $H_{21A/B}$ (downfield at 4.83 ppm, upfield at 4.27 ppm) and H_{23} and H_{23}' (separated by chemical shifts to higher and lower frequencies) (Figures 5-3 to 5-8). The gradual addition of acetone to BDP in $CDCl_3$ did not lead to any changes except for a relatively small chemical shift of the signal assigned to $H_{11(OH)}$ (Table 5-5, Figure 5-9). The polarity of the hydroxyl group and the formation of hydrogen bonds appeared to be critical for the development of intermolecular interaction (Figure 5-10).

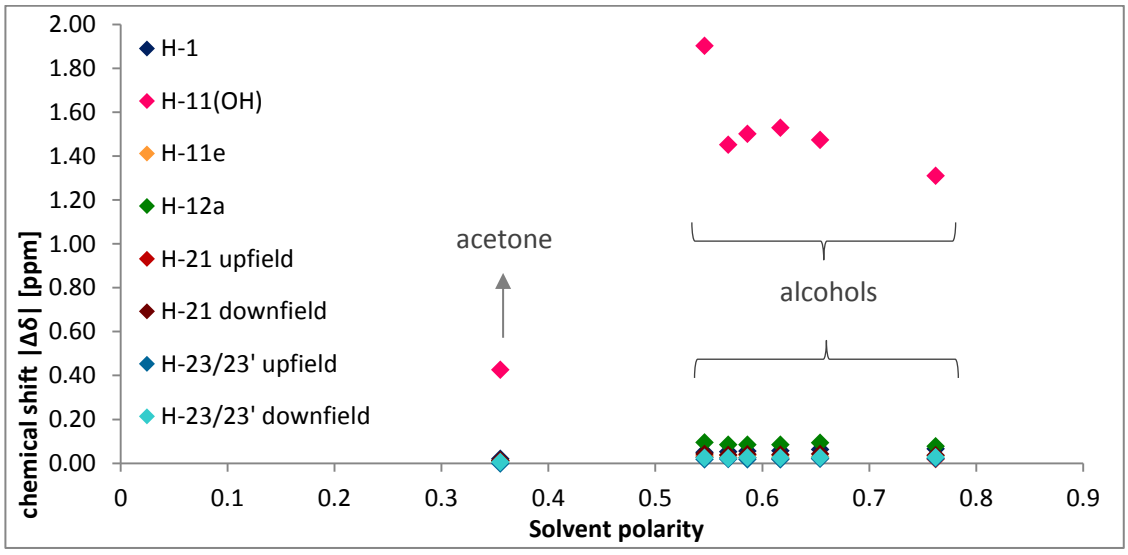

Figure 5-10. Solvent polarity and the magnitude of the chemical shift |Δδ| (ppm) observed in NMR titration at a BDP:solvent ratio of 1:250.

5.2.2 Diffusion Ordered Spectroscopy

DOSY spectra were obtained from all BDP-solvent mixtures with a molar ratio of 1:250 (BDP:solvent). The solvent and BDP molecules could be distinguished based on their diffusion constant. In addition, $CDCl_3$ (δ_{CDCl3} = 7.26 ppm) and water impurities (δ_{H2O} = 1.56 ppm) were seen in the pseudo 2D spectra. The visible signals were assigned under consideration of chemical shifts observed in NMR titration (Table 5-5) and the signals characteristic of each solvent (Yamaji et al., 2014). As expected, the smaller solvent molecules moved faster than the larger BDP molecules (Figure 5-11 to 5-17) and the molecules were clearly distinguishable based on their relative diffusion coefficients (vertical axis, f_1). Due to the extreme solvent excess, satellite signals (asterisk in Figure 5-11) were visible in a symmetrical arrangement on the left and right of the signals characteristic of each solvent.

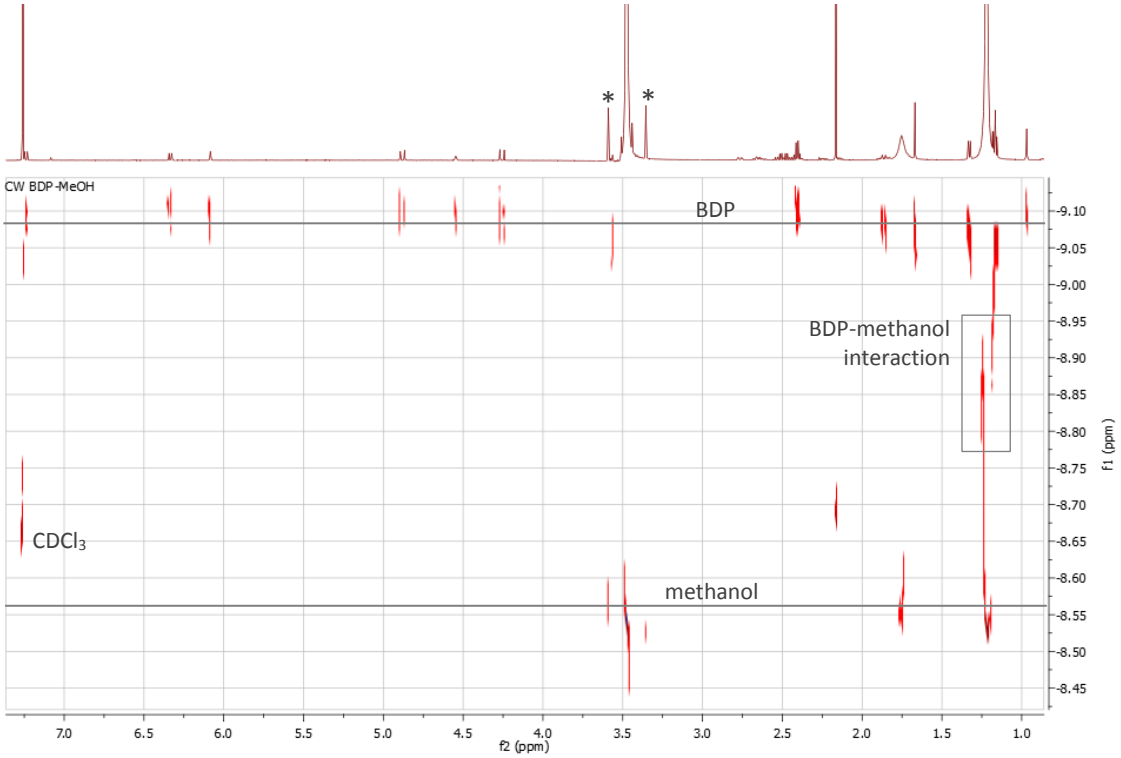

Figure 5-11. DOSY spectrum (600 MHz) of BDP:methanol 1:250 in $CDCl_3$. The marked signals indicated intermolecular interaction between BDP and methanol led to a fraction of the alcohol being diffused at a lower rate than the free alcohol. Asterisks: satellite signals, similar constellations observed in all spectra.

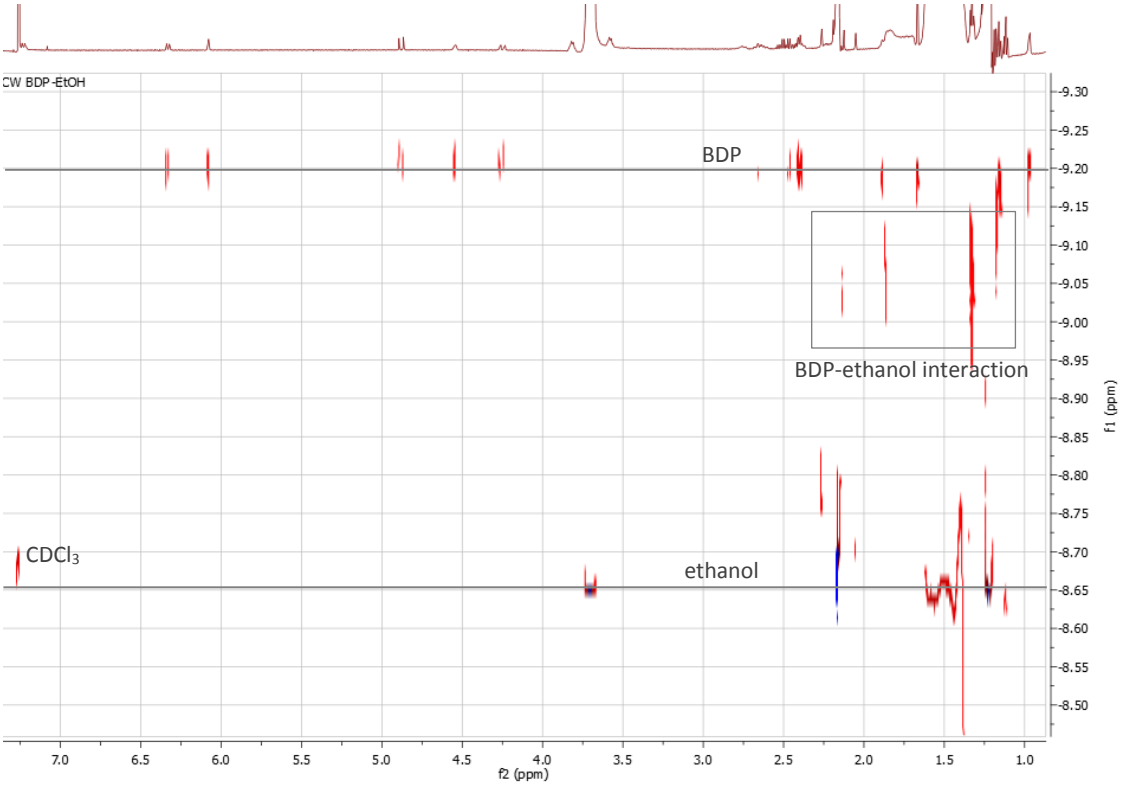

Figure 5-12. DOSY spectrum (600 MHz) of BDP:ethanol 1:250 in $CDCl_3$. The marked signals indicated intermolecular interaction between BDP and ethanol led to a fraction of the alcohol being diffused at a lower rate than the free alcohol.

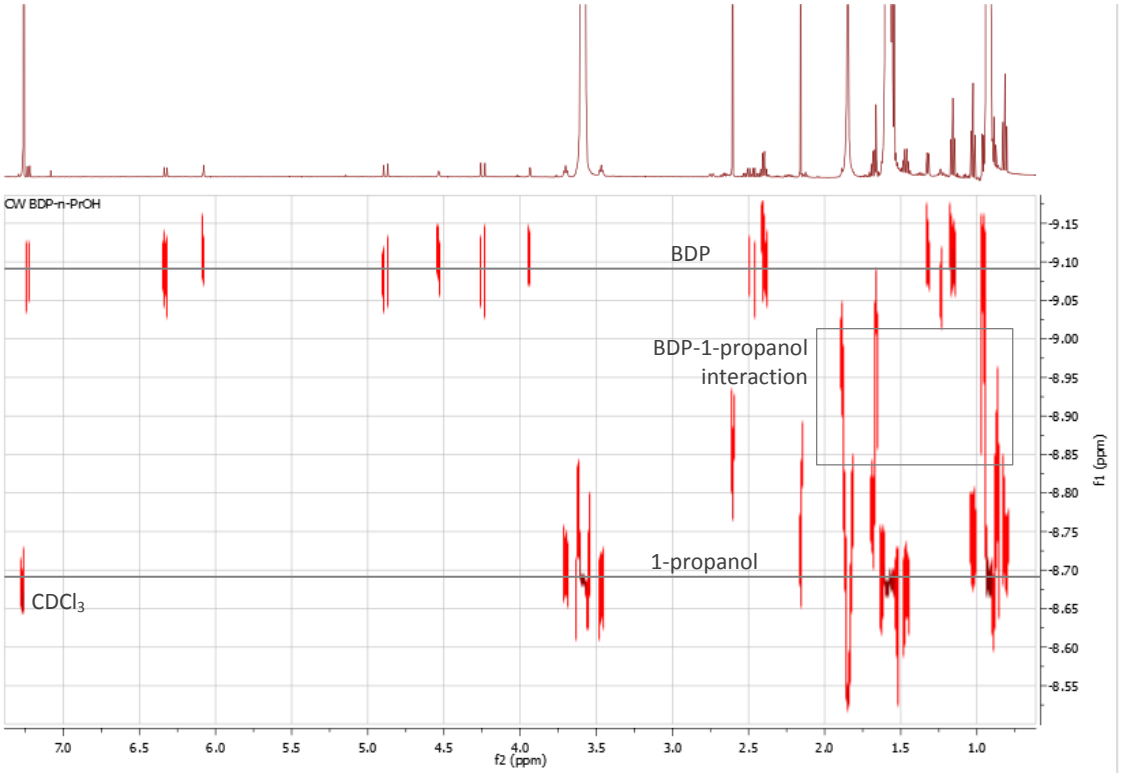

Figure 5-13. DOSY spectrum (600 MHz) of BDP:1-propanol 1:250 in $CDCl_3$. The marked signals indicated intermolecular interaction between BDP and 1-propanol led to a fraction of the alcohol being diffused at a lower rate than the free alcohol.

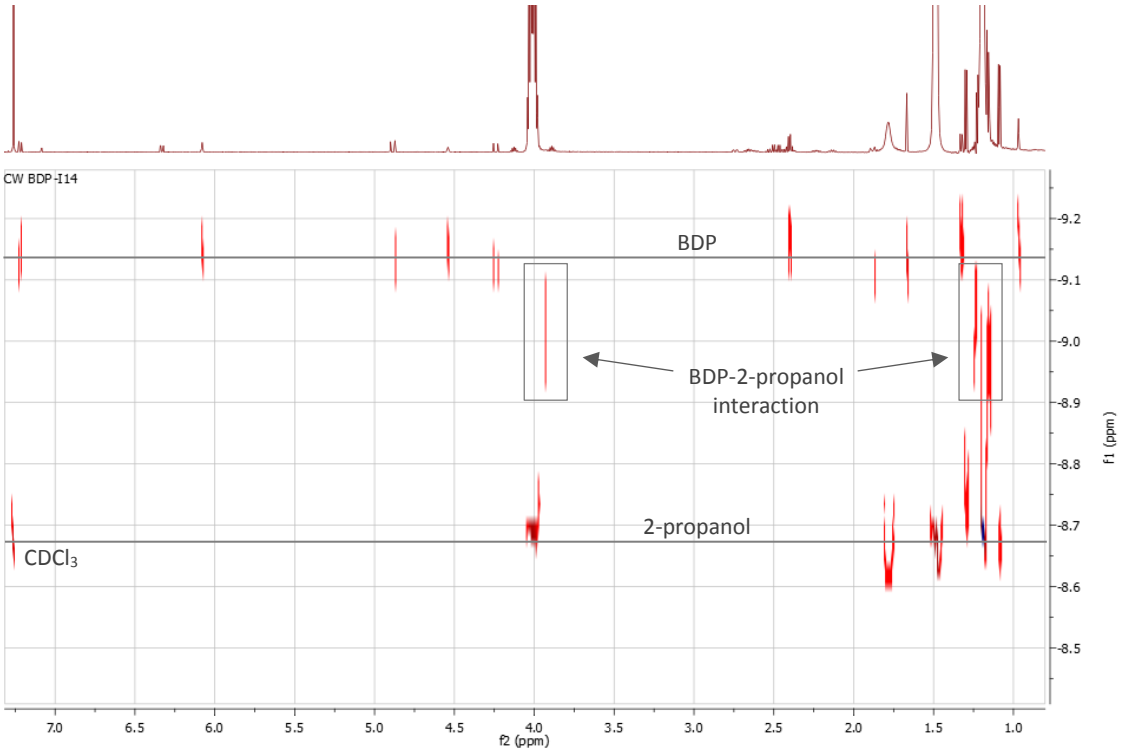

Figure 5-14. DOSY spectrum (600 MHz) of BDP:2-propanol 1:250 in $CDCl_3$. The marked signals indicated intermolecular interaction between BDP and 2-propanol led to a fraction of the alcohol being diffused at a lower rate than the free alcohol.

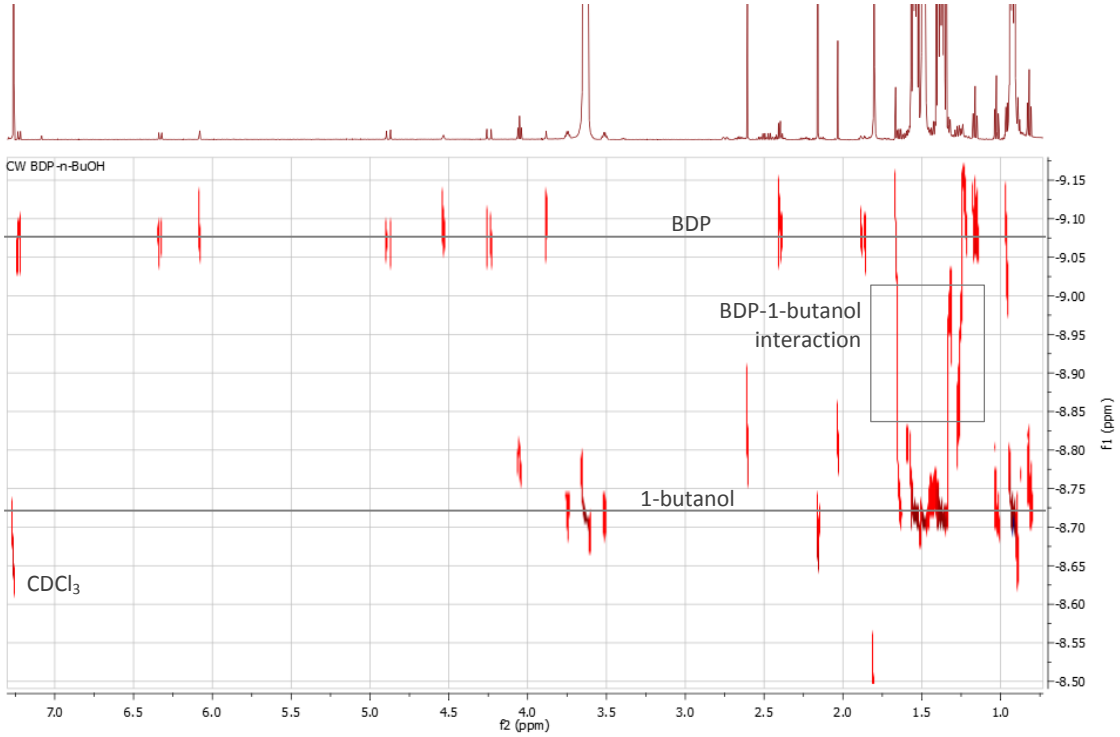

Figure 5-15. DOSY spectrum (600 MHz) of BDP:1-butanol 1:250 in $CDCl_3$. The marked signals indicated intermolecular interaction between BDP and 1-butanol led to a fraction of the alcohol being diffused at a lower rate than the free alcohol.

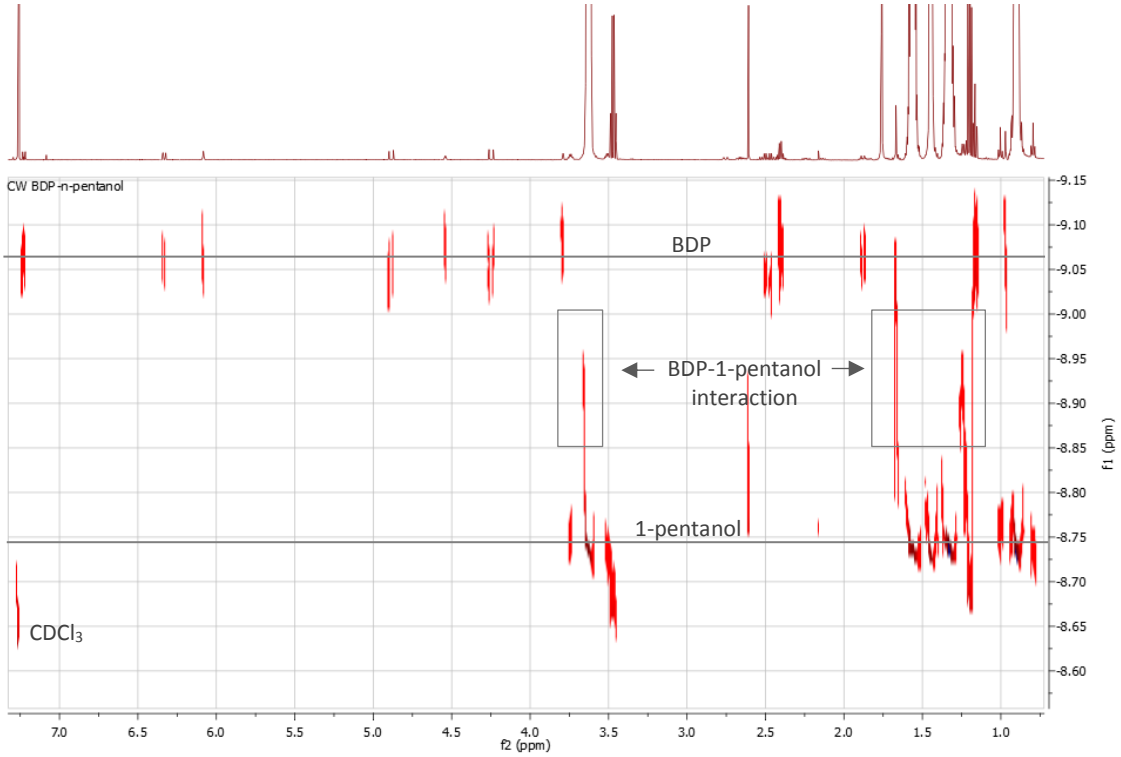

Figure 5-16. DOSY spectrum (600 MHz) of BDP:1-pentanol 1:250 in $CDCl_3$. The marked signals indicated intermolecular interaction between BDP and 1-pentanol led to a fraction of the alcohol being diffused at a lower rate than the free alcohol.

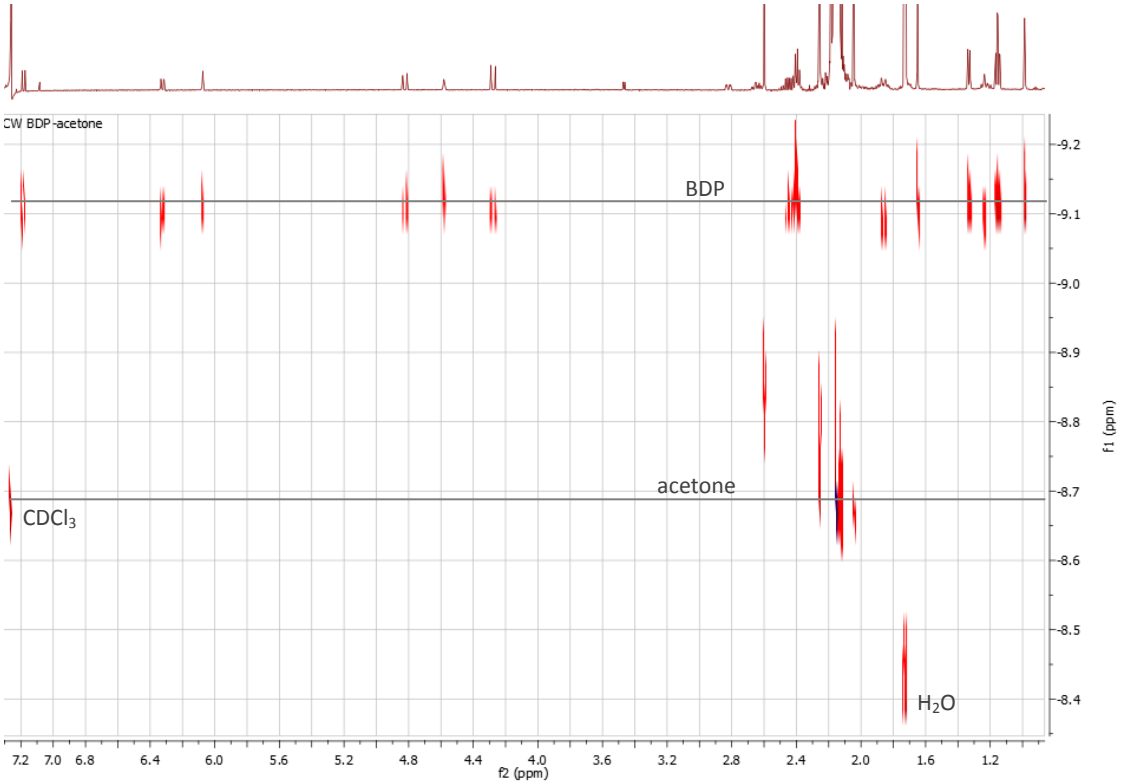

Figure 5-17. DOSY spectrum (600 MHz) of BDP:acetone 1:250 in $CDCl_3$. The small acetone and the larger BDP were separated by their diffusion coefficient without showing any intermolecular interactions.

The linear alcohols and 2-propanol were partly retained by BDP. The characteristic solvent signals were found to diffuse at two different rates (marked in Figures 5-11 to 5-15) which very likely was caused by an intermolecular interaction between BDP and the respective solvent.

In comparison, BDP and acetone were completely separated by their distinct diffusion coefficients and the DOSY spectrum did not show any signs of acetone being retained by intermolecular interaction (Figure 5-17).

Another interesting detail was observed with regard to the BDP hydroxyl proton $H_{11(OH)}$. The signal assigned to $H_{11(OH)}$ had advanced further downfield with the maximum downfield shift occurring in the BDP 1-propanol sample ($\delta_{H11(OH)}$ = 3.94 ppm) and the BDP 2-propanol sample ($\delta_{H11(OH)}$ = 3.93 ppm). There was a time lag of 30 min up to several hours between the acquisition of the 1D ^1H NMR data and the DOSY spectrum of the same sample. The increased downfield shift therefore indicated that the kinetics involving $H_{11(OH)}$ were slow and may evolve even further over a longer period of time. DOSY, however, showed no indication of intermolecular interaction between the solvent hydroxyl group and the BDP $H_{11(OH)}$.

5.3 Discussion

NMR titration spectra (Figures 5-3 to 5-9) were used to visualise how the chemical shifts of certain protons were affected by the addition of an increasing amount of solvent. The results were analysed quantitatively (Equation 5-2, Figure 5-18).

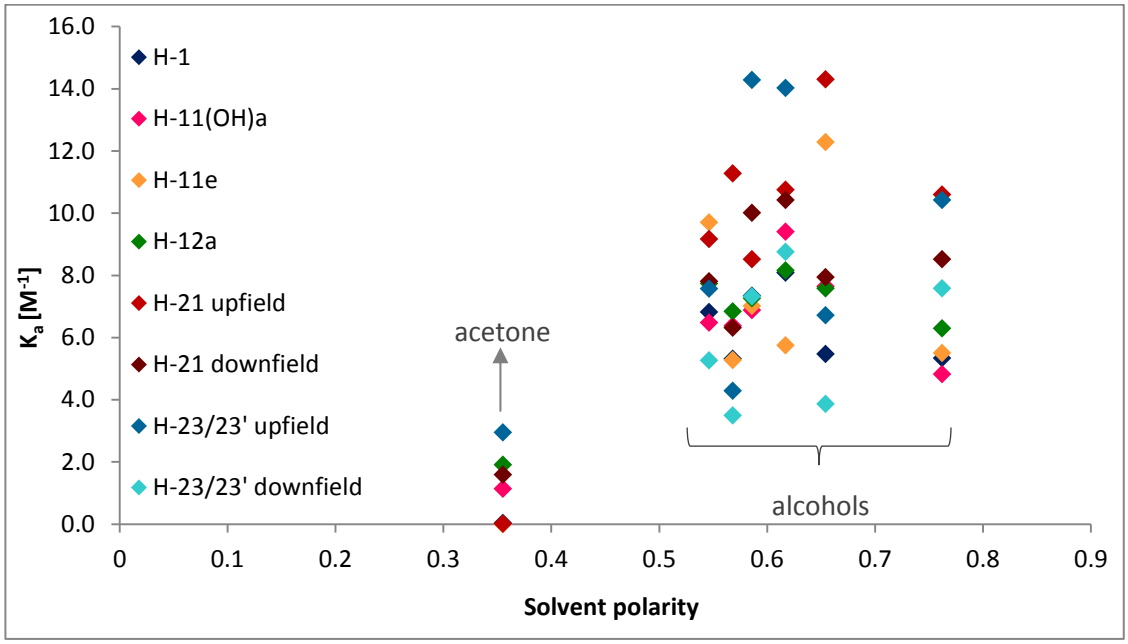

Figure 5-18. Solvent polarity and calculated association constants K_a (M^{-1}) based on NMR titration with n ≥ 10 BDP:solvent ratios (pure BDP to BDP:solvent 1:250).

NMR titration carried out with linear alcohols and 2-propanol indicated the development of weak interaction between the molecules in solution. The chemical shift associated with the solvent hydroxyl groups suggested that hydrogen bonding may have taken place.

Initially, at a BDP:solvent ratio of 1:12.5, the proton belonging to the solvent hydroxyl group experienced a significant upfield shift, possibly caused by the BDP molecules separating the solvent molecules, thus preventing the formation of strong intermolecular hydrogen bonding as it usually occurs in pure solvents. This would also lead to the typically singlet signal being split into a doublet (2-pentanol), triplets (ethanol, 1-butanol, 1-pentanol) and a quartet (methanol). When adding additional amounts of solvent, the proton signal was seen to gradually revert into broad singlets (methanol, ethanol, 1-propanol, 2-propanol) or widening into a broad triplet (1-butanol, 1-pentanol). At the same time, a downfield shift was observed which indicated the development of hydrogen bonding. Hydrogen bonding between the increasing number of solvent molecules (up to a molar ratio of BDP:solvent of 1:250) was facilitated and (partially) caused this downfield shift (Figure 5-2). Despite the high solvent content, however, the hydroxyl protons did not appear at the frequencies characteristic of the pure solvent (Yamaji et al., 2014) (Table 5-4). At the same time, $H_{11(OH)}$, the proton belonging to the hydroxyl group in C_{11} position,

displayed a significant downfield shift, probably due to hydrogen bonding. Due to an increasing amount of solvent molecules becoming available for bonding, BDP may have developed weak hydrogen bonds to solvent molecules in the immediate vicinity which would have resulted in a downfield shift of the BDP hydroxyl proton. This would have also slowed down the downfield shift of the solvent hydroxyl protons back to their characteristic frequencies in pure solvent. Other sites on the BDP molecule (carbonyl and ester groups) were also available for hydrogen bonding yet the most prominent chemical shift was the downfield shift of $H_{11(OH)}$ which appeared to be the result of a slow kinetic reaction.

BDP contains several functional groups that are able to interact with the solvent hydroxyl groups via hydrogen bonding: the carbonyl groups in the C_3 and C_{20} positions, the ester groups at C_{22} and $C_{22'}$ and the hydroxyl group at C_{11}. In its anhydrous form, BDP is known to form hydrogen bonds between the C_{11} hydroxyl proton and the oxygen at C_3 (Millard and Myrdal, 2002). The same oxygen was therefore considered very likely to interact with the alcohol which, due to mesomeric stabilisation within the conjugated ring, would lead to a decreasing electron density at H_1. The downfield shift of the H_1 signal further supported that assumption (Table 5-5).

Similarly, the oxygens at C_{22} and $C_{22'}$ are known to form hydrogen bonds to a water molecule together with the hydroxyl group in C_{11} position (Hunt and Padfield, 1989). Both were therefore likely to interact with the hydroxyl group of alcohol. The nearest ^1H at C_{23} and $C_{23'}$ experienced both a downfield and an upfield shift (Table 5-5). Since it was not possible to distinguish between the branches when carrying out the NMR titration, it could only be assumed that this was caused either by one propionate branch being the preferred group for intermolecular interaction or by the alcohol aligning in a way that would decrease the electron density around one proton at $C_{23}/C_{23'}$ while shielding the second proton and restricting molecular movement. The former would result in one set of protons experiencing a downfield shift while the latter would end the magnetic equivalence of both nuclei and the quartet would be split into a doublet of quartet in addition to the protons resonating at different frequencies. Indeed, NMR titration led to the quartet gradually separating into two quartets, one shifting to higher frequencies, the other one to lower frequencies which was considered supportive of the second assumption.

In addition, the oxygen at C_{20} was available for hydrogen bonding. Hydrogen bonding in this position would be noticed through the position of the ^1H at the nearest carbon, C_{21}. As shown by 2D HSQC-TOCSY (Figure 3-6) and the reciprocal interaction, the protons at C_{21} were not part of a larger spin system and only coupling with each other ($^2J_{HH}$ =16.4 Hz) , resulting in two doublets at 4.83 ppm and 4.27 ppm with noticeable roofing. Reduced movement due to sterical hindrance led to the protons being magnetically inequivalent despite their chemical equivalence. When increasing the solvent:BDP ratio, the two doublets were separated even further. The signal

at 4.83 ppm moved downfield and the doublet at 4.27 ppm upfield (Table 5-5). One proton was therefore in an area of higher electron density, the other one in an area of lower electron density. Hydrogen bond formation between an alcohol and the oxygen in C_{20} position would have affected both protons equally. Hydrogen bonding at the C_{23} oxygen, however, would affect the immobile protons differently by changing the electron density in spatial proximity. Together with the separation of the quartet assigned to $H_{23/23'}$ this observation strengthened the assumption that the alcohol hydroxyl group preferably interacts with the C_{23} oxygen.

The hydroxyl group at C_{11} was affected by the addition of alcohol and acetone (Table 5-5). This functional group is able to form hydrogen bonds with other hydroxyl groups (alcohol) but also with keto groups (acetone). In addition, all samples contained water as an impurity. The chemical shift of hydroxyl protons may vary with the presence of impurities and strength of interaction (Bruice, 2011). Analysis of the position of the H_2O proton signal with increasing solvent:BDP ratio indicated the development of hydrogen bonding between water and other molecules but it was not possible to detect the origin of this downfield shift.

The strength of host guest interactions and the respective association constants K_a again showed little to no interaction when acetone was used whereas all alcohols appeared to interact only weakly (K_a = 4 to K_a = 15) with the functional groups of BDP. Despite the C_{11} hydroxyl group showing the largest chemical shift upon increasing the solvent:BDP ratio (Figure 5-10), the calculated strength of interaction (based on K_a) was similar to that between the alcohols and all other functional groups available for hydrogen bonding (Figure 5-18). The solvent polarity, while affecting the chemical shift observed in the solvent hydroxyl proton itself, appeared to have no immediate impact on the association constant and strength of interaction between BDP and the solvent. The presence or absence of the hydroxyl group was seen as the decisive factor (Figure 5-18). Acetone did not interact with BDP.

The same was observed in DOSY (Figures 5-11 to 5-17) which confirmed the assumption of weak intermolecular interactions between BDP and the alcohol solvent molecules. It appeared that only a fraction of the total amount of solvent present interacted with the BDP which was expected on account of the large excess of alcohol (molar ratio BDP: alcohol 1:250). This also confirmed the assumption of the downfield shift of the alcohol hydroxyl proton seen in NMR titration (Table 5-2) as the solvent molecules were in an increasingly solvent dominated environment with only a relatively small number of BDP available for interaction.

Based on NMR titration and DOSY, alcohol molecules appeared to develop weak hydrogen bonds to certain functional groups on BDP which would prevent these groups from interacting with other BDP molecules. This in turn would facilitate the formation of channels solvates through bonding via the more accessible sites where intermolecular BDP-BDP bonding is

favoured over weak BDP-solvent bonding. The alcohol molecules, being trapped within the evolving channel structure, maintain weak hydrogen bonding to the available sites but also form stronger bonds between each other, thus developing an increased mobility. As the channels form and become more regular, the solvent molecules are aligned within the structure and through their presence add to the stability of the crystalline compound. Their loss through evaporation was seen to lead to the recrystallisation of the compound into the anhydrous form (Figures 4-7, 4-8, 4-9).

Thermal analysis, however, suggested the formation of a BDP acetone solvate and only three alcohol based BDP solvates. DSC and TGA indicated that only BDP ethanol, BDP 1-propanol and BDP 2-propanol solvates had crystallised from the respective solutions. NMR titration and DOSY, in contrast, did not show any signs of any BDP-acetone interactions and the mechanism of solvate formation could not be explained in line with the formation of alcohol based BDP solvates. The formation of solvates may simply have been caused by the presence of acetone in excess and BDP being forced to form intermolecular bonds between the most reactive sites, trapping acetone between them while doing so. This would also explain the differences in thermal analysis where acetone was seen to evaporate in either two or three steps followed by recrystallisation in either one or two steps (Figures 4-7, 4-8, 4-9; Table 4-7).

NMR titration and DOSY showed similar interactions between BDP and all alcohol solvents used although, based on XRPD and thermal analysis, only some were assumed to form solvates. Two scenarios could explain the discrepancy between NMR based analysis and thermal analysis: solvate formation may have occurred and unstable solvates may have formed (scenario 1), solvate formation may have started but solvent characteristics may have prevented the completion of the solvated compound (scenario 2):

Scenario 1

One possibility is that the formation of solvates followed a similar mechanism in all cases where alcohol was used. However, the BDP methanol, BDP 1-butanol and BDP 1-pentanol solvates forming less stable compounds than those based on ethanol, 1-propanol and 2-propanol. The decrease in stability might be due to the size and polarity of the solvent molecules incorporated within the channels. Large molecules such as 1-butanol and 1-pentanol, while still interacting with BDP in solution, may be too large to be accommodated in excess inside the channels. The lack of solvent molecules for solvent-solvent intermolecular bonding would lead to the weak hydrogen bonding between BDP and solvent molecule being the only force keeping 1-butanol and 1-pentanol in place. Such a structure would be susceptible to decomposition at low temperatures or when taken out of solution.

In contrast, methanol is a small molecule with relatively high polarity and low boiling point (Table 4-1), thus prone to prefer intermolecular solvent-solvent bonding over BDP-solvent interactions and also prone to evaporate at low temperatures. During solvate formation, a large number of methanol molecules might become included within the channels which then proceed to form hydrogen bonds with each other rather than maintain the very weak hydrogen bonding to BDP. Methanol might therefore behave more like a pure solvent than ethanol, 1-propanol or 2-propanol within the channels which in turn might lead to methanol contributing less to the stability of the structure. Being trapped inside the channels while in a solution like environment, methanol would display mixed behaviour as observed in thermal analysis (Figures 4-7, 4-8, 4-9; Table 4-7). The solvent would easily migrate towards the open ends of the channels and evaporate at low temperatures, thus causing the early onset of recrystallisation. However, the amount of methanol evaporating within a certain time at room temperature is limited by the diffusion of the solvent and a small fraction of methanol still inside the channel at the time of thermal analysis would be forced to evaporate at temperatures above its boiling point as additional energy is necessary to fasten the diffusion of the left-over solvent.

Scenario 2

The size and polarity of 1-butanol and 1-pentanol might have prevented the formation of solvates while still facilitating the onset of solvate formation. Following the mechanism described in scenario 1, the process of solvate formation may have been interrupted due to 1-butanol and 1-pentanol being forced out of the evolving channels due to their size and the preference of solvent-solvent interaction over BDP-solvent interaction. Without any solvent present to support the channel structure, the compound would have collapsed as it formed and recrystallized into the more stable anhydrous form.

Both scenarios would explain the differences observed in NMR titration, DOSY and thermal analysis but additional analytical methods such as XRD and solid state NMR might add to understanding the process of solvate formation and the intermolecular bonding within the solvates.

5.4 Conclusions

NMR titration gave valuable information about the interaction between the solvent and BDP in solution. The presence of polar hydroxyl groups appeared to be decisive for the formation of weak hydrogen bonds between the BDP and the alcohols. This was seen in the chemical shifts of the signals characteristic of the BDP protons H_1, H_{11}, $H_{11(OH)}$, H_{12A}, H_{21A}, H_{21B}, H_{23} and H_{23}'(Table 5-5). DOSY NMR showed that a fraction of the alcohol molecules was retained by BDP, causing the diffusion efficient of the smaller solvent molecule to decrease. Using acetone,

in contrast, did not result in any comparable intermolecular interactions between the solvent and BDP.

Two possible mechanisms were proposed to explain why solvate formation appeared to only occur when ethanol, 1-propanol, 2-propanol and acetone were used (thermal analysis, Chapter 4). One possibility was that solvates may initially have formed in all cases with the BDP methanol, 1-butanol and 1-pentanol solvates being very instable compounds. The other possibility, relating to the compounds crystallised from 1-butanol and 1-pentanol solution, was that solvate formation may have started but could not be completed due to the large molecules not fitting well into the channels which have a limited diameter of 7.5 Å (Kuehl et al., 2003).

Additional studies, based on single crystal XRD and solid state NMR, were carried out to analyse the intermolecular interactions between the BDP and solvent in the channel solvates and to better understand the role of the solvent in maintaining the channel structure.

5.5 References

Bruice, P. Y. 2011. *Organische Chemie: studieren kompakt*, Pearson Deutschland GmbH.

Choudhary, M. I. 2015. *Applications of NMR Spectroscopy*, Elsevier.

dos Santos, P. M., Hall, A. J. & Manesiotis, P. 2016. Stoichiometric molecularly imprinted polymers for the recognition of anti-cancer pro-drug tegafur. *Journal of Chromatography B*, 1021, 197-203.

Dudzik, K., Wojcik, J., Ejchart, A. & Nowakowski, M. 2017. Size makes a difference: Chiral recognition in complexes of fenchone with cyclodextrins studied by means of NMR titration. *Chirality*, 29, 747-758.

Einstein, A. 1905. Über die von der molekularkinetischen Theorie der Wärme geforderte Bewegung von in ruhenden Flüssigkeiten suspendierten Teilchen. *Annalen der Physik*, 322, 549-560.

Gottlieb, H. E., Kotlyar, V. & Nudelman, A. 1997. NMR chemical shifts of common laboratory solvents as trace impurities. *The Journal of Organic Chemistry*, 62, 7512-7515.

Harris, J. A., Carducci, M. D. & Myrdal, P. B. 2003. Beclomethasone dipropionate crystallized from HFA-134a and ethanol. *Acta Crystallographica Section E: Structure Reports Online*, 59, o1631-o1633.

Hunt, J. H. & Padfield, J. M. 1989. *Micronised beclomethasone dipropionate monohydrate compositions and methods of use*. US Patent 4,866,051.

Jinks, P. A. 1989. *Physically modified beclomethasone dipropionate suitable for use in aerosols*. US Patent 4,810,488.

Kuehl, P. J., Carducci, M. D. & Myrdal, P. B. 2003. An ethanol solvate of Beclomethasone dipropionate. *Acta Crystallographica Section E: Structure Reports Online*, 59, 1888-1890.

Lamm, J. H., Niermeier, P., Mix, A., Chmiel, J., Neumann, B., Stammler, H. G. & Mitzel, N. W. 2014. Mechanism of Host–Guest Complex Formation and Identification of Intermediates through NMR Titration and Diffusion NMR Spectroscopy. *Angewandte Chemie International Edition*, 53, 7938-7942.

Millard, J. W. & Myrdal, P. B. 2002. Anhydrous beclomethasone dipropionate. *Acta Crystallographica Section E: Structure Reports Online*, 58**,** o712-o714.

Othman, A., Harris, R. K., Hodgkinson, P., Christopher, E. A. & Lancaster, R. W. 2008. Structural characterisation of two pharmaceutically important steroids by solid-state NMR. *New Journal of Chemistry*, 32, 1796-1806.

Page, P. R. & Heggie, W. 1990. *Preparation and use of new solvates of beclomethasone 17, 21-dipropionate*. US Patent 4,913,892.

Schlörer, N. E., Cabrita, E. J. & Berger, S. 2002. Characterization of Reactive Intermediates by Diffusion-Ordered NMR Spectroscopy: A Snapshot of the Reaction of 13CO2 with [Cp2Zr (Cl) H]. *Angewandte Chemie International Edition*, 41, 107-109.

Thordarson, P. 2011. Determining association constants from titration experiments in supramolecular chemistry. *Chemical Society Reviews*, 40**,** 1305-1323.

Wierzbicka, C., Liu, M., Bauer, D., Irgum, K. & Sellergren, B. 2017. Cationic pTyr/pSer imprinted polymers based on a bis-imidazolium host monomer: Phosphopeptide recognition in aqueous buffers demonstrated by μ-liquid chromatography and monolithic columns. *Journal of Materials Chemistry B*, 5, 953-960.

Yamaji, T., Saito, T., Hayamizu, K., Yanagisawa, M., Yamamoto, O., Wasada, N., Someno, K., Kinugasa, S., Tanabe, K. & Tamura, T. 2014. *Spectral database for organic compounds, SDBS*. Electronic resource: http://sdbs. db. aist. go. jp/sdbs/cgi-bin/cre_index. cgi.

CHAPTER 6

STRUCTURAL ANALYSIS OF BECLOMETHASONE DIPROPIONATE SOLVATES

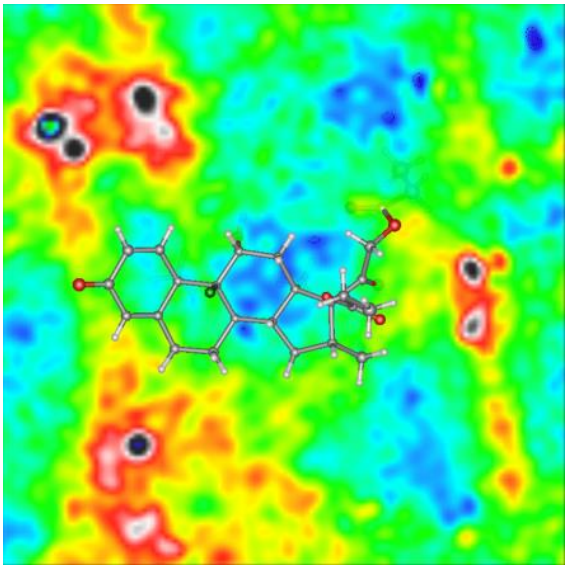

Figure 6. Electron density map of BDP ethanol solvate based on XRD data.

6 Structural Analysis of Beclomethasone Dipropionate Solvates

Despite NMR titration, DOSY and thermal analysis giving a better understanding of how solvate formation occurs in solution, the results do not give any conclusion about intermolecular interactions within the crystalline structure of the BDP solvates. It was assumed that solvates could only be obtained from acetone, ethanol, 1-propanol and 2-propanol solutions while the crystalline compound prepared from methanol, 1-butanol and 1-pentanol appeared to be anhydrous BDP. Two possible crystallisation mechanisms were discussed, both depending on solvent polarity and size. One mechanism was assumed to lead to the formation of stable and unstable solvates, the second mechanism considered the onset of solvate formation with the completion of the crystalline channel structure being either supported or obstructed by the respective solvents. Single crystal XRD of the compounds, obtained immediately after crystallisation, may give additional information about crystallisation, solvate stability and solvent mobility within the channel structure.

Several BDP solvates have been prepared from supersaturated solutions (Kuehl et al., 2003, Harris et al., 2003, Nachiengtung, 1997, Page and Heggie, 1990, Jinks, 1989) and the crystalline structures of the anhydrous form, the ethanol solvate, the HFA-134 ethanol solvate and the ethyl-acetate solvate have been filed in the crystalline database (Cambridge Crystallographic Data Centre, CCDC). In addition, the formation of further alcohol based solvates was reported (Jinks, 1989) but not fully characterised. XRD and solid state NMR (SSNMR) are common methods to analyse crystalline structures. A novel approach, combining electron density maps calculated from single crystal XRD and NMR data, was used here to further investigate the crystalline BDP compounds obtained from methanol, ethanol, 1-propanol, 2-propanol, 1-butanol, 1-pentanol and acetone solution.

6.1 Materials and Methods

6.1.1 Materials

BDP solvates were prepared from supersaturated solutions as outlined in Chapter 4.

6.1.2 Single Crystal X-ray Diffraction

Single crystal XRD was carried out using an Agilent Supernova XRD (Agilent Technologies). Prior to finalising the analyses, each unit cell was compared to the data available on the CCDC database and the measurement was interrupted if the unit cell matched that anhydrous BDP. The structure refinement and modelling was based on the Hirshfeld atom refinement (HAR) method which uses aspherical scattering factors based on quantum mechanical molecular electron densities to convert XRD data into a crystalline structure (Capelli et al., 2014, Jayatilaka and Dittrich, 2008). This method has proven useful for modelling strong hydrogen bonds (Woińska

et al., 2014) and was recently added to the Olex^2 Crystallography Software (OlexSys) (Bourhis et al., 2015, Dolomanov et al., 2009).

6.1.3 Solid State Nuclear Magnetic Resonance Spectroscopy

Solid-state nuclear magnetic resonance (SSNMR) spectroscopy is an extremely useful technique to study molecular conformations, intermolecular interactions and dynamics or to detect the structures of crystals, amorphous material and biomolecules which makes the technique valuable for the characterisation of pharmaceutical materials. Similar to solution state NMR, SSNMR is based on the interactions of nuclear spins with an applied magnetic field; yet the essential interactions – chemical shielding, dipole-dipole and quadrupole coupling - are anisotropic and cause broad signals in the spectrum. The sensitivity of the technique is restricted by the limited number of active nuclei and, in the case of SSNMR, the long relaxation times. These effects can be reduced by using cross polarisation (CP) to increase sensitivity and magic angle spinning (MAS) to increase resolution.

^{13}C CPMAS SSNMR was carried out using an Avance III Bruker 400 MHz NMR spectrometer. Chemical shifts were referenced by setting the methylene peak of adamantane to 38.48 ppm. For comparison a SSNMR spectrum was also obtained for anhydrous BDP.

6.2 Results

6.2.1 Single Crystal X-ray Diffraction

Single crystal XRD data was obtained from BDP samples prepared from methanol, ethanol, 1-propanol, 2-propanol, 1-butanol, 1-pentanol and acetone. Each crystal was kept in solution prior to analysis and, when taken out of solution, immediately immersed in paraffin oil, transferred onto the platinum wire holder and placed into the XRD chamber where nitrogen was used to create an inert atmosphere.

In a pre-screening run, the unit cells were determined and compared to CCDC data. The pre-screening showed that anhydrous BDP was prepared from methanol, 1-butanol and 1-pentanol as the unit cell matched the unit cell of the orthorhombic anhydrous BDP with a $P2_12_12_1$ crystalline space group (Millard and Myrdal, 2002) (Figure 6-1a). The measurements were interrupted at this point for all except one run, based on BDP crystallised from 1-butanol, which was completed as a representative example of anhydrous BDP and used as a reference (Figure 6-1b).

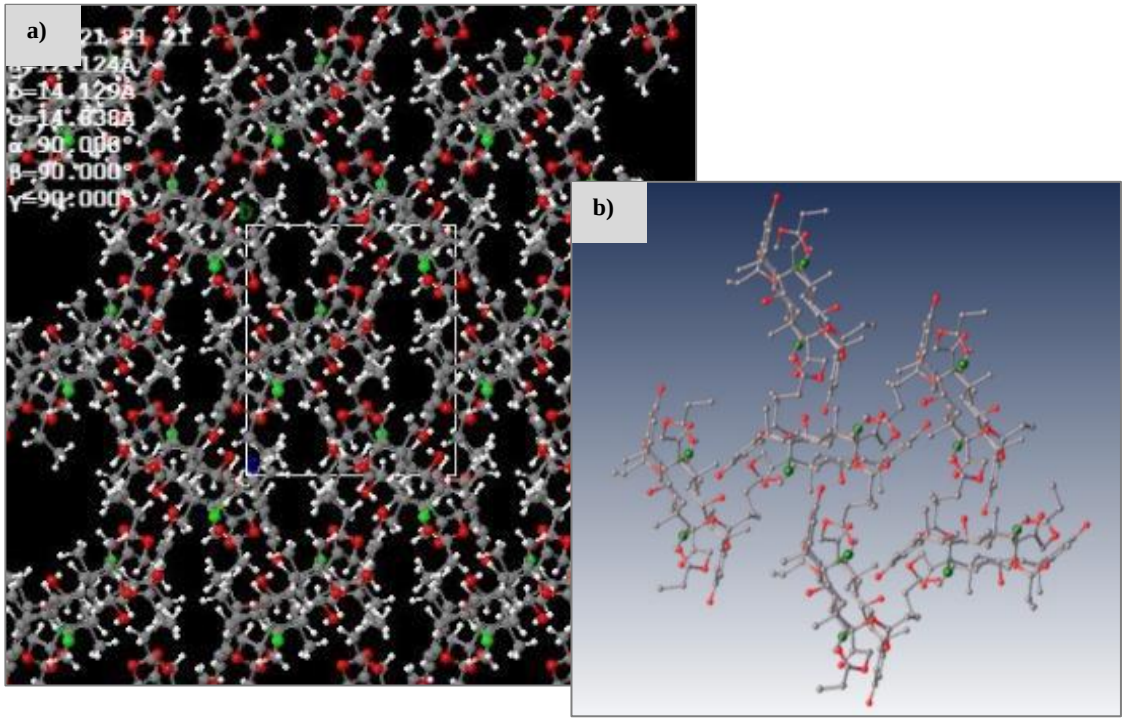

Figure 6-1. Crystalline structure of anhydrous BDP; a) structure available on the CCDC database (Millard and Myrdal, 2002) and b) structure modelled from XRD data. White: hydrogen, grey: carbon, red: oxygen, green: chlorine.

BDP crystallised from ethanol, 1-propanol, 2-propanol and acetone was found to match the unit cell filed for the BDP ethanol solvate (Kuehl et al., 2003) which was reported to crystallise trigonally in a $P3_121$ space group forming a channel with a diameter of 7.5 Å (Figures 6-2a, b). Six BDP molecules are staggered in a circle in a herringbone pattern forming a channel in which the solvent molecules are present (Kuehl et al., 2003, Harris et al., 2003).

The XRD measurements were analysed and refined using the Olex^2 HARt (Hirshfeld atom refinement) interface (Bourhis et al., 2015, Dolomanov et al., 2009) (Figure 6-2c). The models both visualised the intermolecular bonding between the hydroxyl group of one BDP with the oxygen in C_{23}' position of a second BDP molecule which leaves the longer side branch ($C_{21\text{-}24}$) pointing inwards and making the respective oxygen groups available for (weak) hydrogen bonding with the solvent molecules inside the channel.

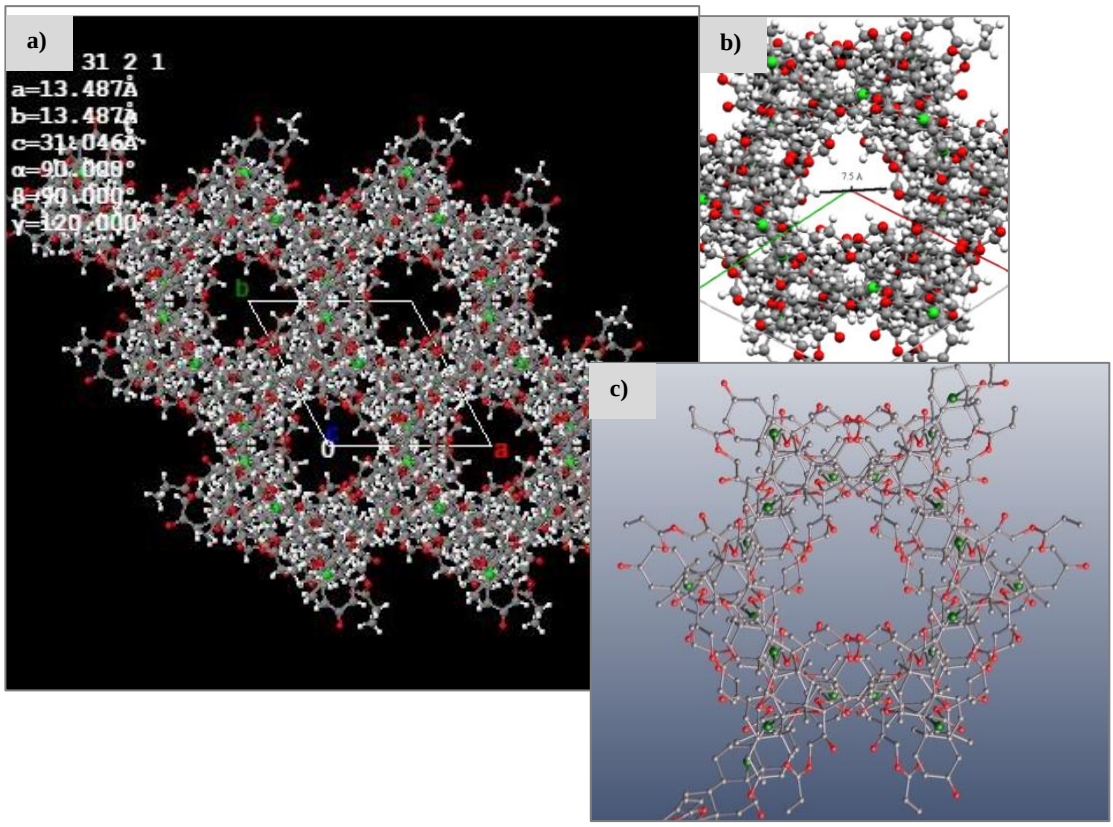

Figure 6-2. Crystalline structure of the BDP ethanol solvate; a) structure of the BDP ethanol solvate with b) showing the average diameter of the channel (Kuehl et al., 2003) and c) structure modelled from XRD data using Olex^2. View along the 001 axis. White: hydrogen, grey: carbon, red: oxygen, green: chlorine.

Based on the electron density distribution only one ethanol molecule could be fitted and a heat map was generated to display the probable location of additional ethanol molecules within the channels and the voids accessible to solvents (Figure 6-3). The software allows one to model the heat map at any level along the channel based on XRD data. The heat map shows the most likely position of molecules and is calculated from the theoretical probability density which is proportional to the square of the wave function and was the basis of the HAR calculations. For consistency and clarity, the same level was chosen to reveal the position of the carbonyl group at C_{23}, the group reaching into the channel which was assumed to interact with the solvent molecules. The position of one ethanol molecule could be modelled yet additional solvent molecules may have been shared between the BDP molecules. It was not possible to solve the complete structural arrangement of the BDP structure and all ethanol molecules which was seen as proof of the high mobility of the solvent inside the channel solvate. It was excluded in all further maps for comparability.

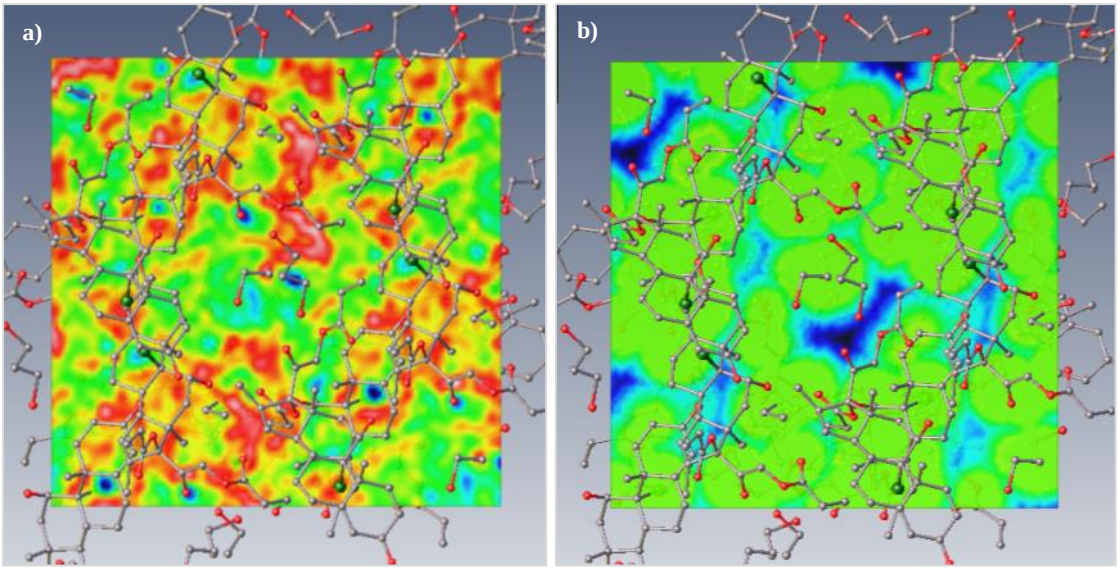

Figure 6-3. Heat maps showing a) the electron density distribution across the channel of the BDP ethanol solvate (BDP:ethanol ratio modelled as 1:1 ratio – 3 ethanol molecules visible due to 3 BDP molecules being displayed above the plane where the heat map is positioned) and b) the possible location of voids (blue) accessible to additional solvent molecules.

The heat maps (Figure 6-3) were modelled based on a BDP:ethanol ratio of 1:1. The automated Hirshfeld atom refinement (HAR) calculated the position of one ethanol molecule. Considering the thermal analysis results (Table 4-10) which gave a stoichiometric ratio of 1:1.33 (BDP:ethanonl) and literature where a BDP:ethanol ratio of 1:2 was assumed (Kuehl et al., 2003), this might be a good approximation but does not necessarily represent the true stoichiometry. Additional ethanol molecules may be present and the ratio may change depending on the mobility of the solvent within in the channel. A direct comparison of the heat maps in Figure 6-3 revealed a void close to the oxygen in the C_{23} position pointing into the channel (Figure 6-3b) and a higher electron density (red), indicating the possible location of an additional solvent molecule in this area (Figure 6-3a). When using a manual approach, it was impossible to refine the molecular structure of the BDP ethanol solvate in a way that allowed the exact determination of all solvent molecules. Ethanol was therefore assumed to move within the channel (Kuehl et al., 2003, Harris et al., 2003), thus allowing the solvent molecules to be shared between several BDP molecules which supported the assumption of a true stoichiometric ratio larger than 1:1 but below 1:2 (BDP:ethanol).

To verify the applicability of heat maps, the ethanol molecule was removed from the structure and both heat maps were generated from the remodelled BDP channel structure (Figure 6-4).

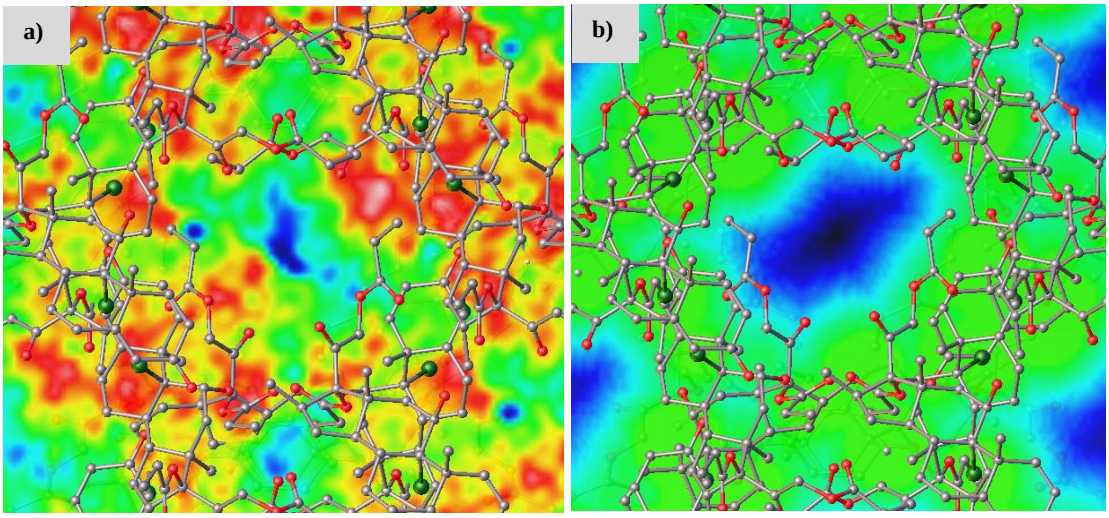

Figure 6-4. Heat maps showing a) the electron density distribution across the channel of the BDP ethanol solvate and b) the possible location of voids accessible to solvent molecules.

The electron density heat map (Figure 6-4a) suggested a higher electron density distribution along the edges of the channel (red) with low density areas (blue) in the middle despite the complete channel being accessible to guest molecules (Figure 6-4b). The results also confirmed the orientation of the ethanol molecules shown in Figure 6-3a. The more electronegative hydroxyl groups pointed towards the BDP propionate branch reaching into the channel, the less electronegative carbon tail of the alcohol was directed towards the centre of the channel. In addition, the electron density heat map shown in Figure 6-4a again confirmed the mobility of ethanol inside the channel structure: the green areas were areas of medium electron density. This was possibly due the mobile solvent molecules moving through the channel. They appeared to have been held in place for a slightly longer period of time by weak hydrogen bonding at the edges of the channel where the red areas indicated a higher probability density.

Similar heat maps showing the accessible voids and the electron density distribution within the channels were prepared for the BDP 1-propanol solvate (Figure 6-5), BDP 2-propanol solvate (Figure 6-6) and the BDP acetone solvate (Figure 6-7). When compared to one theoretical unit cell volume, the accessible void appeared to equal approximately 30% of the cell volume regardless of the solvent used.

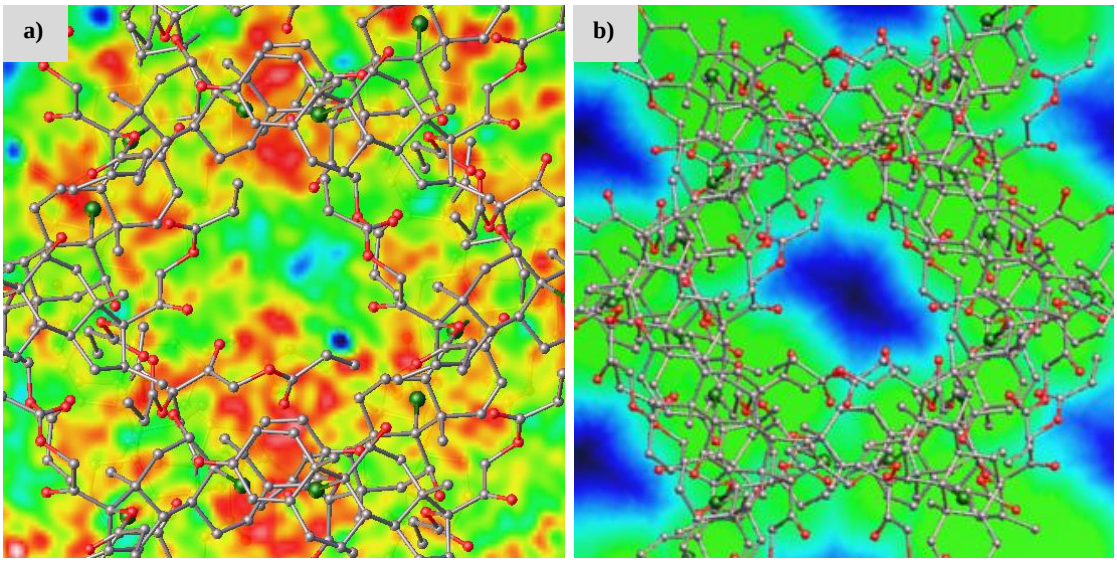

Figure 6-5. Heat maps showing a) the electron density distribution across the channel of the BDP 1-propanol solvate and b) the possible location of voids accessible to solvent molecules.

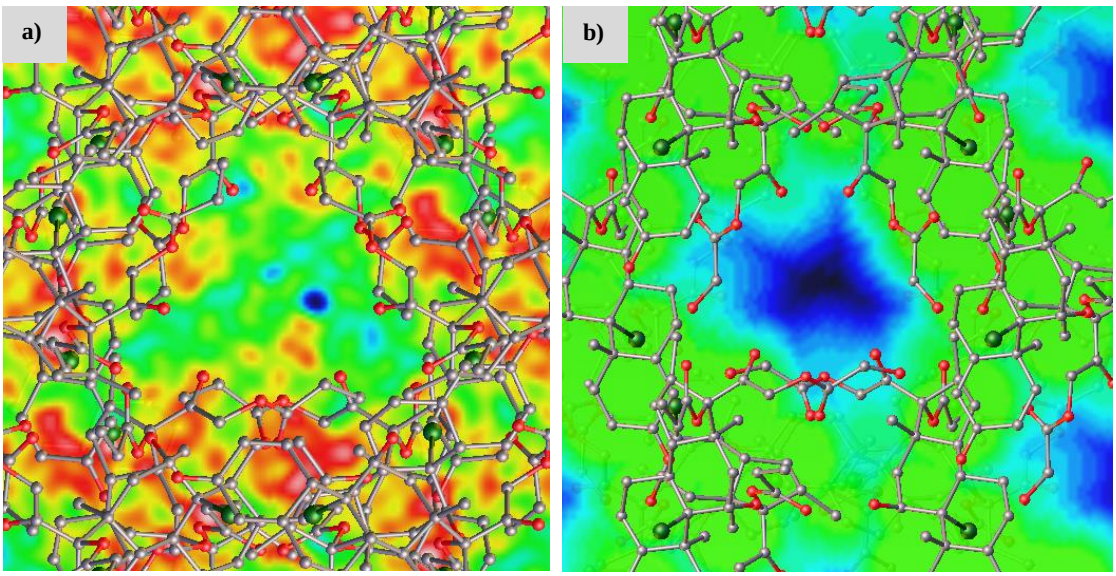

Figure 6-6. Heat maps showing a) the electron density distribution across the channel of the BDP 2-propanol solvate and b) the possible location of voids accessible to solvent molecules.

In comparison, the alcohol based solvates appeared to have similar accessible voids in the centre of the channel but each heat map displayed unique probability densities indicating that the arrangement and most likely position of each solvent within the channels changed with the solvent used. Ethanol (Figure 6-4a) and 2-propanol (Figure 6-6a) appeared to be more evenly distributed across the whole accessible volume of the channel with a slightly higher probability at the edges where the alcohol hydroxyl groups might have interacted weakly with the BDP propionate branch directed towards the channel.

The heat map visualising the electron distribution within the BDP 1-propanol solvate, however, suggested a high probability density in the part of the channel which extended towards the BDP

propionate branches (Figure 6-5a). The most likely position a 1-propanol molecule thus might be a position where the alcohol hydroxyl group formed weak hydrogen bonds to the propionate oxygen of one BDP with the 1-propanol carbon tail directed towards the centre of the channel. Due to the molecules being slightly longer than ethanol, 1-propanol might be less easily accommodated along the channel.

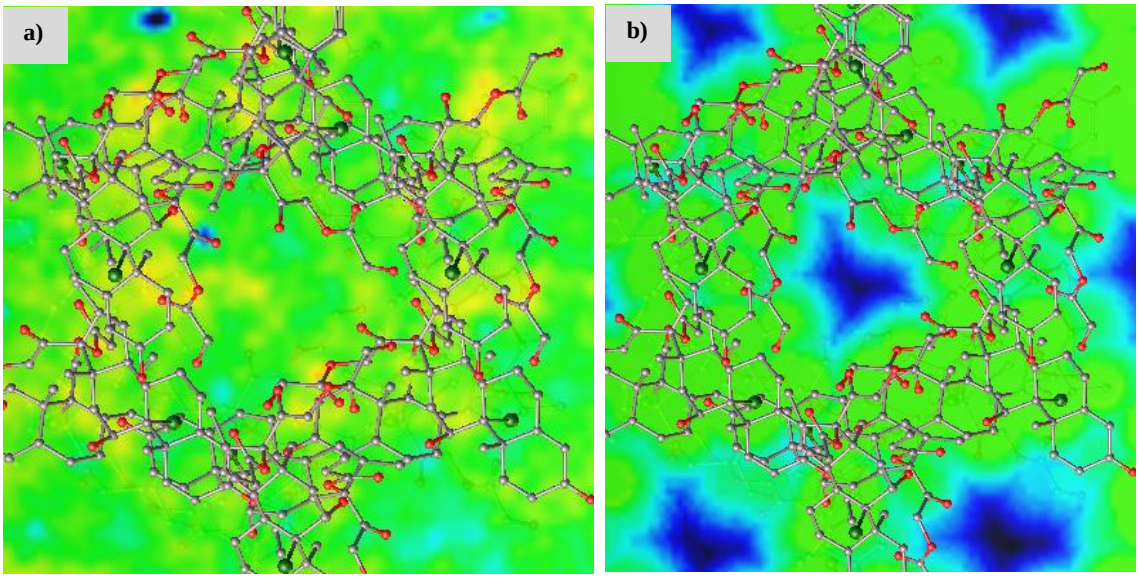

Figure 6-7. Heat maps showing a) the electron density distribution across the channel of the BDP acetone solvate and b) the possible location of voids accessible to solvent molecules.

The BDP acetone solvate, despite having the same structure as the alcohol based solvates, appeared to have more evenly distributed electron density within the channel (Figure 6-7). Since acetone was assumed not to interact in any way with the BDP propionate branches or any other functional groups (Chapter 5), the even probability density was interpreted as the acetone molecules being highly mobile. Their fast exchange and solution like behaviour resulted in the average probability position being equally distributed along the channel.

In contrast to the BDP solvates, the structure of the more densely packed anhydrous BDP did not provide any voids accessible to solvent molecules and the electron density distribution along the crystalline structure appeared to be even without any areas of particularly high or low electron density (Figure 6-8).

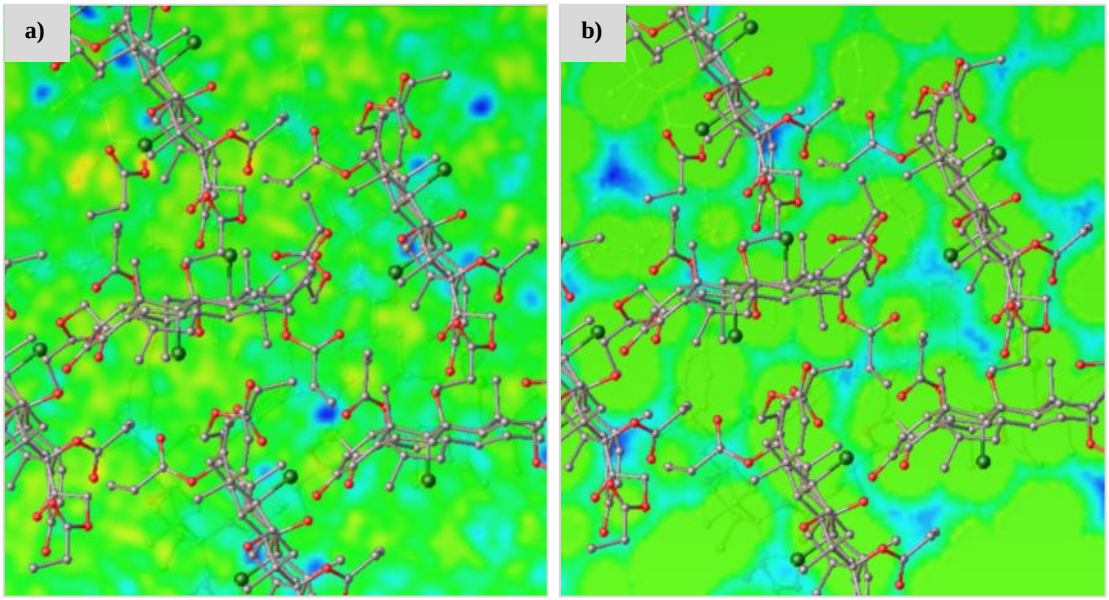

Figure 6-8. Heat maps showing a) the electron density distribution across the crystalline structure of anhydrous BDP and b) the possible location of voids accessible to solvent molecules.

6.2.2 Solid State Nuclear Magnetic Resonance Spectroscopy

Based on XRD results, only confirmed BDP solvates prepared from ethanol, 1-propanol, 2-propanol and acetone were analysed using SSNMR. The spectra showed clear differences between the anhydrous BDP and the BDP solvates (Figure 6-9) with all solvates exhibiting a larger number of ^{13}C signals compared to the anhydrous sample. Comparing the signals to the ^{13}C CPMAS SSNMR spectra of anhydrous BDP, the BDP monohydrate and the BDP ethyl acetate solvate (Table 6-1) (Christopher, 1993) showed that all samples were a mixture of BDP solvate, anhydrate and monohydrate which also included traces of solvent (Tables 6-2 to 6-5), thus confirming the solvated state of the compounds. The signals assigned with the solvates (Table 6-6) were found at nearly identical positions which matched the results seen in single crystal XRD where each solvate appeared to crystallise in the same space group and was found to have the same unit cell.

Over time, when kept at room temperature inside the rotor used for SSNMR, the BDP solvates were found to transition into the anhydrous form (Table 6-7, 6-8) due to the instability of the solvates at ambient conditions.

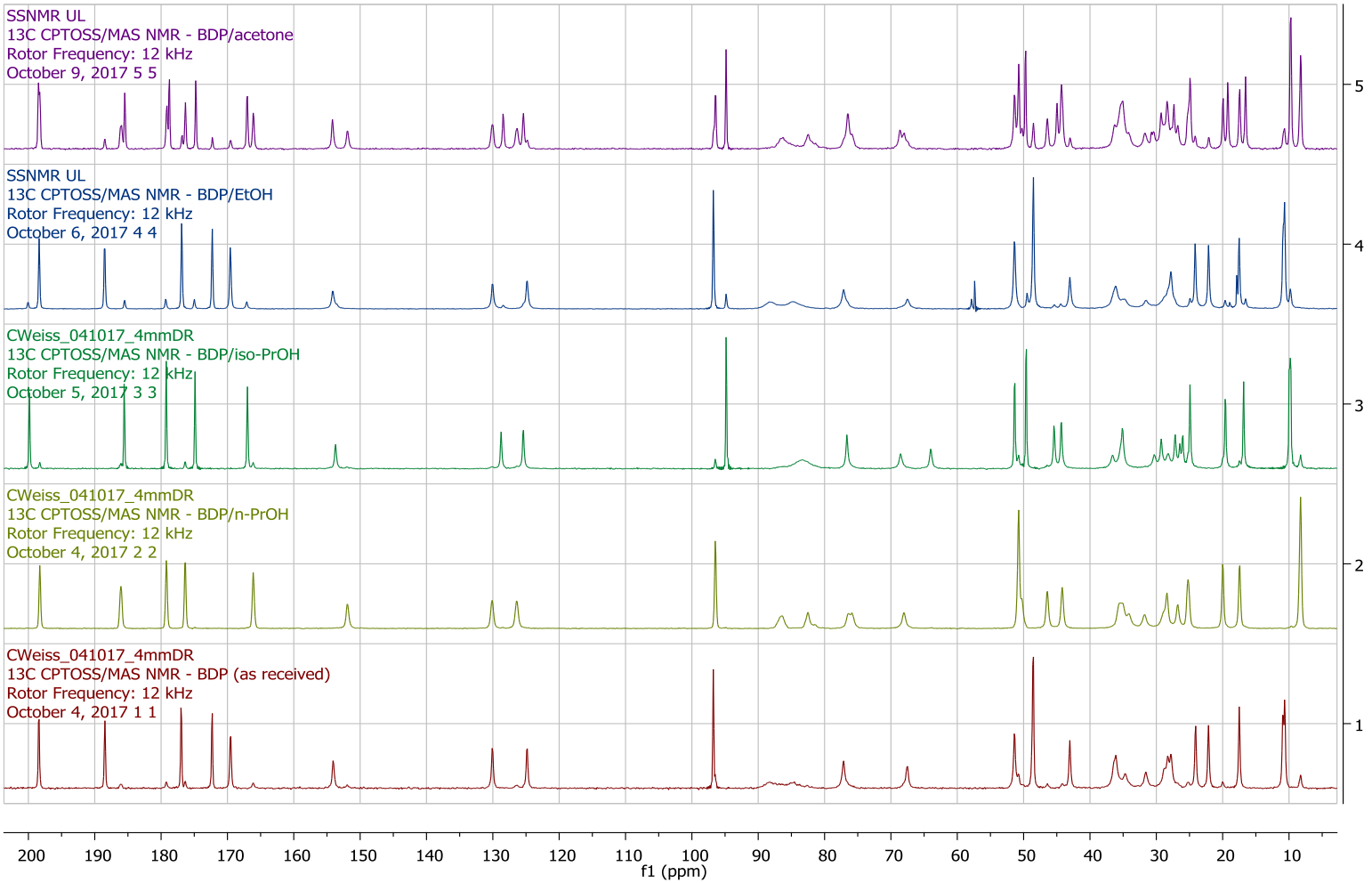

Figure 6-9. ^{13}C CPMAS SSNMR of (top to bottom) BDP acetone solvate, BDP ethanol solvate, BDP 2-propanol solvate, BDP 1-propanol solvate and anhydrous BDP as-received. Signals summarised in Tables 6-1 to 6-5.

Table 6-1. ^{13}C CPMAS SSNMR: Chemical shifts [ppm] in anhydrous BDP (assignment of signals based on known data (Christopher, 1993)). BDP monohydrate (Christopher, 1993) and BDP ethyl acetate solvate (Christopher, 1993) for comparison.

	Anhydrous BDP (this study)	Anhydrous BDP[1]	BDP monohydrate[1]	BDP ethyl acetate solvate[1]
C_{20}	198.4	198.5	198.4	197.8
C_3	188.5	188.4	185.9	185.5
C_{22}'	177.0	177.0	179.4	179.2
C_{22}	172.3	172.4	176.5	175.2
C_5	169.5	169.5	166.3	167.2
C_1	154.1	154.0	152.1	153.4
C_2	130.1	130.2	130.1	128.4
C_4	124.8	124.9	126.3	125.4
C_{17}	96.8	96.8	96.5	94.7
C_9	(90 – 80 ppm)	92.5	86.9	90.0
C_{11}	77.1	77.3	76.6	76.6
C_{21}	67.5	67.8	68.2	68.7
C_{10}	51.4	51.3	50.9	51.2
C_{13}	48.6	48.7	50.9	49.4
C_{16}	48.6	48.7	46.5	45.0
C_{14}	43.0	43.1	44.3	44.3
C_{12}	36.1	36.4	36.5	36.3
C_6	34.7	34.8	35.4	35.4
C_{15}	31.6	31.7	34.3	30.8
C_6	28.8	28.9	32.0	29.5
C_7	28.3	28.5	30.0	28.4
C_{23}	27.8	28.0	28.3	27.4
C_{19}	24.1	24.1	25.3	24.9
C_{25}	22.1	22.3	20.2	19.8
C_{18}	17.5	17.5	17.7	16.2
C_{24}	10.9	10.9	8.4	9.9
C_{23}'			27.0	
C_{24}'	10.7			9.7

[1] Assignments of propionate side chains and some steroid carbons unclear in reference (Christopher, 1993).

Table 6-2. ^{13}C CPMAS SSNMR: Chemical shifts [ppm] of BDP ethanol solvate. Signals were assigned to solvate, anhydrous BDP, BDP monohydrate and ethanol as indicated.

	BDP ethanol solvate[1, 2]	Anhydrous BDP	BDP monohydrate
C_{20}		198.4	198.4
C_3	185.5	188.5	186.0
C_{22}'	179.3	176.9	179.3
C_{22}	175.0	172.3	176.4
C_5	167.1	169.6	166.1
C_1	153.5	154.1	128.5
C_2	128.5	130.1	130.1
C_4	125.4	124.9	126.4
C_{17}	94.8	96.8	96.5
C_9			
C_{11}	76.6	77.1	76.6
C_{21}	68.5	67.6	68.5
C_{10}	51.3	51.3	50.8
C_{13}	49.5	48.6	50.8
C_{16}	45.4	48.6	46.4
C_{14}	44.4	43.0	44.4
C_{12}	36.1	36.1	
C_6	35.1		35.1
C_{15}	30.4	31.6	
C_6	29.3		
C_7	28.3	28.3	
C_{23}	27.2	27.8	28.3
C_{19}	24.9	24.1	
C_{25}	19.7	22.2	
C_{18}	16.6	17.5	17.5
C_{24}	9.8	10.9	8.3
C_{23}’			27.2
C_{24}’	9.8	10.7	
	Ethanol		
$C_{(etoh)}$	57.9, 57.4, 17.9		

[1] Additional ^{13}C signal at 200.1 ppm, only visible in BDP ethanol solvate.

[2] Assignments of ethanol ^{13}C signals based on solution state ^{13}C NMR (Yamaji et al., 2014).

Table 6-3. ^{13}C CPMAS SSNMR: Chemical shifts [ppm] of BDP ethanol solvate. Signals were assigned to solvate, anhydrous BDP, BDP monohydrate and 1-propanol as indicated.

	BDP 1-propanol solvate[1,2]	Anhydrous BDP	BDP monohydrate
C_{20}		198.3	198.3
C_3			186.1
C_{22}'	179.2		179.2
C_{22}			176.4
C_5			166.1
C_1			151.9
C_2			130.1
C_4			126.4
C_{17}			96.5
C_9			
C_{11}	76.4		76.4
C_{21}			68.0
C_{10}	50.8		50.8
C_{13}			50.8
C_{16}			46.4
C_{14}	44.2		44.2
C_{12}			
C_6	35.5		35.5
C_{15}		31.8	34.1
C_6			31.8
C_7	28.4	28.4	
C_{23}			28.4
C_{19}			25.2
C_{25}			20.0
C_{18}			
C_{24}			8.3
C_{23}'			26.8
C_{24}'	9.7		
	1-Propanol		
$C_{(1\text{-proh})}$	63.9		

[1] Assignments of 1-propanol ^{13}C signals based on solution state ^{13}C NMR (Yamaji et al., 2014).

[2] Very small 1-propanol ^{13}C signal at 63.9 ppm, no other visible signals due to overlapping with BDP and noise.

Table 6-4. ^{13}C CPMAS SSNMR: Chemical shifts [ppm] of BDP iso-propanol solvate. Signals were assigned to solvate, anhydrous BDP, BDP monohydrate and 2-propanol as indicated.

	BDP 2-propanol solvate[1]	Anhydrous BDP	BDP monohydrate
C_{20}		198.3	198.3
C_3	185.6		185.6
C_{22}'	179.2		179.2
C_{22}	174.9		176.4
C_5	167.0		166.1
C_1	153.7	153.7	
C_2	128.8	130.2	130.2
C_4	125.4		
C_{17}		96.5	96.5
C_9			
C_{11}	76.6		76.6
C_{21}	68.5		68.5
C_{10}	51.4	51.4	50.8
C_{13}	49.6		50.8
C_{16}	45.4		
C_{14}	44.3		44.3
C_{12}	36.6		36.6
C_6	35.1	35.1	35.1
C_{15}			
C_6	29.3		
C_7	28.2		30.3
C_{23}	27.2	28.2	28.2
C_{19}	24.9		
C_{25}	19.6		
C_{18}			17.5
C_{24}	9.8		8.3
C_{23}'			27.2
C_{24}'	9.8		
	2-Propanol		
$C_{(2\text{-proh})}$	64.0, 25.2		

[1] Assignments of 2-propanol ^{13}C signals based on solution state ^{13}C NMR (Yamaji et al., 2014).

Table 6-5. ^{13}C CPMAS SSNMR: Chemical shifts [ppm] of BDP acetone solvate. Signals were assigned to solvate, anhydrous BDP, BDP monohydrate and acetone as indicated.

	BDP acetone solvate[1,2]	Anhydrous BDP	BDP monohydrate
C_{20}		198.5	198.3
C_3	185.5		186.0
C_{22}'	179.2		179.2
C_{22}	174.8		176.4
C_5	167.1		166.1
C_1		154.2	151.9
C_2	128.5	130.1	130.1
C_4	125.4		126.4
C_{17}	94.9		96.5
C_9			
C_{11}	76.5		76.5
C_{21}	68.7	68.0	68.0
C_{10}	51.4	51.4	50.8
C_{13}	49.7		50.8
C_{16}	45.0		46.4
C_{14}	44.3		44.3
C_{12}	36.3	36.3	
C_6	35.1	35.1	35.1
C_{15}	30.8	31.8	
C_6	29.3		
C_7	28.4	28.4	
C_{23}	27.4		28.4
C_{19}	24.9		
C_{25}	20.0		20.0
C_{18}	16.6	17.5	
C_{24}	9.8		8.3
C_{23}'			
C_{24}'	9.8		
	Acetone		
$C_{(acetone)}$	30.8, 30.4		

[1] Assignments of acetone ^{13}C signals based on solution state ^{13}C NMR (Yamaji et al., 2014).

[2] Acetone ^{13}C signal at 206.55 ppm not visible, ^{13}C signal at 30.8 ppm may be overlapping with BDP solvate.

Table 6-6. Comparison of ^{13}C CPMAS SSNMR signals [ppm] assigned to BDP alcohol and acetone solvates.

	BDP ethanol solvate[1]	BDP 1-propanol solvate	BDP 2-propanol solvate	BDP acetone solvate
C_{20}				
C_3	185.5		185.6	185.5
C_{22}'	179.3	179.2	179.2	179.2
C_{22}	175.0		174.9	174.8
C_5	167.1		167.0	167.1
C_1	153.5		153.7	
C_2	128.5		128.8	128.5
C_4	125.4		125.4	125.4
C_{17}	94.8			94.9
C_9				
C_{11}	76.6	76.4	76.6	76.5
C_{21}	68.5		68.5	68.7
C_{10}	51.3	50.8	51.4	51.4
C_{13}	49.5		49.6	49.7
C_{16}	45.4		45.4	45.0
C_{14}	44.4	44.2	44.3	44.3
C_{12}	36.1		36.6	36.3
C_6	35.1	35.5	35.1	35.1
C_{15}	30.4			30.8
C_6	29.3		29.3	29.3
C_7	28.3	28.4	28.2	28.4
C_{23}	27.2		27.2	27.4
C_{19}	24.9		24.9	24.9
C_{25}	19.7		19.6	20.0
C_{18}	16.6			16.6
C_{24}	9.8		9.8	9.8
C_{23}'				
C_{24}'	9.8	9.7	9.8	9.8

[1] Additional ^{13}C signal at 200.1 ppm, only visible in BDP ethanol solvate.

Table 6-7. ^{13}C CPMAS SSNMR of BDP ethanol solvate after preparation of solvate and after 2 days.

	BDP ethanol solvate[1, 2]		Anhydrous BDP	
	0d	**2d**	**0d**	**2d**
C_{20}			198.4	198.4
C_3	185.5	185.5	188.5	188.5
C_{22}'	179.3	179.3	176.9	176.9
C_{22}	175.0	175.0	172.3	172.3
C_5	167.1	167.1	169.6	169.6
C_1	153.5		154.1	154.1
C_2	128.5	128.4	130.1	130.1
C_4	125.4		124.9	124.8
C_{17}	94.8	94.8	96.8	96.8
C_9				
C_{11}	76.6		77.1	77.1
C_{21}	68.5		67.6	67.5
C_{10}	51.3		51.3	51.4
C_{13}	49.5	49.5	48.6	48.5
C_{16}	45.4	45.4	48.6	48.5
C_{14}	44.4	44.4	43.0	43.0
C_{12}	36.1		36.1	36.1
C_6	35.1			34.8
C_{15}	30.4		31.6	31.6
C_6	29.3			
C_7	28.3		28.3	
C_{23}	27.2		27.8	27.8
C_{19}	24.9	24.9	24.1	24.1
C_{25}	19.7	19.6	22.2	22.1
C_{18}	16.6	16.5	17.5	17.5
C_{24}	9.8	9.8	10.9	
C_{23}'				
C_{24}'	9.8	9.8	10.7	10.7
	Ethanol			
$C_{(etoh)}$	57.9, 57.4, 17.9			

[1] Additional ^{13}C signal at 200.1 ppm, visible in BDP ethanol solvate at 0d and 2d.

[2] Assignments of ethanol ^{13}C signals based on solution state ^{13}C NMR (Yamaji et al., 2014).

Table 6-8. ^{13}C CPMAS SSNMR of BDP acetone solvate after preparation of solvate and after 5 days.

	BDP acetone solvate[1,2]		Anhydrous BDP	
	0d	**5d**	**0d**	**5d**
C_{20}			198.5	198.5
C_3	185.5	185.5		198.3
C_{22}'	179.2	179.1		176.8
C_{22}	174.8			172.3
C_5	167.1	167.0		169.5
C_1			154.2	154.2
C_2	128.5	128.4	130.1	130.1
C_4	125.4	125.4		124.8
C_{17}	94.9	94.8		96.4
C_9				
C_{11}	76.5	76.5		
C_{21}	68.7	68.6	68.0	
C_{10}	51.4		51.4	51.4
C_{13}	49.7	49.7		48.5
C_{16}	45.0	45.0		48.5
C_{14}	44.3	44.3		43.0
C_{12}	36.3		36.3	36.3
C_6	35.1	35.1	35.1	35.1
C_{15}	30.8	30.7	31.8	31.7
C_6	29.3	29.3		
C_7	28.4		28.4	28.4
C_{23}	27.4	27.4		
C_{19}	24.9	24.9		24.1
C_{25}	20.0	19.9		22.1
C_{18}	16.6	16.6	17.5	17.4
C_{24}	9.8	9.8		
C_{23}’				
C_{24}’	9.8	9.8		10.7
	Acetone			
$C_{(acetone)}$	30.8, 30.4			

[1] Assignments of acetone ^{13}C signals based on solution state ^{13}C NMR (Yamaji et al., 2014).

[2] Acetone ^{13}C signal at 206.55 ppm not visible, ^{13}C signal at 30.8 ppm may be overlapping with BDP solvate.

6.3 Discussion

Single crystal XRD, despite not allowing the determination of the exact arrangement of all solvent molecules relative to BDP, gave a good estimation of the most likely position of the solvent within in the channel. This estimation was based on heat maps showing the probability density calculated on the basis of an automated Hirshfeld atom refinement. A similar approach, assigning the position of atoms though an electron density heat map, has been used successfully to determine the position of atoms within metal organic frameworks (MOFs) (Takashima et al., 2014) but has not yet been used to analyse the structure of BDP solvates.

The results (Figures 6-5 to 6-7) confirmed the formations of channels incorporating mobile solvent molecules. It appeared that solvent size, polarity and configuration influenced the most likely position of the solvent molecules within the channel. Despite both being linear alcohols, ethanol (Figure 6-4a) and 1-propanol (Figure 6-5a) appeared to be incorporated in different ways with ethanol being more evenly distributed within the channel. Ethanol and 1-propanol have similar relative polarities (ethanol: 0.654, 1-propanol: 0.617; Table 4-1) and differ in length by only one carbon. However, the addition of one carbon appeared to be a big enough difference to affect the alignment of the solvent molecules within the fixed volume voids available for their incorporation. In both cases, however, the alcohol appeared to be in close proximity to the propionate branch of the BDP host molecules which was found to be a preferred site for intermolecular interaction through hydrogen bonds.

Compared to the linear alcohols, 2-propanol (polarity: 0.546; Table 4-1) appeared to be more evenly distributed across the accessible volume of the channel with a lower probability of hydrogen bonding. Considering that 2-propanol is less polar that 1-propanol the molecule may be less prone to form weak hydrogen bonds to the In addition, 2-propanol has a different configuration with the hydroxyl group in C_2 position which may cause a steric hindrance when approaching the propionate branch and also be detrimental to the alignment of the solvent molecules along the channel.

Acetone with a polarity of 0.355 (Table 4-1) and no hydroxyl group available for hydrogen bonding did not appear to occupy any preferred position. In contrast to the alcohol based solvates, the heat map did not show a higher electron density along the edges of channel but rather suggested a very even distribution across the cross section (Figure 6-7a) which supported the assumption that no intermolecular interaction took place between acetone and BDP and that acetone is highly mobile within the channels as suggested by NMR titration and thermal analysis.

SSNMR supported the results seen in single crystal XRD. Each solvate was found to include ^{13}C signals characteristic of the respective solvent in solution which confirmed the presence of the

alcohols and acetone in a solution like surrounding. This would only be the case if the solvent molecules were mobile within the channels as suggested previously and reported in literature (Kuehl et al., 2003).

In addition, SSNMR confirmed that the structures of all solvates, regardless of the solvent used, were similar to each other (Table 6-6). The solvates were also found to have identical unit cells when running pre-screening single crystal XRD measurements. As assumed when carrying out thermal analysis (Figures 4-7, 4-8, 4-9) and observing the decomposition of solvate crystals under nitrogen (Figures 4-1, 4-2), the BDP solvates gradually transitioned into the anhydrous form. Repeated SSNMR analysis showed an increasing number of ^{13}C SSNMR signals characteristic of the anhydrous form when keeping the BDP ethanol and the BDP acetone solvate under ambient conditions for a prolonged time (Tables 6-7, 6-8). This instability might have been the reason for the small number of ^{13}C SSNMR signals seen in the BDP 1-propanol solvate (Table 6-3). Single crystal XRD led to the assumption of 1-propanol being aligned across the channel (Figure 6-5a) with possible weak hydrogen bonding to the BDP propionate branch rather than being evenly distributed. This might have contributed negatively to the overall stability of the solvate and led to the partial desolvation of the compound when being spun during SSNMR analysis. SSNMR further showed that a fraction of anhydrous BDP and BDP monohydrate was present in all samples which further confirmed the relative low stability of the compounds. The results also explained the peak broadening observed in XRPD (Figure 4-11) which was caused by impurities in the form of both the BDP monohydrate and the BDP anhydrate.

6.4 Conclusions

Both single crystal XRD and SSNMR confirmed the formation of four BDP solvates with identical channel structures incorporating mobile solvent molecules as previously assumed on the basis of thermal analysis and XRPD (Chapter 4). The results further supported the assumption of the arrangement and degree of mobility of the solvent molecules depending on size, configuration and polarity. It was further confirmed that BDP solvates were only obtained from ethanol, 1-propanol, 2-propanol and acetone solution despite NMR titration and DOSY showing that an affinity between all alcohols and the BDP host. This added to the understanding of solvent formation. Two scenarios were presented in the previous chapter: solvate formation may have occurred and instable solvates may have formed from 1-butanol and 1-pentanol solution or solvate formation may have started but solvent characteristics may have prevented the completion of the solvated compound. Since single crystal XRD was carried out immediately after taking the crystals out of solution, scenario two appeared to be the more likely option. Investigating the desolvation mechanism and analysing the material characteristics of desolvated BDP prepared from each solvate may add weight to this assumption.

6.5 References

Bourhis, L. J., Dolomanov, O. V., Gildea, R. J., Howard, J. A. & Puschmann, H. 2015. The anatomy of a comprehensive constrained, restrained refinement program for the modern computing environment–Olex2 dissected. *Acta Crystallographica Section A: Foundations and Advances,* 71**,** 59-75.

Capelli, S. C., Bürgi, H.-B., Dittrich, B., Grabowsky, S. & Jayatilaka, D. 2014. Hirshfeld atom refinement. *IUCrJ,* 1**,** 361-379.

Christopher, E. A. 1993. *Solid-state NMR study of polymorphism in pharmaceuticals.* Durham University.

Dolomanov, O. V., Bourhis, L. J., Gildea, R. J., Howard, J. A. & Puschmann, H. 2009. OLEX2: a complete structure solution, refinement and analysis program. *Journal of Applied Crystallography,* 42**,** 339-341.

Harris, J. A., Carducci, M. D. & Myrdal, P. B. 2003. Beclomethasone dipropionate crystallized from HFA-134a and ethanol. *Acta Crystallographica Section E: Structure Reports Online,* 59**,** o1631-o1633.

Jayatilaka, D. & Dittrich, B. 2008. X-ray structure refinement using aspherical atomic density functions obtained from quantum-mechanical calculations. *Acta Crystallographica Section A: Foundations of Crystallography,* 64**,** 383-393.

Jinks, P. A. 1989. *Physically modified beclomethasone dipropionate suitable for use in aerosols*. US Patent 4,810,488.

Kuehl, P. J., Carducci, M. D. & Myrdal, P. B. 2003. An ethanol solvate of Beclomethasone dipropionate. *Acta Crystallographica Section E: Structure Reports Online,* 59**,** 1888-1890.

Millard, J. W. & Myrdal, P. B. 2002. Anhydrous beclomethasone dipropionate. *Acta Crystallographica Section E: Structure Reports Online,* 58**,** o712-o714.

Nachiengtung, N. 1997. Solid-state characterization of beclomethasone dipropionate solvates and polymorphs. PhD Thesis, Purdue University, IN, USA.

Page, P. R. & Heggie, W. 1990. *Preparation and use of new solvates of beclomethasone 17, 21-dipropionate*. US Patent 4,913,892.

Takashima, Y., Long, D.-L. & Cronin, L. 2014. Towards imaging electron density inside metal–organic framework structures. *Chemical Communications,* 50**,** 2271-2274.

Woińska, M., Jayatilaka, D., Spackman, M. A., Edwards, A. J., Dominiak, P. M., Woźniak, K., Nishibori, E., Sugimoto, K. & Grabowsky, S. 2014. Hirshfeld atom refinement for modelling strong hydrogen bonds. *Acta Crystallographica Section A,* 70**,** 483-498.

Yamaji, T., Saito, T., Hayamizu, K., Yanagisawa, M., Yamamoto, O., Wasada, N., Someno, K., Kinugasa, S., Tanabe, K. & Tamura, T. 2014. Spectral database for organic compounds, SDBS. *Electronic resource: http://sdbs. db. aist. go. jp/sdbs/cgi-bin/cre_index. cgi*.

CHAPTER 7

PREPARATION AND CHARACTERISATION OF ANHYDROUS BECLOMETHASONE DIPROPIONATE FROM BECLOMETHASONE DIPROPIONATE SOLVATES

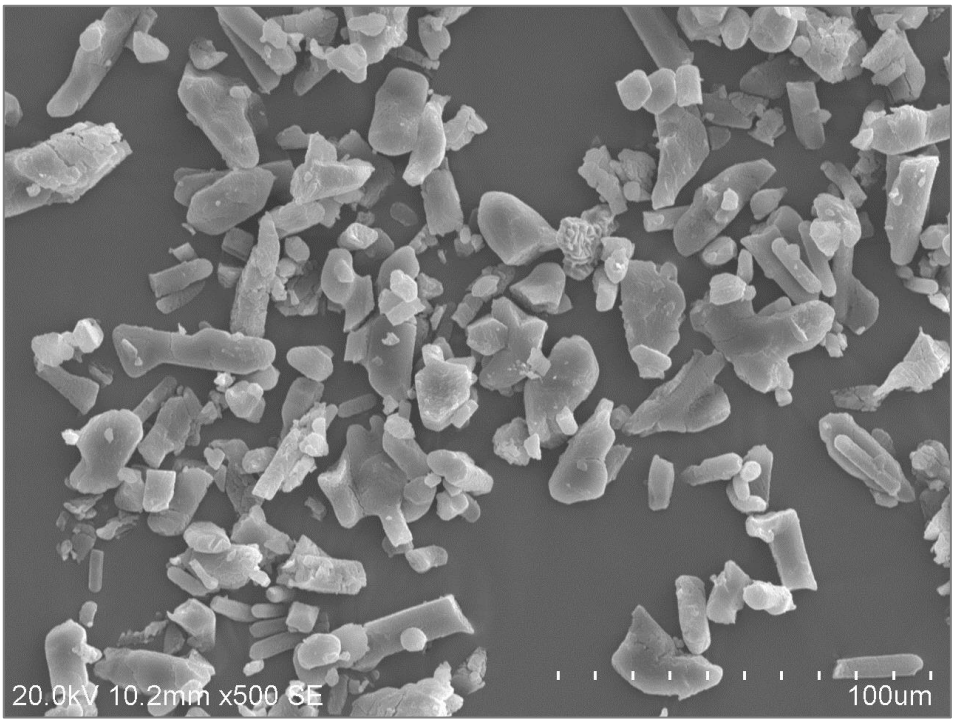

Figure 7. SEM image (x500) of anhydrous BDP prepared from the BDP 2-propanol solvate.

7 Preparation and Characterisation of Anhydrous Beclomethasone Dipropionate from Beclomethasone Dipropionate Solvates

BDP alcohol and acetone solvates, containing toxic organic solvents, are not suitable for administration to the patient in the solvated form. They can, however, potentially be used as intermediate precursors for the preparation of respirable anhydrous particles with defined physicochemical characteristics. The possibility to control the desolvation process is crucial for the development of future applications.

While crystallisation from methanol, 1-butanol and 1-pentanol resulted in predominantly anhydrous BDP, only the use of ethanol, 1-propanol, 2-propanol and acetone led to the formation of solvates. Yet NMR titration together with thermal analysis, single crystal XRD and SSNMR confirmed that only weak interactions between the solvent and the BDP molecule keep the crystalline channel structure of BDP solvates in place. Under vacuum and nitrogen, at low relative humidity, high temperatures and even at room temperature if kept for a longer time, the solvent gradually evaporates, leading to recrystallisation into the anhydrous form. The particle size decreases during this process. The BDP solvates were therefore considered a potential species for the controlled preparation of crystalline anhydrous BDP.

For comparision, all BDP anhydrates were analysed alongside the solvates to evaluate differences between those prepared from BDP solvates and those that did not include this intermediate step. The impact of desolvation on particle size, particle shape, surface area, surface topology and surface energetics was analysed since these characteristics were expected to have a major influence on interparticulate forces within a DPI formulation with surface energetics also affecting the stability of the formulation. Since the desired particle size lies within a range of 1 – 5 μm , ball milling and similar techniques are used to micronise the particles. Such processes put the crystals under physical and mechanical stress and spontaneous recrystallisation of induced amorphous material and uncontrolled crystal growth could negatively affect the formulation. Thus it is suggested that, instead of mechanically micronizing BDP crystals into fine crystallites, these could be precipitated from solution with optimised experimental parameters. This would eliminate the micronisation step and keep the crystalline surface intact, leading to a more stable product with potentially tailored surface properties which depend on the chosen solvate precursor.

7.1 Materials and Methods

7.1.1 Preparation of Anhydrous BDP

Anhydrous BDP particles were prepared by desolvating the BDP solvates crystallised from acetone, ethanol, 1-propanol and 2-propanol at controlled conditions under nitrogen. The weight loss was monitored using thermogravimetric analysis (Q 50 TGA, TA Instruments, UK).

10 – 15 mg of sample was heated at 10 °C/min to 160 °C followed by an isothermal step at 160 °C until the weight had stabilised. FTIR spectroscopy was used to confirm the preparation of anhydrous BDP (Nachiengtung, 1997). For comparison, the crystalline BDP prepared from methanol, 1-butanol and 1-pentanol was subjected to the same treatment and analysed correspondingly.The anhydrous BDP was stored in closed glass vials at 4 °C.

7.1.2 Thermal Analysis, Headspace GC-MS, X-ray Powder Diffraction, Gas Sorption,

Thermal analysis, headspace GC-MS, XRPD and gas sorption were carried out as described in Chapters 2 and 4.

7.1.3 Particle Sizing

The particle size distribution was measured as outlined in Chapter 2.

7.1.4 Scanning Electron Microscopy, Atomic Force Microscopy

The samples were visualised using SEM and AFM as outlined in Chapter 2.

7.2 Results

7.2.1 Thermal Analysis and Headspace GC-MS

Thermal analysis (DSC, TGA) did not show any endothermic signals caused by desolvation and solvent evaporation nor were any exothermic peaks visible that would indicate phase transition into another crystalline form (Figure 7-1).

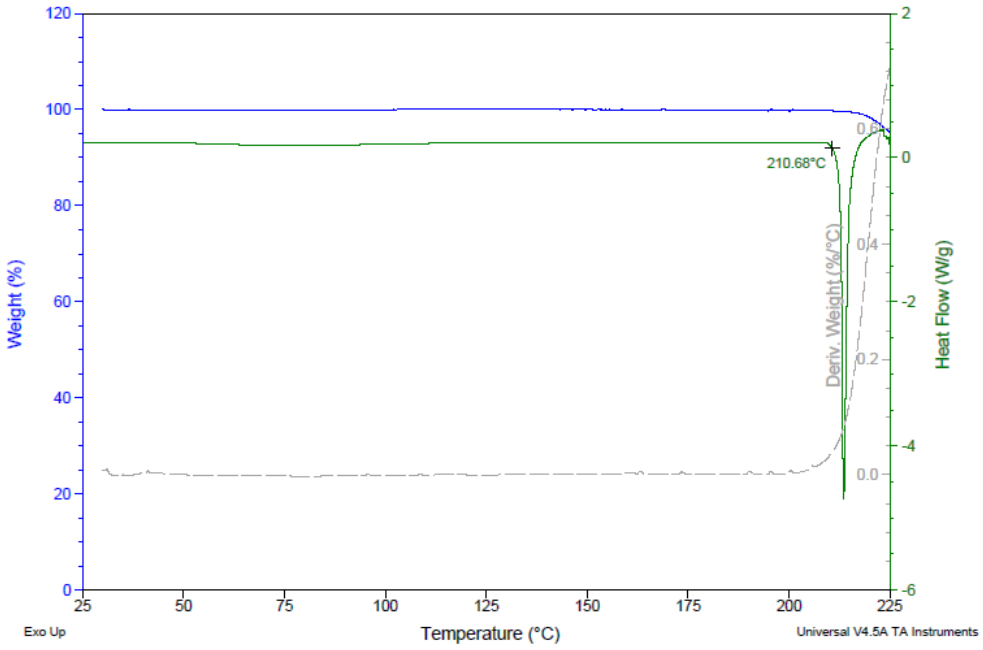

Figure 7-1. Thermal analysis (DSC, green, and TGA, blue: weight change, grey: first derivative) of anhydrous BDP prepared from BDP solvate.

Only the sharp endothermic signal at approximately 213 °C characteristic of the melting of the anhydrous form was seen (Nachiengtung, 1997). No weight loss was monitored in TGA until the onset of degradation at temperatures above the melting point. Headspace GC-MS was used to detect the possible presence of residual solvent. No signals were visible at the characteristic retention times and it was assumed that all solvents had been removed to amounts below the detection limit of the MS based method.

7.2.2 X-ray Powder Diffraction

BDP prepared from alcohol or acetone solution was found to either form the anhydrous form or to transition into anhydrous BDP upon solvent removal. Thermal analysis was the first indicator of this phenomenon (Figures 4-7, 4-8) which was then confirmed by SSNMR and XRD (Chapter 6). Despite having different initial conditions (BDP solvates containing ethanol, 1-propanol, 2-propanol or acetone and anhydrous BDP), all samples were thermally treated to remove any incorporated or residual solvent and, where the starting material was a solvate, to cause transition into the anhydrous form.

XRPD was used to compare the samples after thermal treatment. The signal at $18.7 \pm 0.1\ ^\circ 2\theta$ (Figure 7-2), characteristic of anhydrous BDP (Wang et al., 2007, Nachiengtung, 1997), showed that all BDP solvates had been converted into anhydrous BDP. This also confirmed that the samples that had existed in the anhydrous form prior to thermal treatment had not been affected in any undesired way.

Peak broadening (Figure 7-2) as seen predominantly in the desolvated BDP acetone (orange) and 1-propanol samples (dark blue) indicated the possible presence of amorphous material, only partially collapsed structures or other impurities.

The desolvated BDP ethanol sample (green) exhibited extremely sharp peaks, similar to samples that were crystallised directly into the anhydrous form (e.g. the sample prepared from methanol solution, blue), suggesting a crystalline anhydrous sample with few impurities.

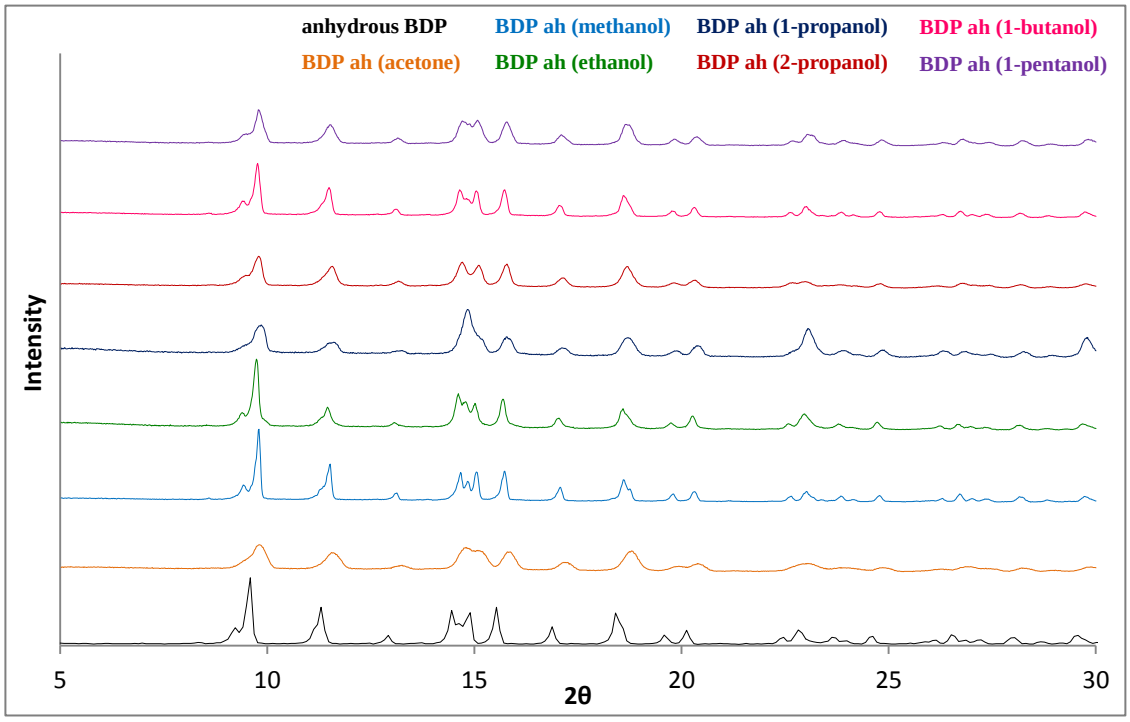

Figure 7-2. XRPD of desolvated BDP. Precursor material as indicated in legend, solvent used for crystallisation given in brackets. XRPD of anhydrous (ah) BDP as-received included for comparison. All XRPD spectra show the characteristic signal between 18.6 and 18.8 °2θ.

7.2.3 Nitrogen Sorption

Nitrogen sorption was carried out to compare the specific surface area of all anhydrous BDP samples. The removal of solvent molecules from the channel structure might have led to a partial porosity or amorphous material. The presence of pores accessible by nitrogen would have an impact on the BET specific surface area and the hysteresis of the adsorption and desorption isotherms.

Yet despite repeating the measurements several times using prolonged degassing times, degassing temperatures up to 130 °C and running the same samples several times, reliable results could only be obtained from the desolvated BDP prepared from the BDP ethanol, BDP 2-propanol and BDP acetone solvates (Table 7-1).

Table 7-1. BET specific surface area SSA_{BET} (m^2g^{-1}) (± standard deviation) and C factor. Anhydrous BDP as-received included for comparison.

Sample	SSA_{BET} [m^2g^{-1}]
BDP prepared from BDP ethanol solvate	1.21 ± 0.02
BDP prepared from BDP 2-propanol solvate	2.93 ± 0.02
BDP prepared from BDP acetone solvate	3.69 ± 0.01
Anhydrous BDP (as received)	2.22 ± 0.04

The BET specific surface area of anhydrous BDP obtained through thermal treatment of these BDP solvates was similar to the surface area of as-received anhydrous BDP. The isotherms did not show any significant hysteresis and matched the isotherms observed for the as-received anhydrous material. This indicated that the desolvated material was non-porous without any residual voids or partially collapsed channels. The small differences in the BET surface area of the anhydrous compounds may be due to slightly different particle sizes as surface area increases with decreasing particle size.

The BET specific surface area of all other samples varied form run to run and values of less than 1 m^2g^{-1} with a standard deviation exceeding the actual value of the specific surface area were recorded. Monitoring the degassing process prior to analysis of the BDP sample prepared from the BDP 1-propanol solvate showed that the compound liquefied partially and recrystallized into large irregular particles that appeared to be slightly yellow and sticky and could not be removed from the sample tube (Figure 7-3).

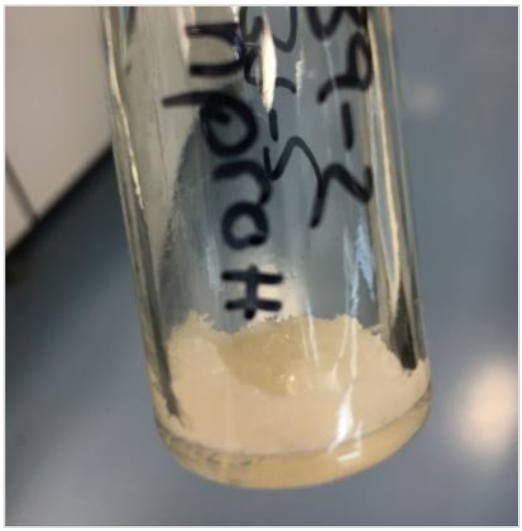

Figure 7-3. Recrystallisation of BDP prepared from BDP 1-propanol solvate liquefied partially when being degassed under nitrogen.

This was facilitated by solvent which was released from the crystal, condensed and trickled back into the sample tube where some of the crystal was dissolved. This suggested that the recorded surface area values were not measurements of the prepared BDP but of sample that had recrystallized during degassing, resulting in very large particles with low surface areas. The surface area values varied from run to run depending on the extent of recrystallisation during preparation.

7.2.4 Particle Sizing

Dry particle size analysis was carried out to evaluate the impact of heat treatment and, if applicable, desolvation on the particle size. Comparing the d_{90} percentile of the samples before and after heat treatment showed that the particle size decreased in all cases (Table 7-2).

The d_{10} and d_{50} values indicated that a fraction of the particles was within the size range of below 10 µm (Hunt and Padfield, 1989), ideally below 5 µm (Cui et al., 2014), which is the desirable particle size range for respiratory delivery. All samples were smaller than the as-received anhydrous reference sample which had similar d_{10} and d_{50} values but a much larger d_{90} value (Table 7-2).

Table 7-2. PSD (µm, percentile d_{10}, d_{50}, d_{90}) of anhydrous BDP after thermal treatment. Percentage difference to d_{90} of BDP before heat treatment. Anhydrous BDP as-received included for comparison.

Sample (BDP precursor)	d_{10} [µm]	d_{50} [µm]	d_{90} [µm]	Reduction (d_{90}) [%]
BDP (BDP/methanol)	2.6	6.9	16.6	-7
BDP (BDP ethanol solvate)	2.2	6.0	15.6	-39
BDP (BDP 1-propanol solvate)	2.7	9.4	28.2	-12
BDP (BDP 2-propanol solvate)	2.6	7.6	17.5	-18
BDP (BDP/1-butanol)	2.7	8.7	22.4	-44
BDP (BDP/1-pentanol)	2.7	8.2	25.1	-36
BDP (BDP/acetone)	2.4	7.8	21.8	-69
Anhydrous BDP (as received)	2.1	10.4	60.9	-

The d_{90} percentile value, however, showed that the size of the majority of the particles had been reduced notably through thermal treatment. The samples prepared from methanol, ethanol and 2-propanol were the smallest with d_{90} values below 20 µm. Considering the crystalline structures of each sample before exposure to thermal treatment, two different mechanisms were assumed to have led to this decrease in particle size.

Mechanism 1 (BDP prepared from methanol, 1-butanol and 1-pentanol)

The anhydrous BDP prepared from methanol, 1-butanol and 1-pentanol solution may have formed agglomerates with the excess solvent present on the particle surfaces facilitating cohesion. Thermal analysis indicated the loss of excess surface solvent (Figure 4-7) which may have caused dispersion, thus showing a reduced particle size after thermal treatment. The particle size of the sample prepared from methanol decreased to a lesser extent by only 7 %. This suggested that desolvation had already taken place prior to thermally induced desolvation. As described in Chapter 6 (solvate formation: scenario 1), a transient solvate could have crystallised from solution which then quickly desolvated and transformed into the anhydrous form, thus resulting in a small PSD.

While the particle size of BDP prepared from methanol decreased by only 7 %, BDP based on 1-butanol and 1-pentanol appeared to decrease by an average of 40 % (Table 7-2). Considering the boiling points of each alcohol (Table 4-1), this difference may be due to excess methanol

evaporating faster than the longer linear alcohols. Faster evaporation would reduce the cohesive forces between the particles, thus leading to dispersion at an earlier stage, possibly before thermal treatment.

Mechanism 2 (BDP prepared from ethanol, 1-propanol, 2-propanol and acetone):
In contrast to the as-received anhydrous BDP, desolvation followed by monotropic solid-solid phase transition was observed in thermal analysis (Figures 4-7, 4-8). The BDP solvates recrystallized into the anhydrous form which was associated with the particles breaking up (Figure 4-2) and resulted in a reduced particle size.

7.2.5 Scanning Electron Microscopy

From a purely visual perspective, the anhydrous BDP prepared from the BDP 2-propanol solvate appeared to be the only compound that had retained its previous elongated shape with a comparatively smooth surface (Figure 7-4).

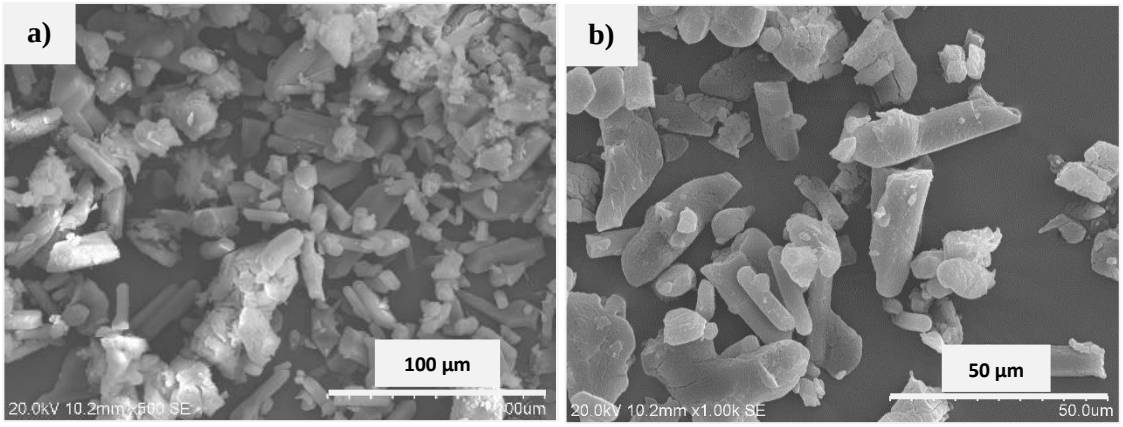

Figure 7-4. SEM images of a) BDP 2-propanol solvates (x500) and b) anhydrous BDP prepared from BDP 2-propanol solvates (x1,000).

The desolvated BDP ethanol, 1-propanol and acetone samples were seen to be of irregular shapes and the samples contained fines, flakes and more compact particles similar to the dispersed anhydrous BDP particles (Figure 7-5). The surface morphology appeared have become uneven and fines were stuck to the larger particles.

SEM imaging was used to visually confirm the reduction of the particle size in all cases (Figures 7-4, 7-5).

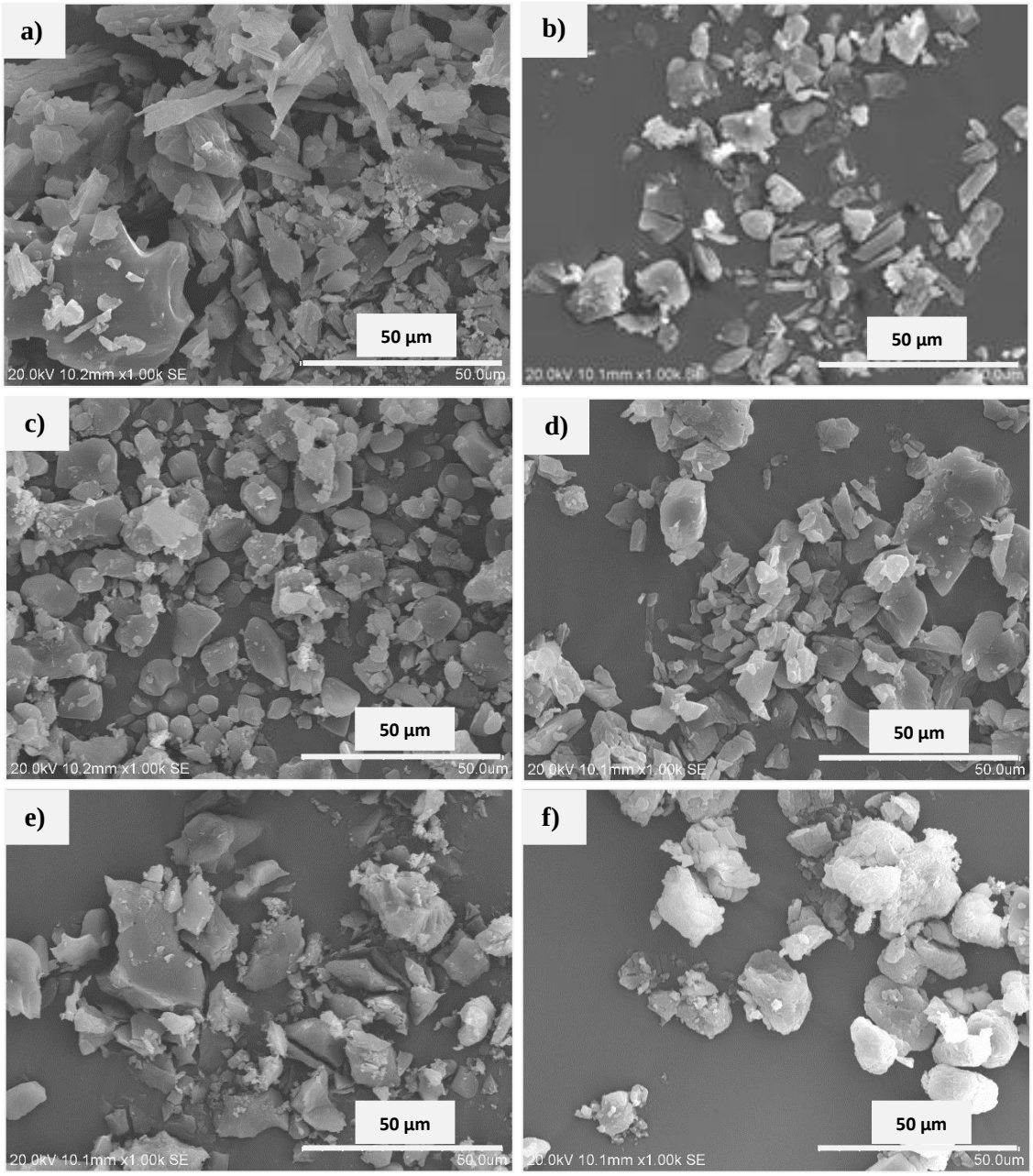

Figure 7-5. SEM images (x1,000) of anhydrous BDP based on a) BDP prepared from methanol solution, b) BDP ethanol solvate, c) BDP 1-propanol solvate, d) BDP prepared from 1-butanol solution, e) BDP prepared from 1-pentanol solution, f) BDP acetone solvate.

7.2.6 Atomic Force Microscopy

The surface roughness (Table 7-3) was quantitatively determined from AFM height maps as outlined in Chapter 4 and the R_q and R_a values were calculated according to Equations 4-1 and 4-2. Since the surface characteristics of the anhydrous particles is of particular importance for DPI formulations, the post thermal treatment surface morphology of BDP were considered crucial for subsequent experimental work.

Table 7-3. Average surface roughness (root mean square, R_q and arithmetic average, R_a) of anhydrous BDP after thermal treatment. Results based on n=10 measurements.

Sample (BDP precursor)	R_q [nm]	R_a [nm]
BDP (BDP/methanol)	53.1 ± 20.0	43.0 ± 17.5
BDP (BDP ethanol solvate)	18.9 ± 6.9	15.0 ±5.33
BDP (BDP 1-propanol solvate)	39.7 ± 14.3	30.9 ± 11.2
BDP (BDP 2-propanol solvate)	40.1 ± 18.4	31.6 ± 12.8
BDP (BDP/1-butanol)	34.5 ± 11.2	28.1 ± 9.1
BDP (BDP/1-pentanol)	49.4 ± 13.3	38.6 ± 10.4
BDP (BDP/acetone)	68.1 ± 18.9	54.3 ± 18.8

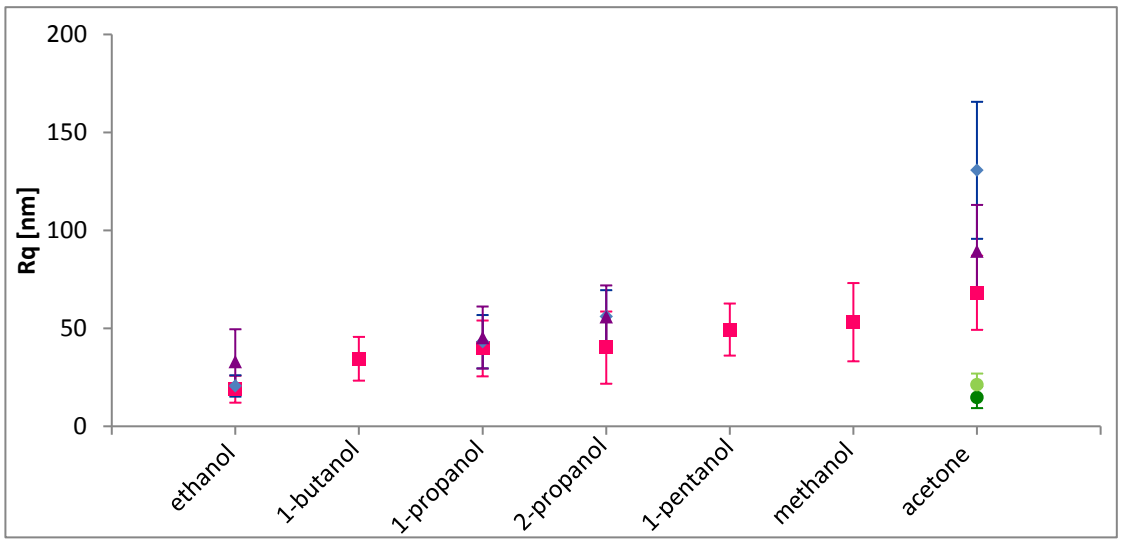

Figure 7-6. Roughness R_q (nm) of all anhydrous BDP particles. To show particle to particle variations, each colour represents one particle on which n=10 spots were measured. Anhydrous BDP labelled with regard to the solvent used in their preparation/the preparation of the precursor solvate.

The desolvated BDP ethanol sample appeared to have the smoothest surface while the anhydrous BDP prepared from the BDP acetone solvate was found to have the most uneven surface which varied significantly depending from particle to particle (Figure 7-6). In contrast to SEM based observations, the anhydrous BDP based on the BDP 1-propanol and the BDP 2-propanol solvates exhibited similar degrees of surface roughness. The surface of the anhydrous sample prepared from 1-butanol solution was relatively low compared to the anhydrous BDP prepared from methanol and 1-pentanol.

The differences in surface roughness may have their origins in the different events taking place during thermal treatment which in turn are based on the formation of either a solvate or the anhydrous form from saturated solution. Depending on the polymorphic form before thermal treatment, the solvates either were subject to desolvation and recrystallisation or, if already

existing in the anhydrous form, lost their excess surface solvent and deaggregated. Pre and post thermal treatment parameters, based on R_q, are summarised in Table 7-4.

Table 7-4. Average surface roughness (R_q) pre and post thermal treatment (pre ΔT, post ΔT); n=10.

Sample (BDP precursor)	R_q [nm]		Difference [%]
	pre ΔT	post ΔT	
BDP (BDP/methanol)	52.8 ± 23.6	53.1 ± 20.0	+0.6
BDP (BDP ethanol solvate)	13.1 ± 8.4	18.9 ± 6.9	+44.3
BDP (BDP 1-propanol solvate)	17.0 ± 7.2	39.7 ± 14.3	+133.5
BDP (BDP 2-propanol solvate)	67.2 ± 25.4	40.1 ± 18.4	-40.3
BDP (BDP/1-butanol)	65.0 ± 25.3	34.5 ± 11.2	-46.9
BDP (BDP/1-pentanol)	150.2 ± 65.5	49.4 ± 13.3	-67.1
BDP (BDP/acetone)	92.8 ± 23.1	68.1 ± 18.9	-26.6

The anhydrous BDP prepared from methanol solution showed the same surface roughness before and after thermal treatment which confirmed the assumption of the sample being only insignificantly affected by increasing temperatures. In contrast to the anhydrous BDP prepared from 1-butanol and 1-pentanol solution, the methanol based sample was assumed to have transformed into the anhydrous form shortly after crystallisation and, due to methanol evaporating at low temperatures, would have separated at an earlier stage.

The increasing surface roughness of anhydrous BDP prepared from the two smoothest BDP solvates, the BDP ethanol and the BDP 1-propanol solvate, was caused by recrystallisation which led to a significant decrease in particle size (Table 7-2). In contrast, the BDP acetone and the BDP 2-propanol solvate became smoother when recrystallizing into the anhydrous form. It appeared that desolvation and recrystallisation reduced extreme surface parameters to a certain degree. However, the BDP acetone solvate, which was previously seen to be the least reproducible and most instable of the confirmed BDP solvates, crystallised into the most irregular shaped anhydrous BDP with the most uneven surface.

7.3 Discussion

XRPD confirmed the preparation of anhydrous BDP through controlled thermal treatment (Figure 7-2). Peak broadening observed in the XRPD pattern of the desolvated BDP prepared from BDP 1-propanol may have been due to the presence of amorphous BDP or impurities. Further irregularities were found when monitoring the degassing process before gas sorption. The anhydrous sample prepared from BDP 1-propanol solvate appeared to still contain solvent

despite thermal analysis suggesting otherwise. It was possible to desolvate the sample carefully under nitrogen when increasing the temperature in small increments or applying a temperature gradient of 10°C/min. This was seen as another indication of thermally induced desolvation being dependent on the solvent incorporated in the channel structure. Fast desolvation and transition into the anhydrous form would have led to a larger PSD on account of the evaporating solvent condensing, trickling back and partially dissolving the crystalline material as seen when degassing the samples prior to nitrogen sorption (Figure 7-3).

This and previous observations regarding the stability of the solvates (Chapter 4), the solvent dependent formation of solvates (Chapters 4 to 6) and the structural composition of confirmed BDP solvates, led to the assumption that both solvent inclusion and evaporation are controlled by solvent properties. Solvent size and polarity appeared to be decisive for the formation of relatively stable solvates. The same properties appeared to also be responsible for the variations seen in their desolvation (Chapter 4) followed by the gradual collapse of the previously solvent filled channels. Depending on how fast evaporation occurred, the crystalline structure was maintained over certain period of time which may in turn have affected the size and surface roughness of the resulting anhydrous BDP.

With the possible exception of the anhydrous BDP prepared from the BDP 1-propanol solvate the specific surface area of all desolvated samples (Table 7-1) was similar to that of the as-received anhydrous BDP which suggested that all channels had collapsed and that the resulting particles were similar in size. In addition, the presence of pores and void channels would have been become visible in the hysteresis.

Thermal treatment also caused a significant size reduction in all anhydrous compounds prepared from BDP solvates which was attributed to evaporation, channel collapse and transformation.

Furthermore, thermal treatment affected the physical properties of the anhydrous BDP crystallised from higher alcohols. The residual 1-butanol and 1-pentanol on the surface of the particles evaporated, thus leading to the dispersion of larger agglomerates. These already anhydrous compounds maintained their rather irregular and often flake-like shapes (Figure 7-5). Methanol in contrast led to the almost immediate formation of anhydrous BDP from solution. Any residual surface solvent evaporated quickly, thus leading to deaggregation. The surface roughness, particle shape and PSD were therefore barley affected by thermal treatment.

Anhydrous BDP prepared through thermally induced desolvation and phase transition of BDP solvates was found to either assume the typical irregular shape of anhydrous BDP (Figure 7-5) or to maintain the elongated shape of the solvated precursor (Figure 7-4). The still slightly elongated shape of the desolvated BDP 2-propanol solvate resembled that of the solvated

compound. XRD results indicated the more even distribution of 2-propanol across the accessible volume of the channel solvate. This may have led to a more evenly progressing desolvation process which in turn may have been beneficial to the maintenance of the elongated particle shape.

The linear alcohols were aligned within the channel structure and were assumed to have formed weak hydrogen bonds to the propionate branch reaching into the channel. The disruption of even such weak bonds may have caused a more irregular desolvation process and a more uncontrolled collapse of the channel structure.

The desolvation of the BDP 1-propanol solvate was only successful when carried out at a rate of 10 °C per minute. In addition, SSNMR (Table 6-6) had suggested the possible formation of BDP monohydrate over time. This would explain the different desolvation behaviour, the peak broadening seen in XRPD and the exceptional increase in surface roughness of the anhydrous BDP compared to the solvated species.

The desolvation of the BDP acetone solvate, the solvate that had previously been found to exhibit the most unpredictable thermal behaviour, resulted in highly irregular anhydrous particles (Figure 7-5) with the highest surface roughness (Table 7-3).

7.4 Conclusions

Thermal treatment appeared to affect already anhydrous BDP by allowing the deaggregation of agglomerates and BDP solvates by prompting solvent evaporation and transformation into the anhydrous form. Depending on the arrangement and positioning of the solvent molecules within the channel structure, evaporation was found to lead either to the disruption of weak hydrogen bonds followed by the gradual collapse of the channel structure or, in the case of the BDP 2-propanol solvate, to a more evenly disintegration and recrystallisation.

This was reflected in the particle shape and roughness. The relatively uncontrolled evaporation of acetone resulted in extremely irregularly shaped anhydrous BDP with a high surface roughness. The anhydrous BDP prepared from the BDP 2-propanol solvate, in contrast, maintained the elongated shape of the solvate whereas the BDP 1-propanol and the BDP ethanol solvates disintegrated into a mix of still slightly elongated but also more compact particles with the latter having the lowest surface roughness, and highest crystallinity based on the sharpness of XRPD peaks.

The controlled, thermally induced desolvation process (under nitrogen, temperature increase of 10 °C/min) allowed the preparation of elongated anhydrous BDP particles from BDP 2-propanol solvates and highly crystalline anhydrous BDP with low surface roughness from BDP ethanol solvates. The preparation of anhydrous BDP through desolvation of BDP 1-propanol solvates

under identical conditions was found to yield particles with a reproducible surface roughness similar to that of the anhydrous sample prepared from BDP 2-propanol solvates. Therefore, all three compounds were considered valuable for the targeted manufacture of anhydrous BDP with defined characteristics

The desolvation of the BDP acetone solvate appeared to be less predictable. The shape of the anhydrous BDP prepared from this solvate was comparatively irregular and showed large variations in its surface roughness. This was therefore not considered a promising precursor for the production of defined anhydrous BDP and was not included in subsequent studies.

7.5 References

Cui, Y., Schmalfuß, S., Zellnitz, S., Sommerfeld, M. & Urbanetz, N. 2014. Towards the optimisation and adaptation of dry powder inhalers. *International journal of pharmaceutics*, 470**,** 120-132.

Hunt, J. H. & Padfield, J. M. 1989. *Micronised beclomethasone dipropionate monohydrate compositions and methods of use*. US Patent 4,866,051.

Nachiengtung, N. 1997. Solid-state characterization of beclomethasone dipropionate solvates and polymorphs. PhD Thesis, Purdue University, IN, USA.

Wang, Z., Chen, J.-F., Le, Y., Shen, Z.-G. & Yun, J. 2007. Preparation of ultrafine beclomethasone dipropionate drug powder by antisolvent precipitation. *Industrial & engineering chemistry research*, 46**,** 4839-4845.

CHAPTER 8

ANALYSIS OF INTERPARTICULATE FORCES IN DRY POWDER INHALER FORMULATIONS

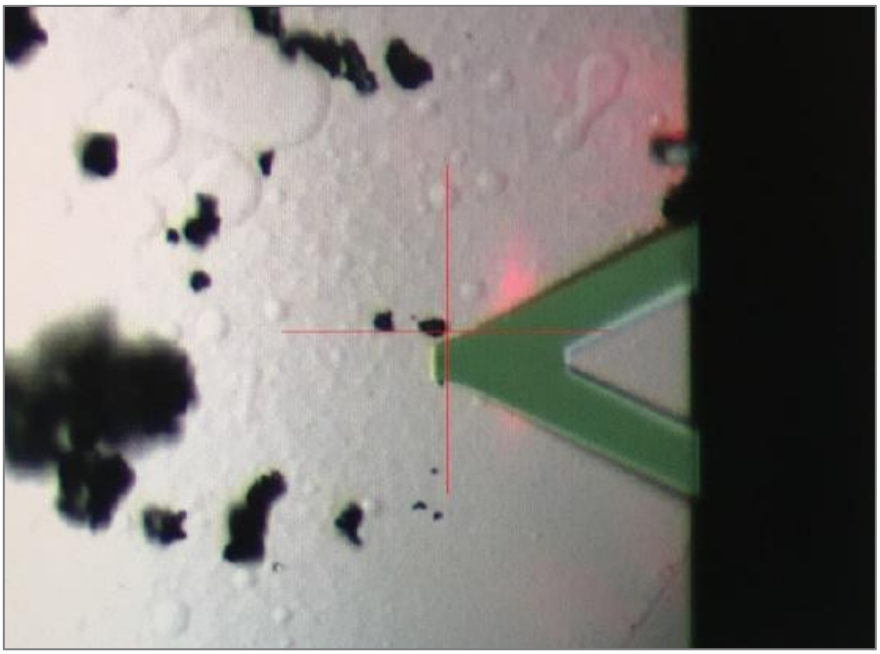

Figure 8. Measurement of interparticulate forces using colloidal probe AFM.

8 Analysis of Interparticulate Forces in Dry Powder Inhaler Formulations

Anhydrous BDP, when used in DPI formulations such as Beclazone (IVAX Pharmaceuticals/TEVA) or Beclate (Cipla Pharmaceuticals) is combined with α-lactose monohydrate as a carrier material. The performance of binary formulations and the efficiency of respiratory drug delivery depend on a number of factors including the forces acting between the components. In DPI formulations these forces are dominated by interparticulate interactions, more specifically on the adhesive and cohesive forces between the compounds of the formulation (Cui et al., 2014).

Adhesion and cohesion depend on particulate properties such as size, surface roughness, crystallinity, surface energetics and combinations of these. While traditional methods focus on the evaluation of bulk properties and their impact on DPI formuulations, AFM enables the determination of local surface characteristics and the direct measurement of interparticulate forces using the colloidal probe technique (Butt, 1991, Ducker et al., 1991). Understanding the impact of the surface properties of one particle on the interparticulate forces between this particle and a substrate allows the direct correlation of certain characteristics to the performance of binary formulations. With the additional knowledge of how these specific particle characteristics can be controlled during manufacture, this would contribute to the targeted improvement of DPI formulations.

Interparticulate forces are best measured with well-defined parameters to facilitate normalisation. Due to many factors, including environmental settings and the exact contact area between the materials at each time during the measurement affecting the results and making replication difficult, interpariculate forces are often evaluated as relative quantities. Estimations, approximations, the application of suitable models and the reduction of external influences add to the quality of the results. The complexity of colloidal probe AFM can be reduced by keeping as parameters constant as possible throughout a series of experiments. For this reason, lactose was initially chosen as the preferred substrate while the more irregular shaped anhydrous BDP particles were used as colloidal probes. Under controlled conditions, lactose gives large regularly shaped crystals with a relatively even surface (R_q = 9.65nm ± 4.33 nm). Thus, major differences in the surface roughness of the substrate could be excluded. Using BDP as colloidal probes led to the additional benefit of using the same probe on different substrates, thus eliminating the need of normalising the force against the (estimated) contact radius. For comparison, additional experiments were carried out using spherical glass beads as colloidal probes with BDP and lactose samples as substrates.

In all cases, force curves were recorded and the forces acting between colloidal probe and substrate were calculated at the point where the probe snaps off the substrate (E, Figure 8-1).

Force spectroscopy relies on the attractive or repulsive forces acting between the tip of the probe and the substrate as the probe approaches the surface and is withdrawn again to its initial position (Figure 8-1).

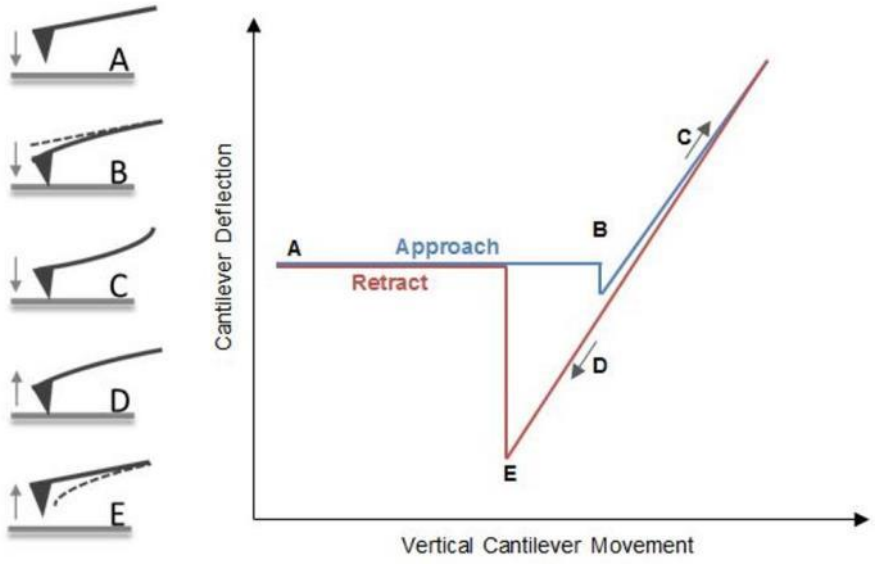

Figure 8-1. Cantilever deflection recorded in force distance curve. Cantilever deflection vs. cantilever movement in one approach and withdraw cycle. The cantilever deflection is then converted into force to result in a force curve, showing the point of snap-on, B, and the point of snap-off, E.

The attractive and repulsive forces acting between sample surface and probe cause the cantilever to deflect. A laser beam reflected from the cantilever surface captures this movement using a photodiode and the position of the reflected beam is used to determine the the cantilever deflection, x_c. This value is then converted into a force, F, using Hooke's law (Equation 8-1), where k_{eff} is the effective spring constant of the cantilever (Butt et al., 2005).

$$F=-x_c k_{eff} \tag{8-1}$$

The force is plotted against the tip-sample separation, D, (Equation 8-2) given by the sum of the cantilever deflection, x_c, and the piezo position, x_p (Butt et al., 2005).

$$D = x_c + x_p \tag{8-2}$$

Initially, no interactions are present between the bodies (A, Figure 8-1) as the probe approaches the sample. At a certain tip-sample separation, the attractive forces cause the tip to snap to the surface (snap-in, B). However, once the tip has snapped to the surface, the repulsive forces gradually start to grow as the tip continues to approach the surface until they exceed the attractive forces and a net repulsive force is recorded. This continues until a pre-defined peak force is reached (C) and the probe is withdrawn from the substrate. The repulsive forces then decrease

(D) until the attractive forces are dominant, holding the tip on the surface and preventing the probe from being withdrawn further. The tip only breaks away from the sample when the force pulling the cantilever back is larger than the adhesive forces holding the tip on the surface (snap-off, E) and the probe then continues to withdraw to its original position. The adhesion between tip and substrate is measured at the snap-off (E).

8.1 Materials and Methods

Anhydrous BDP was supplied by Intatrade GmbH, Germany, and recrystallized using analytical grade ethanol, 1-propanol and 2-propanol (Sigma Aldrich UK). Monodisperse silica beads for colloidal probe AFM were bought from Cospheric (California, USA) and Sigma Aldrich provided α-lactose monohydrate. AFM cantilevers were purchased from Bruker Nano, CA, USA.

8.1.1 Anhydrous BDP

BDP solvates were prepared from acetone, ethanol, 1-propanol and 2-propanol solutions as described in Chapter 7. The samples were fully characterised before being desolvated in a controlled environment under nitrogen (TGA, Q50, TA Instruments, UK; ramping to 160° C at 10° C/min, isothermal at 160 °C). The desolvated BDP crystals were then glued onto clean glass slides (Fisher Scientific) or silicon wafers (Wacker Chemie AG) using Tempfix mounting adhesive (Agar Scientific). Additional samples of anhydrous BDP for colloidal probe AFM were stored in plastic containers wrapped in Parafilm.

8.1.2 Crystallisation of α-Lactose Monohydrate

Anti-solvent vapour crystallisation (Begat et al., 2004a) on a clean, even substrate was used to prepare crystalline α-lactose monohydrate with a smooth surface. In accordance with the previously chosen procedure, 9.75 g α-lactose monohydrate was dissolved in 50 mL deionised water at 40 °C (El-Sabawi et al., 2006) and stirred at 300 rpm for 60 min. The warm solution was filtered through a 45 µm nylon filter (Millipore) and immediately dropped onto a clean glass slide (cleaned in ultrasonic methanol bath methanol) which was then placed over a petri dish filled with ethanol. A beaker was used to cover the set-up, thus minimalizing the loss of ethanol vapour. The crystals were grown for 24 h. Loosely attached particles were blown off the glass with inert gas.

The roughness of the samples was measured on five crystals and found to be 9.65nm ± 4.33 nm (measured on an area of 1 μm^2 each, n=10 measurements per spot).

8.1.3 Colloidal Probes

The AFM (Dimension Icon, Bruker) at the National Graphene Institute at the University Manchester was used to prepare colloidal probes using glass spheres (7.75 µm, 4.08 µm, 1.7 µm) and anhydrous BDP prepared from three selected BDP solvates: BDP ethanol solvate (BDP2), BDP 1-propanol solvate (BDP3) and BDP 2-propanol solvate (BDP1). A series of adhesion and cohesion measurements was carried out with these colloidal probes. BDP (prepared from BDP ethanol/1-propanol/2-propanol solvates and glued onto glass slides) and lactose monohydrate (grown on glass slides using anti-solvent vapour crystallisation) were used as substrates. The same lactose crystals were used each time for consistency.

All AFM based experiments were completed in a clean room.

8.1.3.1 Preparation of Colloidal Probes

Colloidal probes were prepared in soft tapping ramp mode using tipless AFM cantilevers (NP-O10, cantilever A, f_0 = 65 kHz, k_0 = 0.35 Nm^{-1}, Bruker Nano, CA, USA). Glass beads in three different sizes (7.75 µm, 4.08 µm, 1.7 µm) and crystalline BDP particles were mounted onto the free end of the cantilevers (Figure 8-2).

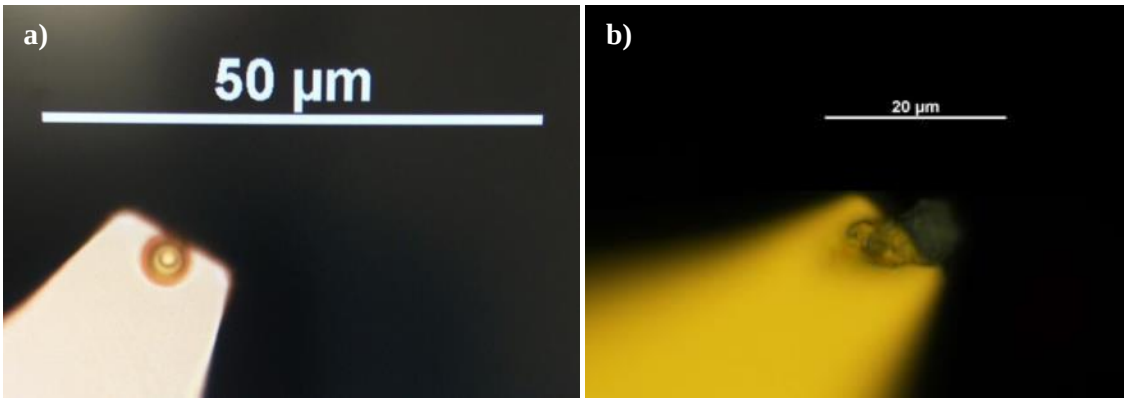

Figure 8-2. Colloidal probes consisting of (a) a glass bead (1.7 µm) and (b) a particle of anhydrous BDP prepared from BDP ethanol solvate (BDP2).

To fix the glass beads and BDP onto the cantilever, minute amounts of two component epoxy resin (UHU plus endfest 300, UHU GmbH & Co KG, Germany) were spread onto a microscope glass slide with a needle. While monitoring the vertical movement of the tipless cantilever, it was gradually brought closer to a streak of glue until the tip was seen to touch the surface. The tip was then retracted immediately and the presence of glue was confirmed visually. The area covered in glue appeared darker compared to the rest of the cantilever. If too much glue appeared to have been taken up, the excess glue was wiped off on the surface of the glass slide. Once a small area at the free end of the cantilever was covered in glue, the frequency was recalibrated. This procedure was necessary to ensure the accuracy of the cantilever movements and it also served to proof that a small amount of glue had been picked up by the cantilever. The addition of glue at the free end of the cantilever decreased the resonance frequency slightly. The

recalibrated cantilever was then positioned precisely above a glass bead or BDP particle on a glass slide and lowered until the tilt of the cantilever indicated that it was in contact with the sphere or particle. After about 20 s the cantilever was retracted and left overnight for curing. The position of the glass beads and BDP was controlled under the microscope and the probe was screened for contamination (glue, debris). Due to an additional weight at the free end of the cantilever, the frequency and spring constant had to be determined again (Table 8-1) using the thermal noise method provided by Bruker's NanoScope software which is accurate for such small spring constants. The spheres and particles were all attached very close to the free end of the cantilevers to avoid corrections due to off-end loading (Green et al., 2004, Glotzbach et al., 2013). The deflection sensitivity was calibrated on a sapphire substrate and calculated using NanoScope Analysis (Bruker).

Table 8-1. Colloidal probes: frequency, f (Hz), cantilever constant, k (Nm), deflection sensitivity (nm V^{-1}).

Cantilever	Particle	f [kHz]	k [Nm]	def. sensitivity [nm V^{-1}]
GB-2µm-1	glass bead, 1.70 µm	69.16167	0.4112	58.37
GB-4µm-2	glass bead, 4.08 µm	67.62207	0.4524	56.64
GB-8µm-1	glass bead, 7.75 µm	53.41511	0.5538	46.75
BDP1-1	anhydrous BDP (BDP 2-propanol solvate)	67.48193	0.3936	59.00
BDP1-2	anhydrous BDP (BDP 2-propanol solvate)	67.43429	0.5120	57.27
BDP1-3	anhydrous BDP (BDP 2-propanol solvate)	67.52539	0.5022	53.29
BDP2-1	anhydrous BDP (BDP ethanol solvate)	66.83242	0.4261	57.49
BDP2-2	anhydrous BDP (BDP ethanol solvate)	67.56332	0.5262	45.41
BDP2-3	anhydrous BDP (BDP ethanol solvate)	69.21178	0.3703	63.39
BDP3	anhydrous BDP (BDP 1-propanol solvate)	69.27195	0.4841	43.05
BDP3-2	anhydrous BDP (BDP 1-propanol solvate)	66.58651	0.4027	58.41
BDP3-3	anhydrous BDP (BDP 1-propanol solvate)	69.34819	0.4256	52.63

8.1.3.2 Adhesion Measurements

A commercial ScanAsyst probe and three colloidal probes made from differently sized glass beads (7.75 μm, 4.08 μm, 1.7 μm) were calibrated (spring constant, resonant frequency, deflection sensitivity) and used in peak force quantitative nanomechanical mapping (PFQNM) mode. A peak force of 50 nN was applied. To evaluate the quality of adhesion and topography mapping in scan mode, images were acquired on lactose and one anhydrous BDP particle (prepared via desolvation of crystalline BDP 1-propanol solvates).

In addition, the probes were scanned across the samples' surface in auto mode. The sharp tip (8 nm) of the ScanAsyst probe got caught in the BDP particles and caused damage. The dull probes, while not damaging the substrates, tended to gradually loosen the substrate from the glass slides or silicon wafers. Due to the probe size in relation to the scale of the substrate texture, the image quality was inconsistent and smaller morphological details were not captured in the height maps.

For this reason, all adhesion measurements were carried out in ramp mode and only the colloidal probes were used. To obtain a representative range of quantitative results, two defined lactose crystals and at least three randomly picked BDP particles were selected and more than 500 force curves were recorded on different spots. PFQNM mapping was carried out to visualise the results where possible but not used for qualitative analysis.

8.1.3.3 Comparative Measurements

Comparative measurements were carried out using BDP colloidal probes (three different BDP samples, three probes prepared from each sample – nine probes in total). 200 force curves were recorded in PFQNM ramp mode at a peak force of 50 nN. Lactose was used as a substrate and adhesion measurements were carried out on two selected areas to assess the adhesive properties of the crystalline BDP particles relative to each other.

Furthermore, the interparticulate forces between the BDP colloidal probe and the corresponding BDP particle glued onto a glass slide were measured to enable the comparison of the particles' cohesive properties.

The preparation of anhydrous BDP through the desolvation of BDP solvates had a significant impact on the surface roughness of the anhydrous material. For this reason, and also to reflect DPI formulation conditions where BDP crystals are unlikely to be completely smooth and planar, anhydrous BDP particles were used as prepared from BDP solvates.

8.2 Results

All force curves were allowed to stabilise before being analysed quantitatively. Irregular forces curves resulting from physical tip-sample interaction or a damaged substrate or tip were excluded from the analysis. Measurements carried out with damaged probes were repeated with replacement probes.

8.2.1 Adhesion to Glass Beads

The adhesion between differently sized glass beads and lactose and between the same glass beads and anhydrous BDP was analysed quantitatively (Table 8-2, Figure 8-3).

Table 8-2. Force of adhesion (F_{ad}) between glass beads and lactose and between glass beads and anhydrous BDP prepared through desolvation of BDP ethanol, 1-propanol and 2-propanol solvates; n ≥ 500[1].

Diameter	F_{ad} [nN]			
[µm]	Lactose	BDP1	BDP2	BDP3
1.70	69.23 ± 2.27	16.06 ± 2.06	55.16 ± 8.60	27.98 ± 5.74
4.08	277.65 ± 14.62	79.87 ± 17.58	96.12 ± 11.18	59.95 ± 7.71
7.78	300.54 ± 12.74	121.03 ± 20.84[1]	253.79 ± 12.74	107.76 ± 11.41

[1] Due to irregularities only 325 force curves were included in the analysis.

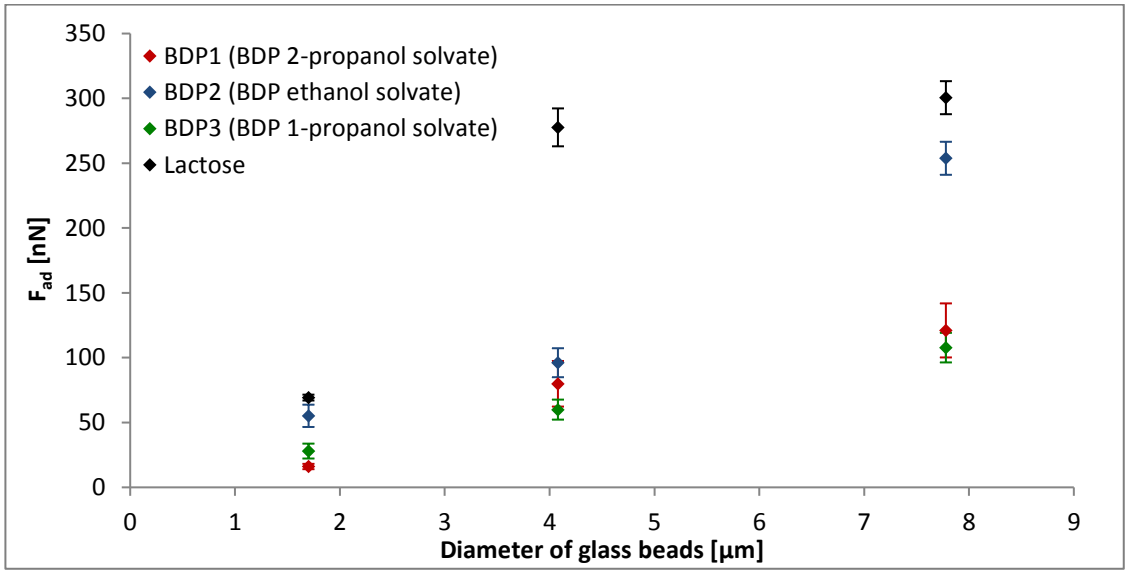

Figure 8-3. Force of adhesion (F_{ad}) between glass beads and lactose (black) and glass beads and anhydrous BDP prepared through desolvation of BDP ethanol (blue), 1-propanol (green) and 2-propanol solvates (red).

Lactose, having a comparatively even surface (R_q = 9.65 nm ± 4.33 nm) was used to evaluate the impact of an increasing contact area on the overall force of adhesion. As expected, the force of adhesion increased together with the size of the glass beads. It appeared, however, that the increase from 1.70 µm to 4.48 µm had a larger influence on the force of adhesion between glass

and lactose than the subsequent increase to 7.78 µm. In each case, the interaction between the lactose substrate and the glass bead solely depended on the contact area since the same materials were used. The surface of lactose is relatively smooth and has an average roughness (R_q) of less than 10 nm. The contact area between the lactose surface and the smaller colloidal probes therefore increased along with the increasing probe diameter (1.70 µm to 4.08 µm). The area of interaction between lactose and the largest glass bead with a diameter of 7.78 µm was large enough to be affected by the surface roughness of the lactose substrate. Assuming an ideally smooth surface, the contact area would increase with the probe diameter. In reality, any surface irregularities smaller than the colloidal probe prevent unbroken contact between probe and surface, thus reducing the actual area of interaction compared to the theoretical contact area (Figure 8-4).

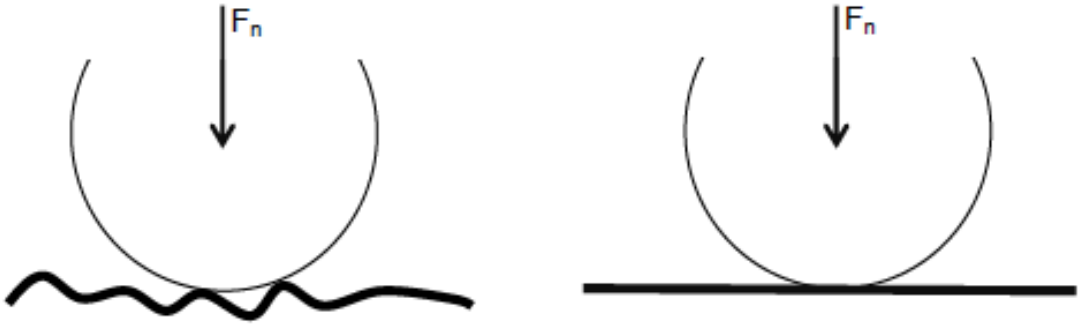

Figure 8-4. Impact of roughness (left) on the area of interaction compared to a smooth surface (right) when using colloidal probe microscopy and applying a force F_n normal to the substrate surface.

The general trend of the force of adhesion increasing with the size of the colloidal probe was also seen when anhydrous BDP was used as substrate (Table 8-2, Figure 8-3). Yet in contrast to lactose, the adhesive forces appeared to increase more linearly. While lactose was found to be relatively smooth, anhydrous BDP had a rough surface (Table 7-3). The actual contact area between each probe and the respective BDP sample was therefore affected by surface roughness even at small probe diameters.

The adhesive forces between the colloidal glass beads and anhydrous BDP prepared from the 1-propanol solvate (BDP3) and the 2-propanol solvate (BDP1) were within the same range (Figure 8-3) and increased by a similar degree with increasing colloidal probe size. This was expected on account of both samples having a surface roughness of about 40 nm (Table 7-3). In contrast, anhydrous BDP prepared from the BDP ethanol solvate (BDP2) was much smoother which had a significant impact on the adhesive forces between this sample and the glass probe. The contact area between probe and substrate was larger which led to a higher force of adhesion.

Protruding areas (Figure 8-5, height sensor; more clearly visualised in peak force error mapping) appeared to adhere more strongly to the glass bead (Figure 8-5, adhesion) than the areas that

could not be reached by the relatively large glass bead. This significantly reduced the actual contact area between the BDP and the colloidal probe.

Using a smaller probe (diameter of 4.08µm instead of 7.78 µm) increased the resolution slightly (Figure 8-5a: 7.78 µm, Figure 8-5b: 4.08 µm). The risk of damaging the probe, however, also increased. The smaller probes, in particularly those with a diameter of only 1.70 µm, were more likely to get physically stuck. For this reason, no PFQNM maps were recorded except for visual evaluation after successful acquisition of several hundred force curves in ramp mode.

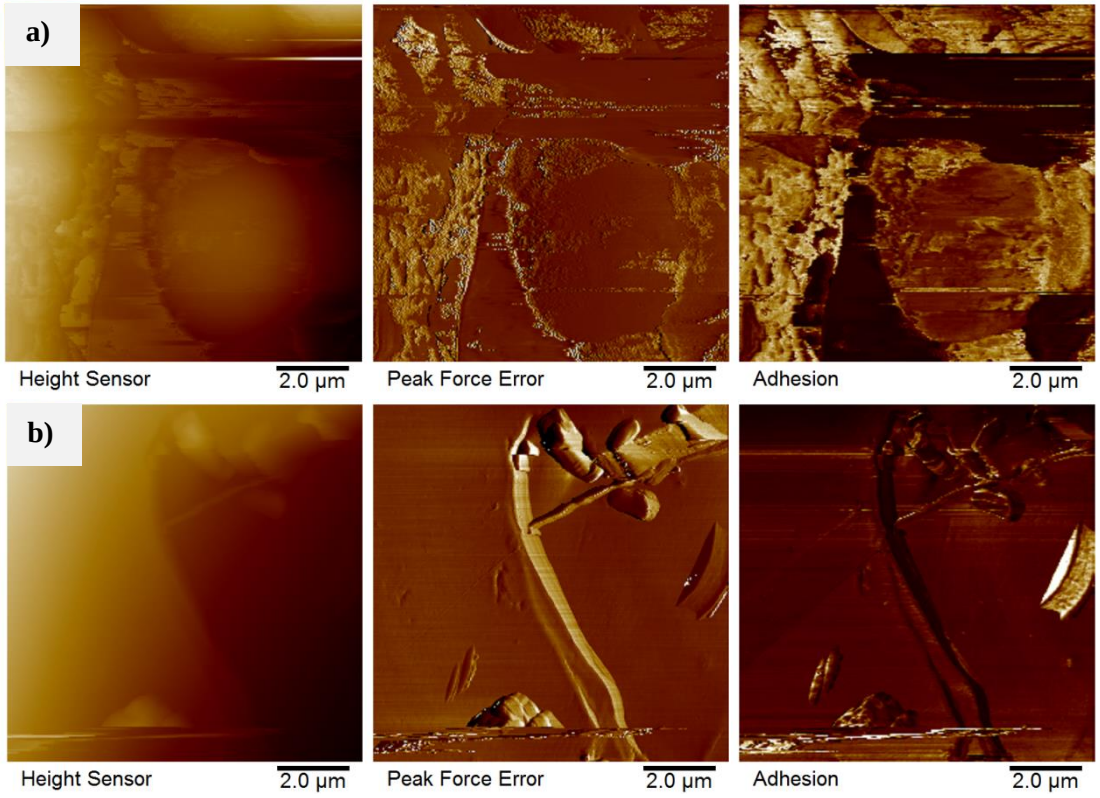

Figure 8-5. PFQNM mapping (height map, peak force map, adhesion map as labelled; lighter areas indicate asperities and larger adhesive forces) at a peak force of 50 nN. Substrate: BDP3. Colloidal probe: a) glass bead, 7.78 µm and b) glass bead, 4.08 µm.

The anhydrous BDP prepared through desolvation of the BDP ethanol solvate had the lowest roughness of about 19 nm whereas the samples prepared from the BDP 1-propanol and the BDP 2-propanol both had an average roughness of 40 nm (Table 7-3). This was reflected in the adhesion (Figure 8-6) which increased less distinctly with increasing surface roughness.

Rougher surfaces exhibited a lower range of forces and the material was less dependent on the curvature of the probe, thus being affected to a lesser degree by the surface of coarse excipient particles in a binary formulation.

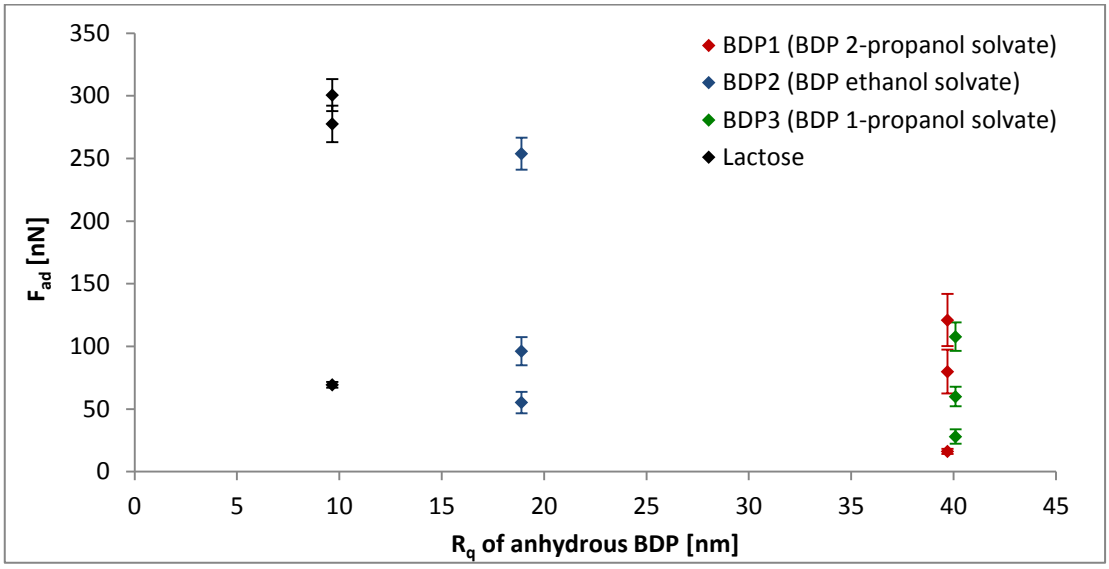

Figure 8-6. Impact of surface roughness (R_q) of anhydrous BDP and lactose on force of adhesion (F_{ad}) between anhydrous BDP, lactose (substrates) and glass beads (colloidal probes)

8.2.2 Adhesion and Cohesion Measurements using Colloidal BDP Probes

The interpartculate forces between colloidal probes prepared from anhydrous BDP (were measured to get a better understanding of the cohesive and adhesive forces acting in a binary DPI formulation consisting of BDP and lactose.

Interparticulate forces strongly depend on the characteristics of the colloidal probe and the substrate. The adhesion between each colloidal probe and lactose was measured on the same areas on the same lactose crystals. Similarly, the cohesive forces between BDP prepared from the same precursor solvate were measured on the same spots on the same substrate. This ensured that adhesion and cohesion measured with one colloidal BDP could be compared. In addition, the results obtained from using different probes on the same substrate were comparable to each other.

The probes that appeared to adhere stronger to lactose also developed higher cohesive forces (Table 8-3, Figures 8-6 to 8-8). Yet despite following the same trend, adhesion between BDP and lactose exceeded BDP to BDP cohesion in all cases which may be attributed to a combination of particle size, surface roughness and surface energetics.

Table 8-3. Adhesion (F_{ad}) between anhydrous BDP (BDP1 prepared from BDP 2-propanol solvate, BDP2 prepared from BDP ethanol solvate, BDP3 prepared from BDP 1-propanol solvate) and lactose; cohesion (F_{co}) between anhydrous BDP (colloidal probe) and BDP substrate; n ≥ 200[1].

Probe	F_{ad} [nN]	F_{co} [nN]		
[µm]	Lactose	BDP1	BDP2	BDP3
BDP1-1	21.57 ± 4.34	11.28 ± 2.78		
BDP1-2	26.17 ± 2.14	15.33 ± 7.23		
BDP1-3	95.74 ± 9.53	35.73 ± 2.73		
BDP2-1	98.91 ± 11.81		85.70 ± 12.60[1]	
BDP2-2	154.10 ± 2.11		104.66 ± 5.09	
BDP2-3	170.61 ± 15.44		109.52 ± 10.13	
BDP3-1	12.29 ± 0.68			5.00 ± 2.11
BDP3-2	69.68 ± 15.81			25.36 ± 10.31
BDP3-3	148. 73 ± 16.63			51.63 ± 9.48

[1] Due to irregularities only 125 force curves were analysed.

8.3 Discussion

Adhesion and cohesion were both seen to increase albeit at different rates (Figures 8-7 to 8-9). The same colloidal probes that showed a stronger adhesion to lactose also showed a stronger cohesion to BDP.

Surface roughness, however, was the decisive factor affecting adhesion due its impact on the contact area between probe and substrate. The force of adhesion between the anhydrous BDP samples and the glass probes therefore depended strongly on the roughness of the BDP substrate. BDP2, prepared from the BDP ethanol solvates, had a smoother surface both BDP1 and BDP3 and the adhesion measurements carried out with glass beads on the BDP2 substrate showed a stronger dependency on the radius of the colloidal probe. Therefore, BDP2 would be more affected by the local curvature of the surface of the carrier material, hence also by number of fines and the surface characteristics of the excipient. BDP1 and BDP3 would be affected to a lesser extent. Considering that the surface properties and the shape of anhydrous BDP based on the BDP 2-propanol solvate precursor was reproducible and less susceptible to variations, this was the preferred compound for potential use in DPI formulations.

When comparing the adhesion between anhydrous BDP and lactose and the cohesion between anhydrous BDP prepared from the same solvated precursor (Figures 8-7 to 8-9), the differences in the contact area caused by surface roughness was only one contributing factor. The affinity of the materials to each other and physical interactions also affected the interparticulate forces.

.

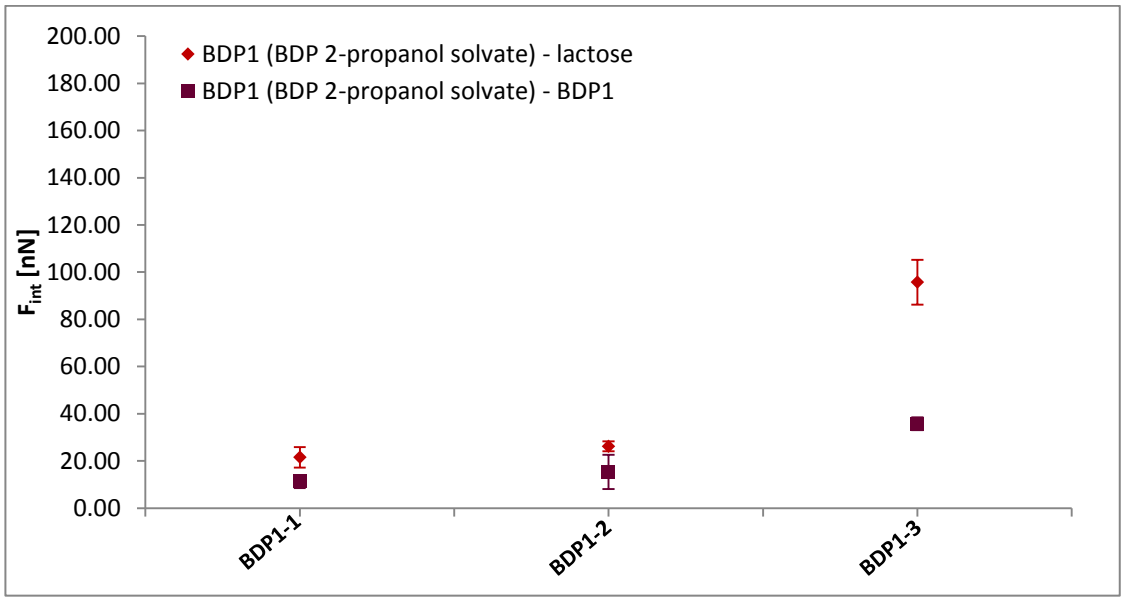

Figure 8-7. Interparticulate forces (F_{int}) (adhesion: red, cohesion: dark red) measured with three colloidal probes prepared from anhydrous BDP (desolvated BDP 2-propanol solvate); n ≥ 200.

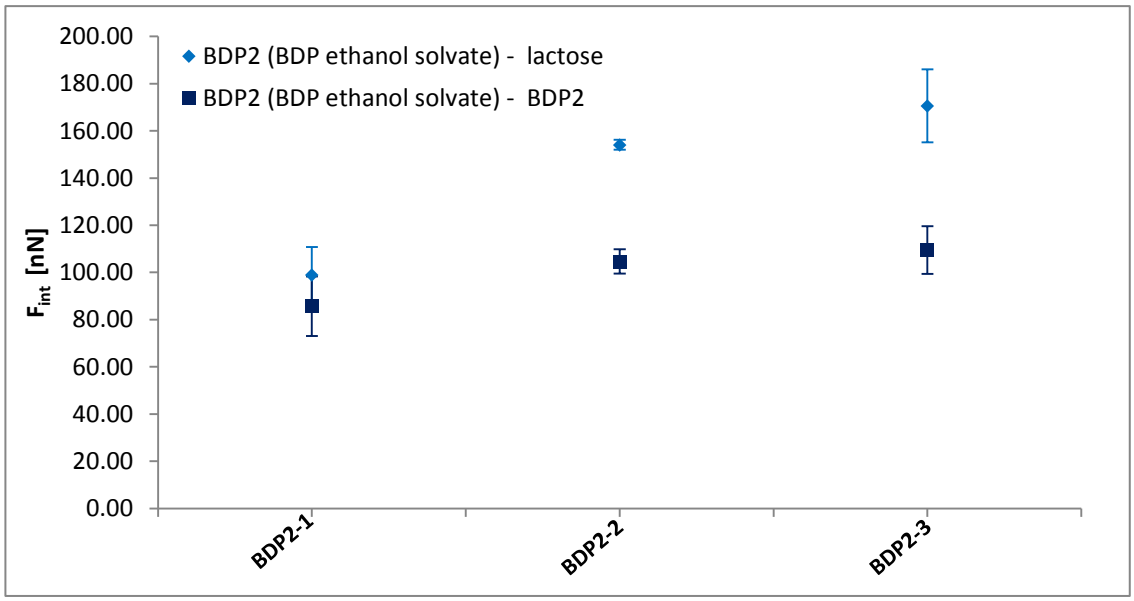

Figure 8-8. Interparticulate forces (F_{int}) (adhesion: blue, cohesion: dark blue) measured with three colloidal probes prepared from anhydrous BDP (desolvated BDP ethanol solvate); n ≥ 200 (cohesion BDP2-1/BDP2: due to irregularities only 125 force curves were analysed).

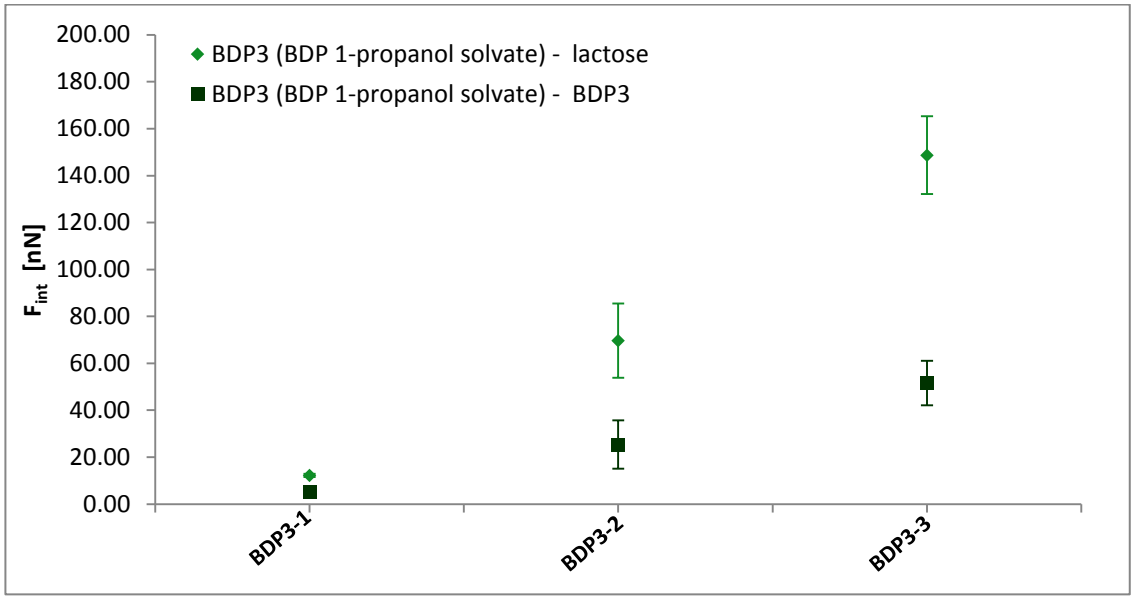

Figure 8-9. Interparticulate forces (F_{int}) (adhesion: green, cohesion: dark green) measured with three colloidal probes prepared from anhydrous BDP (desolvated BDP 1-propanol solvate); n ≥ 200.

If the probe and both substrates had had a uniform surface without any irregularities, the difference in cohesion and adhesion could have been explained by surface energetics, van der Waals forces and long-range electrostatic forces (Leite et al., 2012). Cohesive adhesive balance (CAB) measurements make use of that (Begat et al., 2004b, Begat et al., 2004a). CAB is based on specifically grown crystals with smooth surfaces which act as colloidal probes and substrates. Surface roughness, the size of the colloidal probe and differences in the actual contact area as causes for increased or decreased adhesion and cohesion are therefore virtually excluded. The comparison of adhesive and cohesive forces acting between the same probe and different surfaces is known to give valuable information.

CAB, however, does not reflect the conditions in a DPI formulation where small, irregularly shaped drug particles are mixed with larger lactose particles and fines. In an attempt to mirror such conditions, large lactose crystals and relatively small particulate BDP was used. While not matching the size distributions in an actual DPI formulation, the use of both BDP and lactose on a larger scale gave an indication of the preferred interparticulate forces acting between drug and carrier and drug and drug. As expected, adhesive forces exceeded cohesive forces: Among other purposes, carrier material such as lactose is meant to prevent the agglomeration of drug particles (Zeng et al., 2000).

Despite the actual contact area between probe and substrate being unknown, the increasing difference between adhesive and cohesive forces was also to a certain extent assigned to surface roughness. Regardless of the precursor solvates used in their preparation, the anhydrous BDP particles used as colloidal probes had the same crystalline structure and their surface energetics were assumed to be in a close range. They did, however, have different degrees of surface roughness (Table 7-3) and the particles prepared from the BDP 2-propanol solvate appeared to be slightly elongated (Figure 7-4).

The strongest adhesive forces between colloidal BDP probes and lactose appeared to act between lactose and the anhydrous sample prepared from BDP ethanol solvate. Anhydrous BDP prepared through desolvation of the BDP ethanol solvate also showed the highest adhesion to glass (Figure 8-6) and was known to have the lowest surface roughness.

Interpreting the results with regard to the average surface roughness of anhydrous BDP (Figure 8-10) confirmed the considerable contribution of surface roughness to the overall forces of adhesion. The adhesive force between the smoother anhydrous BDP prepared from the BDP ethanol solvate, was higher than the adhesive forces between the same lactose substrate and anhydrous BDP prepared from BDP 1-propanol and 2-propanol solvates. Yet the results could only serve as a supplement to previous assumptions as the actual contact area, and the exact influence of surface roughness to the actual contact area, were not measured.

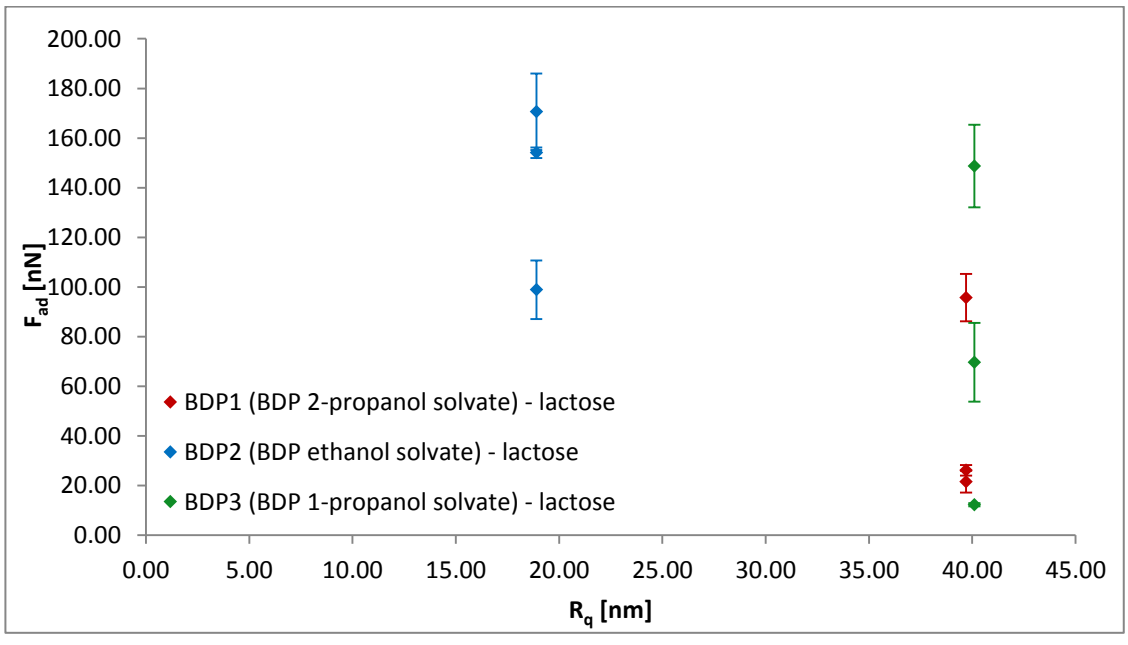

Figure 8-10. Impact of surface roughness (R_q) of anhydrous BDP on force of adhesion (F_{ad}) between lactose (substrate) and anhydrous BDP (colloidal probe).

The considerable impact of surface roughness was further indicated when plotting the cohesive forces acting between anhydrous BDP particles against the surface roughness of each anhydrous sample (Figure 8-11). The relatively smooth anhydrous BDP prepared from the BDP ethanol solvate showed the highest cohesion while the cohesive forces between the two samples prepared from BDP 1-propanol and BDP 2-propanol were lower . Both had a relatively rough surface with the average roughness about than twice as high as that of the desolvated BDP ethanol compound. Again, the results were only considered as an additional indication due to the uncertain contribution of surface roughness to the actual contact area.

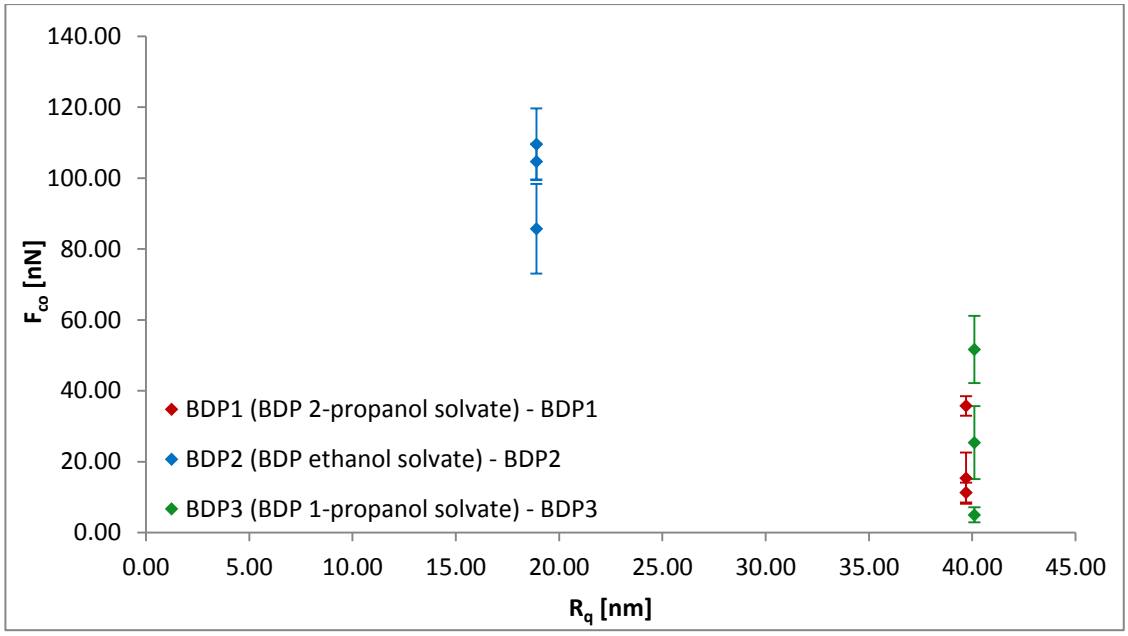

Figure 8-11. Impact of surface roughness (R_q) of anhydrous BDP on force of cohesion (F_{co}).

8.4 Conclusions

Colloidal probe AFM confirmed the importance of surface roughness with regard to interparticulate forces in binary DPI formulations. The adhesion between drug and carrier was replicated based on a simplified model where a large crystalline lactose substrate represented the excipient and relatively small BDP particles were used as colloidal probes. The results indicated a considerable influence of surface roughness on adhesion. Additional studies, using glass beads as colloidal probes and anhydrous BDP as substrates, further confirmed that increasing surface roughness caused a decrease in adhesion.

Since cohesion between drug particles is one of the reasons why excipients are used in DPI formulations, the strength of lactose-BDP adhesion was compared to BDP-BDP cohesion. As expected, cohesion was lower than adhesion in all cases and appeared to decrease with increasing surface roughness.

Out of the three samples used in this study, the BDP prepared from the BDP 2-propanol solvate was the most suitable for targeted manufacturing. The anhydrous BDP had distinct characteristics which are beneficial for DPI formulations: a high surface roughness which can be controlled by desolving the solvate under defined conditions and a slightly elongated shape which facilitates delivery to the lung. The anhydrous BDP prepared from the ethanol solvate had the smoothest surface of all three samples used in colloidal probe AFM and could be reproduced under defined manufacturing conditions. The smooth surface, however, was not seen as an advantage for DPI formulations since this leads to an increased force of cohesion, thus facilitating the formation of agglomerates and also makes the particles prone to adhesion to carrier fines. Preparing anhydrous BDP from BDP 1-propanol solvates was found to be a less reproducible process. The precursor appeared to be less stable and the desolvation process could not be controlled as well as in the other cases. The sample was therefore not considered for use in DPI formulations despite showing the same surface roughness and similar adhesive properties as its counterpart prepared from BDP 2-propanol solvates.

The results showed the reverse relationship between surface roughness and interparticulate forces. Throughout the study, the adhesive and cohesive forces associated with the anhydrous BDP prepared from BDP ethanol solvate appeared to be relatively high compared to those associated to anhydrous BDP prepared from either BDP 1-propanol and BDP 2-propanol solvate. While the former was found to have the smoothest surface with an average roughness (R_q) below 20 nm, the latter both had an average surface roughness of about 40 nm. The surface roughness was shown to be influenced by the initially prepared BDP solvate which in turn were crystallised from supersaturated solutions and subsequently desolvated under controlled conditions. This showed that it is possible to control the interpartculate forces between the components of a binary DPI formulation through the initial choice of solvent and a controlled recrystallisation process.

8.5 References

Begat, P., Morton, D. A., Staniforth, J. N. & Price, R. 2004a. The cohesive-adhesive balances in dry powder inhaler formulations I: direct quantification by atomic force microscopy. *Pharmaceutical research,* 21**,** 1591-1597.

Begat, P., Morton, D. A., Staniforth, J. N. & Price, R. 2004b. The cohesive-adhesive balances in dry powder inhaler formulations II: Influence on fine particle delivery characteristics. *Pharmaceutical research,* 21**,** 1826-1833.

Butt, H.-J. 1991. Measuring electrostatic, van der Waals, and hydration forces in electrolyte solutions with an atomic force microscope. *Biophysical Journal,* 60**,** 1438-1444.

Butt, H.-J., Cappella, B. & Kappl, M. 2005. Force measurements with the atomic force microscope: Technique, interpretation and applications. *Surface science reports,* 59**,** 1-152.

Cui, Y., Schmalfuß, S., Zellnitz, S., Sommerfeld, M. & Urbanetz, N. 2014. Towards the optimisation and adaptation of dry powder inhalers. *International journal of pharmaceutics,* 470**,** 120-132.

Ducker, W. A., Senden, T. J. & Pashley, R. M. 1991. Direct measurement of colloidal forces using an atomic force microscope. *Nature,* 353**,** 239-241.

El-Sabawi, D., Price, R., Edge, S. & Young, P. M. 2006. Novel temperature controlled surface dissolution of excipient particles for carrier based dry powder inhaler formulations. *Drug development and industrial pharmacy,* 32**,** 243-251.

Glotzbach, C., Stephan, D. & Schmidt, M. 2013. Measuring interparticle forces: Evaluation of superplasticizers for microsilica via colloidal probe technique. *Cement and Concrete Composites,* 36**,** 42-47.

Green, C. P., Lioe, H., Cleveland, J. P., Proksch, R., Mulvaney, P. & Sader, J. E. 2004. Normal and torsional spring constants of atomic force microscope cantilevers. *Review of scientific instruments,* 75**,** 1988-1996.

Leite, F. L., Bueno, C. C., Da Róz, A. L., Ziemath, E. C. & Oliveira, O. N. 2012. Theoretical models for surface forces and adhesion and their measurement using atomic force microscopy. *International journal of molecular sciences,* 13**,** 12773-12856.

Zeng, X. M., Martin, G. P. & Marriott, C. 2000. *Particulate Interactions in Dry Powder Formulation for Inhalation*, Taylor & Francis.

CHAPTER 9

CONCLUSIONS AND FUTURE WORK

9 Conclusions and Future Work

The structures of BDP solvates crystallised from solutions of methanol, ethanol, 1-propanol, 2-propanol, 1-butanol and 1-pentanol were studied. In order to be able to correctly interpret the chemical shifts in NMR spectroscopy, the complete structure of BDP in its anhydrous form has been assigned to its ^{1}H NMR spectrum for the first time. Based on 1D and 2D NMR spectra, the axially and equatorially aligned protons of the steroid structure were assigned.

The fully solved ^{1}H NMR spectrum was a valuable reference for the analysis of chemical shifts observed in NMR titration. NMR titration, DOSY, thermal analysis and single crystal XRD allowed the interpretation of the mechanisms facilitating either the crystallisation of solvates or the formation of anhydrous BDP from solution. However, the stability of the BDP solvates appeared to depend on a controlled environment. Where possible, the solvates were analysed immediately after crystallisation. Further studies in controlled environments could elucidate the factors affecting solvate formation and stability.

NMR titration and DOSY showed that BDP interacted in a similar way with all alcohol solvents. Based on this, the crystallisation of solvates was found to depend on both solvent polarity and on the size of the solvent molecules. Solid state NMR and XRD confirmed the formation of channel solvates from ethanol, 1-propanol, 2-propanol and acetone solution and gave further information about the mechanism leading to either anhydrous or solvated BDP. In addition, the mobility of ethanol, 1-propanol, 2-propanol and acetone solution within the channel was confirmed. Weak hydrogen bonding as identified by NMR titration was found to be present between ethanol, 1-propanol, 2-propanol and the available carbonyl group on the propionate branch of BDP that reaches into the channel. The arrangement of the solvent molecules and their mobility within the channel, however, were again found to depend on both solvent polarity and molecular size. The uniform channel volume restricted the accommodation of larger solvent molecules.

Thermal treatment led to the desolvation of the BDP solvates, followed by the collapse of the channels structure which appeared to be maintained by the presence of mobile solvent molecules. Eventually, all solvates were seen to undergo solid-solid phase transition into the anhydrous form. The particle size (d_{90}) of all anhydrous samples prepared from BDP solvates was smaller than that of the as-received anhydrous BDP. However, the successful delivery of DPI formulations to the lung requires an aerodynamic diameter below 10 µm (Hunt and Padfield, 1989), ideally below 5 µm (Cui et al., 2014). To reduce the size of the desolvated BDP to the ideal size range between 1 and 5 µm, two approaches could be followed: The particle size of the solvated BDP will be reduced by either changing the parameters such as temperature and stirring speed during crystallisation (Morissette et al., 2004, Wang et al., 2007) or by adjusting the

conditions of the desolvation process. Analysing the impact of different combinations of manufacturing conditions will show how to best reduce the average size (d_{90}) to a respirable size. Preliminary work has been carried out. The impact of a combination of different stirring speeds (1500 rpm, 300 rpm) and temperatures (-19 °C, 4 °C) on BDP crystallised from ethanol, 1-propanol, 2-propanol and acetone has been studied using a Polar Bear System (Cambridge Reactor Design, UK) to control the conditions. Due to instabilities during crystallisation and a delay of several days between crystallisation and particle size analysis, agglomerates had formed and the true PSD could not be measured.

The surface roughness of the particulate anhydrous BDP, the physical characteristic that is one of the key factors affecting adhesion and cohesion in a DPI formulation, was found to depend on the solvate precursor and could thus be influenced by the initial choice of solvent. The BDP 1-propanol solvate and the BDP 2-propanol solvates transformed into anhydrous BDP samples with similar degrees of surface roughness. Due to being more stable during desolvation and giving more reproducible results, the sample prepared from the BDP 2-propanol solvate was the preferred precursor. Thermal treatment of the BDP ethanol solvate gave smooth anhydrous BDP particles which were highly crystalline. Smooth particles, however, are prone to form agglomerates and adhere more strongly to fines in a DPI formulation.

The results of this study demonstrate an alternative way to prepare anhydrous BDP with defined particle properties through the desolvation of BDP solvates. It was shown that it is possible to prepare anhydrous BDP with a specific shape and a defined surface roughness using BDP solvates as intermediate species and controlling both their crystallisation and the desolvation mechanism. Since the interpartculate forces between the excipients and drug particles in DPI formulations depend, among other factors, on the contact area between excipient and API, the control of the surface roughness is a step towards the targeted preparation of well-defined formulations that can be tailored to specific patient needs. Using either ethanol or 2-propanol to crystallise BDP solvates and removing the solvent in a controlled thermal process was thus shown to give anhydrous BDP particles with distinct characteristics.

In further studies, the actual performance of DPI formulations containing BDP prepared from BDP ethanol and BDP 2-propanol solvates could be evaluated using a next generation impactor (NGI) (Marple et al., 2003) which mimics the conditions of an airstream through the respiratory system. The method allows the determination of the fine particle fraction (FPF) that would be delivered in a typical application and gives information about the uniformity of the delivered dose. Correlations between the FPF would further link the formulation performance to interparticulate forces, material characteristics and initial processing parameters.

References

Cui, Y., Schmalfuß, S., Zellnitz, S., Sommerfeld, M. & Urbanetz, N. 2014. Towards the optimisation and adaptation of dry powder inhalers. *International journal of pharmaceutics,* 470**,** 120-132.

Hunt, J. H. & Padfield, J. M. 1989. *Micronised beclomethasone dipropionate monohydrate compositions and methods of use*. US Patent 4,866,051.

Marple, V. A., Roberts, D. L., Romay, F. J., Miller, N. C., Truman, K. G., Van Oort, M., Olsson, B., Holroyd, M. J., Mitchell, J. P. & Hochrainer, D. 2003. Next generation pharmaceutical impactor (a new impactor for pharmaceutical inhaler testing). Part I: Design. *Journal of aerosol medicine,* 16**,** 283-299.

Morissette, S. L., Almarsson, Ö., Peterson, M. L., Remenar, J. F., Read, M. J., Lemmo, A. V., Ellis, S., Cima, M. J. & Gardner, C. R. 2004. High-throughput crystallization: polymorphs, salts, co-crystals and solvates of pharmaceutical solids. *Advanced drug delivery reviews,* 56**,** 275-300.

Wang, Z., Chen, J.-F., Le, Y., Shen, Z.-G. & Yun, J. 2007. Preparation of ultrafine beclomethasone dipropionate drug powder by antisolvent precipitation. *Industrial & engineering chemistry research,* 46**,** 4839-4845.

APPENDIX I

AWARDS

VCU RDD Peter R Byron Graduate Student Award 2017, funded by the Virginia Commonwealth University's Medical College of Virginia Foundation, awarded at Respiratory Drug Delivery 2017, Antibes, 25-28 April 2017.

Young Researcher Award 2016, funded by the Chemistry of Construction Materials Division of the German Chemical Society (GDCh), awarded at International Conference on the Chemistry of Construction Materials 2016, Munich, 10-12 October 2016.

PUBLICATIONS

Weiss, C., McLoughlin, P., Cathcart, H. (2015) 'Characterisation of Dry Powder Inhaler Formulations Using Atomic Force Microscopy', International Journal of Pharmaceutics, 494, p393-407. Citations to date (May 2018): 8.

Weiss, C., McLoughlin, P., Manesiotis, P., Redington, W. and Cathcart, H. (2018) 'Preparation and Characterisation of Beclomethasone Dipropionate Solvates'. Submitted to *Crystal Growth & Design*. Accepted with minor corrections.

PRESENTATIONS

Donegan, S. and Weiss, C. (2017) 'Chemistry, Alchemy and Magic', presented at II Encuentro de Ciencia, Magia y Educación, Madrid, 1-3 December 2017.

Weiss, C., McLoughlin, P., O'Mahony, J., Manesiotis, P., Nockemann, P. and Cathcart, H. (2017) 'Synthesis and Materials Characterisation of Crystalline BDP: A Novel Approach Using NMR, XRD and AFM', presented at 69th Irish Universities Chemistry Research Colloquium 2017, Dublin, 22-23 June 2017.

Weiss, C., Kraft, A, Hergeth, W.-D. and Müller, I. (2016) 'Application of atomic force microscopy on cementitious surfaces', presented by invitation of Wacker Chemie AG at International Conference on the Chemistry of Construction Materials 2016, Munich, 10-12 October 2016.

Weiss, C., McLoughlin, P., and Cathcart, H. (2016) 'Preparation and Characterisation of Beclomethasone Dipropionate for Inhalation', presented at WIT Research Day 2016, Waterford, 3 May 2016.

POSTER PRESENTATIONS

Weiss, C., McLoughlin, P., Manesiotis, P., Nockemann, P. and Cathcart, H. (2017) 'Crystallisation of BDP: The Impact of Solvent Properties on Crystalline APIs', presented at Drug Delivery to the Lungs 2017, Edinburgh, 6-8 December 2017.

Weiss, C., McLoughlin, P., O'Mahony, J., Manesiotis, P., Nockemann, P. and Cathcart, H. (2017) 'Analysing and Predicting the Physical Properties of the Anti-inflammatory Drug Beclomethasone Dipropionate: A Novel Approach Using NMR, XRD and AFM, presented at WIT Research Day 2017, Waterford, 4 May 2017.

Weiss, C., McLoughlin, P., Manesiotis, P., Nockemann, P. and Cathcart, H. (2017) 'Synthesis and Materials Characterization of BDP Solvates as Precursors for Anhydrous BDP Particles for Dry Powder Formulations', presented at Respiratory Drug Delivery Europe 2017, Antibes, 25-28 April 2017.

Weiss, C., McLoughlin, P., Manesiotis, P., Nockemann, P. and Cathcart, H. (2017) 'Synthesis and Materials Characterization of BDP Solvates as Precursors for Anhydrous BDP for DPI Formulations', presented at IOP Spring Meeting, Dublin, 10 March 2017.

Weiss, C., McLoughlin, P., and Cathcart, H. (2015) 'Correlation of Particulate Characteristics and Interparticulate Forces in Dry Powder Formulations', presented at GDCh Wissenschaftsforum 2015, Dresden, 30 August – 2 September 2015.

Weiss, C., McLoughlin, P., and Cathcart, H. (2015) 'Characterisation of Dry Powder Formulations for Inhalation using Atomic Force Microscopy', presented at Limerick Postgraduate Research Conference, Limerick, 28 May 2015.

Weiss, C., McLoughlin, P., and Cathcart, H. (2015) 'Characterisation of Dry Powder Formulations for Inhalation using Atomic Force Microscopy', presented at WIT Research Day 2015, Waterford, 28 April 2015.

PUBLICATIONS IN PROGRESS

Weiss, C., McLoughlin, P. and Cathcart, H. (2018) 'Complete NMR Spectroscopic Analysis of Anhydrous BDP'. In preparation.

Weiss, C., McLoughlin, P., Manesiotis, Nockemann, P. and Cathcart, H. (2018) 'Structural Analysis of BDP Solvates and Solvate Formation'. In preparation.

APPENDIX II

Characterisation of Dry Powder Inhaler Formulations Using Atomic Force Microscopy

Weiss, C., McLoughlin, P., Cathcart, H. (2015), International Journal of Pharmaceutics, 494, p393-407. DOI: 10.1016/j.ijpharm.2015.08.051

Inhalation formulations are a popular way of treating the symptoms of respiratory diseases. The active pharmaceutical ingredient (API) is delivered directly to the site of action within the deep lung using an inhalation device such as the dry powder inhaler (DPI). The performance of the formulation and the efficiency of the treatment depend on a number of factors including the forces acting between the components. In DPI formulations these forces are dominated by interparticulate interactions. Research has shown that adhesive and cohesive forces depend on a number of particulate properties such as size, surface roughness, crystallinity, surface energetics and combinations of these. With traditional methods the impact of particulate properties on interparticulate forces could be evaluated by examining the bulk properties. Atomic force microscopy (AFM), however, enables the determination of local surface characteristics and the direct measurement of interparticulate forces using the colloidal probe technique. AFM is considered extremely useful for evaluating the surface topography of a substrate (an API or carrier particle) and even allows the identification of crystal faces, defects and polymorphs from high-resolution images. Additionally, information is given about local mechanical properties of the particles and changes in surface composition and energetics. The assessment of attractive forces between two bodies is possible by using colloidal probe AFM. This review article summarises the application of AFM in DPI formulations while specifically focussing on the colloidal probe technique and the evaluation of interparticulate forces.

Preparation and Characterization of Beclomethasone Dipropionate Solvates

Weiss, C., McLoughlin, P., Manesiotis, P., Redington, W. Cathcart, H. (2018), Crystal Growth & Design, in print. DOI: 10.1021/acs.cgd.8b00465

Active pharmaceutical ingredients (APIs) in dry powder inhaler (DPI) formulations need to have well-defined material properties. These can be influenced by the choice of processing parameters. The impact of methanol, ethanol, 1-propanol, 2-propanol, 1-butanol, 1-pentanol and acetone on the crystallization of beclomethasone dipropionate (BDP), an anti-inflammatory agent, was studied using X-ray powder diffraction, thermal analysis, gas chromatography with mass spectrometry, scanning electron microscopy and atomic force microscopy. Crystallization from methanol, 1-butanol and 1-pentanol resulted in particulate BDP with a predominantly anhydrous character. In contrast, BDP solvates were formed using ethanol, 1-propanol, 2-propanol or acetone. The solvates had different crystalline structures depending on the solvent used. Distinct thermal properties confirmed the inclusion of ethanol, 1-propanol, 2-propanol and acetone within the crystalline BDP host. Furthermore, the size, shape and surface characteristics of the crystalline particles were found to be influenced by the choice of solvent in a reproducible way. These properties were also found to translate to the anhydrous products prepared from the solvates through controlled desolvation. Such information is of value to the pharmaceutical industry where knowledge of how specific factors affect the crystalline product would potentially allow one to tailor BDP to have specific material properties. Knowledge of how to control these properties by controlling specific processing parameters and to adjust them as desired would be of great benefit to dry powder inhaler (DPI) formulations where surface properties are crucial to the efficacy of the treatment.